MODELLING OF GAS-CONDENSATE FLOW IN RESERVOIR AT NEAR WELLBORE CONDITIONS

by

SALMAN MOHAMMED AL-SHAIDI,
BSCE, MSE

Submitted for the Degree of Doctor of Philosophy in
Petroleum Engineering

Department of Petroleum Engineering
Heriot-Watt University
Edinburgh, UK
August 1997

To my father. the late.

Mohammed Ibin Salman Ibin Hassan Al-Shidi.

May Allah bless his sole and place him in the day of judgement

amongst the believers and prophets.

TABLE OF CONTENTS

LIST OF SYMBOLS

A = area.

E_a = average absolute relative error.

E_i = average relative error.

f = fractional mobility.

f_L = liquid fractional flow mobility.

f_{υ} = vapour fractional flow mobility.

f_w = water fractional flow mobility.

I = X-ray beam intensity, counts/s.

J = Leverett's capillary-pressure function.

k = permeability.

k_e = effective permeability.

k_r = relative permeability.

k_{rcb} = base or initial relative permeability to condensate.

k_{rcm} = relative permeability to condensate under miscible conditions.

k_{rgb} = base or initial relative permeability to gas.

k_{rgm} = relative permeability to gas under miscible conditions.

k_{rL} = relative permeability to liquid.

k_{rnw} = nonwetting phase relative permeability.

$k_{r\upsilon}$ = relative permeability to vapour.

k_{rw} = relative permeability to water.

k_{rw} = wetting phase relative permeability.

k_w = effective permeability to water.

L = total length.

L = path length of x-ray beam, cm.

MW = molecular weight.

N_c = capillary number (as defined).

N_{cb} = base or initial capillary number value.

N_p = oil pore volume produced.

N_{Po} = cumulative volume of oil produced.

n = relative permeability scale function exponent.

nr = residual saturation scale function exponent.

n^c = condensate Corey's exponent.

n^g = gas Corey's exponent.

P = pressure.

P_c = critical pressure.

P_c = capillary pressure.

P_{cb} = threshold capillary pressure or bubbling pressure.

P_{cgo} = oil/gas capillary pressure.

PV = pore volume.

PV_{inj} = pore volume injected.

Q = cumulative production.

Q_i = pore volume injected.

q,Q = injection rate.

R_e = Reynold's number.

S = saturation.

S_{cr} = residual condensate saturation.

S_{crb} = base or initial residual condensate saturation.

S_g^* = normalised gas saturation.

S_{gr} = residual gas saturation.

S_{grb} = base or initial residual gas saturation.

S_{gt} = trapped gas saturation.

S_o' = normalised oil saturation.

S_{or} = residual oil saturation.

S_{ori} = initial residual oil saturation.

S_υ = vapour saturation.

S_w = water saturation or wetting phase saturation.

S_w' = normalised water saturation.

S_{wavg} = average water saturation.

S_{wi} = initial or connate water saturation.

t = time.

T = temperature.

T_b = boiling point temperature.

T_c = critical temperature.

u, v = Darcy velocity.

U = uncertainty function.

V = volume.

V_c = critical volume.

V_{inj} = cumulative volume of liquid injected.

V_L = cumulative volume of liquid produced.

V_w = cumulative volume of water injected.

WF = weight fraction, fraction.

WF_{PHC} = weight fraction of pure hydrocarbon component, fraction.

WF_{BrHC} = weight fraction of bromated hydrocarbon component, fraction.

WF_{CH4} = weight fraction of methane, fraction.

WF_{C3H7Br} = weight fraction of bromopropane, fraction.

X_i = scale function for phase i.

X_{ri} = scale function for residual saturation of phase i.

β = turbulence factor.

γ = two-phase turbulence multiplier (as defined).

λ = pore-size distribution factor.

ρ = density.

μ = viscosity.

μ_b = viscosity of fluid used to find absolute permeability.

μ_e = effective viscosity.

$\bar{\mu}_e$ = average effective viscosity.

μ_L = liquid viscosity.

μ_υ = vapour viscosity.

μ_w = water viscosity.

η = mass absorption coefficient, cm2/g.

ϕ = porosity.

Φ = fluid potential.

θ = time weighting parameter.

σ = interfacial tension.

σ_b = initial or base interfacial tension value.

υ = interstitial velocity.

τ_{rx} = shear stress.

ΔP = differential pressure across the sample during the flood.

ΔP_b = differential pressure across the sample to calculate absolute permeability.

$\Delta P/\Delta L$ = pressure gradient.

Subscripts

1.2 = refers to the fluid 1 and fluid 2.

2 = refers to the outlet or end values.

c = condensate.

g = gas.

i = phase index.

o = oil.

r = rock.

Abbreviations

1D: = one dimensional.

3P PR EOS = three parameter Peng-Robinson equation of state.

BHP = bottom-hole pressure.

BIC = binary interaction coefficient.

BL = Bardon and Longeron.

CCE = constant composition expansion.

CCS = critical condensate saturation.

CGR: = condensate gas ratio in vol./vol. both at reservoir conditions.

CVD = constant volume depletion.

EOS = equation of state.

GOR = gas to oil ratio.

HWU = Heriot-Watt University.

HCPV = hydrocarbon pore volume.

IFT = interfacial tension.

IMPES = implicit in pressure but explicit in compositions and saturations.

JBN = Johnson, Bossler and Naumann.

JR = Jones and Roszelle.

LBC = Lohrenze, Bray and Clark.

NFA = Nghiem, Fong and Aziz.

PVT = pressure-volume-temperature.

SS = steady state.

STB = stock tank barrel.

STD = standard deviation.

UC = unit cell.

USS = unsteady state.

LIST OF TABLES

LIST OF FIGURES

ACKNOWLEDGEMENTS

I have the honour of working under the supervision of Professor Ali Danesh and Professor Dabir H. Tehrani of the Department of Petroleum Engineering at Heriot-Watt University. Their technical guidance, professional support, and encouragement made the completion of this work successful. Their interest in my professional development as a researcher in this field is also gratefully acknowledged.

I am privileged to be a member of the Gas Condensate Recovery Project team. Hence, the contribution of all the members in this project is appreciated.

The financial support of Petroleum Development - Oman LLC. (PDO) through their full scholarship to conduct this work is acknowledged. I am grateful for Dr. M. Samir Al-Kharusi of PDO for his moral and professional support in making this scholarship possible. Special thanks go to the members of PDO/HTR staff for their co-operation during this research programme.

The co-operation of the academics, senior and associate researchers and members of support staff of the Department of Petroleum Engineering at Heriot-Watt University is acknowledged. Also, special thanks go to Steve Furnival of Geoquest Inc. for his simulation aid that is required for successfully completing this work.

Finally, the financial support for this programme is also provided by: The UK Department of Trade and Industry, British Gas plc, BP Exploration Operating Company Ltd, Chevron UK Ltd, Conoco (UK) Ltd, Elf UK, Marathon Oil UK, Mobil (North Sea) Ltd, Phillips Petroleum Co (UK) Ltd, Shell Exploration and Development, and Total Oil Marine Plc that is gratefully acknowledged.

S. Sh.
August, 1997
HWU
Edinburgh, Scotland

ABSTRACT

The behaviour of gas condensate flow in the porous media is distinctly different from that of gas-oil flow. The differences are attributed to the difference in fluid properties, phase behaviour, and condensation and vaporisation phenomena that distinguishes gas condensate fluids from the aforementioned fluid types. These differences manifest themselves into an important flow parameter that is typically known as relative permeability.

Relative permeability is known to be related to the phase saturation, and the interfacial tension (IFT). Also, at high phase velocities, its reduction with increasing velocity, known as Forchheimer (turbulence) or inertia effect, is well documented. An unconventional behaviour of gas condensate fluids has been experimentally proven in Heriot-Watt laboratory and confirmed by other experimental studies performed elsewhere. These tests have shown that at intermediate velocities, before the inertia becomes significant, the gas and the condensate relative permeabilities are significantly improved by increase in velocity. This phenomenon is referred to as the rate-effect. None of the conventional relative permeability models include this experimentally proven favourable rate effect.

In this work the flow of gas condensate fluids in porous media is modelled with emphasis on near wellbore conditions. Theoretical, empirical as well as simulational investigations are used to improve the present technology on the treatment of the flow of gas condensate in reservoirs. The use of X-ray or γ-ray devices to monitor saturation profile during displacement experiments is investigated and the appropriate test conditions leading to reliable measured relative permeability data are determined.

The regimes of the gas condensate flow at the core level, where the rate effect is evident, are investigated using the concept of Reynolds number. Then a mechanistic flow model, where the flow of gas condensate fluids is assumed to follow an annular-mist flow criterion, is presented to capture the essence of the rate effect in perforations.

The favourable IFT and rate effects are incorporated into the modelling of gas condensate relative permeability by correlating it with capillary number (N_C). Two forms of the correlation are presented.

The impact of IFT and N_C together with the Forchheimer (inertia) on well deliverability is thoroughly investigated using the above correlation. The gas condensate relative permeability correlation is combined with the Forchheimer effect and used in a specially modified version of a commercial simulator, Eclipse 300V 98a development, to investigate the impact of IFT, N_C, and inertia on well productivity. The impact is found to accelerate production from gas condensate reservoirs. At practical production rates, the significance of the impact on phase recoveries cannot be ignored regardless of reservoir fluid richness or absolute permeability.

CHAPTER 1

INTRODUCTION

As world oil reserves dwindle the challenge of producing more oil out of existing reservoirs has been elevated to higher degrees of competency on knowledge and technology. Such a challenge requires a solid understanding of the basic concepts of reservoir engineering. As technology and knowledge grew so did the benefit of better understanding of such concepts that evolved to become an integral part of any reservoir study. Today hardly any project will materialise before a comprehensive study is conducted; such a study must take into account the effect of relative permeability and phase behaviour on well deliverability and hence recoverable hydrocarbons. Consequently, the uncertainties associated with the development of new fields and production from existing ones have been reduced.

Furthermore, in the process of understanding the aforementioned concepts, technological advancements in the area of experimental measurements and computer simulation have enabled us to observe and quantify unforeseen, maybe previously overlooked, behaviours. This is specially true for gas-condensate reservoirs where until recently treated just like gas reservoirs. Reservoir engineers always expect a reduction in gas-condensate well deliverability due to condensate drop-out, but they could not experience this consistently. In some cases it is so and in other cases not and in few cases they even observed improvement, without being able to explain the reasons.

The recognition of distinct reservoir and flow characteristics for gas-condensate reservoirs in comparison with black oil, volatile oil, or gas reservoirs had opened a new frontier where hardly any concept (i.e. relative permeability or phase behaviour) typically applied for these three reservoirs can be taken for granted. Each concept has to be rigorously investigated and modified before applying it to gas-condensate reservoirs. Failure to do so inevitably hinders the ongoing effort in finding solutions for existing problems associated with gas-condensate reservoirs such as loss of well deliverability.

Since gas-condensate reservoirs present unique challenges for petroleum engineers and scientists, they deserve a significant portion of the research and development effort financed by the petroleum industry. Recognising the significant produced stock-tank oil from such a reservoir makes the economics of developing such reservoirs much more viable especially when gas prices are low.

Steady state gas condensate relative permeability curves are calculated based on Darcy flow equation. In the Darcy flow equation relative permeability is treated as a constant with respect to pressure drop or flow rate and it is variable only with respect to phase saturation. This assumes that the two fluids flow as though they are hydrodynamically independent; each fluid is flowing in separate channels of the network. However, this flow behaviour is not true of gas-condensate flow at low interfacial tension, (IFT) or high flow rates (at near the wellbore region). Furthermore, it contradicts the recent experimental finding that at constant low IFT, relative permeabilities of gas and condensate are dependent on flow rate, referred to throughout this thesis as "Rate-Effect". Therefore, relating gas condensate relative permeability to saturation (or even saturation and IFT) is not adequate to define the relative permeability accurately.

Hence, the goal of this research is to contribute to the understanding of the flow of gas-condensate systems in the near wellbore region . This is accomplished by theoretically modelling measured relative permeability of gas condensate flowing in porous media with emphasis on the aforementioned flow behaviour

Chapter 2 gives an introductory literature review on gas condensate reservoirs. The current understanding of the behaviour of the gas condensate fluid systems, the nature of the retrograde condensation and flow mechanism, production methods, sampling and well testing, gravity drainage and well deliverability of gas condensate reservoirs are defined.

Two-phase flow in porous media where the concept of relative permeability is thoroughly explored in chapter 3 with emphasis on the difference between gas condensate and the customary gas-oil or water-oil relative permeabilities. It includes a complete description of the experimental laboratory set-up currently employed, at the Department of Petroleum Engineering of Heriot-Watt University, to conduct core experiments to measure the gas-condensate relative permeability. Also, the possibility of successfully using x-ray or γ-ray absorption methods in measuring condensate saturation profile during gas condensate relative permeability displacement experiment is investigated. The viability (in terms of expected possible total error in measured condensate saturation) of using X-ray or γ-ray devices to measure phase saturation is determined. Measured PVT-data for a methane/bromated propane mixture is used in phase behaviour modelling and hypothetical core displacement experiment using Eclipse simulator. The extra errors in measured condensate saturation added by PVT-data and the dynamic of the displacement are quantified for X-ray or γ-ray devices with accuracy similar to those reported for doped gas/oil/water systems.

To be applicable for the flow of gas-condensate systems at near wellbore conditions, the Darcy flow equation is extended by modifying the relative permeability definition. This is done by linking the relative permeability (previously treated as a function of saturation) with velocity and interfacial tension simultaneously.

First, to model the rate effect it is imperative to know the nature of the fluid flow during the steady-state relative permeability tests where rate effect is reported. Therefore, in Chapter 4 the flow regimes during those tests are categorised. The concept of a modified Reynolds number is used in conjunction with various flow models to investigate the possible occurrence of the Forchheimer (Inertia) flow.

Initially, gas-condensate flow at near wellbore conditions is mechanistically modelled at the pore level where a certain fluid distribution is assumed to be responsible for the aforementioned gas condensate relative permeability dependence on velocity. This approach is detailed in chapter 5 where the flow near the wellbore is assumed to be an annular-mist flow in perforations.

Secondly, chapter 6 details a comprehensive approach in developing a general and simple yet efficient relative permeability correlation for gas condensate systems at near wellbore conditions. This approach concentrates on the micro-picture of the dependence of relative permeability on capillary number so that the investigation is performed at constant phase saturation. This resulted in two gas-condensate relative permeability expressions as a function of capillary number ratio (N_{cb} / N_c). The investigation is then reconciled with some literature data to come up with the final form for the gas condensate relative permeability correlation with N_{cb} / N_c.

Finally, the aforementioned relative permeability expressions are combined with the Forchheimer equation to further modify the gas condensate relative permeability to account for the Forchheimer (Inertia) effects. The resultant expressions have been incorporated into the Eclipse 300 compositional simulator and used in a comprehensive study to determine the impact of rate and IFT (N_c-effect) and Forchheimer effects on well productivity as detailed in chapter 7.

Chapter 8 summarises the conclusions reached in this work and provides the recommendations for further work.

CHAPTER 2
GAS CONDENSATE RESERVOIRS

2.1 INTRODUCTION

Developing and operating gas-condensate reservoirs for optimum flow capacity is different from oil or dry gas reservoirs. The difference lies in the fact that condensate liquid accumulation occurs near wellbore when the pressure falls below the dew-point pressure of the reservoir fluids[1]. This phenomenon complicates the prediction of phase saturation and pressure distributions in the reservoir, especially near producing wells, and total fluid production rate as a function of the BHP. Therefore, thorough understanding of gas-condensate fluid and flow properties together with proper consideration of other aspects of a reservoir such as economics, rock properties and geological conditions is vital for optimising formation flow capacity.

Accurate fluid characterisation is very important before setting production development of a gas condensate reservoir. The identification of the type of fluid in a gas condensate reservoir is determined by laboratory experiments. These usually take time to conduct and analyse, therefore, initial classification, as a rule of thump, is based on the producing gas-oil ratio (GOR), API gravity, and colour of the produced liquids[2]. Experimental laboratory determination requires reliable estimates of reservoir temperature (from well-log runs), initial pressure (from repeat-formation or drillstem tests) and representative fluid samples.

The initial reservoir pressure of a retrograde gas condensate reservoir is usually above the saturation (dew-point) pressure; therefore, the fluid is a single phase gas. As the reservoir pressure declines, liquid starts condensing in the reservoir and in surface separation equipment. There are two main challenges associated with optimising recoveries from a gas condensate reservoir. The first is to obtain maximum liquid yield from the gas produced at the surface, and the second is to economically minimise the loss of liquids by retrograde condensation in the reservoir[3].

Condensate distribution throughout the pore spaces coupled with relatively low interfacial tension (IFT) values between the hydrocarbon phases compared to gas-oil systems are responsible for the non-conventional flow behaviour associated with gas-condensate systems. Capillary forces play a major role in defining the multi-phase flow for the high IFT gas-oil systems. However, this is not the case for low IFT gas condensate systems where capillary forces are much less important in comparison with the role played by viscous forces (near the wellbore) and gravity forces (in reservoir bulk).

The existence of two phases (gas and condensate) in the pore spaces reduces the formation flow capacity to the gas phase significantly below its original flow capacity to single phase gas flow. Therefore, the phenomena of relative permeability and condensate blocking play a significant role in controlling well productivity. In recent years, a greater awareness of the impact of the condensate formation (drop-out) on the ultimate hydrocarbon recovery and well deliverability has been achieved. However, the complete impact of such a phenomenon is far from being fully understood.

2.2 PHASE BEHAVIOUR

As far as reservoir conditions are concerned, Fig. 2.1 shows a schematic pressure/temperature diagram for a multi-component hydrocarbon system (typically known as the phase behaviour diagram or PVT diagram). The two-phase region in the diagram is defined by the bubble point line, critical point, and the dew point line and divided into constant liquid fraction lines. When initial reservoir pressure is above the cricondenbar; when the reservoir temperature is below the critical temperature the system is referred to as a bubble-point system. When the reservoir temperature is between the critical temperature and the cricondentherm the system is referred to as a gas-condensate system.

Two characteristics separate a gas condensate system from the other fluid types: the condensation of liquid at reservoir conditions during an isothermal depletion and the retrograde (re-vaporisation) nature of such a condensation[2]. To illustrate this retrograde behaviour, consider a reservoir temperature (typically higher than critical temperature and lower than the cricondentherm) with initial pressure at P_1 (typically above the cricondenbar in the single phase gaseous state). As soon as the isothermal depletion reaches the saturation pressure at P_2 the liquid fraction starts to increase from 0% until it reaches a maximum liquid drop out of, in this example about 7%, at P_3 then it starts decreasing to 4% at abandonment pressure represented here by P_4. Theoretically, as suggested by such a diagram, if such a depletion continues one would expect a complete re-vaporisation of the liquid phase at significantly low pressures. However, the real situation is different[5] and such a re-vaporisation will be limited by other factors such as the high pressure condensation of liquid is greater than the low pressure re-vaporisation, lighter fluid components will tend to re-vaporise leaving the heavier ones causing appreciable loss of valuable liquid constituents, and liquid surface tension will tend to retain the condensate in liquid phase.

Initial reservoir pressure for gas condensate reservoirs is typically in the range of 3000 to 15000 psia[7] with reservoir temperatures in the range of 200 to 400 °F. Such a wide range of temperature and pressure gives gas condensate a great variety of physical conditions at which they may exist. Gas condensate produced fluids can be recognised by their light colour or colourless at stock tank conditions with an API gravity of greater than 45° and producing CGR something higher than 300 STB/MMscf, as reported for the Headlee Devonion field in West Texas[6]. They are also recognised by much lower heptanes and heavier components than those observed for crude oil systems.

2.3 THE CONDENSATION MECHANISM

A significant contribution to the understanding of the process of retrograde condensation in gas condensate reservoirs was offered by the micro-model visual studies performed at the Petroleum Engineering Department of Heriot-Watt University[32]. The work involved the use of high pressure glass micro-models to investigate the flow mechanism of gas condensate fluids at simulated reservoir conditions.

The micro- model consists of two plates. A model pore structure is etched on the inside of one plate and the inlet and outlet is etched on the other before joining them to create a single-unit glass micro-model. The glass micro-model can be oriented either horizontally or vertically to simulate a specific process. The highly pressurised gas condensate fluid can be injected into the glass micro-model at rates as low as 0.01 cc/hr. Both real gas condensate fluid systems (as obtained from North Sea gas condensate reservoirs) and synthetic ones[28-32] were used to observe the retrograde condensation in horizontally and vertically oriented glass micro-models.

Depletion tests were simulated on horizontally oriented micro-models. Condensate liquid was observed to form in all highly curved surfaces with connate water such as pore throats and other water bridges[31]. Isolated grains that are not bridged by water were observed not to accumulate condensate liquid. Further increase of condensate continues to fill all the available pore space that is bridged by water in scattered locations in the micro-model.

Contrary to the discontinuity suggested by the scattered nature of the condensate liquid formation in the micro-model, the condensed liquid was found to be in communication through thin films spreading on water and consequently separating the gas phase from the water phase.

The depletion tests conducted on vertically oriented micro-models revealed a completely different picture of condensate liquid formation[31] than the horizontally oriented tests. The effect of gravitational forces was clearly observed particularly at low IFT condition (around 14.5 to 29 psia below the dew point pressure). At these conditions condensate liquids mainly accumulate as dish-type cavities at the upper side of grains and as a thick curved layer hanging at the lower side of grains held by IFT forces. The isolated grains also accumulated condensate at their lowest surfaces that later drained to the lower parts of the model[31]. As IFT increased, following consequent depletion, more condensate retained in the pores; hence, capillary domination of the flow mechanism is evident. Eventually condensate liquid formed permanent bridges and filled all the pore space that is not occupied by connate water[31]. Whereupon the drainage process reverted to the conventional thin-film flow in a similar manner observed in the aforementioned horizontal depletion tests.

The balance between capillary forces (IFT) and gravitational forces (density contrast) together with nature of the porous medium (permeability) will determine the point of cross-over between the two flow mechanisms. A dimensionless group known as the Bond Number, N_B, (Eq. 2.1) is used to give some indication of such a cross-over point. Gravitational forces are considered significant at a value of greater or equal to E-5. Capillarity dominates the flow at low N_B values where IFT is significantly high.

$$N_B = \frac{\Delta\rho\, g\, k}{\sigma} \qquad \text{...(2.1)}$$

The effect of connate water saturation manifests itself through two functions: (1) Connate water fills the tighter pores reducing condensate trapping. (2) Connate water coats the grains providing lubrication for the flow of condensate at low capillary forces. Therefore, the presence of connate water helps mobilises the condensed liquid at much lower condensate saturation. In the above micro-model work[31] also a third manifestation of the effect of connate water on condensate flow was observed. It forms dead-end pores blocking the passage way for the condensate liquid to flow. Hence, both the magnitude and the distribution of connate water are important for the flow of gas condensate fluids.

2.4 SAMPLING AND WELL TESTING

To have accurate experimental data that describe the actual fluids in place a representative fluid sample must be collected. The sample must have the same composition as the initial composition of the reservoir fluids; therefore, such a sample must be collected early when the reservoir conditions are close to initial reservoir conditions (i.e. flowing BHP must be above, or close to, the dew-point pressure with high production rate to ensure that no liquid hold-up occurs in any part of the production string or surface lines)[2]. This sample is equivalent to a sample obtained by combining high pressure separator vapour and liquid phase at the measured GOR. This ideal case is compromised by the fact that most wells must be flowed for cleanup before the produced stream consists solely of reservoir fluids and many gas condensate reservoirs are discovered near their dew point pressure. Hence, the often preferred method for obtaining a representative fluid sample is to recombine surface separator gas and liquid samples collected at low and stable rates[2]. However, a successful sampling program must consider well conditioning before sampling, choice of collection site, collection mechanics, and quality control checks[2].

Well tests are performed on gas condensate wells for a number of reasons including obtaining a representative fluid sample, and to determine formation and well characteristics. These tests include drillstem tests, build-up, and draw down tests.

2.5 EXPERIMENTAL INVESTIGATIONS

Experimental investigations are vital in predicting the behaviour of the transformation that gas condensate reservoirs undergo during their productive life. The experiments are performed to measure important properties such as saturation pressure and compositional, viscosity, and liquid drop-out changes with depleting reservoir pressure. These tests are performed in a pressure/volume/temperature (PVT) cell at reservoir temperature. Constant composition expansion (CCE) test is usually performed to measure saturation (dew-point) pressure. In this test the fluid composition is maintained while pressure is lowered (at stages) by expanding the volume of the cell until the first drop of condensate is observed to form. This pressure value is recorded and recognised as a dew-point pressure. Above the dew point pressure the information commonly reported is the initial composition of the total fluid and the gas-deviation factor (Z-factor) as a function of pressure. The composition is reported to the C_{40+} fraction when a tuned equation of state (EOS) description is planned. Constant volume depletion (CVD) test is performed to measure liquid drop-out, viscosity and other properties at different pressure stages in an attempt to mimic the depletion process of a gas-condensate reservoir. In this test the volume is maintained constant while pressure is lowered by removing gas at a constant rate and replacing it with mercury at every stage of the depletion process at which measurements of the properties are measured.

Experimental measurements are not always possible to satisfy the requirement for all the range of reservoir engineering calculations; also they are expensive and time consuming. Therefore, cubic EOS models such as Ping-Robinson (1976)[8], Soave-Redlich-Kwong (1972)[9], Zudkevitch-Joffe-Redleich-Kwong (1970)[10] and Patel-Teja (1982)[11] are substituted to fill in the gap and sometimes to be a useful, reliable, and much less expensive alternative to experimental measurements. Few experimental measurements (i.e. liquid viscosity or liquid drop-out curve) are customary used to tune equation of state to accurately predict the behaviour of gas-condensate system at other not measurable field conditions. Fig. 2.2 shows an experimental and predicted liquid drop-out curve for a gas condensate system using the Ping-Robinson EOS. The tuned EOS model is then used in performing simulation studies; hence, reducing uncertainties in developing production strategies to exploit hydrocarbon from gas condensate reservoirs.

2.6 PRODUCTION METHODS

Gas condensate reservoirs are produced by three different methods. The appropriate production method is usually based on an economic feasibility study that is conducted by integrating the available geological and engineering information on the reservoir with the prevailing economic conditions (mainly gas prices). The three production methods are pressure depletion, pressure maintenance by dry gas recycling, and pressure maintenance by water injection[12,13]. Pressure depletion method corresponds to primary recovery and it is analogous to CVD experiment conducted in the laboratory; hence, the recovery factor can be approximated from CVD test results. The main assumption in this method is that the condensed liquid never reaches the critical condensate saturation (CCS) to enable flow. Hence, it is considered unrecoverable. This assumption is practically valid for lean gas condensate reservoirs away from the wellbore. However, it cannot be applied to rich gas condensate systems where liquid saturation may reach a high enough saturation level to mobilise to producing wells. Hence, the importance of measuring gas and liquid relative permeabilities becomes evident for any production forecast using simulator and analytical models[4,12,13].

Produced gas is injected back into the reservoir in what is known as pressure maintenance by gas cycling. Gas is cycled to maintain pressure high to keep the amount of retrograde condensation at minimum. In addition, dry gas is miscible with virtually all reservoir gas condensate systems that makes it the primary choice for cycling. Gas cycling also has other two economically driven advantages; it provides an economically viable use for gas when the gas market is sluggish and the means to produce valuable liquid from gas condensate reservoirs. However, the attractiveness of gas cycling projects is controlled by many other factors such as product prices, the cost of processing and compression, liquid contents of reservoir gas, and the degree of reservoir heterogeneity where both vertical and lateral permeability variations can have marked impact on recoveries by cycling. The impact of gas cycling on other valuable hydrocarbon phases in the reservoir must be also carefully assessed (i.e. impact on oil phase when the gas condensate is situated above it as a gas-cap) before commissioning the scheme[12,13].

Water is also injected into gas condensate reservoir to improve production in deep and high pressure reservoirs. Because dry gas compression and re-injection are expensive for deep high reservoirs, particularly in offshore development, water is used for injection; this production method is known as pressure maintenance by water injection. The purpose of water injection is the same as that for gas cycling, however, the uncertainty associated with trapped gas saturation at high pressure and the effect of pore geometry on recovery must be clearly identified before high pressure water injection is commenced. Furthermore, to minimise the loss of liquid in the formation through retrograde condensation the water drive must provide sufficient support for pressure maintenance. Also water breakthrough is strongly affected by permeability distribution; hence, reservoirs with large permeability contrast between different parts of the reservoir are prone to have an early breakthrough during water injection[12,13].

2.7 GRAVITY DRAINAGE

Gravity drainage may play a role in liquid recovery from high permeable unfractured gas condensate reservoirs. The logic behind this phenomenon is that liquid accumulated at various parts of the reservoir will drain down to the bottom of the reservoir given the low IFT (hence low Pc) and low critical condensate. This liquid can be eventually produced by completing the wells at the appropriate lower part of the pay zone. The production of liquid from a fractured tight reservoir can also be influenced, to a lower extent, by gravity drainage; however, the process is much more complex than it appears initially[14].

2.8 WELL DELIVERABILITY

Production rate from wells is affected by several natural variables such as reservoir pressure and permeability, PVT properties, and time; it is also influenced by other production induced variables such as turbulence (non-Darcy flow, mechanical skin, and capillary pressure), multi-phase flow (relative permeability), and formation impairment (skin). All the above variables are related together in a functional form to define the rate-equation or what is commonly referred to as the well deliverability equation. Each variable manifests its control on production rate in a unique and well-quantified manner; however, the interaction between such variable to accurately define the well-deliverability equation for a specific gas condensate reservoir is not so well understood. While some workers tried to redefine and further enhance the understanding of the role of each variable, the overall picture is far from completely realised. Condensate blockage and losses of condensate by retrograde condensation are still unsolved significant problems.

Well deliverability is defined in two ways: wellhead deliverability and wellbore deliverability. The former definition of well deliverability is the most common one and it accounts for all the sources of pressure loss from the reservoir to surface separators (reservoir bulk, wellbore vicinity, tubing, flow lines); the latter definition is used mainly in reservoir simulation studies and it considers the sources of pressure loss in the reservoir and well skin only.

The type of reservoir ultimately defines the contribution of each source of pressure loss to the total pressure with reservoir permeability playing the major role. In tight gas condensate reservoirs (with permeability < 50 mD) the reduction in both wellbore and wellhead deliverabilities due to reservoir sources such as condensate blockage can be significant. On the other hand, in higher permeability reservoirs (>200 mD) the reduction of wellbore deliverability due to reservoir sources such as condensate blockage can still be significant, yet the reduction in wellhead deliverability due to the same source of pressure loss is negligible because tubing pressure losses are dominant[3].

Three fundamental factors influence the effect of condensate blockage on wellbore deliverability. They are relative permeability, PVT properties, and production mechanism (constant rate or constant BHFP). The effect of condensate blockage is only relevant when BHFP is below the dew-point pressure and the well is on the decline. Relative permeability is stated here as a major controlling factor of the influence of condensate blockage on wellbore deliverability; however, this might be true for simulation purposes where relative permeability is used as an input parameter, but in reality relative permeability near the wellbore can represent condensate blockage and the vice versa.

Condensate blockage was addressed by Muskat[15], Fetkovich[16], Kniazeff and Naville[17], Eilerts et al.[18,19] and Gondouin et al[20]. Also, various functional formulations of well deliverability as functions of the aforementioned constraining variables were provided since the 1967 where O'Dell and Miller[6] presented the first gas rate equation using pseudopressure function to describe the effect of condensate blockage. These efforts were followed by the work of Fussell[21], Coats[22], Hinchman and Barree[23], van de Leemput et al.[24], Alonso and Nectoux[27], Jones and Raghavan[26], and recently the work of Fevang and Whitson[3,25]. The works of the above investigators have emphasised the importance of condensate blockage, gravity drainage, non-Darcy flow, PVT properties and relative permeability in constraining well deliverability.

Since, the objective of this research program is to define gas condensate relative permeability near producing wells a detailed literature review on the concept of relative permeability with specific interest on gas condensate fluids together with the latest findings on the subject is revealed in the next chapter.

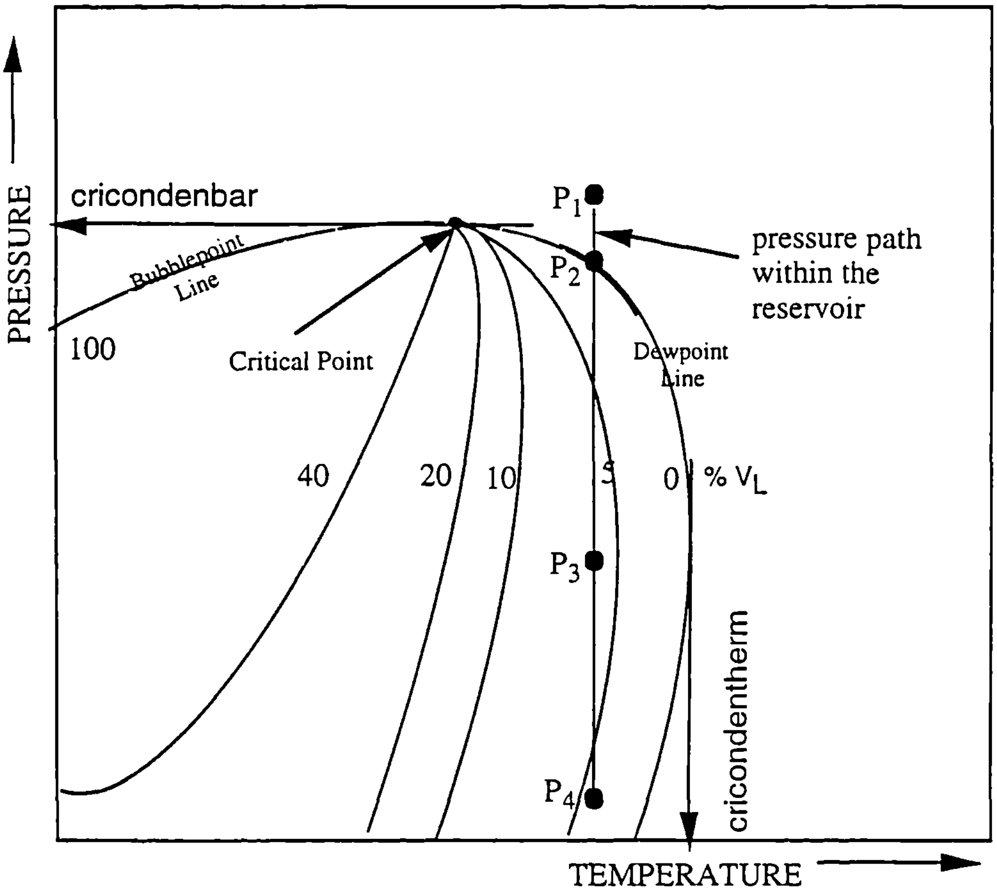

Figure 2.1: A Qualitative Pressure / Temperature Diagram Used For The Classification of Hydrocarbon Systems

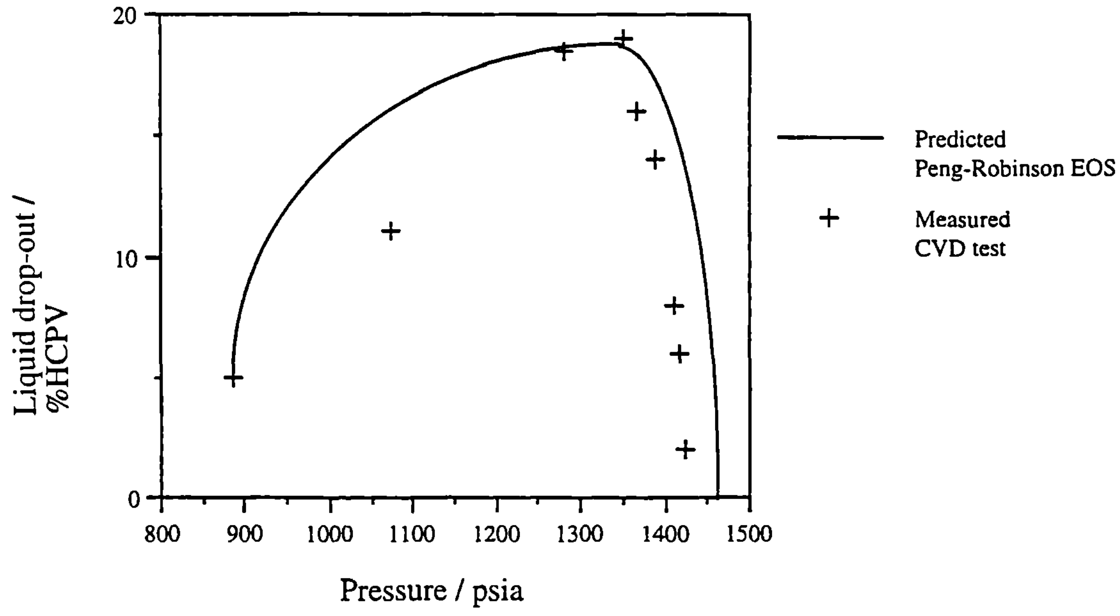

Fiqure 2.2: Liquid drop-out curve at 120^{o}C for binary gas-condensate system

CHAPTER 3

RELATIVE PERMEABILITY

3.1 INTRODUCTION

The dynamic nature of this research work requires a constant literature review effort to keep-up with the latest advances in the area of relative permeability of gas-condensate over the research period. However, it is essential to conduct a general introductory literature review of the relative permeability of gas-condensate with emphasis on the difference between it and the customary gas-oil or water-oil relative permeability. Therefore, the purpose of this literature review is to establish the foundation for reported knowledge on the relative permeability of gas-condensate flowing in porous media and related topics.

3.2 TWO-PHASE RELATIVE PERMEABILITY

The absolute permeability, as defined by Darcy's flow equation, the empirical equation that is widely used to describe laminar fluid flow in porous media, is the proportionality constant that relates the macroscopic velocity (flux) of a fluid with known viscosity to the associated pressure drop. Hence, it is a measure of the porous media ability to conduct flow and it is a function of the geometry of the pore network. For multi-phase flow in porous media the concept of effective permeability has been developed to describe the flow of one fluid in the presence of another. The sum of two effective permeabilities defined for two phases flowing in a porous media is not necessarily equal to the absolute permeability because of flow interference between the two fluids. Multi-phase fluid flow in porous media is also described by relative permeability that is simply the ratio of the phase effective permeability to absolute permeability. Relative permeability is dependent on fluid properties, viscosity, wettability, interstitial fluid distributions and saturation history. Relative permeability dependence on the interstitial fluid distribution and saturation history, explain the so called hysteresis effect. Hysteresis effect is a term that describes the possible difference in relative permeability versus saturation values obtained by drainage (reducing wetting phase saturation) and those obtained by imbibition (increasing wetting phase saturation). Relative permeability data are very essential to enable the estimation of productivity, injectivity, and ultimate recovery from a hydrocarbon reservoir.

3.2.1 Relative Permeability Measurements

Two methods are used to measure relative permeability in the laboratory: Steady-state and unsteady-state methods[33]. In the steady-state method the fluids, at a certain ratio, are injected simultaneously at constant rate or pressure until equilibrium (fluid ratio of influent = fluid ratio of effluent) is attained; then saturation, flow rate and pressure drop are measured. For different ratios of the injected phases, different saturation levels are created and the process is repeated for every saturation level. The steady-state method gives more applicable and reliable relative permeability measurement and the calculation scheme is based on Darcy's law, but it is more time-consuming because it could take several hours or days to reach the equilibrium at each saturation level. The steady-state equilibrium concept is the basis for the following commercially known steady-sate methods: Hassler method, single-sample dynamic, stationary phase, Penn State, and modified Penn State[33]. These methods differ only in the approach used in establishing capillary equilibrium between the fluids and in reducing end effects (error introduced in the measurements by possible higher saturation and high pressure drop at the end of the core sample).

The unsteady-state method involves the displacement of in-situ fluids by constant rate or constant pressure injection of a driving fluid while monitoring the effluent volume continuously. The unsteady-state method contains many uncertainties in the pertaining calculation schemes, and that capillary equilibrium does not prevail sometimes prevents the manifestation of the role of wettability, but this method takes only few hours to generate relative permeability curves making it more attractive than the steady-state method.

3.2.2 Relative Permeability Calculations

Depending on the method used to measure the relative permeability in the laboratory the corresponding set of relative permeability versus saturation can be calculated. For the steady-state method relative permeability curves are generated by applying Darcy's law to the measured saturation, flow rate and pressure drop at every saturation level to calculate the corresponding effective permeability of each phase.

The unsteady-state method production data is analysed using various mathematical methods. The Buckley-Leverret[34] theory for linear displacement of immiscible and incompressible fluids is the basis of analysis for all the mathematical methods. The Welge[36], Johnson-Bossler-Neumann (JBN)[35], Jones-Roszelle[37], and Bardon-Longeron[42] methods are the most widely used mathematical methods. Welge[36] has extended the Buckley-Leverret theory and used it to calculate the relative permeability ratios. It assumes a linear sand section and a constant pressure with respect to position and time; hence, negligible changes in density, solubility, and reservoir volume factor are expected. Johnson, Bossler, and Neumann[34] have extended the Welge technique to create a method (the JBN) to calculate individual relative permeability rather than relative permeability ratios, as done by Welge. To simulate immiscible and incompressible fluid flow they assumed constant flow velocity at all cross sections of the linear porous body. Furthermore, they introduced large pressure gradient enough to minimise capillary pressure effects. Both Jones-Roszelle[37], and Bardon and Longeron[42] combined the Welge and JBN methods to create graphical techniques for calculating relative permeability. The following sections detail these two methods.

Jones-Roszelle Method

Jones-Roszelle[37] Method is applicable for constant rate, constant pressure, or variable pressure displacement where overall material balance is used to determine average saturation in the core. Relative permeability is calculated from the saturation history at the outlet of the core where the fractional flow at this point is conveniently equal to produced oil or water. The point value of the pressure gradient per unit injection rate instead of average value is used in the calculation.

When gravity and capillary pressure effects are ignored, the relative permeabilities for oil and water can be expressed as follow:

$$k_{rw} = \frac{\mu_w f_{w2}}{\mu_{e2}} \qquad \text{...(3.1)}$$

$$k_{ro} = \frac{\mu_o f_{o2}}{\mu_{e2}} \qquad \text{...(3.2)}$$

where 2 refers to the outlet end of the core, and

f_w and f_o = water and oil fractional flow, respectively.

μ_w and μ_o = water and oil viscosities, respectively.

μ_e = effective viscosity = $\frac{kA}{q}\left(-\frac{dP}{dl}\right) = \left(\frac{k_{ro}}{\mu_o} + \frac{k_{rw}}{\mu_w}\right)^{-1}$

q = total liquid flow rate

This method simply involves the calculations of both the fractional flow values for each phase (f_w and f_o) and the effective viscosity (μ_e) at the outlet end of the core, at any point during the core flood (at a specific saturation value), and then calculating the corresponding relative permeability for each phase. The graphical analysis for this method can be divided into two parts.

Part A: Fractional flow calculations where the following data are used: initial water saturation (S_{wi}), cumulative volume of oil produced (N_{PO}) and commutative water injected (w_i) versus time, and total core pore volume (PV).

Step 1: Non-dimensionalise the data by dividing by PV and calculating average saturation at the outlet:

$$Q_i = w_i / PV \qquad ...(3.3)$$

$$S_{wavg} = S_{wi} + \frac{N_{PO}}{PV} \qquad ...(3.4)$$

Step 2: Plot average saturation Eq. (3.4) versus pore volume injected Eq. (3.3) and calculate the saturation at the outlet by graphically measuring the slope of the curve $(\frac{d(S_{wavg})}{d(Q_i)})$ at any value of pore volume injected and using the following equation:

$$S_{w2} = S_{wavg} + Q_i(\frac{d(S_{wavg})}{d(Q_i)}) \qquad ...(3.5)$$

Step 3: Calculate the fractional flow of both water and oil at the outlet of the core for any time during the flood using the following equations:

$$f_{o2} = \frac{(S_{wavg} - S_{w2})}{Q_i} \qquad ...(3.6)$$

$$f_{w2} = 1 - f_{o2} \qquad ...(3.7)$$

Par B: Effective viscosity calculations; where the following information is used: pressure drop(ΔP) and pore volume injected(Q_i) versus time and the corresponding flow rate (q) together with the pressure drop (ΔP_b) for flow of a fluid with a known viscosity (μ_b) through the core at a certain rate (q_b).

Step 1: For every saturation value at the outlet, the effective average viscosity (μ_{eavg}) of the fluids can be calculated at any point during the flood using the following equation:

$$\mu_{eavg} = \mu_b \left(\frac{(\Delta P / q)}{(\Delta P_b / q_b)} \right) \qquad \text{...(3.8)}$$

Where subscript b denotes the base single-fluid flow of fluid of known viscosity μ_b.

Step 2: The average effective fluid viscosity (μ_{eavg}) versus total pore volume injected (Q_i) can be plotted and the slope $(\frac{d\mu_{eavg}}{dQ_i})$ at any value of Q_i can be graphically determined as was done for average saturation that was described in part A.

Step 3: The average effective viscosity at the outlet now can be calculated using the following equation:

$$\mu_{e2} = \mu_{eavg} - Q_i \left(\frac{d\mu_{eavg}}{dQ_i} \right) \qquad \text{...(3.9)}$$

Bardon-Longeron Method

Bardon and Longeron[42] used Jones-Roszelle[37] technique to calculate relative permeability assuming linear porous medium and constant pressure or constant rate injection. Similar to Jones-Roszelle they also did not incorporate the effect of gravity or capillary pressure into their model. For a core that is initially saturated with 100% of liquid, the vapour saturation at the outlet can be expressed by:

$$S_v = \frac{100}{PV} \Delta V_L^* \qquad \text{...(3.10)}$$

where,

$$\Delta V_L^* = V_L - t\left(\frac{dV_L}{dt} \right) \qquad \text{...(3.11)}$$

So the relative permeability values that correspond to the above saturation are:

$$k_{rv} = f_v(\frac{\Delta P_v}{\Delta P^*}) \quad ...(3.12)$$

and $$k_{rL} = f_L(\frac{\Delta P_L}{\Delta P^*}) \quad ...(3.13)$$

where,

$$\Delta P_v = \frac{\mu_v q L}{Ak} \quad ...(3.14)$$

$$\Delta P_L = \frac{\mu_L q L}{Ak} \quad ...(3.15)$$

f_L = fractional flow of liquid = $\frac{dV_L}{dV_{inj}}$

f_V= fractional flow of Vapour = 1- f_L

$$\Delta P^* = \Delta P - t(\frac{d(\Delta P)}{dt}) \quad ...(3.16)$$

ΔP_v or ΔP_L are calculated assuming only one phase flow at the rate of the experiment; and ΔP is the pressure drop across the core sample during the experiment. For this graphical technique three different steps can be recognised:

Step 1: Plot production data: V_L versus pore volume injected and ΔP versus pore volume injected.

Step 2: Determine the values of ΔV_L^* from the slope of the tangent of the first curve at any point in time and Eq.(3.11); and the values of ΔP^* from the slope of the tangent of the second curve at any point during the flood and Eq.(3.16).

Step 3: Using Eq.(3.10), calculate the vapour saturation and the rest of the above equations to calculate the relative permeabilites.

3.3 GAS-CONDENSATE RELATIVE PERMEABILITY

Saeidi and Handy[38] found lower gas to oil relative permeability for gas-condensate systems than that of bubble-point systems by investigating phase and flow behaviour of Methane-Propane binary mixtures. Furthermore, their relative permeability measurements indicated lower critical liquid saturation for gas-condensate system as compared to bubble point systems; and their observation indicated no evidence of condensate mobility during depletion experiments.

Depletion experiments[38,29,31,27,43] are unsteady-state experiments. The core is initially saturated with the selected gas-condensate system at a pressure above the dew point. Gradual condensate formation in the pores is achieved by reducing the pressure through a back-pressure valve. To calculate liquid drop-out, a phase behaviour model is used together with measured effluent gas composition, which can be used to determine condensate saturation in the core. The relative permeability is calculated in a method similar to unsteady-state experiments.

Relative permeability of gas-condensate at low IFT values was studied by Asar and Handy[39] using highly volatile Methane-Propane mixtures. They demonstrated that low IFT causes low residual liquid saturation and increased flow rates. Furthermore, they observed that as IFT value approaches zero, the curvature of the gas-condensate relative permeability curves becomes less pronounced and the irreducible gas and oil saturation approached also zero. Gravity effects for the horizontally oriented experiments were assumed to be negligible and experiments were conducted without interstitial water that may affect the flow of condensate. Haniff and Ali[39] also used the same binary mixtures to study gas-condensate relative permeability at low IFT. They observed, what they termed, a critical IFT value due to phase distribution. Below this value, capillary forces are negligible and condensate establishes a complete wetting condition where condensate assumes film flow and results in low residual liquid saturation. Above the aforementioned critical value of IFT, flow is capillary controlled causing high residual liquid saturation.

A ternary mixture was used by Gravier et al.[41] in an experimental study to determine gas-condensate relative permeability and critical condensate saturation. They noted the high critical condensate saturation for this gas-condensate system; and the higher rate of reduction in gas relative permeability as condensate saturation increased as compared to that of gas-oil systems.

Bardon and Longeron[42] studied, in a series of displacement experiments, the aspects of relative permeability of various binary hydrocarbon systems. They found that both relative permeability and residual oil saturation obtained by unsteady-state displacement tests are strongly affected by IFT, especially at IFT of lower than 0.04 mN/m.

Khazam[4] pointed out that although many of the conclusions stated by the above authors are important in understanding the flow behaviour of gas-condensate, they do not always take full account of the factors influencing their results. For instance, the effects of gravitational and viscous forces, continuous mass transfer between the phases, liquid and gas phase-distribution and the effect of interstitial water and rock characteristics make the gas-condensate relative permeability to be more complicated than gas-oil systems.

Many answers on the formation and flow of gas-condensate were provided by Danesh et al.[28,29,30,31] where depletion experiments on horizontally and vertically mounted cores and micro-models were conducted. The formation of condensate in the reservoir was found to form by the process of film formation; and hydraulic continuity being maintained throughout the pores. This film flow together with low values of gas-condensate IFT were found to significantly enhance the role of gravity drainage on gas-condensate flow in the reservoir. Furthermore, the presence of interstitial water was found to greatly influence the growth and flow of condensate in the pores.

To evaluate the critical condensate saturation and determine the effect of connate water saturation on the condensate mobility, Danesh at al.[31] conducted a number of experiments on water-wet Clashach and Berea cores. The critical condensate saturation was found to decrease with increasing connate water saturation. This is attributed to the presence of connate water in the tighter capillary pores leaving fewer sites for condensate to accumulate. This observation agrees with micro-model studies.

The most interesting part about gas-condensate flow behaviour was found in the experimental work performed on gas-condensate systems as part of a GCR Project[44,45]. In this work a binary mixture that consists of 76% Methane and 24% normal-Butane was used in conducting horizontal core displacement tests to simulate gas-condensate flow near the wellbore. A 61 cm long homogeneous Berea sandstone core with 18.2% porosity, 92 mD permeability and 26.4% irreducible water saturation was used in this study. It was found that at high capillary number (E-5 to E-3) and low IFT (0.12 mN/m) where capillary forces are negligible and flow is dominated by viscous forces, both the gas and the condensate relative permeabilities increase with increasing flow rate. This relative permeability rate dependence was found to be more pronounced at high condensate saturation than at low ones. At high condensate saturation, the condensate relative permeability was found to double between the flow rate of 100 cc/hr and 800 cc/hr (0.61 and 4.88 HCPV/hr). Furthermore, gas and condensate in a gas-condensate system were observed to flow as slugs of both fluids in the same channels. The flow can be represented by intermittent gas and condensate flow in pipes where the two phases are not completely segregated as in Darcy flow and not fully mixed as in single flow. This hydrodynamic dependence is known as fluid coupling.

In a related simulation work reported by Khazam[4] on the same core using 5-component synthetic fluid at flow rate of 10 cc/hr have shown that at a high IFT value of 0.4 mN/m capillary pressure has no effect on relative permeability measured from the horizontal core tests; and at low IFT value of 0.05 mN/m gravity segregation effects on relative permeability measured from horizontal displacements are minimal at flow rates in access of 100 cc/hr (0.65 HCPV/hr).

It is evident from the above cited recent findings that the gas and condensate relative permeabilities are indeed functions of fluid properties, viscosity, wettability and saturation history that gas-condensate flow behaviour differs from that of gas-oil systems. Indeed, the flow behaviour of gas-condensate system is even more complicated than that of gas-oil systems when acknowledging the rate dependence of gas-condensate relative permeability at low IFT.

3.4 COUPLED FLOW RELATIVE PERMEABILITY

Coupled flow as defined by Dullien[46] is a characteristic of two-fluid flow in porous media at low IFT. At low IFT the assumed network flow of the two fluids begins to break first at large pores followed by smaller pores at even lower IFT values; and slugs of both fluids start travelling in the same pores. Darcy flow equation has been modified to incorporate the coupling flow phenomena for two-phase flow in porous media and reported by a number of authors[47-60]. The coupled flow formulations by those authors were summarised by Dullien[46]. Dullien stated the following relationships to be valid for the coupled two-phase flow in porous media provided that both fluid phases are continuos:

$$u_1 = -\frac{k_{11}}{\mu_1}\Delta P_1 - \frac{k_{12}}{\mu_2}\Delta P_2 \qquad ...(3.17)$$

$$u_2 = -\frac{k_{21}}{\mu_1}\Delta P_1 - \frac{k_{22}}{\mu_2}\Delta P_2 \qquad ...(3.18)$$

Where, kii refers to the apparent relative permeability where the second fluid is considered part of the rock. kij or kji refer to the relative permeability of one phase induced by the pressure-drop in the second phase.

Also Dullien applies the above two equations to a coupled two-phase flow in porous media where one of the two fluids is emulsified in the other. For instance, when fluid 2 is emulsified in fluid 1, fluid 1 becomes the continuos phase and fluid 2 is discontinuous; and the viscosity of the emulsion is that of the continuos fluid 1.

$$u_1 = -\frac{k_{11}}{\mu_1}\Delta P_1 \qquad \text{...(3.19)}$$

$$u_2 = -\frac{k_{21}}{\mu_1}\Delta P_1 \qquad \text{...(3.20)}$$

Most workers agree on the existence of coupled flow phenomena in two-phase flow in porous media. However, they differ in their views on the importance of such a phenomenon. The case of the existence of coupled flow in porous media was built on the concept of momentum exchange across fluid-fluid boundaries. Philip(1972)[53], concluded that the matter of such a momentum exchange, and therefore, coupled flow, is for most practical purposes, a non-problem. His conclusion was based on the fact that surfactants are always present in real systems making fluid interface highly resistant to shear. Whiteker (1986)[53] provided some formulation to quantify the coupled flow phenomena or what he called the non-traditional terms in the equation of motion that describes two-phase flow in porous media. He admitted that the complicity in his formulation presents extremely complex computational problem for theoretical determination of the importance of such non-traditional terms. Rose (1988)[49] and Kalaydjian (1990)[59] provided experimental venues to measure the transport coefficients that appear in the extended Darcy's law Eqs. (3.17) and (3.18). Although their approaches are important in supporting the existence of coupled flow phenomena they do not provide any additional theoretical insight that can explain the rate effect on the gas and condensate relative permeabilities.

The effect of flow rate on relative permeability of gas condensate at low IFT has been experimentally proven, with great confidence, to exist by the recent finding stated earlier in this report. Yet, up to our knowledge, it has not been reported to be theoretically modelled using extensive steady-state experimental data any where in literature.

Recent experimental findings (HWU 1993-94) showed that gas and condensate relative permeabilities in both steady and unsteady-state tests conducted on Berea Sandstone cores are dependent on flow rate especially at low IFT. This rate effect is more pronounced at high condensate saturation values than at low condensate saturation values. Furthermore, from experimental observations of micro-models associated with the above findings, it was concluded that rate effect is a manifestation of the aforementioned coupled flow phenomena. Moreover, since the viscosities of the two phases involved in the experiments (gas phase and condensate phase) are not of equal order of magnitude, the coupled flow phenomenon in this case was most likely caused by fluid distribution rather than momentum exchange between the gas and condensate phases.

Hence, the appropriate approach to take to theoretically quantify the coupled flow phenomenon observed in the flow of gas-condensate systems of low IFT in porous media is to mechanistically model the flow. Such a modelling must incorporate the experimental observations regarding fluid (phase) distribution and come-up with an equivalent velocity profile. The resultant equivalent velocity profile must explain the rate effect and theoretically quantifies the coupled flow phenomena. Alternatively, such rate-effected relative permeability data can be correlated to provide an empirical mean of quantifying such a rate effect.

3.5 HERIOT-WATT EXPERIMENTAL SET-UP[32]

3.5.1 Apparatus

The modified core facility that is currently used at Heriot-Watt University to conduct core displacement experiments to measure relative permeability of gas-condensate systems can be seen in Fig. 3.1[32]. The test fluids are present in piston cells, with water being injected into or withdrawn from the base of the cells by the high pressure twin barrel displacement pumps to circulate the fluids around the flow system. In the high pressure core facility there are two 1-litre gas piston cells, one of which is full of gas and the other empty at the beginning of each steady-state test. Using one of the twin barrels of displacement pumps, gas is displaced through the core from the piston cell initially full of gas to the large 100 cc sight glass at the core outlet, from where gas is recovered from the top of the sight glass to fill the initially empty gas cell by withdrawing water using the second barrel of the pump. A similar procedure is followed for the condensate using the other pump, with the condensate being recovered from the base of the sight glass at the core outlet. The pumps used to circulate the fluids have a resolution of 0.01 cc, with the volumes of fluid displaced into the core being checked independently using linear transducers with a resolution of 0.01 cc. There was no detectable leak rate from the pumps.

To increase the accuracy of the mass balance measurements used to calculate fluid saturation, two small 6 cc sight glasses are located at the outlet of the fluid cells upstream of the core. The sight glass in the gas line is filled with gas and acts as a trap to accumulate any small amounts of condensate that may flow from the gas cell. The sight glass in the condensate line is filled with condensate that will accumulate any gas that may flow from the condensate cell during a test. This ensures that the exact volume of fluid (gas and condensate) injected will indeed flow into the core.

The differential pressure is measured using two quartzdyne quartz crystals high accuracy transducers located at the inlet and outlet of the core. The transducers have been found to be accurate to within 0.01 psi, giving stable differential pressure measurements during the tests.

The absolute pressure of the system can be measured to within 0.01 psi, with the measurements indicating that there is no leak from the flow system.

3.5.2 Core Test Procedures

First the core must be prepared according to the following procedure:

Initially the core samples are weighed and the length/area measurements are taken to estimate the bulk volume. Before the core is loaded into viton rubber sleeve, they are wrapped in two layers of PTFE tape and aluminium foil. This is necessary to prevent the gas condensate mixture attacking the rubber, which has previously occurred and caused the rubber to swell and become permeable to gas. Two end pieces, with low internal volumes, are then attached to either end of the core before it is placed in the rubber sleeve. Once loaded into a core holder, the helium porosity and nitrogen permeability of the core are measured. This is followed by evacuation of the core, after which the core is injected with a 1% brine solution. The amount of brine imbibed into the core is measured and gives a second measurement of pore volume. A 1% sodium chloride/calcium chloride brine solution is used to sensitise any clay minerals and prevent them from swelling and restricting flow. The water permeability is measured, before core characterisation.

Before the connate water saturation being established, tracer analysis of the core is conducted to ensure that there are no problems with the core such as fractures or permeability layers which if not detected may influence the results of the core tests. This procedure also provides an accurate measurement of the pore volume of the core.

Second, connate water saturation must be established in the core according to the following procedure:

Initially a viscous mineral oil with a viscosity of approximately 30 cP is injected into the brine saturated core. After flushing with the oil until the water production is greatly reduced, the viscous oil is displaced by decane over a period of days to ensure that all the mineral oil is removed. Decane is then displaced by the injection of methane, with the effluent from the core being monitored on the gas chromatograph until there is no trace of decane.

Third, gas condensate is introduced and dew point is observed according to the following procedure:
Single phase gas condensate at ~500 psi above the dew point, can then be injected into the core to displace methane. Two HCPV of gas condensate are injected and left for 24 hours, after which further gas condensate injected until the composition from the core matches the original gas mixture from the storage vessel. The single phase gas permeability can now be measured before depletion to the retrograde region.

To further ensure that the gas condensate mixture in the core is of the correct composition, a sample of the produced gas from the core is collected in the sight glass at the core outlet. The sight glass is then isolated from the core, and the pressure is reduced by constant composition expansion to ensure that the dew-point of the fluid and the measured liquid drop-out match the PVT supplied data.

The core is now at a stage when the planned experiment can begin, which starts with the depletion of the core to the dew point of the gas. The depletion is initially controlled through a BPR that is connected to a 200 cc vessel of nitrogen from which the pressure is dropped. The pressure is depleted fairly rapidly at a rate of ~10 psi/minute until 50 psi above the dew point. At this stage the BPR is isolated from the system, and the rate of pressure reduction is decreased to 1 psi/minute by withdrawing water from the sight glass located at the outlet of the core, with the lower level partly filled with water, and the gas condensate mixture occupying the remainder of the volume. When the dew point is reached, a condensate mist can be seen to form resulting in a layer of condensate being deposited on the water surface. At this stage it is necessary to reduce the rate of pressure reduction to ensure equilibrium behaviour of the gas.

Forth, gas-condensate steady-state points are measured according to the following procedure:
Using PVT information, the liquid dropout at any pressure below the dew-point is known, which enables the condensate saturation in the core deposited by condensation during depletion to be calculated. The initial condensate saturation in the core varied from approximately 27 to 32 %, depending on the test pressure.

When establishing steady-state flow, equilibrium gas and condensate are added to the core until steady-state conditions are established (when the fractional flow of gas and condensate from the core outlet are equal to the fractional flow of gas and condensate being injected). Initially, to provide data at lower condensate saturation, the initial fractional flow (CGR, volume condensate/volume gas) used in the tests was 0.005; the lowest practical CGR determined by the specification of the displacement pumps. This reduced the condensate saturation in the core at steady-state conditions to a lower value than that initially established by injection. Subsequent increases in the CGR increased the condensate saturation in the core. At each CGR several steady-state relative permeability points were measured at different gas injection rates. During the test sequence the flow rate was increased in four stages from a minimum total injection rate of 105 cc/hour to a maximum rate of 840 cc/hour, before the rate was reduced in steps back to the initial value. An example of the test sequence can be seen in Table 3.1, where the flow rate is shown as hydrocarbon pore volumes (HCPV)/hour, and superficial pore velocity for gas.

The velocity was initially increased followed by a decrease at the same CGR to investigate rate hysteresis caused by variation in velocity. After the tests were conducted at the CGR of 0.05, the CGR was increased to 0.10 and the sequence of seven tests was repeated. The test sequence was conducted for all CGR's from 0.05 to 0.4.

The effect of compositional variations due to differential pressure on the flow behaviour is not believed to be significant, due to the low rate of condensate re-vaporisation.

Fifth, gas-condensate unsteady-state drainage relative permeability is measured according to the following procedure:
Following the initial condensate saturation being established in the core by condensation, injection of equilibrium gas was occasionally initiated to measure the subsequent recovery of condensate from a core, allowing the unsteady-state drainage relative permeability to be calculated. However, in the case of conventional unsteady-state relative permeability measurements, the core is either initially saturated with 100 % oil or gas before displacement.

3.5.3 Saturation measurement

At the start of each test programme, the gas and condensate saturation dropped in the core were known from PVT data. The initial volumes of gas and condensate in the flow system (fluid storage cells and lines) were repeatedly measured with the core isolated, before the test programme starting. The measured condensate volume was repeatedly measured to within an accuracy 0.5 cc. After the initial steady-state conditions were established, the condensate saturation in the core was then calculated from the change in the total volume of condensate in the system between the beginning and the end of the test. To make this measurement, the core was isolated and the gas and condensate in the cells, lines and sight glasses were re-equilibrated by simultaneously flowing them through a line bypassing the core. After equilibrating the fluids, one of the condensate cells was completely filled with condensate and the other completely emptied, similar to the situation present at the start of the test. The variation in the volume of condensate present in the large sight glass at the core outlet between the start and the end of the test therefore allowed the new condensate saturation in the core to be calculated.

3.6 SATURATION MONITORING

When measuring gas-condensate relative permeability curves, it is important to have accurate phase saturation measurements too, particularly in unsteady-state experiments. At present phase saturation in the core is calculated based on material balance, but would be more accurate if they were measured directly by methods, such as X-ray or γ-ray attenuation scanning, which are successfully employed in gas-oil and water-oil systems. However, before installing an expensive saturation monitoring facility in the laboratory, it is important to demonstrate its applicability.

The possibility of successfully using the X-ray absorption method to measure condensate saturation in gas condensate systems is investigated using phase behaviour modelling, and hypothetical flow simulation experiments generated by the Eclipse compositional simulator. The analysis is first performed on a purely hypothetical bromated mixture to determine its applicability and justify actual PVT experimental measurements; the results are then validated using measured PVT data on a methane/bromated propane mixture. It is especially important to evaluate dynamic errors associated with the changes in phase-saturation during each X-ray reading throughout displacement experiments.

The viability of using X-ray devices to measure phase saturation is determined in terms of expected possible total error in the measured condensate saturation. Assuming that the X-ray device accuracy is similar to those reported for doped gas-oil-water systems, the extra errors to the measured condensate saturation by the accuracy of the PVT-data and the associated errors of the dynamic displacement are quantified.

The viability of using γ-ray attenuation, with reference to the associated dynamic error, is also discussed.

3.6.1 Theory

The X-ray absorption method is based on the measurement of X-rays received at a detector after they are transmitted through a sample[137]. The transmission of the X-ray beam through a porous medium depends on the phase saturation of the fluids, the density of each phase, the absorption coefficients of the phases and the wavelength of the X-ray beam. In the case of gas and condensate systems, with the connate water assumed to be part of the rock, Lambert's Law is written as:

$$-\ell n(I) = \left[\eta_c \rho_c S_c + \eta_g \rho_g \left(1 - S_c\right)\right] \phi L + \eta_r \rho_r (1 - \phi) L \qquad \text{...(3.21)}$$

where I represents the intensity of the X-ray beam count received at the detector, with the condensate and gas absorption coefficients η_c, η_g being dependent on both the X-ray beam wavelength and the components of the system to be analysed.

Also Lambert's Law for a core with only gas phase present can be written as follow:

$$-\ell n(I_g) = \eta_g \rho_g \phi L + \eta_r \rho_r (1 - \phi) L \qquad \text{...(3.22)}$$

Subtracting Eq.(3.22) from Eq.(3.21) yields the equation of the intensity ratio:

$$-\ell n(I / I_g) = \left[\eta_c \rho_c - \eta_g \rho_g\right] S_c \phi L \qquad \text{...(3.23)}$$

and,

$$S_c = \frac{-\ell n(I / I_g)}{\left[\eta_c \rho_c - \eta_g \rho_g\right] \phi L} \qquad \text{...(3.22a)}$$

where,

η	mass absorption coefficient, cm2/g
S	saturation, fraction
I	X-ray beam intensity, counts/s.
ρ	density g/cc
ϕ	porosity, fraction
L	path length of X-ray beam, cm

c (subscript) refers to condensate phase

g (subscript) refers to gas phase

Eq. 3.22 shows that for a given wavelength the product of the absorption coefficient and the density $\eta\rho$ for both condensate and gas must have a good contrast for the saturation of the two phases to be accurately measurable from the relationship between saturation and X-ray absorption. Hence, a suitable dope agent or a dope component would partition itself mostly in one phase to produce the desired contrast between the $\eta\rho$ of the phases present in the system.

Furthermore, the absorption coefficients in Eq.(3.22) are usually assumed to be constant throughout the range of saturation when this equation is applied to black oil systems. In gas condensate systems this assumption is valid only if the experiment is performed at a constant temperature and pressure, with any change in condensate saturation obtained by changing the CGR in the core by injection. However, when the condensate saturation increases by pressure depletion, its composition (and the composition of vapour) changes, as will the absorption coefficients. The adsorption coefficients can be related to saturation through fluid composition (weight fraction) as shown in the following two equations for condensate and gas phases:

$$\eta_c = \sum_{i=1}^{n}\left(WF_{ci} * \eta_i\right) \qquad ...(3.24)$$

$$\eta_g = \sum_{i=1}^{n}\left(WF_{gi} * \eta_i\right) \qquad ...(3.25)$$

Here the absorption coefficient η_i for each component i is assumed to be known and constant. The weight fraction of the components in condensate, even those of the tracers, are assumed to be calculable (with acceptable accuracy) by phase behaviour models.

3.6.2 The Gas-Condensate Mixture

The doped gas-condensate mixture must have very good contrast in the product of densities and absorption coefficients $\eta\rho$ between the two phases for the Lambert's absorption method to work. Also, for experimental consideration, the mixture must form a retrograde behaviour at temperature around 40 ^oC to eliminate the need for a high-temperature experimental environment. A binary fluid, instead of a multi-component mixture, is believed to increase the accuracy of the data, as the properties of the two phases will be dependent only on the system pressure and temperature.

A binary methane/bromopropane (C_3H_7Br) mixture is therefore chosen for this analysis. PVT experimental tests are performed on a single-phase (gas) mixture (76.4% methane, 23.6% Bromopropane) at 37 ^oC. The liquid drop-out curve shown in Fig. 3.2 plots the high liquid drop-out of this mixture (47% at 4520 psia). Phase densities, phase viscosities, mass fractions of each phase, and interfacial tension (IFT) are measured at two different pressures, of 4500 psia (25 psia below the dew point) and at 3000 psia, as shown in Table 3.2.

3.6.3 Static Error

At a given pressure the error in phase saturation as determined by Lambert's Law (Eq. 3.23) can be static or dynamic. Static error is the combined effect of possible measurement error in phase densities (ρ_c, ρ_g), and errors in phase attenuation coefficients (η_c, η_g), both referred hereafter as PVT-errors. Errors are also possible from the X-ray device intensity ratio (I/I_g) reading due to the accuracy limitations of the device, referred to hereafter as intensity ratio (I/I_g)-errors. In gas-oil systems densities and attenuation coefficients for all the phases are assumed constant during the experiment and only measured once. Consequently this source of the static error does not exist in such tests, and the total error in phase saturation is assumed to be directly proportional to the accuracy of the X-ray device[137]; the effect of (I/I_g)-error on fluid saturation has been reported to be around ±3 %HCPV for doped gas/oil/water systems[137]. However, in the case of gas-condensate systems (in depletion experiments) neither the phase densities nor the attenuation coefficients can be considered constant, and must be measured at every pressure value, introducing two sources of static errors.

The assumption of ±3% HCPV in saturation measurements for a gas-oil-water system is on the optimistic side, compared with our gas-condensate system. The gas-oil-water system is apparently at moderate pressure and temperature, and used thin walled core holders. Gas-condensate systems operate at high pressures, and to control the temperature an oven must surround the core holder. The accuracy in I/I_g measurements is likely to be far less than that of the gas-oil-water systems.

As the PVT data for the methane/bromopropane mixture are measured at two extreme IFT values (the first at very low IFT 0.0015 mN/m and the other at relatively high 3.22 mN/m), it is important to also perform the analysis for an intermediate value of IFT. As several of our relative permeability measurements are conducted with a fluid at an IFT value of 0.135 mN/m, this value is chosen for our analysis. The measured PVT-data at the two extreme IFT values together with the measured liquid drop-out are used in a PVT-package to tune equation of state (EOS), to predict PVT-data at any intermediate pressure. The input (to start the regression) critical properties for the bromoprpoane are those of normal hexane (nC6), with the actual specific gravity and molecular weight of bromopropane. The results appeared reliable. The results of the regression analysis (predicted and measured PVT-data) are given in Figs. 3.3a to 3.3f. A flash calculation is then performed using the tuned EOS in the PVT-package to predict the PVT-data at the intermediate IFT of 0.135 mN/m, the results are given in Table 3.3.

The PVT-data is used to calculate the phase attenuation coefficients using Eqs. 3.26 and 3.27 and the intensity ratio (I/I_g) for the three IFT values. The reported ±3 %HCPV[137] error in measured condensate saturation, which is due to the accuracy of the X-ray device, is then translated (using Eqs. 3.28 and 3.29)[95] into a percentage error in intensity ratio (I/I_g) for the IFT values and corresponding condensate saturation. The values are used as the accuracy of the X-ray device in measuring intensity ratio in gas-condensate systems excluding the effect of PVT-error. The total possible static errors in the measured condensate saturation are estimated (using Eqs. 3.30 to 3.35)[95] for different errors in PVT-data, with the results shown in Table 3.4.

The resultant errors in the measured condensate saturation are assumed to follow a normal distribution, and the five different sources of the static errors (measured liquid and vapour densities, measured liquid and vapour attenuation coefficients, and intensity ratio, I/I_g) are assumed to be independent of each other.

$$\eta_c = 0.2\left(WF_{CH_4}\right)_c + 5.4\left(WF_{C_3H_7Br}\right)_c \qquad ...(3.26)$$

$$\eta_g = 0.2\left(WF_{CH_4}\right)_g + 5.4\left(WF_{C_3H_7Br}\right)_g \qquad ...(3.27)$$

where,

WF_{CH4}: weight fraction of methane, fraction

WF_{C3H7Br}: weight fraction of bromopropane, fraction

η_c: attenuation coefficient of condensate.

η_g: attenuation coefficient of gas.

0.2: attenuation coefficient of CH_4[137].

5.4: attenuation coefficient of C_3H_7Br[137].

$$\left(I/I_g\right)_e=\sqrt{\left(\frac{\partial\left(I/I_g\right)}{\partial S_C}\right)^2\left(S_C\right)_e^2} \qquad ...(3.28)$$

where,

$$\frac{\partial\left(I/I_g\right)}{\partial S_C}=\left[-\left(\mu_c\rho_c-\mu_g\rho_g\right)\phi L\right]\exp^{\left[-\left(\mu_c\rho_c-\mu_g\rho_g\right)S_c\phi L\right]} \qquad ...(3.29)$$

$\left(S_C\right)_e$: standard error in measured condensate saturation.

$\left(I/I_g\right)_e$: resultant error in intensity ratio.

$$\left(S_C\right)_e=\sqrt{\begin{array}{l}\left(\frac{\partial S_C}{\partial\left(\rho_C\right)}\right)^2\left(\rho_C\right)_e^2+\left(\frac{\partial S_C}{\partial\left(\rho_g\right)}\right)^2\left(\rho_g\right)_e^2+\left(\frac{\partial S_C}{\partial\left(\eta_C\right)}\right)^2\left(\eta_C\right)_e^2\\+\left(\frac{\partial S_C}{\partial\left(\eta_g\right)}\right)^2\left(\eta_g\right)_e^2+\left(\frac{\partial S_C}{\partial\left(I/I_g\right)}\right)^2\left(I/I_g\right)_e^2\end{array}} \qquad ...(3.30)$$

where $\left(S_C\right)_e$, $\left(\rho_c\right)_e$, $\left(\rho_g\right)_e$, $\left(\eta_C\right)_e$, $\left(\eta_g\right)$, $\left(I/I_O\right)_e$: are the standard errors in measured condensate saturation, liquid density, vapour density, liquid attenuation coefficient, vapour attenuation coefficient, and reported error in intensity ratio (I/Io) respectively. Taking the derivatives of S_C from Eq. 3.22a we obtain:

$$\frac{\partial S_C}{\partial\left(\rho_C\right)}=\frac{S_c\,\eta_c}{\left(\eta_c\rho_c-\eta_g\rho_g\right)} \qquad ...(3.31)$$

$$\frac{\partial S_C}{\partial\left(\rho_C\right)}=\frac{-S_c\,\eta_g}{\left(\eta_c\rho_c-\eta_g\rho_g\right)} \qquad ...(3.32)$$

$$\frac{\partial S_c}{\partial(\eta_c)}=\frac{S_c\,\rho_c}{\left(\eta_c\rho_c-\eta_g\rho_g\right)} \qquad ...(3.33)$$

$$\frac{\partial S_c}{\partial(\eta_g)}=\frac{-S_c\,\rho_g}{\left(\eta_c\rho_c-\eta_g\rho_g\right)} \qquad ...(3.34)$$

$$\frac{\partial S_c}{\partial(I/I_g)}=\frac{-1}{\left(\eta_c\rho_c-\eta_g\rho_g\right)\phi L\left(I/I_g\right)} \qquad ...(3.35)$$

3.6.4 Dynamic Error (γ-Ray)

This type of error is associated mostly with the γ-ray device as the time taken to take measurement is normally minutes, as opposed to seconds for to x-ray system.

During unsteady-state displacement experiments, the rate at which phase-saturation profile changes can cause significant dynamic error. This error results from the fact that at any location of the core the γ-ray device requires a finite time (i.e. 10 minutes) for each reading[126]. The change in phase saturation values at that given location of the core during the reading time can make the measured condensate saturation value un-representative. For instance, if the actual phase saturation at beginning of the reading time is 40%, and at the end of the reading it is 35%, then the dynamic error in the phase saturation value read by the γ-ray device is expected to be up to ± 5 %hcpv. The dynamic error is dependent on fluid properties, injection rate, displacement mechanism (gravity free fall versus horizontal gas-injection). The latter two aspects are investigated in the following sections.

Simulated Core Experiments

To study the effect of gas injection rate on the dynamic error, two horizontal displacement experiments at IFT= 0.135 mN/m are simulated at gas injection rates of 200 cc/hr and 800 cc/hr using the ECLIPSE simulator. To study the effect of the displacement mechanism on the dynamic error, a gravity free fall experiment at the same IFT value (0.135 mN/m), is also simulated.

The dimensions of the horizontal 1-D simulation model are 122 x 1 x 1 with a square cross sectional area of 4.42 cm x 4.42 cm. A grid size of 0.5 cm and time step of 0.01 hr have been determined in earlier sensitivity analysis to be suitable not to cause any numerical dispersion[7]. The different sets of relative permeability curves used in the simulation are given in Fig. 3.4. As shown in this figure the relative permeability curves for IFT of 0.135 mN/m are indeed an extrapolation of experimentally measured relative permeability curves at the two different rates. The dimensions of the vertical 1-D simulation model are 1 x 1 x 123 with a square cross sectional area of 4.42 cm x 4.42 cm, where the last cell has a porosity of 1.0 serving as a tank for the condensate to accumulate at the bottom. The same grid size of 0.5 cm and time step of 0.01 hr. as the ones used for the horizontal displacement.

The core properties used are that of the Berea Sandstone core used in laboratory relative permeability measurements, with the core properties are given in Table 3.5[6]. Condensate saturation versus time and condensate saturation profile along the length of the core are given in Figs. 3.5 to 3.10 for all the three simulated displacement experiments.

Dynamic error calculations

To calculate the possible dynamic error for each of the above simulated core displacement experiments the γ-ray device reading is assumed to represent the condensate saturation value that corresponds to half the reading time. For instance, if the reading time is 10 minutes then the γ-ray device reading is assumed to correspond to condensate saturation at 5 minutes. Hence, the possible dynamic error is taken as half the difference in condensate saturation values between the beginning of reading time and the end of reading time. The γ-ray device is assumed to be located at three different locations along the 61 cm core, and to avoid any end-effects the location of the γ-ray devices are taken as follows: for the horizontal core the locations are at 15 cm, 30 cm, and 45 cm from the inlet of the core; and for the vertical core the locations are at 15 cm, 30 cm, and 45 cm from the top of the core. It is found that the magnitude and behaviour of the dynamic error with time are similar for all the three locations, only the first location is presented here. The resultant dynamic errors for the three different experiments are shown in Figs. 3.11 to 3.13.

If X-ray is used the time required at each location to take accurate reading is less than one minute which is much shorter than the time required for γ-ray device. The simulation studies indicate that under realistic conditions (similar to those in laboratory experiments), in one minute time, the maximum change in saturation ranges from 0.26 to 0.48 %. This does not create significant error.

3.6.5 Analysis Of Results

Static Error

As shown in Table 3.4, for the lowest IFT value case (0.0015 mN/m), the contribution of the PVT-error to the static error can be significant, additional 3 %hcpv for PVT error of 4%. This is attributed to the fact that this case is very close to the critical point of the mixture where the contrasts between phase densities and phase attenuation coefficients are very small forcing the required accuracy range by which the intensity ratio must be measured to be very small indeed. For the highest IFT case (3.22 mN/m), the contribution of the PVT error to the static error is negligible, additional 0.06 %hcpv for PVT error of 4%. The performance of this case, because of the relatively high IFT value, is closer to gas/oil/water systems where PVT-data does not play significant role in affecting the device reading. For the case of the intermediate IFT value (0.135 mN/m), Table 3.6 indicates that a reasonable value of 0.61 %hcpv is the contribution of the PVT error to the overall static error for introduced PVT error of 4%.

Dynamic Error

The dynamic error, as shown in Figs. 3.11, 3.12, and 3.13, for horizontal injection displacement experiments can be 20 fold greater than those for gravity free fall. This is mainly due to the slow displacement mechanism governing the gravity free fall displacement. Also, at the early time of the horizontal displacements, the dynamic error for the 800 cc/hr can be four folds greater than that for the 200 cc/hr. On the other hand, the dynamic error behaviour is the same for all the three experiments. The dynamic error assumes a maximum value at some point during the displacement and then it reduces gradually to almost zero at steady state conditions. The point of maximum occurs almost at the beginning for both horizontal displacements and it occurs at some later time for the gravity free fall.

Total Error

Total error expected for the three experiments is calculated by summing the static and the dynamic errors. Tables 3.6 to 3.8 give the resultant total error together with the associated static and dynamic errors, for different values of errors introduced in measured PVT data and intensity ratio (I/I_g) at three different times during each displacement experiment. The maximum total error expected for the horizontal displacement at 800 cc/hr is 7.42 %hcpv when the error in PVT data is around 4%. For the horizontal displacement at 200 cc/hr for the same amount of error in PVT data the maximum total error is 4.61 %hcpv. For the gravity free fall the maximum total error is 3.61 %hcpv for the same 4 % error in PVT data. For all three experiments the maximum error occurs almost at the beginning of the displacement.

3.6.6 Conclusions

1. Experiments have shown that a binary mixture methane/bromopropane behaves as gas-condensate system at 37 ^{o}C.

2. Critical properties of normal hexane together with the actual molecular weight and specific gravity of bromopropane can be used as starting properties to produce reliable EOS tuning to experimental data of methane/bromopropane.

3. For methane/bromopropane mixture at low IFT (0.0015 mN/m) the use of X-ray to measure condensate saturation profile is not viable because small errors in PVT data can produce large errors in the measured condensate saturation.

4. For methane/bromopropane mixtures at high IFT (3.22 mN/m), the use of X-ray in measuring condensate saturation profile can give similar results to those of doped gas/oil/water systems; where the error associated with the measured PVT data can be small.

5. For methane/bromopropane mixtures at intermediate IFT (0.135 mN/m), the use of X-ray to measure condensate saturation profile is promising. The contribution of the dynamic error is small, therefore, only PVT (static) errors impact the performance of the X-ray device. If the accuracy of the X-ray device in measuring the intensity ratio does not cause errors in condensate saturation of more than 3 %hcpv, the error in measuring PVT data is also controlled to within 4% of actual values. If the X-ray device is not located very close to the inlet or top of core, then the maximum total error should be less than 3.61 %hcpv.

6. For methane/bromopropane mixtures at intermediate IFT (0.135 mN/m), the use of γ-ray in measuring condensate saturation profile is not promising. If the accuracy of the γ-ray device in measuring the intensity ratio does not cause errors in the condensate saturation of more than 3 %hcpv, the error in measuring PVT data is also controlled to within 4% of actual values. If the γ-ray reading time is not more than 10 minutes, and the γ-ray device is not located very close to the inlet or top of core, then the following can be true:

- Maximum total error in horizontal displacement at 800 cc/hr will be around 7.42 %hcpv.
- Maximum total error in horizontal displacement at 200 cc/hr will be around 4.61 %hcpv.
- Maximum total error in gravity free fall will be around 3.61 %hcpv.

7. For the methane/bromopropane mixture the intermediate value of IFT (0.135 mN/m) is at relatively high pressure (4125 psia). This high pressure will require a thicker core holder than the one conventionally used for gas-oil systems X-ray measurements. The X-ray accuracy is reported to measure condensate saturation within ±3 %hcpv for the core holder that can stand pressure of 2700 psia. Thicker core holders might increase this error to 5% hcpv or more.

8. The use of an X-ray device in measuring condensate profile along the core during displacement experiments is more viable than the γ-ray device.

Table 3.1: Test sequence at an IFT of 0.135 dynes/cm and a CGR (vol./vol.)of 0.05

Test	Gas flow rate (cc/hr)	Oil flow rate (cc/hr)	Hcpv / hour	Gas superficial pore velocity (m/day)	Gas-phase capillary number, Nc
1	100	5	0.61	8.8	0.16 E-4
2	200	10	1.22	17.6	0.32 E-4
3	400	20	2.44	35.2	0.64 E-4
4	800	40	4.88	70.4	0.13 E-3
5	400	20	2.44	35.2	0.64 E-4
6	200	10	1.22	17.6	0.32 E-4
7	100	5	0.61	8.8	0.16 E-4

Table 3.2: Measured PVT-Data For Methane/Propylbromide At 37.0 °C

Pressure psia	Vapour Density gm/cc	Liquid Dansity gm/cc	Vapour Viscosity cp	Liquid Viscosity cp	Vapour mole C3H7Br fraction	Liquid mole C3H7Br fraction	IFT mN/m
5000	0.6129		0.0693		0.2360		
4500	0.5100	0.6885	0.0567	0.0908	0.2025	0.2840	0.0015
3000	0.2142	1.0213	0.0234	0.2014	0.0009	0.5289	3.22

Table 3.3: Predicted PVT-Data For Methane/ Propylbromide At 37.0 °C

Pressure psia	Vapour Density gm/cc	Liquid Dansity gm/cc	Vapour Viscosity cp	Liquid Viscosity cp	Vapour mole C3H7Br fraction	Liquid mole C3H7Br fraction	IFT mN/m
4125	0.4080	0.8120	0.0413	0.1188	0.1575	0.3739	0.135

Table 3.4: Static errors for methan/bromopropane at 37 °C

Steady-State			Introduced Errors		Resultant Errors in S_C	
Pressure	IFT	Sc	I/Io	PVT	% of Sc value	%hcpv
psia	dyne / cm	%hcpv	%	%		
3000	3.2240	39	5.94	0	7.69	3.00
		39	5.94	1	7.71	3.00
		39	5.94	2	7.74	3.01
		39	5.94	4	7.86	3.06
4125	0.13500	42	6.23	0	7.14	3.00
		42	6.23	1	7.59	3.26
		42	6.23	2	7.28	3.13
		42	6.23	4	8.40	3.61
4500	0.0015	47	3.76	0	6.38	3.00
		47	3.76	1	6.91	3.26
		47	3.76	2	8.33	3.93
		47	3.76	4	12.50	5.90

Table 3.5: Core Properties

Length (cm)	Area cm2	Porosity %	Permeability @ S_{wi} (md)
61.00	19.55	21	92

Table 3.6: Total error for horizontal displacement at 200 cc/hr.
(reading time is 10 minutes and device location at 15 cm from inlet)

IFT = 0.135 mN/m		Static Errors		Errors in Condensate Saturation			
Time	Cond.Sat	I/Io	PVT	Static	Dynamic	Total	
Minutes	%hcpv	%	%	%hcpv	%hcpv	% of S_c	%hcpv
0	42	6.23	0	3.00	0.00	7.14	3.00
0	42	6.23	1	3.17	1.00	9.93	4.17
0	42	6.23	2	3.26	1.00	10.15	4.26
0	42	6.23	4	3.61	1.00	10.98	4.61
750	17	26.41	0	3.00	0.04	17.85	3.04
750	17	26.41	1	3.00	0.04	17.86	3.04
750	17	26.41	2	3.00	0.04	17.87	3.04
750	17	26.41	4	3.01	0.04	17.93	3.05
1500	14	34.22	0	3.00	0.01	21.53	3.01
1500	14	34.22	1	3.00	0.01	21.53	3.01
1500	14	34.22	2	3.00	0.01	21.54	3.02
1500	14	34.22	4	3.01	0.01	21.57	3.02

Table 3.7: Total error for horizontal displacement at 800 cc/hr.
(reading time is 10 minutes and device location at 15 cm from inlet)

IFT = 0.135 mN/m		Static Errors		Errors in Condensate Saturation			
Time	Cond.Sat	I/Io	PVT	Static	Dynamic	Total	
Minutes	%hcpv	%	%	%hcpv	%hcpv	% of S_C	%hcpv
0	42	6.23	0	3.00	3.81	16.21	6.81
0	42	6.23	1	3.17	3.81	16.62	6.98
0	42	6.23	2	3.26	3.81	16.84	7.07
0	42	6.23	4	3.61	3.81	17.67	7.42
750	8	68.18	0	3.00	0.03	37.81	3.03
750	8	68.18	1	3.00	0.03	37.81	3.03
750	8	68.18	2	3.00	0.03	37.81	3.03
750	8	68.18	4	3.00	0.03	37.82	3.03
1500	6	94.92	0	3.00	0.00	50.02	3.00
1500	6	94.92	1	3.00	0.00	50.02	3.00
1500	6	94.92	2	3.00	0.00	50.02	3.00
1500	6	94.92	4	3.00	0.00	50.03	3.00

Table 3.8: Total error for Gravity free fall
(reading time is 10 minutes with device location 15 cm from top).

IFT = 0.135 mN/m		Static Errors		Errors in Condensate Saturation			
Time	Cond.Sat	I/Io	PVT	Static	Dynamic	Total	
Minutes	%hcpv	%	%	%hcpv	%hcpv	% of S_C	%hcpv
0	42	6.23	0	3.00	0.00	7.14	3.00
0	42	6.23	1	3.17	0.00	7.55	3.17
0	42	6.23	2	3.26	0.00	7.77	3.26
0	42	6.23	4	3.61	0.00	8.60	3.61
750	30	11.30	0	3.00	0.14	10.47	3.14
750	30	11.30	1	3.01	0.14	10.49	3.15
750	30	11.30	2	3.03	0.14	10.57	3.17
750	30	11.30	4	3.12	0.14	10.88	3.26
1500	23	17.15	0	3.00	0.03	13.17	3.03
1500	23	17.15	1	3.00	0.03	13.19	3.03
1500	23	17.15	2	3.01	0.03	13.22	3.04
1500	23	17.15	4	3.04	0.03	13.36	3.07

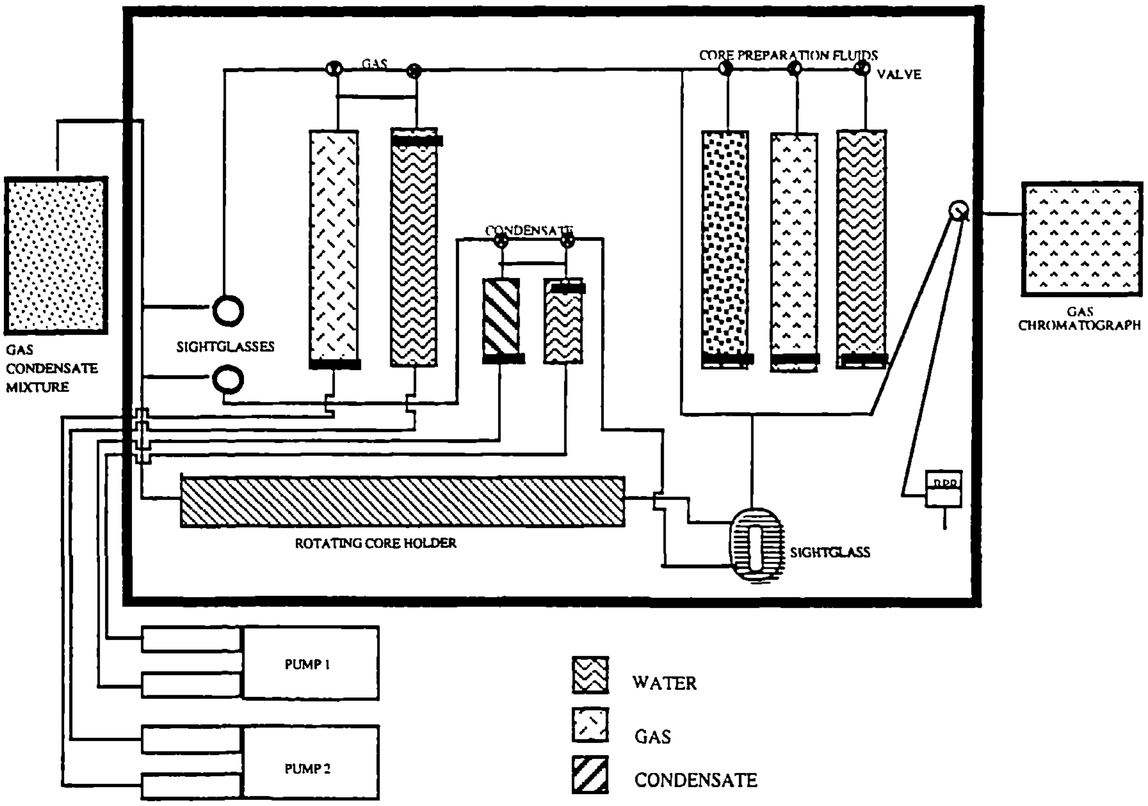

Figure 3.1: Modified core facility (after reference 32).

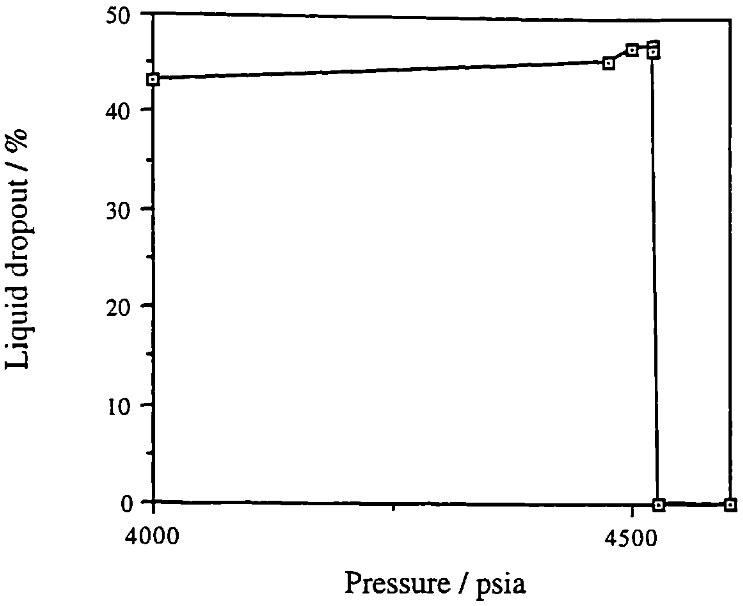

Figure 3.2: Liquid dropout for methane/bromopropane GC mixture at 37 oC

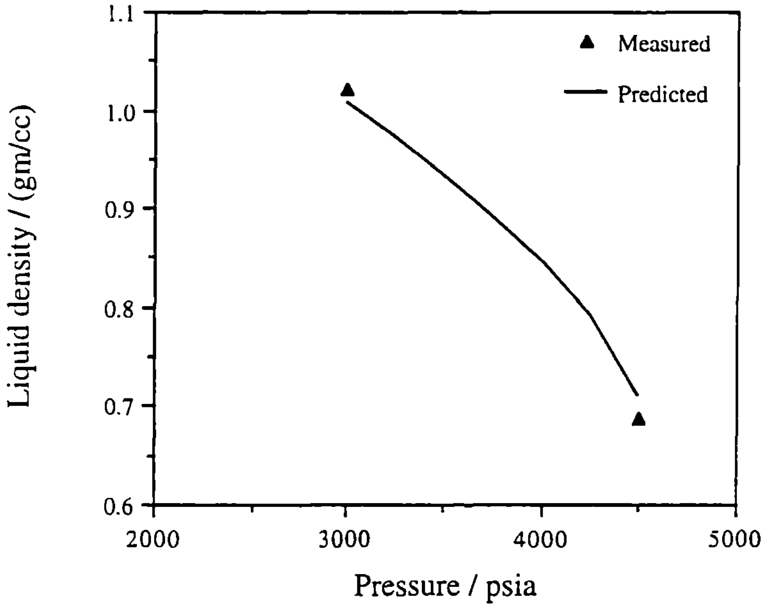

Figure 3.3a: Regressed and measured liquid density

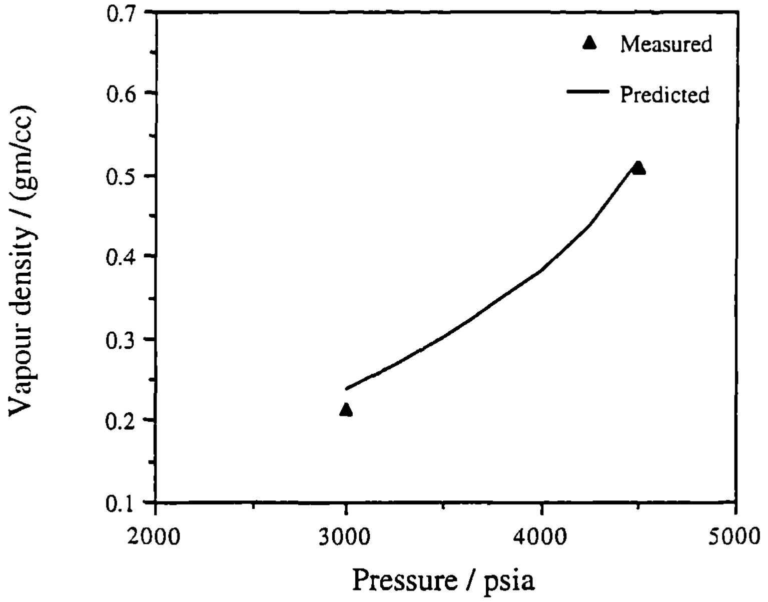

Figure 3.3b: Regressed and measured vapour density

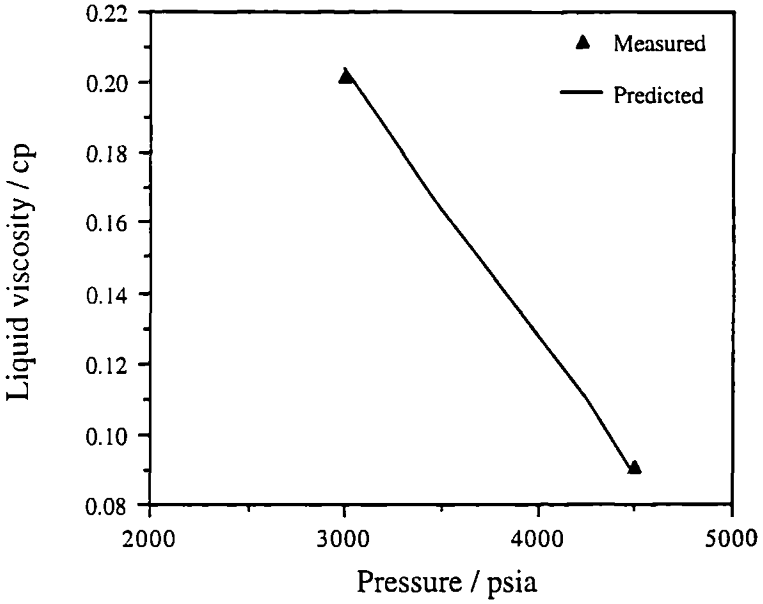

Figure 3.3c: Regressed and measured liquid viscosity

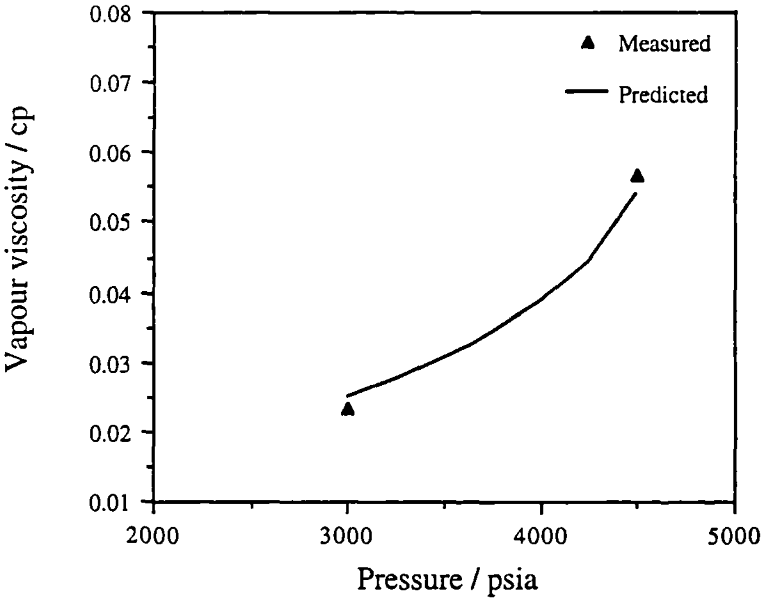

Figure 3.3d: Regressed and measured vapour viscosity

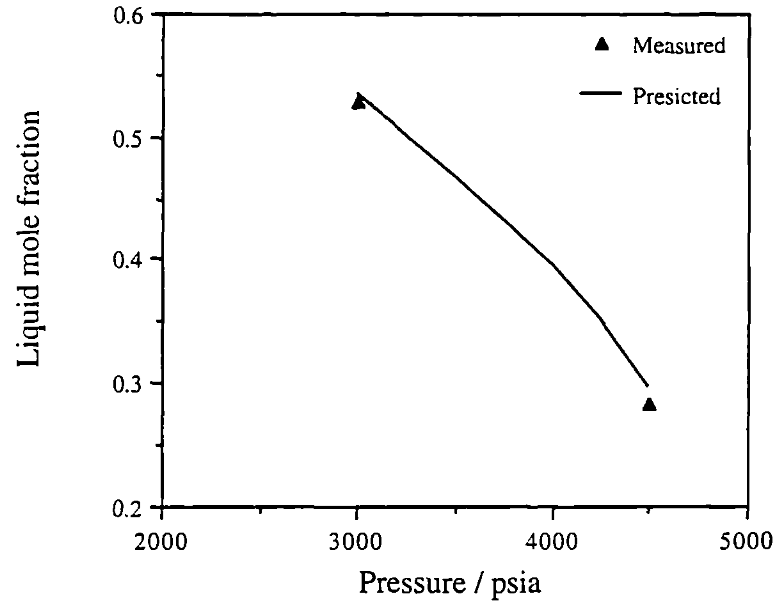

Figure 3.3e: Regressed and measured bromopropane liquid mole fraction

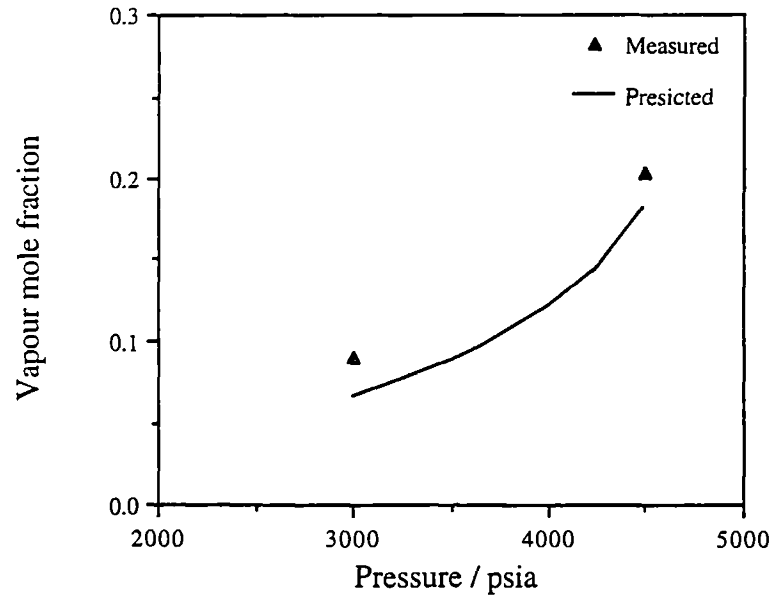

Figure 3.3f: Regressed and measured bromopropane vapour mole fraction

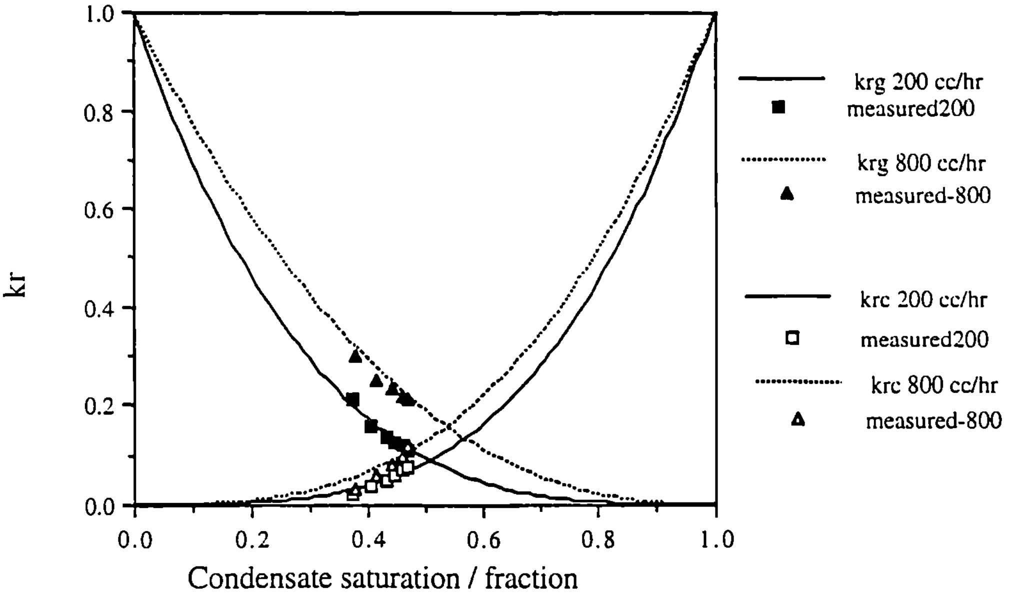

Figure 3.4: Relative premeability curves used in simulation for two different gas flow rates

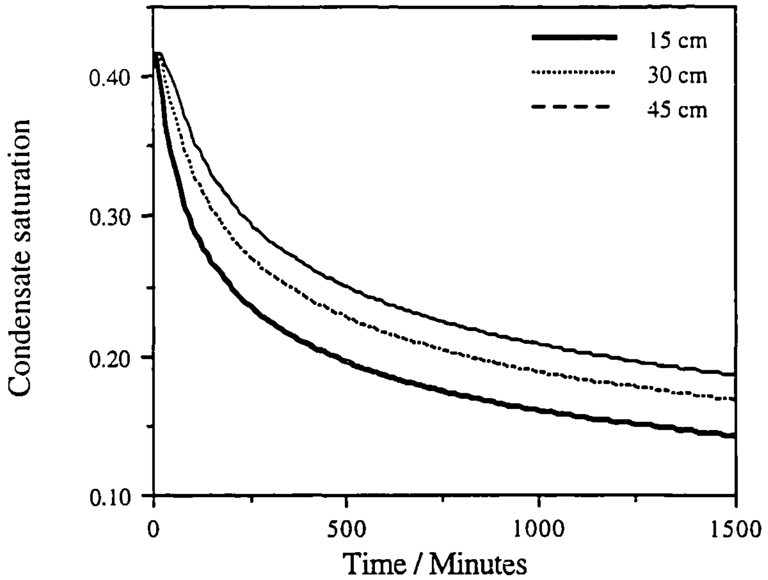

Figure 3.5: Horizontal Displacement for IFT=0.135 mN/m; Rate 200 cc/hr.

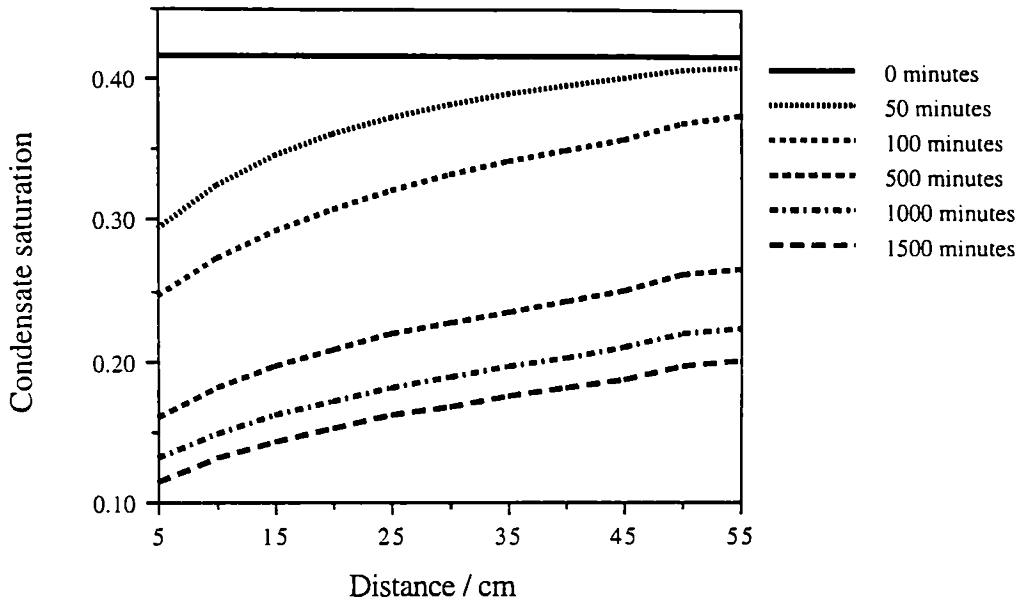

Figure 3.6: Horizontal Displacement for IFT=0.135 mN/m; Rate 200 cc/hr.

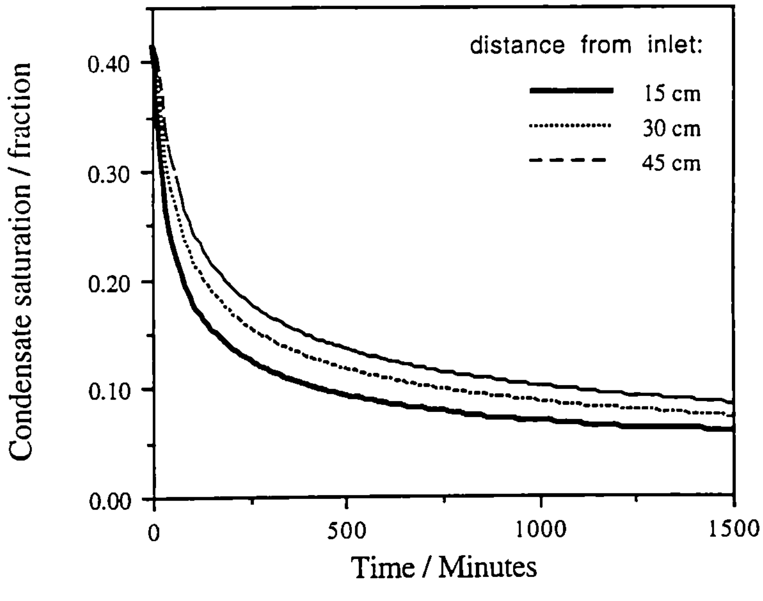

Figure 3.7: Horizontal Displacement for IFT=0.135 mN/m; Rate 800 cc/hr.

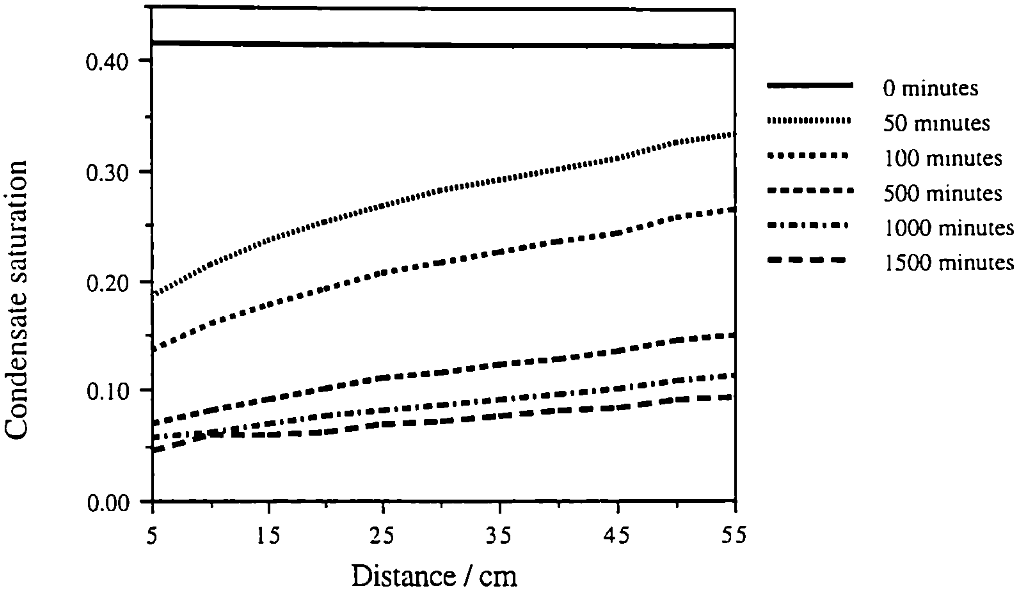

Figure 3.8: Horizontal Displacement for IFT=0.135 mN/m; Rate 800 cc/hr.

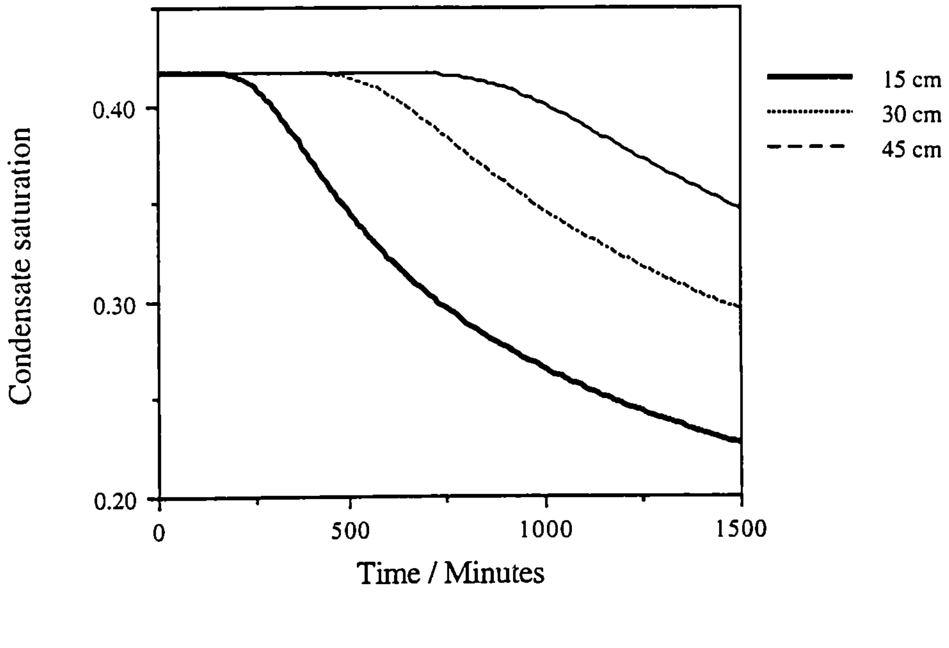

Figure 3.9: Gravity free fall for IFT=0.135 mN/m

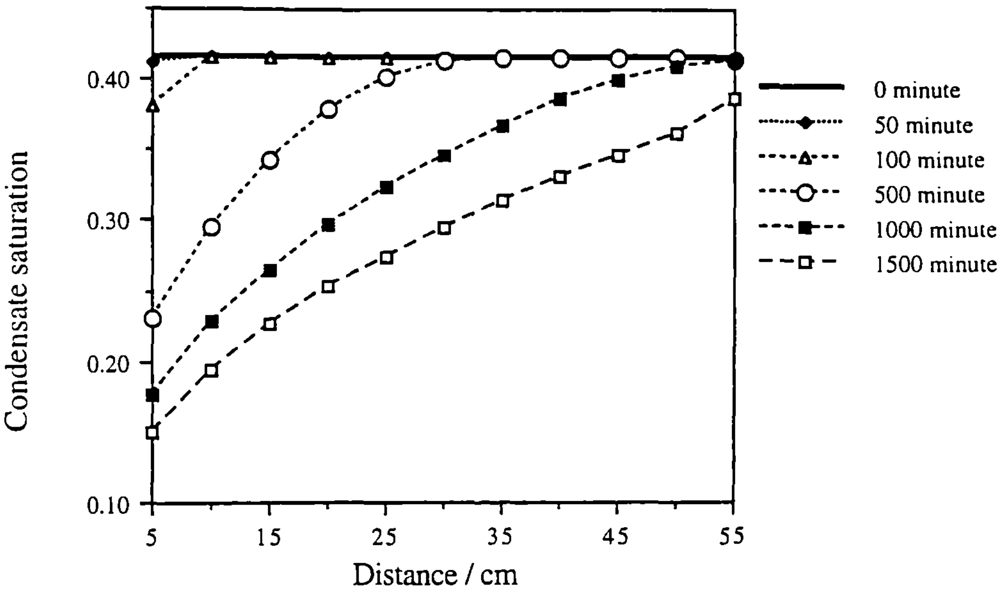

Figure 3.10: Gravity free fall for IFT=0.135 mN/m

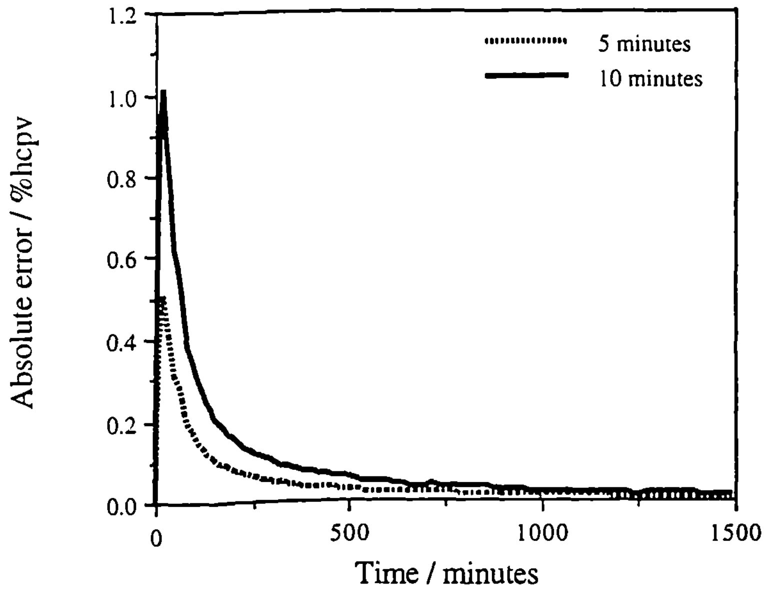

Figure 3.11: Dynamic error of horizontal displacement for IFT=0.135 mN/m; rate= 200 cc/hr, device location at 15 cm from inlet

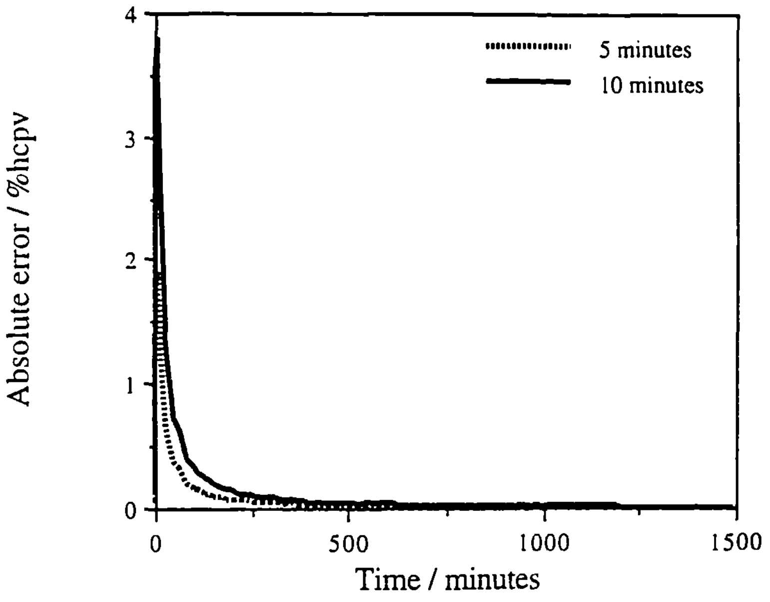

Figure 3.12: Dynamic error of horizontal displacement for IFT=0.135 mN/m; Rate 800cc/hr, device location at 15 cm from inlet

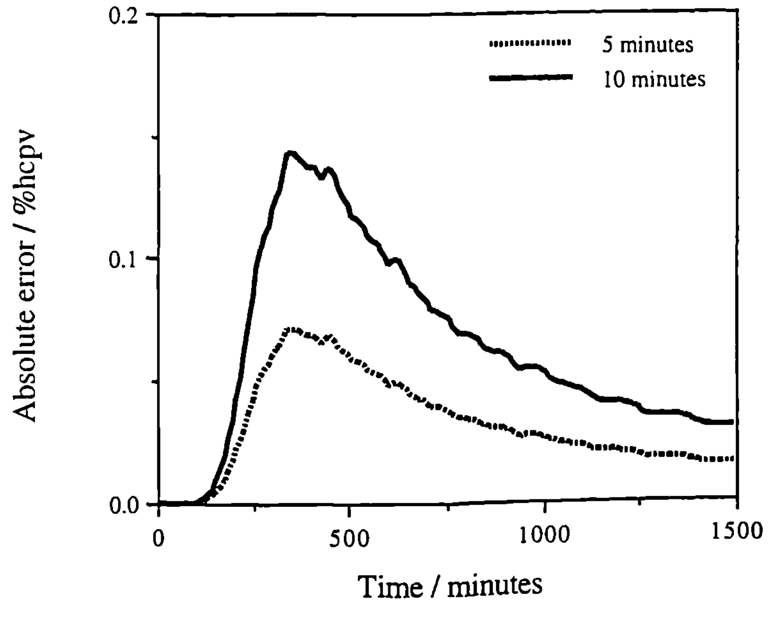

Figure 3.13: Dynamic error of gravity free fall for IFT=0.135 mN/m; device location at 15 cm from top

CHAPTER 4

FLOW REGIMES

4.1 INTRODUCTION

During steady-state relative permeability tests conducted as part of the Gas-Condensate Recovery Project at Heriot-Watt University[61] the relative permeabilities of both gas and condensate were found to be dependent on flow rate. These tests reported the existence of such a rate effect without categorising the nature of the flow or at least describing the type of flow regimes these tests represent. During the above steady-state tests, the relative permeabilities of both phases (gas and condensate) were found to increase with increasing flow rate. Therefore, this rate effect is evidently not caused by inertial forces associated with the non-Darcy flow in porous media that works in the reverse direction (i.e. in high velocity flow the inertial forces create additional pressure-drop causing lower relative permeabilities at higher flow rates). However, for the sake of modelling such a rate effect it is imperative to know the relationship between the flow rate and pressure drop during those tests. In this chapter the flow in the above steady-state relative permeability tests is categorised to prove that the relative permeability rate effect is indeed existing in the laminar flow region.

4.2 THEORY

4.2.1 The Modified Reynolds Number

A dimensionless quantity referred to as Reynolds number (R_e) is the most widely used criteria by which flow is categorised into laminar, transient or turbulent flow regimes. The Reynolds number simply relates fluid properties, i.e. viscosity and density, and superficial flow velocity with a set of parameters associated with the actual porous structure including porosity and a characteristic length scale ratio typical of the internal structure of the porous medium[64]. The above length scale ratio characterises the constituent particle or pore-size, internal surface roughness and bed packing geometry. Ergun (1952)[64,65] defined a version of Reynolds number suitable for flow in porous media. This so called modified Reynolds number is given by Eq. 4.1.

$$R_e = \left(\frac{D_p \rho v}{\mu}\right)\left(\frac{1}{1-\phi}\right) \qquad \ldots(4.1)$$

where,

D_p: characteristic length scale typical of the internal structure of the porous medium.

ρ: density of the flowing fluid.

μ: viscosity of the flowing fluid.

v: superficial fluid velocity.

ϕ: porosity of the medium.

Another version of the Reynolds number for flow in porous media was provided by Cornell and Katz (1953)[66,67]. This was also called a modified Reynolds number and it was developed for the flow of fluids through consolidated formation; it is given by the following equation:

$$R_e = \frac{\beta W k}{\left(6.32 \times 10^{10}\right) A \mu} \qquad \ldots(4.2)$$

where,

$W = A\rho v$: mass flow rate, lb_m/s.

A: cross sectional area available for flow, ft^2.

β: empirical Forchheimer factor that is related to formation permeability (k) (see section 4.2.2 below).

Therefore, the modified Reynolds number as defined by Ergun (1952)[64,65] (Eq. 4.1) as well as the one defined by Cornell and Katz[66,67] are adopted for the calculations presented in this chapter.

4.2.2 Forchheimer β-Factor

Forchheimer modified Darcy's law to better describe the dry-gas non-Darcy flow in 1905. Forchheimer's formulation was put forth by Cornell and Katz in 1953[66] (Eq. 4.3). The additional pressure-drop introduced by inertia forces is represented by a second term added to the typical Darcy's definition of a pressure-drop associated with two-phase flow in porous media. This second term is a function of velocity to the second order which makes it important only at high velocity. It is also a function of the so-called β-factor, therefore, a better definition and understanding of this factor is vital for accurate quantification of the Forchheimer effect on the two-phase flow near the wellbore and hence on well gas-phase productivity.

$$-\frac{dP}{L}=\frac{\mu v}{k\,k_r}+\beta\rho v^2 \qquad \text{...(4.3)}$$

While the exact determination of the multi-phase β-factor is still vague, several workers have reported their efforts in better determining the β-factor for two-phase flow in porous media (Penny and Liang's (1995)[114], Wong(1970)[115], Geertsma (1974)[116], Tek at al. (1962)[117], Fredrick and Graves (1994)[6]. Wong and Geertsma incorporated the multi-phase effect on the β-factor by assuming that the other phase occupies pore space, so that

$$\beta=\frac{0.005}{\left(\phi(1-S_w)\right)^{5.5}k_g^{0.5}} \qquad \text{...(4.4)}$$

where,

S_w: water saturation, fraction

k_g: gas effective permeability, m^2.

ϕ: porosity, fraction

Noman and Archer (1988)[119] stated that the following correlation (Eq. 4.5) presented by Tek et al. (1962)[117] follows the trends better than Geertsma's.

$$\beta = \frac{3.21 \text{ x } 10^4}{k^{1.25}\ \phi^{0.75}} \qquad \text{...(4.5)}$$

where,

k: gas effective permeability, mD.

ϕ: porosity, fraction.

Fredrick and Graves (1994)[118] gave two different correlations for the β-factor accounting for presence of immobile water saturation. They also concluded that these correlations should give the same trends for mobile water saturation. The first was given in term of the gas effective permeability, so that

$$\beta = \frac{1.98 \text{ x } 10^{11}}{k_e^{1.64}} \qquad \text{...(4.6)}$$

where,

k_e: gas effective permeability, mD.

The second was in terms of the effective gas permeability and effective porosity and it was given in three different forms:

<u>Form 1:</u>

$$\beta = \frac{7.89 \text{ x } 10^{10}}{k_e^{1.6}\left[\phi\left(1-S_w\right)\right]^{0.404}} \qquad \text{...(4.7)}$$

Form 2:

$$\beta = \frac{2.11 \text{ x } 10^{10}}{k_e^{1.55}\left[\phi\left(1-S_w\right)\right]} \qquad \text{...(4.8)}$$

Form 3:

$$\beta = \frac{1}{\left[\phi\left(1-\mathrm{S_w}\right)\right]^{2.0}} \cdot \mathrm{e}^{45.0-\sqrt{407+81\ell n(\mathrm{k_e}/(\phi(1-\mathrm{S_w})))}} \qquad \text{...(4.9)}$$

where,

k_e: gas effective permeability, mD.

To extend the applicability of Eq. 4.3 to multi-phase systems, Penny and Liang (1995)[114] proposed multiplying the equation by a multi-phase correction factor (γ) and leaving the β-factor at its fundamental form; so that,

$$-\frac{dP}{L} = \gamma\left(\frac{\mu v}{kk_{r(N_c)}} + \beta\rho v^2\right) \qquad \text{...(4.10)}$$

where,

β : Dry-gas Forchheimer factor

$$\beta = \frac{b}{k^a} \qquad \text{...(4.11)}$$

a = 1.45, b = 0.75, Reported for Jordan Sand.

γ : gas permeability correction factor for the increase in pressure drop due to multi-phase flow.

$$\gamma = \gamma_o + C\left(\frac{X_l}{X_g}\right)^d \qquad ...(4.12)$$

where,

$\gamma_o = 1.25$

C= 25

d= 0.5

$$X_l = \left(\frac{\rho v}{\mu}\right)_l \qquad ...(4.13)$$

$$X_g = \left(\frac{\rho v}{\mu}\right)_g \qquad ...(4.14)$$

While the general form of all the above correlations can be used for the gas-condensate systems, none is specific to gas-condensate flow in porous media. Furthermore, Penny and Liang's (1995)[114] modification to Forchheimer equation is too system dependent. Therefore, Wong and Geertsma's Equation (Eq. 4.4), is adopted for this study for its simplicity and consistency as it gives the correct unit for β, i. e. L^{-1}.

4.2.3 Flow Equations

To calculate the values for Reynolds number (R_e) which describes the flow regimes during the steady-state gas-condensate relative permeability measurements, the values for D_p must first be estimated. Therefore, the flow in the porous medium must be modelled to enable us to calculate D_p. The flow in porous media is often approximated by flow in packed columns where spheres are conveniently chosen to be the packing material[64,65]. Fluid flows in tubes of varied cross sections in the space available for flow between the packing material and D_p is the diameter of the spheres. For this model, the flow is completely described by Ergun (1952)[65] equation as given by the following equation (all terms are in self-consistent units):

$$\Phi = \left(\frac{150\mu v}{D_p^{\,2}}\right)\frac{(1-\phi)^2}{\phi^3} + \left(\frac{1.75\rho v^2}{D_p}\right)\frac{(1-\phi)}{\phi^3} \qquad \text{...(4.17)}$$

where,

$\Phi = \frac{\Delta p}{L}$: pressure gradient across the length of the porous medium.

v : Darcy velocity=total flow rate over total cross sectional area.

For low flow rates (linear-laminar) the value of the second term in Eq. 4.17 becomes negligible compared with the first term reducing it to the Blake-Kozeny[65] equation where,

$$\Phi = \left(\frac{150\mu v}{D_p^{\,2}}\right)\frac{(1-\phi)^2}{\phi^3} \qquad \text{...(4.18)}$$

which is a restatement of the extended Darcy's law in which the porous medium absolute permeability (k) is given by:

$$k = \frac{D_p^{\,2}\phi^3}{150(1-\phi)^2} \qquad \text{...(4.19)}$$

and this equation can be used to calculate D_p for laminar flow in a porous medium of known permeability and porosity.

On the other hand, for high flow rates (non-linear) the first term of Eq. 4.17 will be much smaller than the second term and can be eliminated reducing it to the Burke-Plummer equation[65, pp200] where,

$$\Phi = \left(\frac{1.75 \rho v^2}{D_p} \right) \frac{(1-\phi)}{\phi^3} \qquad \text{...(4.20)}$$

This is not a Darcy flow and the permeability of the flow is not solely dependent on the porous medium, but also it depends on flow rate. Therefore, Eq. 4.20 may be used to calculate D_p for the flow. In this case D_p is no more a characteristic length scale.

4.2.4 Flow Classification

In a study of porous media fluid mechanics using laser anemometry and fluid flow visualisation in porous structure Dybbs and Edwards (1984)[64] have provided a detailed flow regime classification using the modified Reynolds number (R_e). When R_e (as defined by Eq. 4.1 or 4.2) is less than 1.0 the flow is classified to be Darcy laminar flow. When R_e is between 1 and 10 the flow is observed to start developing an inertial core; the role of such an inertial core is considered insignificant at this stage and the linear relationship between the flow rate and pressure drop is still approximately valid. A non-linear steady laminar flow classification, where the flow rate is definitely not linearly related to pressure drop, is given when R_e is between 10 and 150. At R_e of 150 to 250 the flow is classified as unsteady laminar flow; where the flow is still not chaotic. A transitional zone $250 < R_e < 300$ is observed separating the unsteady laminar flow regime and the highly unsteady and chaotic flow regime (turbulent) classified for R_e of greater than 300[64].

4.3 CALCULATIONS AND RESULTS

To apply the previous flow equations for multi-phase flow in porous media, the absolute porosity term (ϕ) which appears in these equations must be substituted by a so called net porosity (ϕ_n). ϕ_n defines the pore volume available for the flow of a specific phase (e.g. gas-phase) by subtracting the pore volume occupied by the other coexisting phases (liquid-phase). Hence, the net porosity associated with the flow of the gas phase for a core with an irreducible water saturation of S_{wi}, and an existing condensate saturation of S_c is:

$$\phi_n = \left(1 - S_{wi} - S_c\right)\phi \qquad \text{...(4.21)}$$

Furthermore, the possibility of Forchheimer effect flow occurrence is highest at high condensate saturation where less pore volume space is available for gas flow, than at low condensate saturation (i.e. the calculation of the R_e number at high condensate saturation will overestimate its value). Therefore, to see the maximum possible effect, the calculations are made at the highest condensate saturation during the steady-state experiment (S_c=50.2%)[61]. If with this maximum value, the Reynolds number is small enough to indicate laminar flow then in all other cases (with $S_c < S_{cmax}$) the flow will also be laminar (see sections 4.3.1 to 4.3.3).

Substituting the above value for S_c together with the information available about core properties as listed in Table 4.1[61], in Eq. 4.21 yielded a net porosity (ϕ_n) of 4.3%. Also, to calculate a value for D_p using Eq. 4.19 an effective permeability (k_e) must be used instead of the absolute permeability value at irreducible water saturation (k_{Swi}) reported in Table 4.1. The effective permeability (k_e) is related to the absolute permeability (k_{Swi}) by the following equation: $k_e = k_{rg} k_{Swi}$. Again using the relative permeability for gas at the maximum condensate saturation (S_c=50.2%) has resulted in an effective permeability of k_e = (0.055)*(92 mD)= 5.06 mD.

4.3.1 Laminar-Flow Procedure (Blake-Kozeny Model)

The procedure for calculating the modified Reynolds number involves the following: the flow regime first is assumed to be laminar then the value for D_p is calculated. This value of D_p is used in Eq. 4.1 to calculate the modified Reynolds number. If the value of the calculated modified Reynolds number lies within the laminar flow range ($R_e \leq 10$)[65] then the above assumption is valid and the flow is indeed laminar. On the other hand, if this value lies outside the above range, the flow is not laminar. Table 4.2 gives the fluid properties that were used in the relative permeability tests as reported in the gas condensate recovery project progress report[61].

The formation effective permeability value of the core in Eq. 4.19 is used to calculated D_p. This value of D_p is then used in Eq. 4.1 to calculate the modified Reynolds number. Using the effective permeability of 5.06 mD and the net porosity ϕ_n = 4.3% into Eq. 4.19 gave a value of D_p= 0.0949 mm. The detailed calculation for D_p is shown below:

From Eq. 4.5:

$$D_p = \left[\frac{150k_e(1-\phi)^2}{\phi^3}\right]^{\frac{1}{2}}$$

$$= \left[\frac{150\left(5.06x10^{-3}x10^{-12}m^2\right)(1-0.042588)^2}{(0.042588)^3}\right]^{\frac{1}{2}} = 9.49x10^{-5}m.$$

The sample calculation, given below, shows how to apply the above procedure using the value of 0.0949 mm for D_p and the fluid properties as given in Table 4.2 together with the superficial gas velocity at total flow rate of 840 cc/hr. The superficial gas velocity is given by Eq. 4.22. Also the results of applying the same procedure for all the tests are given in Table 4.3.

$$v_g = \frac{q_g}{A} \qquad ...(4.22)$$

Sample R_e Calculations: For total flow rate of 840 cc/hr in the relative permeability tests:

$$R_e = \left(\frac{D_p \rho v}{\mu}\right)\left(\frac{1}{1-\phi}\right)$$

$$= \left(\frac{\left(9.4905\text{x}10^{-5}\text{m}\right)\left(167.61\text{kg}/\text{m}^3\right)\left(\frac{7.0488}{86400}\text{m}/\text{s}\right)}{0.0161\text{x}10^{-3}\text{pa.s}}\right)\left(\frac{1.0}{1-0.042588}\right)$$

$$= 0.0842$$

It is evident from Table 4.3 that all the calculated values for the modified Reynolds number are extremely less than 1.0. This suggest that the reported rate-effect is occurring in the laminar flow regime.

4.3.2 Non-Laminar-Flow Procedure (Ergun Model)

This procedure involves using Eq. 4.3 (Ergun equation) to calculate D_p. This value of D_p is then used to calculate the modified Reynolds number as given by Eq. 4.1.

Eq. 4.17 can be written in the form of a quadratic equation , i.e.:

$$a.X^2 + b.X + c = 0$$

where,

$$X = \frac{1}{D_p}$$

$$a = \frac{150\mu v(1-\phi)^2}{\phi^3}$$

$$b = \frac{1.75\rho v^2(1-\phi)}{\phi^3}$$

$$c = -\Phi$$

Table 4.4 shows the calculated values for D_p that resulted from applying this procedure using $\phi_n = 4.3\%$ and the fluid data give in Table 4.2.

Therefore, these D_p values now can be used to calculate the modified Reynolds number. The modified Reynolds number resulted from applying this procedure is given in Table 4.5. Again, the values of the modified Reynolds number are extremely low which suggests that the flow is laminar and inertial core has very limited influence on flow.

4.3.3 Cornell and Katz Model

This approach involves the use of Eq. 4.4 in estimating the β-factor which is then used in Cornell and Katz modified Reynold number definition (Eq. 4.2). Using the gas effective permeability of 5.06 mD together with hydrocarbon porosity $\phi = 13.52\%$ into Eq. 4.4 gave a value of $\beta = 7.03 \times 10^{11}$ ft^{-1}. For the above gas effective permeability value a similar value for β is also read from the reservoir permeability versus β provided by Katz and Cornell[66, 67].

The calculated β factor is substituted in Eq. 4.4 for the highest total flow rate of 800 cc/hr. Other measured properties required for the calculation are given in Table 4.2. The calculated modified Reynold number values is 9.8. The calculated values for the other flow rates are listed in Table 4.6. The highest value for the modified Reynolds number (9.8) indicates that the flow is approching the upper limit (10) of the transitional zone. Hence, the inertial forces are about to be significant.

4.4 CONCLUSION

Since, the Cornel and Katz approach is tailored to describe the flow in porous media, it is more reflective of the flow behaviour than the idealised Ergun or Blake-Kozeny models. Therefore, the Reynolds number values as obtained by using Cornel and Katz model are more appropriate to categorise the flow during the relative permeability measurements. This is evident from the extremely low values obtained by using the other two models.

It is evident, from the forgoing analysis, that the favourable rate dependence of relative permeabilities of gas and condensate, observed during the high velocity steady-state relative permeability tests, are occurring in the upper region of the transitional zone. This rate effect may therefore be explained by fluid distribution resulted from some factors specific to the flow of low-IFT / high-velocity gas-condensate systems during those steady-state such a transitional zone. Hence, the formulation of coupled flow that might be used to describe the flow of low IFT gas-condensate systems in those tests must not be modelled using highly turbulent flow criterion (i.e. the flow rate is still directly proportional to pressure drop across the core).

Table 4.1: Core Properties

Length (cm)	Area cm2	Porosity %	Swi %	Permeability@S_{wi} (mD)
61.00	20.4282	18.2	26.4	92

Table 4.2: Fluid Properties

Binary-system fluid properties Molar mix: 73.6% C1 +26.4% nC4 P= 1550 psia, T=37 °C	
IFT (mN/m)	0.9
Liquid drop-out (%hcpv)	28.5
Condensate density (gm/cc)	0.35714
Gas density (gm/cc)	0.16761
Condensate viscosity (cp)	0.0513
Gas viscosity (cp)	0.0161

Table 4.3: Reynolds number for the reported experiments using the formation permeability approach into the Blake-Kozeny model

Test	Cond. Flow Rate (cc/hr)	Gas Flow Rate (cc/hr)	Superficial Velocity of Gas (m/day)	R_e
1	30	75	0.8811	0.0105
2	60	150	1.7622	0.0210
3	120	300	3.5244	0.0421
4	240	600	7.0488	0.0842

Table 4.4: D_p values for the reported experiments using the pressure-drop / superficial velocity approach into the Ergun model

Test	a	b	c	D_p (mm)
1	0.00029227	0.00037812	-52219.312	0.07481632
2	0.00058454	0.00151249	-95170.279	0.07837892
3	0.00116907	0.00604995	-171803.79	0.08250822
4	0.00233815	0.02419984	-275790.30	0.09211987

Table 4.5: Reynolds numbers for the reported experiments using the pressure-drop / superficial velocity approach into the Ergun model

Test	Pressure Drop Kpa	Gas Flow Rate (cc/hr)	Superficial Pore Velocity of Gas (m/day)	D_p (mm)	R_e
1	31.85378	75	3.766	0.0748	0.0083
2	58.05387	150	7.531	0.0784	0.0174
3	104.80031	300	15.062	0.0825	0.0366
4	168.23208	600	30.124	0.0921	0.0817

Table 4.6: Reynolds numbers for the reported experiments using Cornell and Katz model

Test	Pressure Drop Kpa	Gas Flow Rate (cc/hr)	Superficial Pore Velocity of Gas (m/day)	R_e
1	31.85378	75	3.766	1.22
2	58.05387	150	7.531	2.45
3	104.80031	300	15.062	4.90
4	168.23208	600	30.124	9.80

CHAPTER 5

A MECHANISTIC FLOW MODEL FOR FLOW THROUGH A PERFORATION IN THE WELL LINER

5.1 UNIT-CELL (UC)

On the basis of experimental observations[44,45,61] the following behaviour about the flow of gas condensate near the wellbore is assumed to be valid: 1) capillary forces are minimal due to the low values of IFT, 2) gravity segregation is minimal, if any, compared with the high viscous forces and 3) flow can be represented by intermittent gas and condensate flow in pipes where the two phases are not segregated as in Darcy flow and not fully miscible that act as a single phase. As a first attempt, the unit-cell is taken as a small pipe with a radius of R as shown in Fig. 5.1a. Beside simplicity, the reason for choosing the UC to be a small pipe is that there has been a great deal of literature dealing with fluid distributions (fluid patterns) in pipes for a variety of purposes such as studies of heat exchangers and disperse systems. Hence, the available literature can be used to somehow give us starting reasonable fluid distributions (fluid patterns) which describe two-phase flow in small pipes at a specific flow-rate range for the two phases. It should be noted that the developed model is not expected to capture all the physics of gas-condensate flow during the core tests. It should be more applicable to perforated region around the wellbore, where the assumption of a uniform conduit may be reasonable. While the results from this model can be compared with those observed during the core tests, they may not necessarily suggest that the trend in the perforation is the same as that in the core.

5.2 FLUID DISTRIBUTIONS IN UC

To be able to model the coupled flow of gas and condensate mechanistically experimental observations as well as available information in the literature, as stated above, are utilised to resemble a fluid distribution at the pore level. The closer such a fluid distribution to reality, the more successful the model in mimicking the flow of low IFT gas-condensate systems through porous media will be and consequently the better it is in theoretically quantifying the rate effect and predicting relative permeabilities. Accordingly, the second assumption regarding fluid distribution for our mechanistic model is taken. Fig. 5.1b shows the assumed fluid distribution in UC where the condensate phase is flowing as "entrained droplets" in the core flow and as a film in the annular region of the UC. So that there are two separate regions. Flow can be modelled as two concentric cylinders: a two-phase "core flow" region where gas and "entrained droplets" of condensate flow in the inner cylinder as a mixture; and another one phase "annular flow" region where condensate flows as a film in the outer cylinder.

This type of fluid distribution has been known as "Annular-Mist Flow". It has been identified and studied by several workers for high velocity two-phase fluid system flow at high interfacial tensions in small pipes. Collier and Hewitt (1961)[69], in their analysis of the "Annular-Mist Flow" occurring in vertical flow of air-water mixtures in a 1.25 inch plastic tube, observed that the flow in the liquid film initially increases with increasing the overall liquid flow rate, but eventually levels out at a value largely dependent on gas flow rate. They also observed that at high gas flow rates approximately 95 per cent of liquid is carried as "entrained droplets". This was observed earlier by Wicks and Duckler (1960)[74] and then confirmed later by Aziz and Govier (1962)[68] and Gill, Hewitt, and Lacy (1965)[72] in their study of high velocity flow of air-water mixtures in 11/4 inch tube. Eaton, Andrews, Knowles, Silberberg, and Brown (1967)[70] investigated "Annular-Mist Flow" in the flow of natural gas-water, natural gas-crude oil, and natural gas-distillate systems in 2-, 4-, and 17-inch horizontal pipelines. Levy (1966)[73] presented a correlation for estimating the liquid distribution between the film flowing in the "annular flow" region and the entrained droplets flowing in the "core flow" region. His method requires an independent measurement of the pressure-drop and it assumes that the entrainment is caused mainly by turbulence in the part of the film flow. Therefore, to use Levy's method in our mechanistic model approach we have to simplify it so that only the flow rates of the two phases together with fluid properties and UC characteristics are needed to determine the fluid distribution between the film and the entrained condensate droplets.

Most of the workers and investigators have used the "Annular-Mist Flow" to describe the flow of high interfacial tension fluid systems, such as air-water mixtures (IFT about 70 mN/m or more), at very high gas-phase velocities (about 2 to 6 m/s). Some of those correlations and investigations will be the corner stone for our devising a process for predicting relative permeability for low interfacial tension gas-condensate systems using the "Annular-Mist Flow" fluid distribution in a tube. By doing so, we are assuming that for the case of the gas-condensate systems with low IFT values (less than 5 mN/m) such an "Annular-Mist Flow" fluid distribution occurs at much lower gas flow rate than for the high interfacial tension fluid systems. We shall test the validity of such an assumption later.

First, the governing equations of the Mechanistic Model "Annular-Mist Flow" in a small pipe must be derived together with the final expressions for the relative permeabilities of both gas and condensate phases.

5.3 VELOCITY PROFILES IN UC

To find the steady-state velocity profiles of the two regions a shell momentum balance must be taken. A main assumption regarding the behaviour of the two fluids (gas and condensate) is taken when deriving the velocity profiles. This third assumption is that both fluid phases (gas and condensate) behave like a Newtonian fluid; this condition (as defined by Eq. 5.1)[65] governs the relationship between the velocity of each phase and the corresponding perpendicular shear stress. Also, a fourth assumption of no-slip between the phases or between fluids and the boundary of the UC had to be taken when deriving the velocity profiles in the two regions ("core flow" region A and "annular flow" region B of Fig. 5.1b). Hence, the condensate film in the "annular flow" must have a zero velocity at the wall of the UC (r=R); and both the condensate film in the "annular flow" and the mixture in the "core flow" must flow at the same velocity and have the same shear stress at the core-film interface ($r=\kappa R$, with film thickness = $(1-\kappa)R$). The value of the shear stress at the centre is finite. The detailed derivation is given in appendix A and the resultant steady-state velocity profile for the two-phase mixture present in the "core flow" region A is given by Eq. 5.2. The velocity profile for the one-phase "annular flow" region B is given by Eq. 5.3.

$$\tau^{i}_{rx} = -\mu^{i}\left(\frac{dv^{i}_{x}}{dr}\right) \qquad \text{...(5.1)}$$

where,

τ_{rx} : shear stress

μ : fluid viscosity

v_x : fluid velocity in the x direction (Perpendicular to the shear stress propagation)

i : refer to phase or mixture i

The velocity profile in the two-phase mixture presents in the "core flow" region A is:

$$v^{m}_{x} = \frac{\Delta P\, R^2}{4L\,\mu^{m}}\left[\frac{\mu^{m}\left(1-\kappa^2\right)+\mu^{c}\kappa^2}{\mu^{c}} - \left(\frac{r}{R}\right)^2\right];\quad 0 \le r \le \kappa R \qquad \text{...(5.2)}$$

and the velocity profile of the condensate film present in the annulus region B is:

$$v_x^f = \left[\left(\frac{\Delta P\, R^2}{4L\,\mu^c}\right)\right]\left[1-\left(\frac{r}{R}\right)^2\right]; \quad \kappa R \le r \le R \qquad \text{...(5.3)}$$

where,

f, m : refer to film and mixture respectively

ΔP : pressure-drop across the length L of UC (the tube).

v_x^i : x-velocity of phase or mixture i

R : outer radius of the UC.

κ : ($0 \prec \kappa \prec 1$) dimensionless flow radius ratio between the radius "core flow" and the total radius of the UC, assumed to be constant along the perforation length.

c: (superscript) refers to condensate

5.4 FLUXES

The flow rates for both phases in each region can now be calculated by integrating the above velocity profiles over the appropriate limits. To determine the total flow rate associated with each phase for the entire unit-cell the flow rate of each phase resulting from the above integration for "core flow" region A must be added to the corresponding one for the "annular flow" region B. The average velocities (fluxes) of each phase for the entire UC can then be calculated by dividing the total flow rate associated with each phase by cross sectional area of the unit cell. The details regarding the derivation of these equations are given in appendix A. The flow rate of the mixture of entrained condensate droplets and gas flowing in the "core flow" region A is as follows:

$$q^m = \frac{\pi\,\Delta P\, R^4}{8\; L\,\mu^c}\left[2\kappa^2\left(1-\kappa^2\right)+\left(\frac{\mu^c\kappa^4}{\mu^m}\right)\right] \qquad \text{...(5.4)}$$

and the flow rate of the film of condensate flowing in the annulus region B is as follows:

$$q^{f} = \frac{\pi\,\Delta P\,R^{4}}{8\,L\,\mu^{c}}\left(1-\kappa^{2}\right)^{2} \qquad \text{...(5.5)}$$

where,

m: refers to the mixture of gas and condensate flowing in the "core flow" region A.

f: refers to the unentrained condensate film flowing in the annulus region B.

Also the resultant final expressions for the average velocities are as follows:

for the gas phase

$$v_{g} = \frac{\Delta P\,R^{2}}{8\,L\,\mu^{c}\left(1+\omega\,\kappa^{2}\right)}\left[2\kappa^{2}\left(1-\kappa^{2}\right)+\left(\frac{\mu^{c}\kappa^{4}}{\mu^{m}}\right)\right] \qquad \text{...(5.6)}$$

and for the condensate phase

$$v_{c} = \frac{\Delta P\,R^{2}}{8\,L\,\mu^{c}}\left\{\left(\frac{\omega\,\kappa^{2}}{1+\omega\,\kappa^{2}}\right)\left[2\kappa^{2}\left(1-\kappa^{2}\right)+\left(\frac{\mu^{c}\kappa^{4}}{\mu^{m}}\right)\right]+\left(1-\kappa^{2}\right)^{2}\right\} \qquad \text{...(5.7)}$$

where,

ω: volume fraction of the entrained droplets of condensate in the "core flow" region A, assumed to be constant along the perforation length

5.5 RELATIVE PERMEABILITY EXPRESSIONS

To find the expressions for relative permeabilities for the two phases, Eqs. 5.6 and 5.7 are equated to the conventional Darcy's law for two-phase flow in porous media and solved for the relative permeability for each phase. The detailed derivation is given appendix in A; and the resultant relative permeability expressions are: for the gas phase:

$$k_{rg} = \frac{1}{\vartheta_1\left(1 + \omega\kappa^2\right)}\left[2\kappa^2\left(1 - \kappa^2\right) + \left(\frac{\vartheta_1\kappa^4}{\vartheta}\right)\right] \qquad \text{...(5.8a)}$$

and for the condensate phase:

$$k_{rc} = \left\{\left(\frac{\omega\kappa^2}{1 + \omega\kappa^2}\right)\left[2\kappa^2\left(1 - \kappa^2\right) + \left(\frac{\vartheta_1\kappa^4}{\vartheta}\right)\right] + \left(1 - \kappa^2\right)^2\right\} \qquad \text{...(5.9a)}$$

where,

$$\vartheta = \frac{\mu^m}{\mu^g} \quad \text{and} \quad \vartheta_1 = \frac{\mu^c}{\mu^g}$$

ϑ and ϑ_1 are assumed to be constant along the perforation length.

Eqs. 5.8a and 5.9a can be written in terms of conventional measurable quantities such as condensate saturation (S_c). This task can be achieved by realising the following true relationship about the UC (refer to appendix A for derivation):

$$\omega = \frac{\left(S_c + \kappa^2 - 1\right)}{\kappa^2} \qquad \text{...(5.10)}$$

$$\vartheta = \frac{\kappa^2 + \left(\vartheta_1 - 1\right)\left(\kappa^2 + S_c - 1\right)}{\kappa^2} \qquad \text{...(5.11)}$$

Incorporating Eqs. 5.10 and 5.11 into the relative permeability Eqs. 5.8a and 5.9a has resulted in the following expressions for relative permeability of the gas phase and condensate phase respectively:

$$k_{rg} = \frac{1}{\vartheta_1\left(S_c + \kappa^2\right)}\left[2\kappa^2\left(1 - \kappa^2\right) + \left(\frac{\vartheta_1 \kappa^6}{\kappa^2 + \left(\vartheta_1 - 1\right)\left(S_c + \kappa^2 - 1\right)}\right)\right] \qquad \text{...(5.8b)}$$

$$k_{rc} = \left[1 - \kappa^4 + \left(\frac{\vartheta_1 \kappa^6}{\kappa^2 + \left(\vartheta_1 - 1\right)\left(S_c + \kappa^2 - 1\right)}\right)\right] - \left[\vartheta_1 k_{rg}\right] \qquad \text{...(5.9b)}$$

Checking the above relative permeability expressions for the case of one phase flow. For single phase condensate flow κ=0.0 and S_c=1.0 then Eq. 5.8b reduces to 0.0 and Eq. 5.9b reduces to 1.0. For the single phase gas flow κ=1.0 and S_c=0.0 then Eq. 5.8b reduces to 1.0 and Eq. 5.9b reduces to 0.0.

5.6 CALCULATING RELATIVE PERMEABILITIES

The final expressions for relative permeabilities of both gas and condensate phases as represented by Eqs. 5.8b and 5.9b require the knowledge of the dimensionless ratio between the radius of the "core flow" flow and the radius of the UC, referred hereafter by the flow radius dimensionless ratio (κ). To determine the value of κ we use Levy (1966)[73] correlation, also reported by Govier and Aziz (1972)[72], in which they predicted the thickness of the film flow in terms of the total flow rate, the gas flow rate, condensate saturation, fluid properties, and UC characteristics. The simplified Levy's approximation is given by Eq. 5.12 and the detailed simplification of the correlation is given in appendix A. Hence, at any gas and condensate flow rates and condensate saturation, the κ value can be determined. Therefore, the relative permeabilites for the two phases can be calculated using Eqs. 5.8b and 5.9b. Levy's Function can be given in the following form:

$$\kappa = 1 - b.a^{0.05} \quad ...(5.12)$$

where,

$$a = \left[\frac{4\,q\,\mu^e}{A\,R\,\rho^c}\right]^{1/2}\left(\frac{\rho^c}{\rho^g}\right)^{1/3}\left(\frac{1}{q_g}\right), \mathrm{m}^{-2}. \quad ...(5.13)$$

$$\mu^e = S_c\,\mu^c + \left(1 - S_c\right)\mu^g \quad ...(5.15)$$

A: cross sectional area of the pipe, m^2.

q, q_g : total and gas flow rates respectively, m^3/s

b: constant = 0.1122 which takes the units of $m^{0.1}$.

ρ^c, ρ^g: condensate and gas phase density respectively, kg/m^3.

μ^c, μ^g: condensate and gas phase viscosity respectively, Pa.s.

μ^e : average total fluid viscosity as defined by Eq. 5.15, Pa.s.

D (=2R): diameter of the pipe, m.

S_c: condensate-phase saturation, fraction.

A change in gas or condensate flow rate will introduce a change in the parameter "a" which will introduce a corresponding change in "κ". This change in "κ" may or may not result in significant change in the relative permeability values for both gas and condensate phases. This is checked by a sensitivity analysis study (see section 5.7 below).

Calculation Procedure

Step 1: Given: - gas and condensate flow rates.
- condensate-phase saturation.
- viscosities and densities of the two phases.
- UC radius.

Calculate: - flow radius dimensionless ratio κ (Eqs. 5.12 to 5.15)

Step 2: Given: - flow radius dimensionless ratio κ (from Step 1).
- the condensate-phase saturation.
- fluid viscosities.

Calculate: - gas-phase relative permeability (Eq. 5.8b)
- condensate-phase relative Permeability (Eq. 5.9b).

5.7 SENSITIVITY ANALYSIS

To evaluate the applicability of this model a sensitivity analysis is carried out so that the relative permeabilities for the gas and condensate phases were predicted using the above detailed procedure at different flow rates and condensate phase saturation. First, an arbitrary base-case is selected. For this base-case, the relative permeability values are calculated using this procedure for a range of condensate saturation similar to those encountered in steady-state relative permeability experiments at a total flow rate of 105 cc/hr. Second, the total flow rate is increased from 105 cc/hr to 1000 cc/hr then it is increased to 10, 000 cc/hr at constant fractional flow and the relative permeability values are calculated for both cases. The results are shown in Fig. 5.2 for the case total flow rate of 105 cc/hr, the case of 1000 cc/hr, and the case of 10, 000 cc/hr. Third, the gas flow rate is increased ten fold, i.e. from 100 cc/hr to 1000 cc/hr, then it is increased 100 fold to 10, 000 cc/hr, and the relative permeability values are calculated for both cases. The results are shown in Fig. 5.3 for the 100 cc/hr case together with the cases of 10 fold and 100 fold cc/hr.

5.8 ANALYSIS OF RESULTS

From the sensitivity analysis results, as shown in Fig. 5.2 and Fig. 5.3, according to relative permeability values calculated using this mechanistic approach, the increase in total flow rate at a constant fractional flow increases the relative permeability of condensate and decreases the relative permeability of gas. Similarly, the increase in the gas flow rate increases the relative permeability of condensate and decreases the relative permeability of the gas. Furthermore, this relative permeability dependence on flow rate is more pronounced at low condensate saturation than at high condensate saturation especially for the gas phase relative permeabilities. This mechanistic model is able to exhibit a rate effect. The trends of this rate effect describe the trends of the flow of gas-condensate in the perforation of a well liner.

5.9 CONCLUSION RECOMMENDATION

The mechanistic flow model, as represented by the UC and the "Annular-Mist Flow" fluid distribution, is made to describe the flow of gas condensate in the perforation of the well liner. The model shows a rate effect. The resultant trends of such a rate-effect, are not similar to the trends of the experimentally observed rate-effect during the core tests. Therefore, the experimentally observed rate effect may be a characteristic of the gas condensate flow in regions around the wellbore other than the perforations. In these regions, both entrainment and condensate saturation are high at high flow rates and condensate accumulates in such a way does not hinder the flow of the gas phase. Therefore, to result in a rate-effect similar to the experimentally observed one, the flow in a region around the wellbore, other than the perforation region, must be investigated. For the new region, a different unit cell may be used with fluid distribution without entrainment to accurately predict the rate effect associated with the flow of low IFT gas-condensate systems during the core tests.

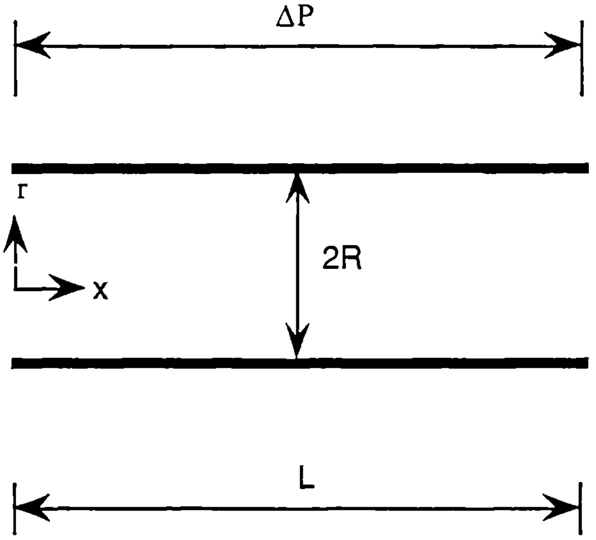

Figure 5.1a: The dimensions of the UC

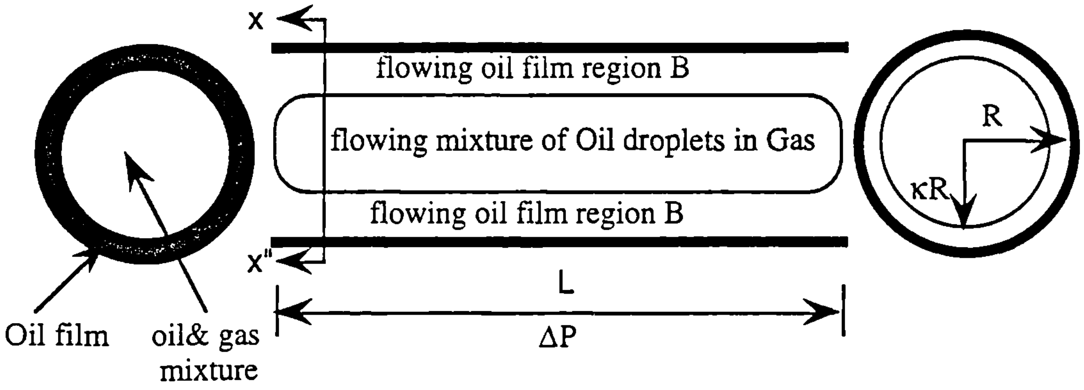

Figure 5.1b: Assumed fluid distribution

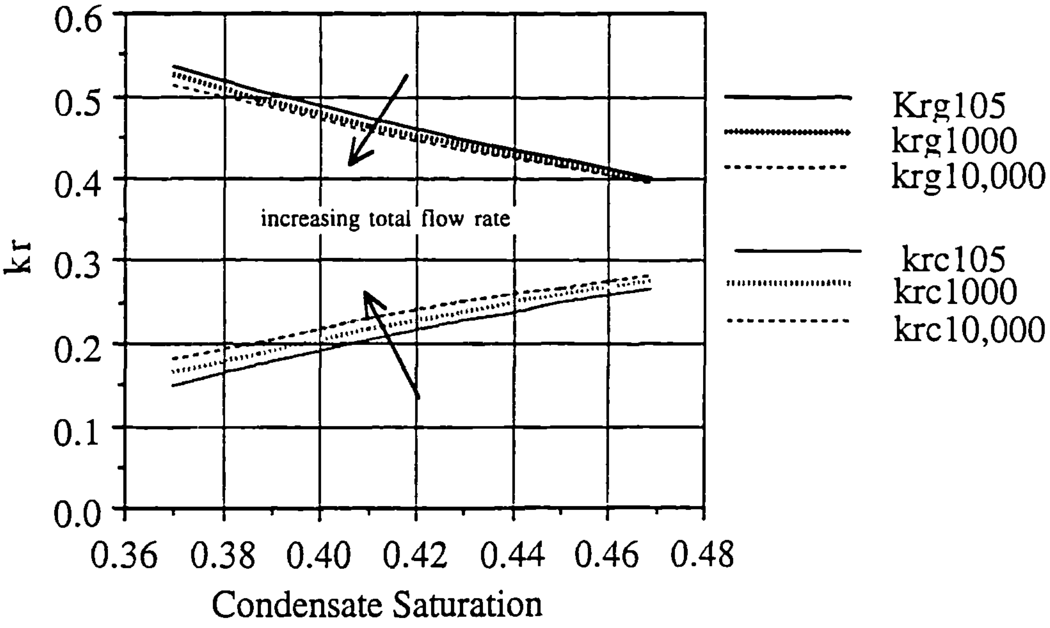

Figure 5.2: Predicted Relative Permeability Curves For Different Total Flow Rates (cc/hr).

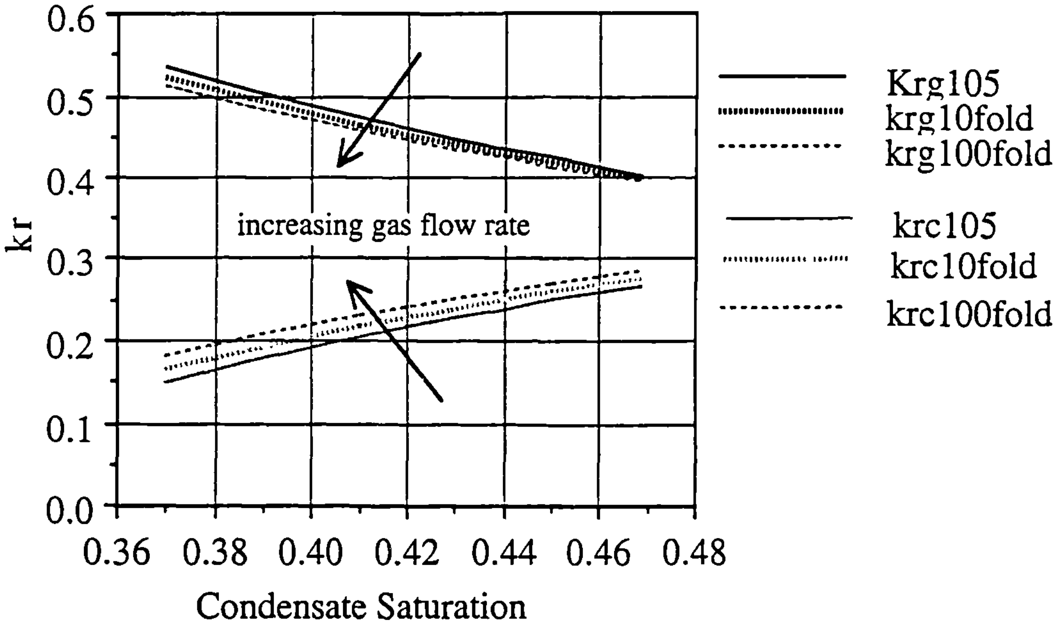

Figure 5.3: Predicted Relative Permeability Curves For Different Gas Flow Rates (cc/hr).

CHAPTER 6

RELATIVE PERMEABILITY CORRELATION

6.1 INTRODUCTION

The dependence of phase relative permeability and residual saturation on IFT had been long observed in laboratory experiments (Moore and Slobod, 1956[76]; Pirson, 1958[77]; Mungan, 1966[78]; Wagner and Leach, 1966[79]; Lefebvre du Prey et al., 1968[80]). Bardon and Longeron (1980)[42] had experimentally validated the strong effect of IFT on the relative permeability in gas-oil binary systems. They conducted unsteady-state measurements at IFTs ranging from 0.0014 mN/m to 12.7 mN/m. Their study and those of Asar and Handy (1988)[39], Hanif and Ali (1990)[40], Gravier et al. (1993)[41], Danesh et al.[28,29,30,31] emphasised the dependence of both the values of relative permeabilities and critical condensate saturation (the minimum condensate saturation required to initiate flow) on IFT especially at low IFT conditions (i.e. less than 0.04 mN/m). Some of those workers even attempted to define a critical IFT value (the IFT value below which such a dependence can not be ignored). Different authors gave different values for the critical IFT because this value depends on, among other factors, the nature of the fluid system used in the study.

Numerous correlations have also been developed for gas-oil or water oil relative permeabilities as a function of IFT (e.g. Coats, 1980[81]; Amaefule and Handy, 1982[82]; Bette et al., 1991[83]; Fultcher et al., 1985[84]; Jankovic, 1985[85]; Pusch and Muller, 1989[86]; Ronde, 1992[87] Hartman and Cullick, 1993[88] and Khazam et al., 1994[75]). Some of these correlations were expressed directly in terms of IFT and others are in terms of a dimensionless quantity referred to as capillary number (N_c). The capillary number represents the ratio between viscous and capillary forces; while it has been expressed in various forms, the following form is the most common:

$$N_c = \frac{v_g \mu_g}{\sigma} \qquad \text{...(6.1)}$$

where,

v_g : interstitial velocity of the gas phase, defined as follow:

$$v_g = \frac{q_g}{A\phi(1 - S_{wi})} \qquad \text{...(6.2)}$$

μ_g : viscosity of the gas phase.

σ : IFT between the oil and gas phases.

One of the earliest attempts to correlate gas-oil relative permeability with IFT is that of Coats (1980)[81]. Coats' correlation (detailed in Eqs. 6.3 to 6.9) was based on the fact that near critical point, interfacial tension between the two phases approaches zero, residual phase saturation decreases toward zero, and relative permeability curves must approach straight lines. Furthermore, his correlation is an intuitive treatment to the observed behaviour and it is not based on any theory or experimental evidence.

$$k_{rg} = k_{rgcw}\left\{f(\sigma)\bar{S}_g^{ng} + [1 - f(\sigma)]\bar{S}_g\right\} \qquad \text{...(6.3)}$$

$$k_{ro} = f(\sigma)\bar{S}_o^{no} + [1 - f(\sigma)]\bar{S}_o \qquad \text{..(6.4)}$$

where,

$$\bar{S}_g = \frac{S_g - S_{gr}^*}{1 - S_{wir} - S_{gr}^*} \qquad \text{...(6.5)}$$

$$\overline{S}_o = \frac{S_o - S^*_{or}}{1 - S_{wir} - S^*_{or}} \qquad ...(6.6)$$

$$f(\sigma) = \left(\frac{\sigma}{\sigma_0}\right)^{1/n_1} \qquad ...(6.7)$$

$$S^*_{gr} = f(\sigma)S_{gr} \qquad ...(6.8)$$

$$S^*_{or} = f(\sigma)S_{or} \qquad ...(6.9)$$

and

σ: interfacial tension (IFT).

s_o: initial interfacial tension(IFT); initial input.

n_1: exponent generally in the range of 4 to 10; initial input.

n_g: Corey's gas saturation exponent; initial input.

n_o: Corey's oil saturation exponent; initial input.

k_{rgcw}: relative permeability to gas at connate water; initial input.

k_{rocw}: relative permeability to oil at connate water; initial input.

S_{wir}: irreducible water saturation; initial input.

S_{or}: residual oil saturation; initial input.

S_{gr}: residual gas saturation; initial input.

Amaefule and Handy (1982)[82] provided a correlation that accommodates the dependence of relative permeabilities of low IFT oil-water systems on IFT. The study used steady- and unsteady-state displacement methods to generate relative permeability curves. By then the advantage of using capillary number rather than IFT to correlate the data was not yet fully realised. Therefore, they related residual saturation, rather than relative permeability as a whole, to the capillary number. This again may be more applicable to oil-water systems than to gas-oil systems or gas-condensate systems.

Fultcher et al. (1985)[84] had stated that the recovery efficiency, hence, relative permeability, was found to be dependent on the capillary number. In their study, they investigated the effect of the capillary number as well as its individual constituents (velocity, viscosity, and IFT) on relative permeability in oil-water systems. They found that the relative permeabilities for both the non-wetting oil phase and the wetting water phase were more function of individual variables rather than the capillary number as a whole. This finding is very much expected for an oil-water system because of the high viscosities of the two phases (0.947 to 954 cp), hence, minimising the changes in capillary number due to change in either IFT or velocity and maximising the changes in capillary number due to changes in viscosity. The critical IFT value was observed to be 2.0 mN/m above this value and no IFT effect was observed. No rate-effect was observed because of the limited range of velocities within this study (4.9 to 24 m/d). Residual oil saturation decreased to approximately zero when the capillary number increased to 0.01. They correlated relative permeability with IFT and viscosity; residual oil saturation with capillary number; and irreducible water saturation with IFT.

Hartman and Cullick (1993)[88] presented a correlation, a mixing function, to represent the dependence of relative permeability on IFT for simulation of gas-oil recovery processes. Both relative permeability and residual oil saturation were represented by the function in terms of IFT. The authors stressed that there was no experimental verification of the proposed empirical relationships. The model was the result of seven slim tube displacement experiments where a set of experimental IFT-depenedent relative permeability curves were developed. Four experiments were conducted using a binary methane/n-butane (C_1/n-C_4) fluid system and the other three were conducted using a ternary carbon dioxide/n-butane/n-decane (CO_2/n-C_4/n-C_{10}). They correlated both the residual oil saturation and relative permeability of both phases directly with IFT. The final form of their correlation was identical to the one proposed by Coats (1980)[81] of course with exponents that fit their own experimental data.

The latest gas-oil relative permeability correlation with IFT was presented by Khazam (1994)[4]. This correlation was also the product of slim tube experiments and it followed a form similar to that of Coats (1980)[81]. Khazam (1994)[4] presented the relationship between the relative permeability of gas-oil systems and IFT as a function of capillary number rather than IFT alone.

The above correlations were developed for either water-oil or gas-oil systems. Hence, such correlations may not be valid for gas-condensate systems because fluid phase properties and phase distribution in pores are much different for those systems than for gas-condensate systems. Furthermore, these correlations, whether they were in terms of IFT or capillary number, were created with experimental data that shows the sensitivity of relative permeability to either IFT or viscosity or both. Non of the above correlations included the experimentally proven velocity dependence of relative permeability.

Following is a correlation for relative permeability of gas-condensate as function of capillary number. The experimental relative permeability data used in achieving this correlation exhibits sensitivity to IFT, viscosity, as well as velocity[44, 45, 61, 62]. Furthermore, the obtained relative permeability correlation is reconciled with other reported low IFT relative permeability measurements. This task involved the collection of published relative permeability data that can be used in our analysis. This task is complicated by the fact that only few workers have experimentally investigated the rate effect and even fewer reported works have included high capillary numbers close to the values achieved during the steady-state experiments at Heriot-Watt University.

6.2 THE CORRELATING PARAMETER

The correlating parameter, the gas phase capillary number (N_c), as given by Eq. 6.1, is chosen because it contains the effects of viscous and capillary forces simultaneously. In this section such a choice will be validated by the actual measured data over the newly extended range of N_c values.

Furthermore, the different forms of N_C are thoroughly investigated to find the most appropriate one. The reason for such an investigation is that the conventional form of the N_C is dependent on the gas phase velocity and viscosity. This may reduce its efficiency when the condensate phase flow becomes significant. Also, Eq. 6.1 does not directly reflect the basic properties (k and ϕ) of the porous medium. This makes the comparison of measured relative permeability data for different rock types difficult. The incorporation of some core properties into the N_C may help define a universal (for all core types) base capillary number above which the relative permeability of the gas and condensate increases with increasing N_C.

Four additional forms of N_C are considered to investigate the possible improvement in correlating the data at the same time incorporating the lithology of the porous medium. These are represented by Eqs. 6.10 to 6.15.

$$N_c = \frac{\sqrt{2\,\phi\,k}\,\Delta P}{\sigma} \qquad \text{...(6.10)}$$

$$N_c = \frac{k\,\Delta P}{\sigma\,L\,\phi} \qquad \text{...(6.11)}$$

$$N_c = \frac{\Delta P}{P_c} \qquad \text{...(6.12)}$$

$$N_c = \frac{4.\mu_g.v_g.L}{\sigma.\sqrt{\dfrac{8k}{\phi}}} \qquad \text{...(6.13)}$$

where,

All in self-consistent units.

k: permeability of porous medium.

ϕ: porosity of porous medium.

$\frac{\Delta P}{L}$: pressure gradient across the porous medium.

P_c: capillary pressure, which is distinctive for every core and every fluid and fluid saturation. For our analysis P_c is represented with the following function, as used by Hagoort (1980)[120]:

$$P_c = \frac{J(S)\,\sigma}{0.46916}\sqrt{\frac{\phi}{k}} \qquad \text{...(6.14)}$$

$$J(S_c) = P_{cb}\left[\frac{(1+c_1-S_c)^{c_2} - c_1^{c_2}}{S_c^{c_3}}\right] \qquad \text{...(6.15)}$$

the units for the terms in Eqs. 6.14 and 6.15 are:

P_c: capillary pressure, Atm.

σ: IFT, mN/m

ϕ: porosity, fraction

k: permeability, darcy.

The constant used for the analysis are those reported for gas condensate system as used in the simulation work of M. Khazam[4]; and they are as follows:

P_{cb}=0.08; C_1=0.095; C_2=-1.8; C_3=0.19

The definition of N_c as given by Eq. 6.12 is dependent on the length of the medium. This might cause problem when comparing data from porous mediums of different length. However, we can overcome this problem by introducing the length of the porous medium in the denominator which makes the dimension of the N_c length^{-1}. The relative permeability data is correlated with N_c ratio rather than N_c which would remove the problem of having a dimensional N_c. In any case, this is not an issue for the time being because in this analysis we are considering the data of the Berea Sandstone core only.

The definition of N_c in Eq. 6.13 was suggested by Kalaydjian et al. (1996)[125] to be a more appropriate correlating parameter for gas condensate relative permeability. On the basis of this definition, the authors claim that only when the value of N_C exceeds 1.0 can the effect of IFT, hence N_C, be observed. Indeed, all the calculated values of this form of N_C for the experiments measured on the Berea Sandstone core are above a value of 2.0. Hence, the claim is supported by this finding yet it is far from being confirmed.

The gas and condensate relative permeability values measured on the Berea Sandstone are plotted against N_C for all the above definitions. The results are shown in Figs. 6.1 to 6.10. As can be seen from these figures all the definitions of the N_C produces similar results for both phases.

The definitions of Eqs. 6.11, 6.12, and 6.13 therefore, offer alternative formulations for N_C which, without compromising the efficiency of the conventional definition of N_C, and incorporate the properties of the porous medium explicitly. Eq. 6.12 requires the additional measurement of the capillary pressure together with relative permeability for a given porous medium. Hence, Eqs. 6.1, 6.11 and 6.13 are the preferred forms for N_C out of the five different forms.

6.3 PROPOSED CORRELATION

6.3.1 Introduction

The gas condensate relative permeability data measured on the Berea Sandstone are taken to be the basis for the correlation because I believe that they are the most reliable and they extend to cover a wide range of N_C values and most importantly all the measured data (i.e. pressure drop, flow rates, phase viscosities, permeabilities, irreducible water saturation, and residual phase saturation) required for our analysis is available.

6.3.2 Methodology

The two stages are involved in correlating the gas condensate relative permeability measured on the Berea Sandstone. They are correlating the phase residual saturation (S_{cr}, and S_{gr}) with N_C and correlating the relative permeability data themselves with N_C. The following two sections detail the above stages:

Correlating Phase Residual saturation

On the basis of experimental observations during the gas-condensate steady-state relative permeability experimental measurements, we believe that the combination of low IFT and high velocity values (i.e. high capillary number values) makes the condensate phase flow continuously as a film, spreading on connate water surfaces. Hence, the critical or residual condensate saturation is zero. This view is supported by many workers as it is evident from the literature review detailed in a later section of this chapter.

The measured gas-phase residual saturation values for different relative permeability curves (i.e. different values of N_C) are correlated with N_C ratio. The base residual gas saturation and the corresponding N_C are that of the curve measured at IFT of 0.78 mN/m and flow rate of 105 cc/hr. (the lowest N_C value). The following two formulations are considered:

$$X_{gr} = \left(\frac{N_{cb}}{N_c} \right)^{\frac{1}{nr}} \qquad \text{...(6.16)}$$

where,

$$X_{gr} = \frac{S_{gr}}{S_{grb}}$$

S_{grb} : gas-phase residual saturation at the base N_C value N_{cb}.

nr: gas-phase residual saturation exponent = 8.0.

or:

$$X_{gr} = 1 - e^{-nr\left(\frac{N_{cb}}{N_c}\right)} \qquad \text{...(6.17)}$$

where,

nr: gas-phase residual saturation exponent = 51.0.

The measured residual gas saturation together with the predicted values using the above two equations are illustrated in Fig. 6.11. As can be seen from this figure, Eq. 6.17 is superior to Eq. 6.16 in predicting the gas-phase residual saturation. Hence, Eq. 6.17 is adopted for the remainder of the analysis in this chapter.

Correlating Relative Permeability Values

In correlating the steady-state gas condensate relative permeability values measured on the Berea sandstone core Coats's formulation that he had proposed for the effect of IFT[81] is adopted. Coats' stated that his correlation is an intuitive one and the exponents have no explicit physical meaning. Furthermore, in Coats formulation, relative permeability values are linearly interpolated between base values and miscible ones. This assumption of linear behaviour has not been proven. Given the extended range of the measured N_c and the corresponding relative permeability data we should be able to validate or provide alternative formulation to Coats'. In other words, we are attempting to incorporate some physical observation / understanding about the flow of gas-condensate systems into the Coats' correlation that may enhance its performance. The two important points that have to be investigated are linearity of the rate of change of the relative permeability and the possibility of the existence of an inflection point (where such a rate of change reaches its maximum) between the base and the miscibility limits.

To have a clearer vision on the behaviour of the slope (rate of change) of relative permeability as a function of N_c, the slope must be investigated at constant phase saturation (as done in the earlier section). Relative permeabilities (k_{rg} and k_{rc}) have been plotted versus N_c at constant phase saturation as shown in Figs. 6.1 to 6.10. Also, they are plotted against N_c ratio (N_{cb}/N_c) as shown in Figs. 6.12 and 6.13. As evident from these figures, at constant condensate saturation, the rate of change, with N_c or N_c ratio, of the relative permeability for both gas and condensate phases is changing considerably between the two limits ($N_c=N_{cb}$ and N_c=infinity). Also, there is no inflection point of such rate of change between the stated limits. Therefore, variation in the rate of change of relative permeability with N_c or N_c ratio and its dependence on phase saturation can be accommodated by the appropriate scale function.

Therefore, the form of the Coats' is simple yet still adequate to correlate gas-condensate relative permeability with capillary number. So that,

$$k_{ri} = X_i . k_{rib} + (1 - X_i). k_{rim} \qquad ...(6.18)$$

where,

i: refers to phase i

k_r: relative permeability

k_{rib}: base relative permeability

k_{rim}: miscible relative permeability:

$$k_{rcm} = S_c \qquad ...(6.19)$$

$$k_{rgm} = \frac{S_g - X_{gr}\, S_{grb}}{1 - X_{gr}\, S_{grb}} \qquad ...(6.20)$$

S_{grb} : critical saturations for the base condensate and gas curves respectively

X_i : relative permeability scale function = f_c (N_{cb} / N_c)

X_{gr} : gas-phase residual saturation scale function , Eq. 6.17.

N_{cb} , N_c: base capillary number and capillary number respectively.

Base values correspond to a set of relative permeability at the lowest N_c.

The relative permeability values versus N_c ratio on log-log scale are shown in Figs. 6.14 and 6.15. The definition of the formulation for the scale function (X_g, and X_c) becomes quite clear. These figures show that relative permeability, hence, the scale functions can be represented as a function of the N_c ratio according to the following two equation:

$$X_i = \left(\frac{N_{cb}}{N_c} \right)^{f(S_i)} \tag{6.21}$$

where,

$$f(S_i) = c_1 S_i^{c_2} \tag{6.22}$$

or

$$f(S_i) = c_1 S_i + c_2 \tag{6.23}$$

The effect of phase saturation is incorporated into the above definitions for the scale functions in the form of Eqs. 6.22 and 6.23.

Eq. 6.21 is used to correlate the relative permeability data together with both Eqs. 6.22 and 6.23. The optimum exponents for the four scale functions are obtained then the functions are used to predict the relative permeability data. The error for every predicted point (E_i) is calculated then the average absolute (E_a) error is calculated for all the points according to the following two equations:

$$E_i = \left(\frac{k_{r(cal.)i} - k_{r(\exp.)i}}{k_{r(\exp.)i}} \right) * \ 100 \tag{6.24}$$

$$E_a = \left(\frac{1}{n} \right) \sum_{i=1}^{n} |E_i| \tag{6.25}$$

where,

n: number of points used in the analysis for all curves at the various IFTs and flow rates.

The average absolute errors for the two different combinations of the scale function for each phase resulted from the above analysis are given in Table 6.1. It is evident from this table that the combination of Eqs. 6.21 and 6.22 predicts the relative permeability values of gas and condensate phases better than the other combination. Therefore, for the two phases the scale function, X_i is:

$$X_i = \left(\frac{N_{cb}}{N_c} \right)^{c_{1i} S_i^{c_{2i}}} \tag{6.26}$$

where,

i: refers to gas or condensate phase.

and,

for condensate phase:

$C_{1c} = 0.1$; $C_{2c} = 1.5$.

for gas phase:

$C_{1g} = 0.06$; $C_{2g} = -0.6$.

Predicted and measured relative permeability values are shown in Figs. 6.16 and 6.17 for the gas and condensate phases respectively.

To appreciate the added efficiency by the introduction of condensate phase saturation into the scale functions the above optimisation process of the scale function are repeated without considering the effect of condensate phase saturation. The following expressions are considered:

$$X_i = \left(\frac{N_{cb}}{N_c} \right)^{\frac{1}{n_i}} \tag{6.27}$$

where,

n_i: constant exponent equals 3.31 and 2.22 for gas and condensate phase respectively.

$$X_i = 1 - e^{-n_i\left(\frac{N_{cb}}{N_c}\right)} \qquad (6.28)$$

where,

n_i: constant exponent equals 0.07 and 0.05 for gas and condensate phase respectively.

The exponents (n_i) for the two phases are calculated for the two formulations of the scale functions. They are used to predict the steady-state relative permeability values for the Berea core and the average absolute errors were calculated using Eqs. 6.24 and 6.25. The results are given in Table 6.2.

It is evident from the values given in Table 6.1 and Table 6.2 that the inclusion of the effect of condensate phase saturation in the scale functions improves the efficiency of the correlation in predicting the steady-state gas condensate relative permeability for the Berea core. The efficiency, in terms of the averaged absolute errors, increases 21% for the gas phase (from 26.81 to 21.82%); and it increases by 25% for the condensate phase (from 19.04 to 15.57 %).

6.4 LITERATURE DATA

6.4.1 Introduction

The relative permeability correlation is based on relative permeability data measured on a single core. It is important that such a correlation is reconciled with relative permeability data reported in literature. There are specific core characteristics, fluid type, experimental setting, experimental procedure, and objectives associated with a specific experimental study of gas-oil and gas condensate relative permeability. Therefore, we do not expect the literature data to perfectly match our data. However, we are seeking to confirm the applicability of our correlation to reasonably predict such data.

Also, by thoroughly examining, the experimental as well as the theoretical investigations of other workers, we seek to improve our understanding of the behaviour of gas-condensate relative permeability in the low IFT domain. By highlighting the different cores' characteristics, fluid types, experimental settings, experimental procedures, and objectives for the different experimental and theoretical studies, we can understand the limitations of each study.

6.4.2 Literature Review

The literature reviewed includes 23 different references [5, 39, 40, 42, 87, 88, 91, 121-136] which either experimentally or theoretically investigate the behaviour of gas-oil or gas condensate relative permeability in the low IFT domain. The detailed review for each source together with the comments on the implication and applicability of each study to our analysis is listed in appendix B.

6.4.3 Discussion

The different studies reported in the literature include steady state and unsteady state measurements of relative permeability for gas-oil and gas-condensate systems. They include depletion, displacement, and two-phase simultaneous injection tests on cores that are dry (with no connate water) or with constant or variable connate water saturations. The core types include sandstone, limestone, and carbonate rocks that cover the Americas, the North Sea, and the Middle East.

While most of the information in these studies is relevant and helpful, in one way or other, to our analysis, there are eight different studies that stand out from the rest because of the proximity of their core characteristics, fluid types, experimental settings, experimental procedures, and objectives to our work. The data generated from these studies can be used in our analysis. The core properties, fluid systems, IFT range, flow rate, the corresponding N_c values, core orientation, number of reported tests, and the effects considered in each study are summarised in Table 6.3. An important fact that must be stated is that not all of the information needed for the analysis, such as flow rate, pressure, phase viscosities, and IFT, are reported in every study. Therefore, some of the information is inferred from other reported information. This makes the task of reconciling the data with the in-house data more difficult. The same information for the data conducted at Heriot-Watt University Petroleum Engineering Department since 1990 is summarised in Table 6.4.

As a summery to the most relevant findings of the literature survey, the following conclusions regarding the relative permeability of gas condensate systems in the low IFT, high N_c, domain can be drawn:

1. Below a certain IFT value (base value), they are dependent on IFT.

2. No real effort reported that can give conclusive base IFT value, however, it is believed to be in the range of 0.05 to 1.0 mN/m. It is most probably dependent on rock and fluid properties.

3. Above a certain combination of low IFT and high flow rate value (base N_c value), they are dependent on N_c (rate effect). This effect is more pronounced at higher condensate saturations than at low ones.

4. No work reported a base N_c value because this will depends on the definition of the N_c , however, by considering the definitions given by Eq. 6.1 and 6.11, its value maybe as low as 6.6×10^{-7} and 4.2×10^{-6} respectively. Also according to Eq. 6.13 it may take a value of 1.0.

5. N_c is a better indicator and a correlating parameter of relative permeability than IFT, because it incorporates both IFT and velocity effects simultaneously.

6. The relationship of gas condensate relative permeability with saturation does not necessarily follow the Corey's type.

7. Temperature effect on the measured values of relative permeability may exist but can be considered negligible (Gravier et al.[41] measured relative permeability at temperature between 70 and 130 °C with limited correction for temperature).

8. Condensate can flow at low condensate saturation, when N_c is high[39,130,40].

9. Gas phase relative permeability is considerably reduced by condensate accumulation.

10. Gravity can have strong influence on relative permeability when viscous and capillary forces are low[128, 40].

11. Straight line relative permeability as a function of saturation are expected at miscibility conditions, IFT = 0 or N_c = infinity.

12. Viscous forces dominate over gravity and capillary forces in the low IFT domain[125,127].

6.4.4 Correlating The Data

The first task in the analysis is to plot all the data, the in-house data for the Berea and the Clashach, and the data gathered from the literature on a single figure to determine the possibility of correlating the data using a single base curve. The trend of the data with N_c (as defined in Eqs. 6.1,6.11, and 6.13) is analysed by plotting all the data on normal and log-log scales for the three constant saturation levels (Sc=0.356, 0.45, and 0.55). The trend is found to be the same at the three different saturation levels. Based on Eq. 6.1 the trend is illustrated in Figs. 6. 18 to 6.21 for condensate saturation of 0.356. Based on Eq. 6.11 it is also illustrated in Figs. 6.22 to 6.25 for condensate saturation of 0.55. Also based on Eq. 6.13 it is illustrated in Figs. 6.26 to 6.29 for condensate saturation of 0.45. The plotted line, in all these figures, shows the trend of the Heriot-Watt Berea data and it indicates that these data are representative of almost all the literature data. The analysis has led to the following observations (also it can be seen clearly in the above figures):

* A single base curve cannot be used to correlate and predict all the data from the different cores. Therefore a separate correlation must be obtained for the different cores.

* data that incorporate either IFT ,or velocity effects or both shows a trend identical to Eq. 6.26 where the exponents C_1 and C_2 naturally depend on, among other things, core and fluid properties, experimental procedure, and the steady-state criteria employed during the test.

* All the three forms of N_c are comparatively similar in their efficiency in correlating data measured on a single core for all the literature data.

To correlate the literature data, including the data of the steady state measured in-house on the Clashach core, a consensus must be reached on the a value for the base N_c. This must be established from the relative permeability measurements that show neither IFT nor velocity dependence (i.e. no N_c dependence). At this point we can not give a single value for the base N_c which will be suitable for all the cases considered here because in all the above studies there was no effort reported to experimentally define either an IFT or N_c base values. However, based on the definition of N_c as given by Eq. 6.13, Kalaydjian et al.[125] suggested that relative permeability becomes sensitive to N_c at values equal to 1.0. In all the literature data analysed in this work the calculated values are in the range of 2.0 to 3474 and they all showed IFT or rate effect.

In correlating the data we assumed that all the reported data that show dependence of N_c is above the base values. Hence, for every set of data reported for a single core, the lowest N_c and the corresponding relative permeability curve are taken as base values. Therefore, the data from each source is correlated independently and the exponents for Eq. 6.26 are calculated. The results are shown in Table 6.5. The resultant equations are used to predict relative permeabilities for both the gas and the condensate for each literature source. The predicted as well as the measured data for all the sources are shown in Figs. 6.30 to 6.37.

For the condensate phase, the exponent C_1, and C_2 are found to in the range of 0.1 to 0.59 and 0.41 to 1.6 respectively for all the correlated data. For the gas phase C_1, and C_2 are in the range of 0.001 to 2.72 and -2.2 to 1.0 respectively.

6.4.5 Error Analysis

The absolute error is calculated for each predicted data point then the average error is taken for each source according to Eqs. 6.24 and 6.25. The averaged absolute errors of all the data points of each source are given in Table 6.6. According to this table the correlation is capable of predicting the literature data with efficiency greater or equal to the efficiency of the correlation in predicting the in-house relative permeability measured on the Berea Sandstone core.

6.5 RECONCILING THE DATA

To reconcile all the relative permeability data the exponent C_2 in Eq. 6.26 is assumed to be equal to 1.0 for all the cores. This value is chosen as an average value from the calculated values obtained in the previous section. Hence, Eq. 6.26 is simplified, having only one exponent (n_i), to the following form:

$$X_i = \left(\frac{N_{cb}}{N_c}\right)^{n_i S_i} \qquad \text{...(6.29)}$$

The second exponent n_i for both phases in every data source is calculated. The variation of the exponent is investigated as a function of some core properties such as porosity and permeability. First the exponent is investigated as a function of the pore-size distribution index (R) using the definition suggested by Kalaydjian et al.[125] where,

$$R = \sqrt{\frac{8k}{\phi}} \qquad ...(6.30)$$

The calculated exponent plotted against R as shown in Fig. 6.38. This figure shows that there is no clear relationship between the exponent and R.

The variation of these exponents is also investigated as a function of another form of the pore-size distribution index (λ), where λ is defined by the slope of the capillary pressure curve on the log-log plot; so that,

$$\lambda = \frac{\Delta \ell n\left(\frac{P_c}{P_{cb}}\right)}{\Delta \ell n(S_c)} \qquad ...(6.31)$$

Since we do not have the capillary pressure curves for the different data, the λ index is back calculated from the relationship given between the λ index and Corey's relative permeability exponent proposed by Brook and Corey in 1964 and detailed by Dullien(1992)[46] and Honapour et al.(1986)[142]. For the base gas phase relative permeability curve (k_{rgb}) the relationship is defined by the following expression:

$$k_{rgb} = \left[1-(S_c)_{eff}\right]^2 \left\{1-\left[(S_c)_{eff}\right]^{\frac{2+\lambda}{\lambda}}\right\} \qquad ...(6.32)$$

where,

$$(S_c)_{eff} = \frac{S_c - S_{wi}}{1 - S_{wi}} \qquad ...(6.33)$$

S_{wi}: wetting phase irreducible saturation.

As shown in Fig. 6.39 the straight line relationship between both the exponents and the pore-size distribution index is evident and the equation for this line is given for both phases as follow:

The condensate phase exponent (n_c) can be calculated as follow:

$$n_c = 0.089\ \lambda + 0.101 \qquad \text{...(6.34)}$$

Also the gas phase exponent (n_g) can be calculated as follow:

$$n_g = 0.934\ \lambda - 1.128 \qquad \text{...(6.35)}$$

6.6 THE FINAL FORM

Therefore, the final form of the relative permeability correlation for gas condensate system, proposed in this work, is as follows:

$$k_{ri} = X_i . k_{rib} + (1 - X_i) . k_{rim} \qquad \text{...(6.18)}$$

where,

i: refers to condensate phase (c), or gas phase (g).

k_r: relative permeability

k_{rib}: base relative permeability

k_{rim}: miscible relative permeability:

$$X_i = \left(\frac{N_{cb}}{N_c} \right)^{n_i\ S_i} \qquad \text{...(6.29)}$$

$$n_c = 0.089\ \lambda + 0.101 \qquad ...(6.34)$$

$$n_g = 0.934\ \lambda - 1.128 \qquad ...(6.35)$$

$$k_{rcm} = S_c \qquad ...(6.19)$$

$$k_{rgm} = \frac{S_g - X_{gr}\ S_{grb}}{1 - X_{gr}\ S_{grb}} \qquad ...(6.20)$$

$$X_{gr} = 1 - e^{-nr\left(\frac{N_{cb}}{N_c}\right)} \qquad ...(6.17)$$

S_{grb} : critical saturations for the base gas curves

nr: = 51.

The above procedure is used to calculate the exponents (n_g and n_c) and then predict the relative permeability data for the different sources. The exponents are given in Table 6.7. The average absolute relative error is also calculated, using Eq. 6.24 and 6.25, and the resultant errors are given in Table 6.8. As can be seen from these error values, the correlation predicted the data effectively.

6.7 CONCLUSION

Five different forms of N_c definitions are analysed and their efficiencies are compared. All the forms are found to be competitive in efficiently correlating the data, however for the sake of consistency when comparing the data from different cores, the N_c definitions as given by Eqs. 6.11 and 6.13 are preferred.

The residual gas saturation for steady-state data is correlated with N_c ratio. Two different forms for the correlation are considered and the exponential form (as given by Eq. 6.17) is found to be the more efficient one.

The behaviour of the steady-state relative permeability data with N_c is analysed and the Coats' IFT model is found to be suitable form for correlating such data. The function as given by Eq. 6.26 is inferred from the analysis of the relative permeability data to be the suitable scale function for both condensate and gas phases.

A comprehensive literature review has been carried out to reconcile the newly found correlation with data from different cores. The major findings resulted from the survey are summarised.

The steady-state relative permeability data found in literature as well as those measured in-house on the Clashach core have been correlated with N_c ratio. It is found that Eq. 6.26 predicts gas and condensate relative permeability reasonably well. The exponents of this equation are calculated for the different reported data. It is found that for the condensate phase, the exponent constants C_1, and C_2 fall in the range of 0.1 to 0.59 and 0.41 to 1.6 respectively and for the gas phase C_1, and C_2 are in the range of 0.03 to 2.72 and -0.7 to 1.0 respectively. These ranges in the exponent values are reasonable and can be explained by the difference in core characteristics and fluid types.

The number of exponents in the Eq. 6.26 is reduced to one. It is demonstrated that this exponent can be related to the pore-size distribution index for the given core. The straight line equation that defines this relationship is determined for both phases and the final form for the relative permeability correlation is realised. A further error analysis using the final form of the correlation demonstrated the efficiency of the such a correlation.

The λ equations (Eqs. 6.33 and 6.34) can be defined further if a value for the base capillary number is established experimentally. The literature data together with the in-house ones support the stipulation of Kalaydjian et al[125] of the existence of such a value that is equal to 1.0 when N_c is defined by Eq. 6.13 (i. e. all the calculated values where N_c dependence is observed are greater than 1.0). According to this concept we can observe no N_C dependence if the relative permeability are measured on the Berea core at a flow rate of less than 50 cc/hr at an IFT of 0.78 mN/m.

Table 6. 1: Average absolute errors for predicted steady-state gas and condensate relative permeability data measured on Berea Sandstone core phase saturation effect is included

Scale Function	Condensate		Gas	
	$f(S_c) = c_1 S_c^{c_2}$	$f(S_c) = c_1 S_c + c_2$	$f(S_c) = c_1 S_c^{c_2}$	$f(S_c) = c_1 S_c + c_2$
	%	%	%	%
$X_i = \left(\frac{N_{cb}}{N_c}\right)^{f(S_c)}$	15.57	17.60	21.82	25.40

Table 6. 2: Average absolute errors for predicted steady-state gas and condensate relative permeability data measured on Berea Sandstone core phase saturation effect is not included

Scale Function	Condensate	Gas
	%	%
$X_i = \left(\frac{N_{cb}}{N_c}\right)^{\frac{1}{n_i}}$	19.04	36.10
$X_i = 1 - e^{-n_i\left(\frac{N_{cb}}{N_c}\right)}$	95.3	26.81

Table 6.3a: Summary of experimetal data of low IFT gas-condensate or gas-oil systems from literature

Ref. No.	Year	Author	Core	Properties				Fluid	System		IFT	Flow Rate	Nc1	Nc2	Core Posit.	Method	No. of Tests	Effects Considered
			Type	ϕ	k	L	D	Comp.	Temp.	water								
				%	mD	cm	cm		^oC	%	mN/m	cc/hr	E-4					
42	1980	Bardon and Longeron	Fontainebleau	9.9	82	38.2	5.0	C1-nC7	71.1	0	0.02 - 12.62	34 - 40	0.0005 - 0.38	0.0005 - 38.0	V	USS	6	IFT
								C1-nC10	37.7		12.5	36.07	0.0006	0.0024-0.06			1	IFT
41	1986	Gravier et al.	Packstone Carbonate	25.8	17.2	20.21	6.6	C1-nC5-nC9	70-130	29.0	1.0	123.1	0.011	0.03-0.7	H	SS	7	Scc , IFT, and k
				16.5	0.37	13.1	6.6			23.0			0.015	0.03-2.1			6	
				22.7	31.8	17.3	6.6			30.0			0.013	0.03-0.4			7	
				18.6	6.0	19.5	6.6			22.2			0.014	0.03-1.0			8	
				19.6	39.2	21.5	6.6			19.5			0.012	0.02-0.4			7	
				19.6	7.4	19.9	6.6			22.5			0.014	0.03-1.0			8	
				23.4	14.5	16.6	6.6			24.3			0.012	0.03-0.4			6	
				14.5	0.90	15.6	6.6			25.4			0.021	0.03-0.4			10	
39	1988	Asar and Handy	Fired Berea Sandstone	20.0	193.0	30.0	5.0	C1-C3	21	0	0.03	260.0	1.06	2.9-3.6	H	SS	4	IFT
											0.18	340.0	0.2	0.5-1.4			7	
											0.43	280.0	0.02	0.2-1.8			6	
											0.82	120.0	0.014	0.1-0.6			5	

Keys: Gas Capillary Number ($N_{c1} = \frac{\mu_g v_g}{\sigma}$), Total Capillary Number ($N_{c2} = \frac{k \Delta P}{\sigma L}$), Vertical (V), Horizontal (H), Steady-State (SS), Unsteady-State (USS).

Table 6.3b: Summary of experimetal data of low IFT gas-condensate or gas-oil systems from literature

Ref. No.	Year	Author	Core	Properties				Fluid	System		IFT	Flow Rate	Nc1	Nc2	Core Posi.	Method	No. of Tests	Effects Considered
			Type	ϕ	k	L	D	Comp.	Temp.	water								
				%	mD	cm	cm		^oC	%	mN/m	cc/hr	E-4					
43	1989	Munkerud	Berea Sandstone	15.3	220.0	50.0	5.08	C1-C2-C3-nC6-nC10	41	0	0.04-	67.9-216.8	≤ 0.43	≤ 0.585	H	USS (Depl.)	8	IFT, Rate
					220.0					0	0.04	138.6	0.897	0.96-1.7		USS (Displ.)	1	
					150.0					30	0.07-	13.4-97.2	≤ 0.04	≤ 0.116		USS (Depl.)	8	
					150.0					30	0.07	141.0	0.455	0.51-1.8		USS (Displ.)	1	
					220.0					0	0.09-	76.9-157.9	≤ 0.02	≤ 0.159		USS (Depl.)	8	
					220.0					0	0.09	133.8	0.312	0.39-3.5	V	USS (Displ.)	1	
40	1990	Haniff and Ali	Spynie Sandstone	22.0	23.0	15.0	5.0	C1-C3	31.7	0	0.001	10.0	1.36	4.4-17.6	H	SS	6	IFT
											0.01		0.144	0.50-2.6			6	
											0.05		0.028	0.11-1.0			6	
											0.1		0.0140	0.06-1.0			6	
											0.2		0.0070	0.04-0.8			6	
126	1994	Bourbiaux and Limborg	Palatinate Sandstone	19.3	4.1	38.4	A = 10.2 cm^2	C1-C3	37.8	16 - 23	0.03	10.0	1.725	≤6.9	H	USS	6	IFT
										22	0.37		0.112	≤1.0		SS	1	
										16.6	0.03		0.1064	0.699			1	
										16.2	0.37		0.0069	0.109			1	

Keys: Gas Capillary Number ($N_{c1} = \frac{\mu_g v_g}{\sigma}$), Total Capillary Number ($N_{c2} = \frac{k \Delta P}{\sigma L}$), Vertical (V), Horizontal (H), Steady-State (SS), Unsteady-State (USS).

Table 6.3c: Summary of experimetal data of low IFT gas-condensate or gas-oil systems from literature

Ref. No.	Year	Author	Core	Properties				Fluid	System		IFT	Flow Rate	Nc1	Nc2	Core Posit.	Method	No. of Tests	Effects Considered
			Type	ϕ	k	L	D	Comp.	Temp.	water								
				%	mD	cm	cm		^oC	%	mN/m	cc/hr	E-4	E-4				
41	1995	Chen et al.	Composite core A	17.4	73.39	73.28	3.81	Real	121.1	20.9	0.025 - 0.35	20.0 - 160.0	0.03-7.81	0.65-12.56	H	SS	40	Rate, IFT
			Composite core B	18.5	11.76	73.67	3.81	Real	126.1	21.5	0.007 - 0.42	20.0 - 160.0	0.122-22.48	1.77-33.08			42	
125	1996	kalaydjian et al.	Palatinate Sandstone	19.3	4.1	38.4	A = 10.2 cm^2	C1-C3	37.8	11.4 - 16.2	0.03 - 0.80	10.0	.00001 - 0.10	0.0002-0.4	H	SS	8	Rate
										11.4 - 24.3	0.03 - 1.41					USS (Drain.)	11	
								C2-C3-C7		11.4	1.33					SS	2	
											1.33					USS (Drain.)	4	
								Real GCS			0.033					SS	2	
											0.12 - 1.0					USS (Drain.)	2	
			Belgium Chalk	39.9	2.0	34.0	A = 9.61 cm^2	C1-C3		6.0	0.134					USS	1	
											0.134					SS	1	
											0.37					USS	1	
											0.37					USS	1	

Keys: Gas Capillary Number ($N_{c1} = \frac{\mu_g v_g}{\sigma}$), Total Capillary Number ($N_{c2} = \frac{k \Delta P}{\sigma L}$), Vertical (V), Horizontal (H), Steady-State (SS), Unsteady-State (USS).

Table 6.4: Summary of experimetal data of low IFT / high capillary number gas-condensate systems performed in-house

No.	Year	Author	Core Properties					Fluid System			IFT	Flow Rate	Nc1	Nc2	Core Posit.	Method	No. of Tests	Effects Considered
			Type	ϕ	k	L	D	Comp.	Temp.	water								
				%	mD	cm	cm		^oC	%	mN/m	cc/hr	E-4	E-4				
1	1990 - 1993	Heriot - Watt University	Berea Sandstone	19.9	120	61.0	5.02	C1-nC3-nC5-nC10-nC16	37	30.0	0.05	10.0-400.0	0.1-4.1	0.4-14.2	H	SS (end points)	6	Rate, IFT, k
													0.097-3.89	0.215-9.36		USS (Displ.)	3	
											0.40	10.0-400.0	0.01-0.4	0.07-5.2		SS (end points)	6	
												10.0 - 100.0	0.006-0.061	0.039-1.424		USS (Displ.)	2	
2	1993 - 1996	Heriot - Watt University	Berea Sandstone	18.2	92	61.0	5.1	C1-nC4	37	26.4	0.037	105.0-840.0	0.47-5.12	1.0-13.71	H		23	Rate, IFT
											0.135	105.0-840.0	0.16-1.30	0.956-6.874			26	
											0.37	105.0-840.0	0.046-0.432	0.156-4.470			21	
											0.78	105.0-840.0	0.017-0.176	0.241-1.559			28	
			Clashach Sandstone	11.6	120	87.5	4.95	C1-nC4	37	15.3	0.041	105.0-420.0	0.59-3.28	2.161-8.310			18	
3	1996 -	Heriot - Watt University	Berea Sandstone	18.2	92	61.0	5.1	C1-nC4	37	26.4	0.015	105.0-840.0	1.240-13.402	2.455-30.52	H	SS	19	Rate, IFT

Keys: Gas Capillary Number ($N_{c1} = \frac{\mu_g v_g}{\sigma}$), Total Capillary Number ($N_{c2} = \frac{k \Delta P}{\sigma L}$), Vertical (V), Horizontal (H), Steady-State (SS), Unsteady-State (USS).

Table 6.5: Exponents for predicting steady-state gas and condensate relative permeabilities for various cores found in literature

Source of Data	Gas Phase		Condensate Phase	
	c_1	c_2	c_1	c_2
Heriot-Watt (Berea Sandstone)	0.25	1.0	0.1	1.5
Heriot-Watt (Clashach Sandstone)	0.76	0.91	0.14	1.13
Asar and Handy(1988)[39] (Fired Berea Sandstone)	0.14	-1.24	0.5	1.60
Hanif and Ali (1990)[40] (Spynie Sandstone)	2.13	-0.19	0.59	1.25
Chen et al.(1995)[127] (Composite core B)	0.53	0.54	0.47	0.41

Table 6.6: Average absolute errors for predicted steady-state gas and condensate relative permeabilities for various cores found in literature

Source of Data	Gas Phase	Condensate Phase
	%	%
Heriot-Watt (Berea Sandstone)	21.82	15.57
Heriot-Watt (Clashach Sandstone)	8.17	0.07
Asar and Handy(1988)[39] (Fired Berea Sandstone)	3.97	15.52
Hanif and Ali (1990)[40] (Spynie Sandstone)	0.42	7.73
Chen et al.(1995)[127] (Composite core B)	6.40	0.98

Table 6.7: The final exponents for predicting steady-state gas and condensate relative permeabilities for various cores found in literature

Source of Data	Gas Phase	Condensate Phase
	c_1	c_1
Heriot-Watt (Berea Sandstone)	0.246	0.06
Heriot-Watt (Clashach Sandstone)	0.801	0.13
Asar and Handy(1988)[39] (Fired Berea Sandstone)	0.587	0.32
Hanif and Ali (1990)[40] (Spynie Sandstone)	4.485	0.48
Chen et al.(1995)[127] (Composite core B)	0.707	0.76

Table 6.8: The final average absolute errors for predicted steady-state gas and condensate relative permeabilities for various cores found in literature

Source of Data	Gas Phase	Condensate Phase
	%	%
Heriot-Watt (Berea Sandstone)	24.75	15.52
Heriot-Watt (Clashach Sandstone)	8.20	0.24
Asar and Handy(1988)[39] (Fired Berea Sandstone)	3.68	17.28
Hanif and Ali (1990)[40] (Spynie Sandstone)	0.65	7.4
Chen et al.(1995)[127] (Composite core B)	6.36	1.88

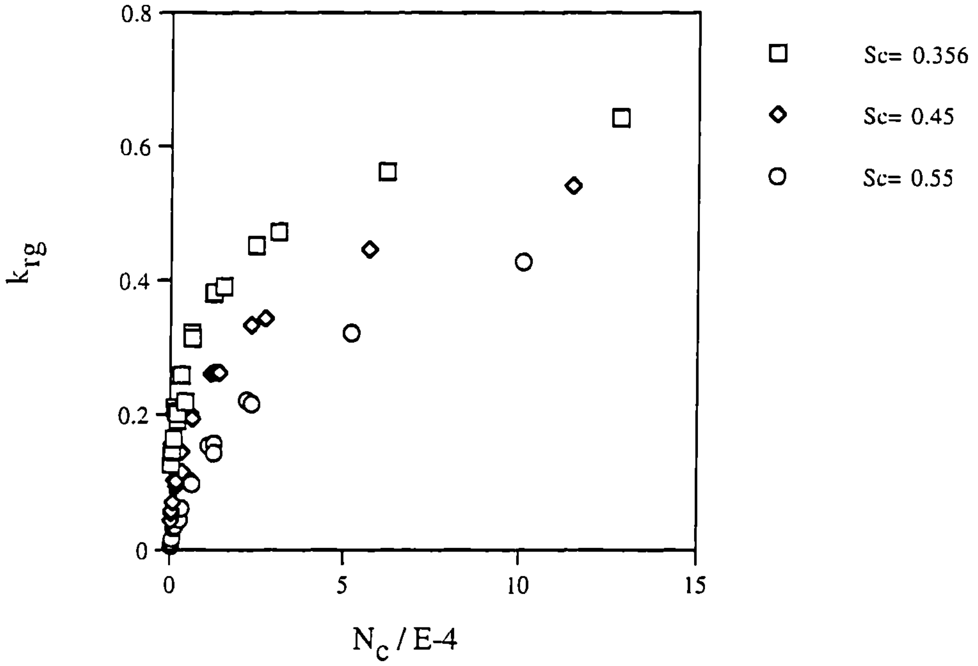

Figure 6.1: The variation of gas relative permeability with capillary number at selected constant phase saturations for all steady-state experiments measured on Berea core, Nc = $\mu_g v_g / \sigma$.

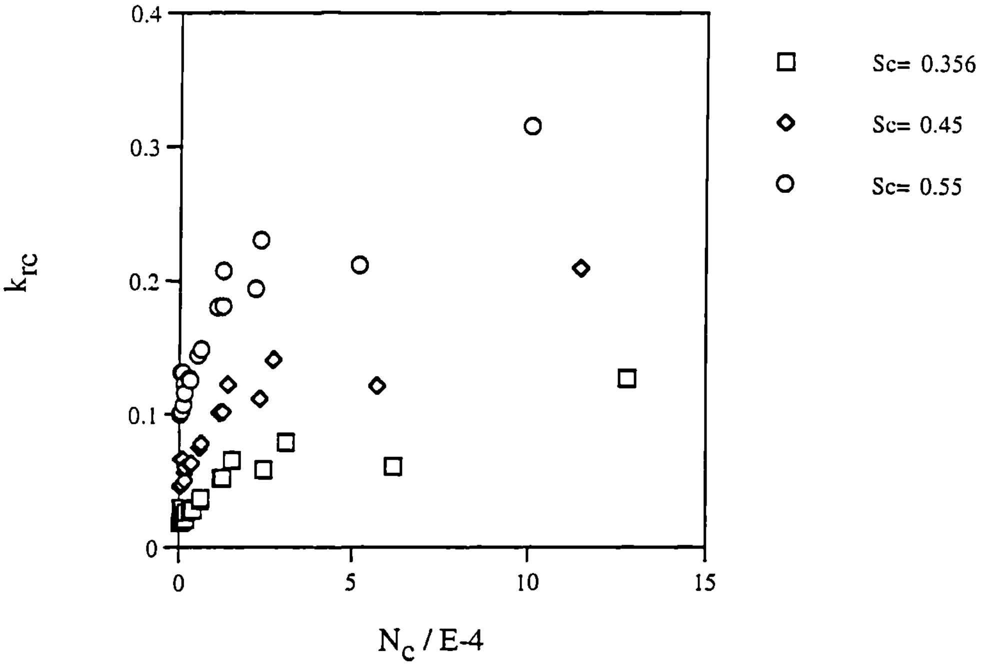

Figure 6.2: The variation of condensate relative permeability with capillary number at selected constant phase saturations for all steady-state experiments measured on Berea core, Nc = $\mu_g v_g / \sigma$.

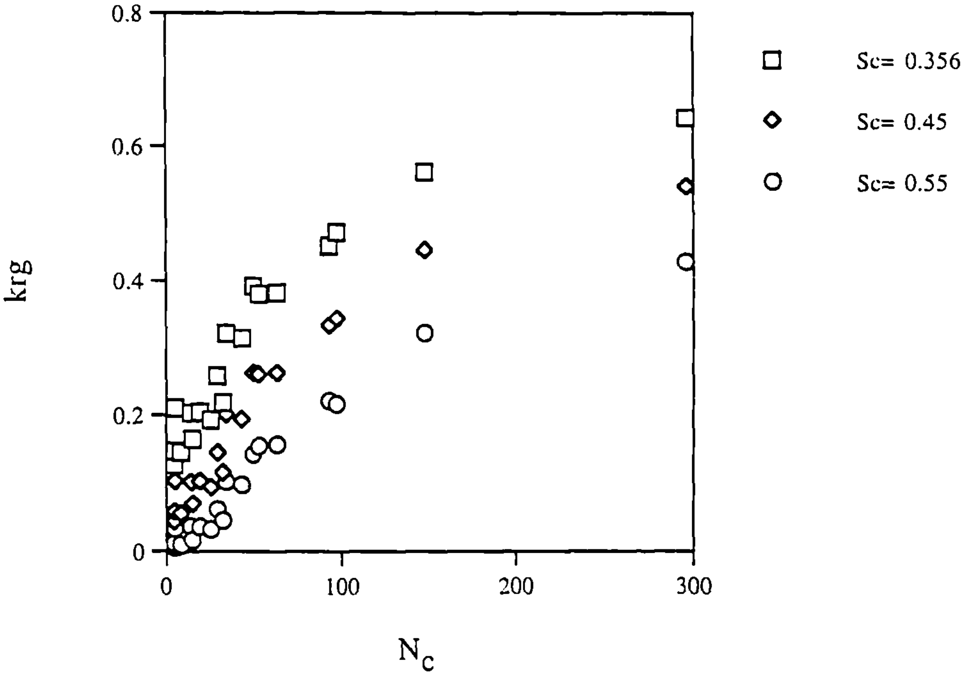

Figure 6.3: The variation of gas relative permeability with capillary number at selected constant phase saturations for all steady-state experiments measured on Berea Sandstone core, $N_c = \Delta P.(2\ \phi\ k\ )\char94 0.5\ /\ \sigma$.

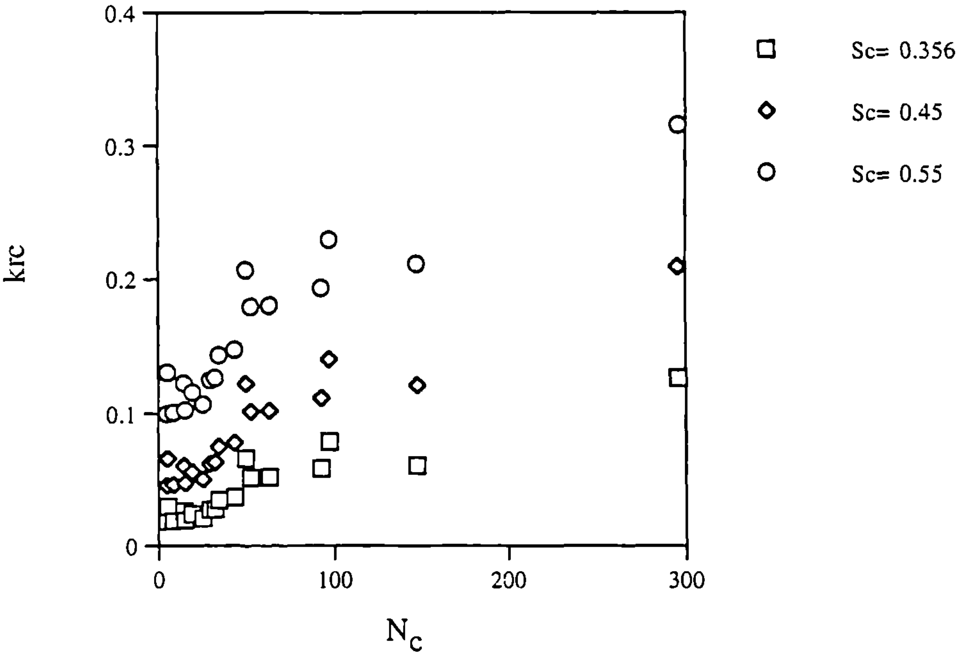

Figure 6.4: The variation of condensate relative permeability with capillary number at selected constant phase saturations for all steady-state experiments measured on Berea Sandstone core, $N_c = \Delta P.(2\ \phi\ k\ )\char94 0.5\ /\ \sigma$.

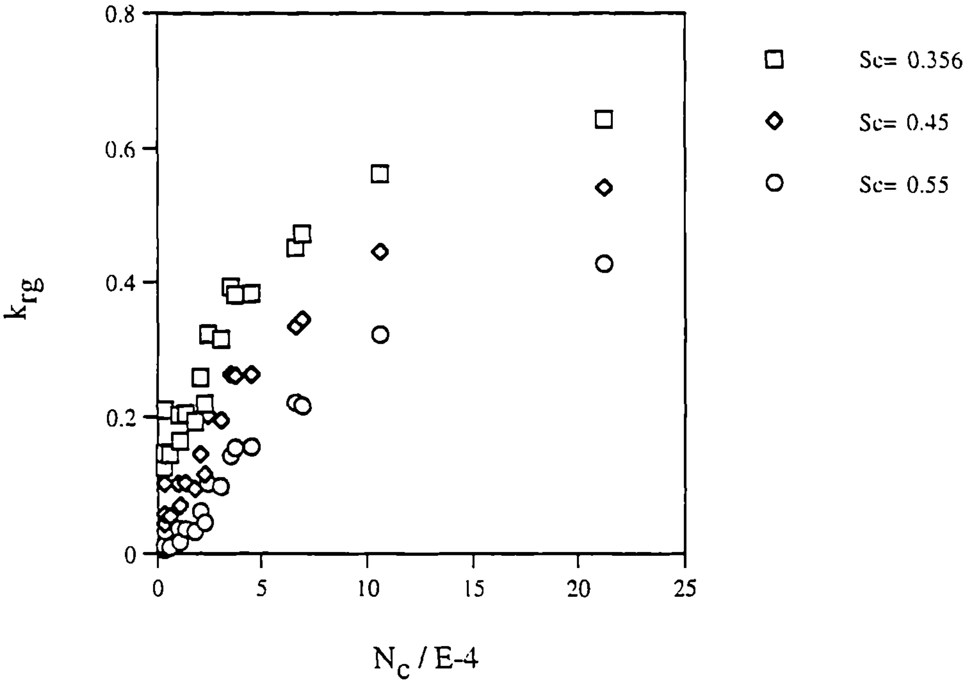

Figure 6.5: The variation of gas relative permeability with capillary number at selected constant phase saturations for all steady-state experiments measured on Berea Sandstone, $N_c = (\Delta P.\ k)\ /\ (\phi.\ \sigma.\ L)$.

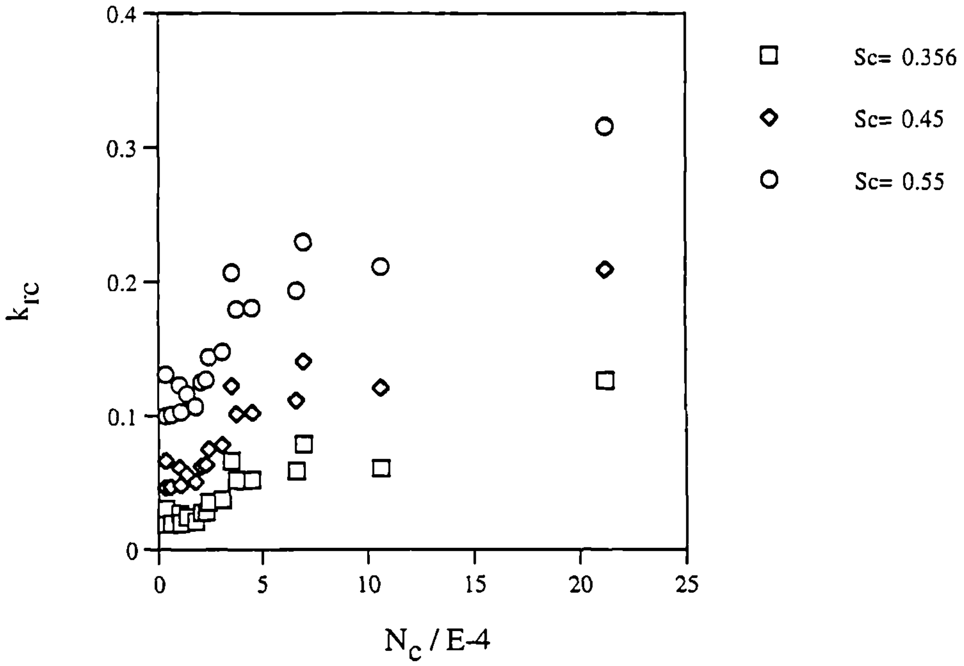

Figure 6.6: The variation of condensate relative permeability with capillary number at selected constant phase saturations for all steady-state experiments measured on Berea Sandstone, $N_c = (\Delta P.\ k)\ /\ (\phi.\ \sigma.\ L)$.

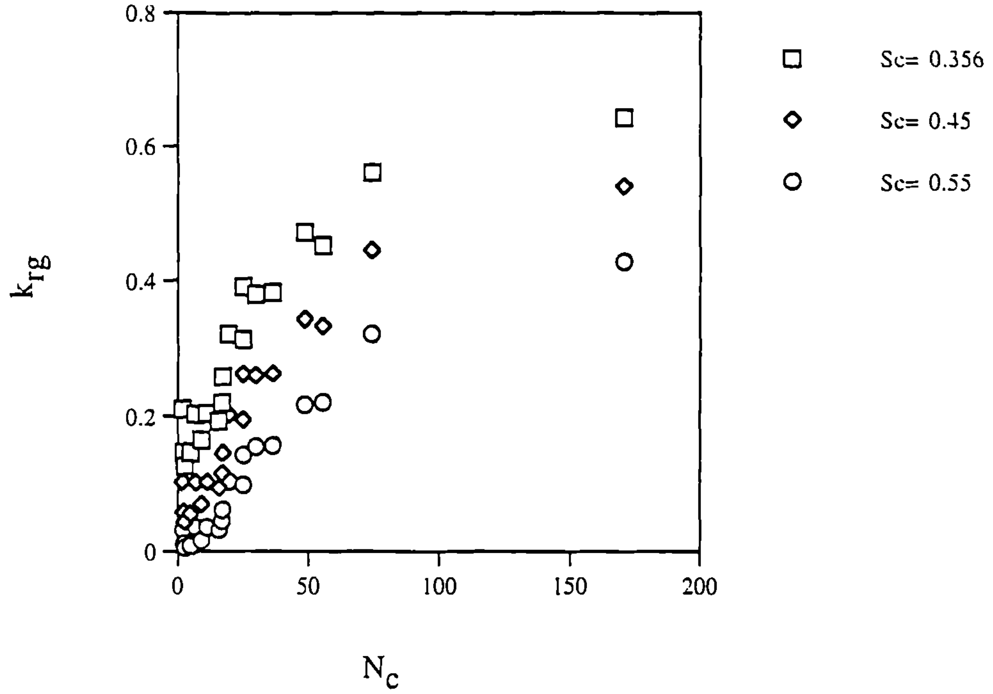

Figure 6.7: The variation of gas relative permeability with capillary number at selected constant phase saturations for all steady-state measured on Berea core experiments, $N_c = \Delta P / P_c$.

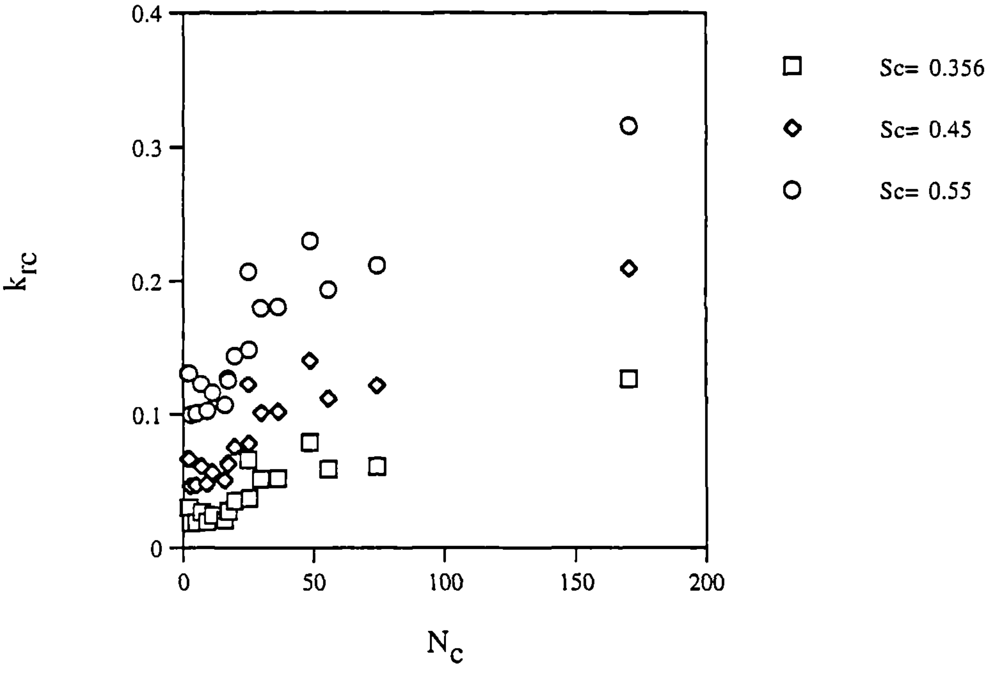

Figure 6.8: The variation of condensate relative permeability with capillary number at selected constant phase saturations for all steady-state measured on Berea core experiments, $N_c = \Delta P / P_c$.

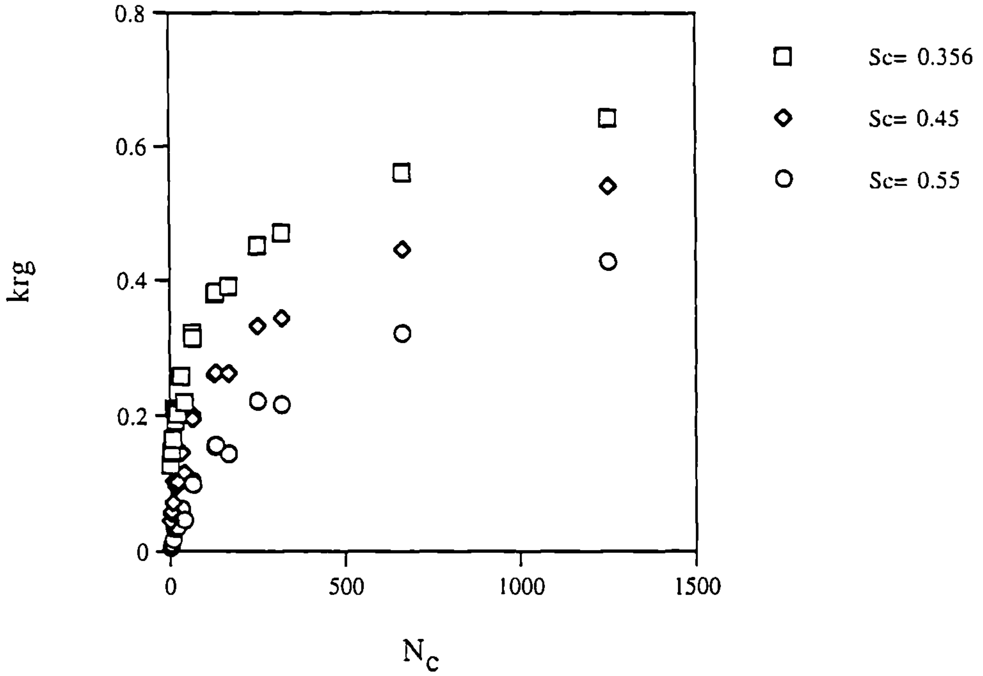

Figure 6.9: The variation of gas relative permeability with capillary number at selected constant phase saturations for all steady-state experiments measured on Berea core, $N_c = (4.\mu_g .v_g) / (\sigma. (8 k / \phi)$^0.5)

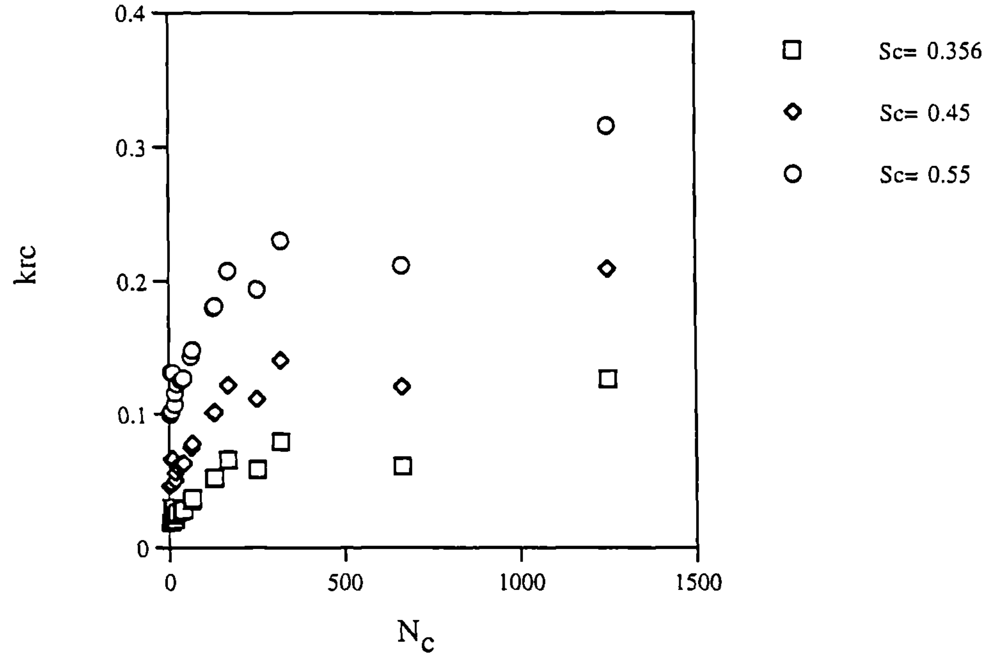

Figure 6.10: The variation of condensate relative permeability with capillary number at selected constant phase saturations for all steady-state experiments measured on Berea core, $N_c = (4.\mu_g .v_g) / (\sigma. (8 k / \phi)$^0.5)

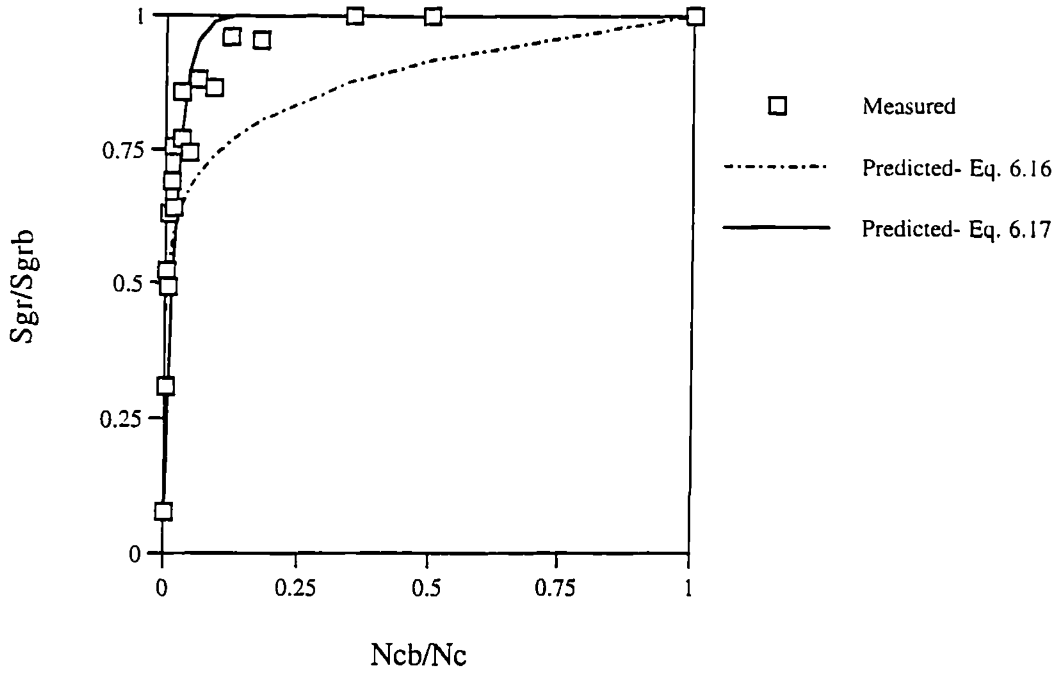

Figure 6.11: Residual gas saturation ratio as a function of capillary number ratio for steady-state relative permeability measurements on Berea Sandstone.

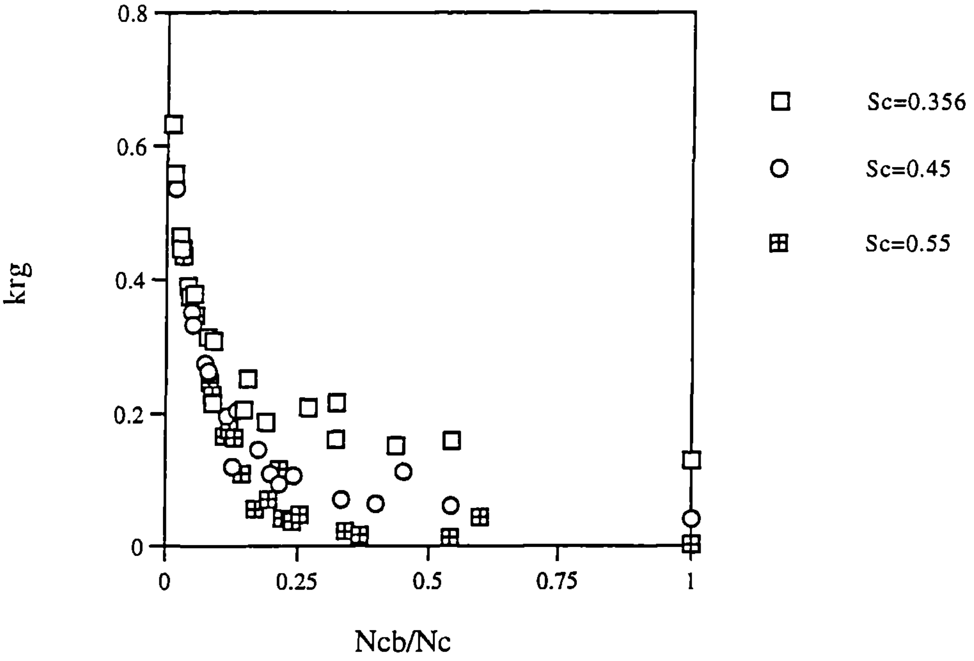

Figure 6.12: The variation of gas relative permeability with capillary number ratio at selected constant phase saturations for all steady-state experiments measured on Berea Sandstone core.

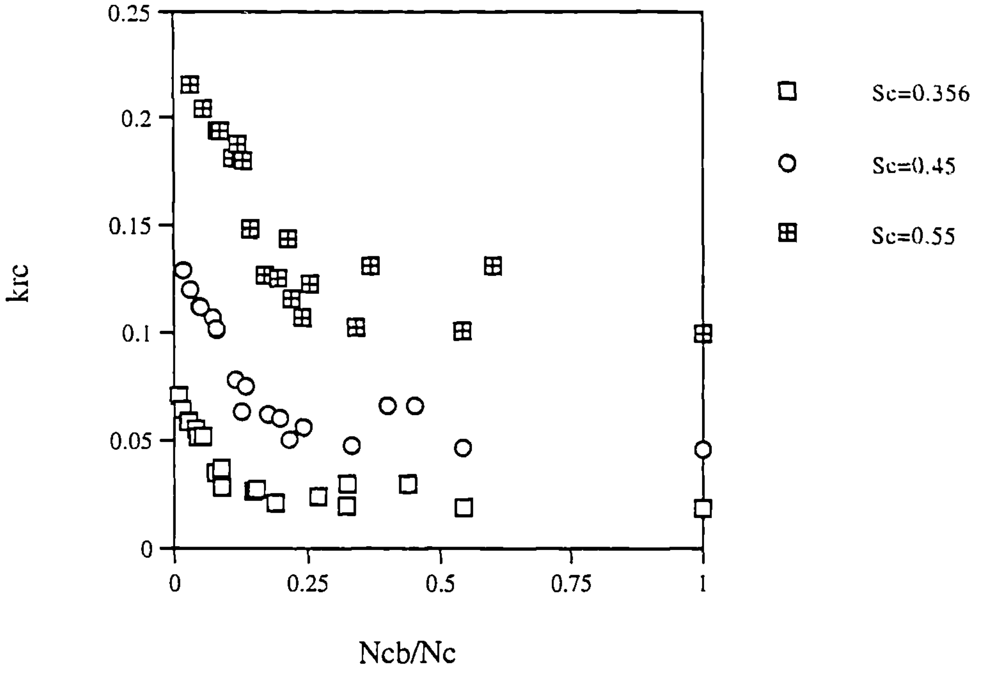

Figure 6.13: The variation of condensate relative permeability with capillary number ratio at selected constant phase saturations for all steady-state experiments measured on Berea Sandstone core.

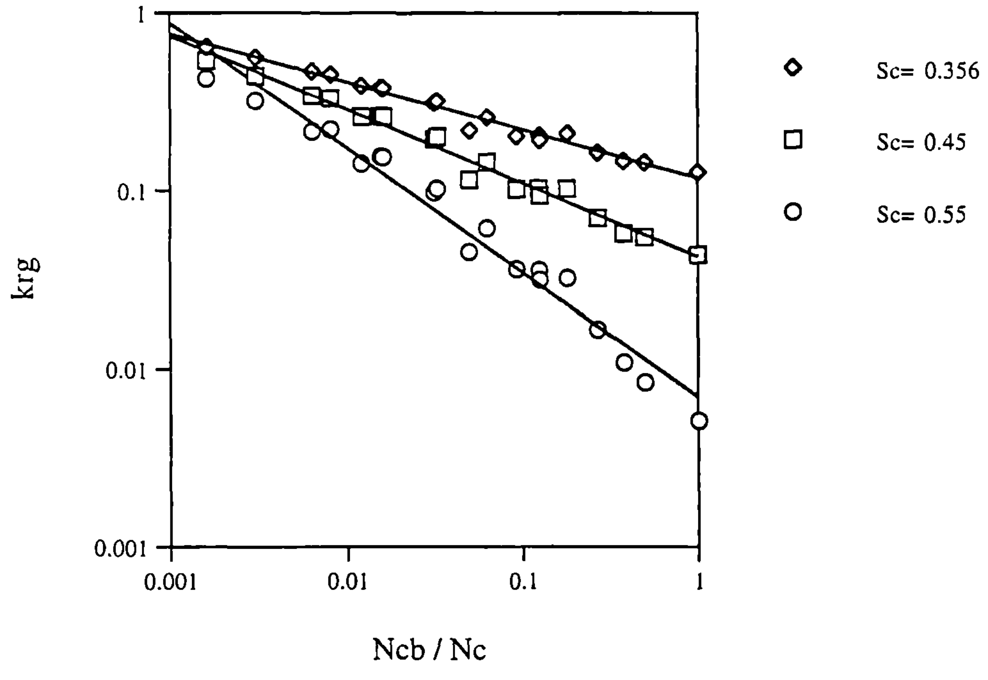

Figure 6.14: The variation of gas relative permeability with capillary number ratio at selected constant phase saturations for all steady-state experiments measured on Berea Sandstone.

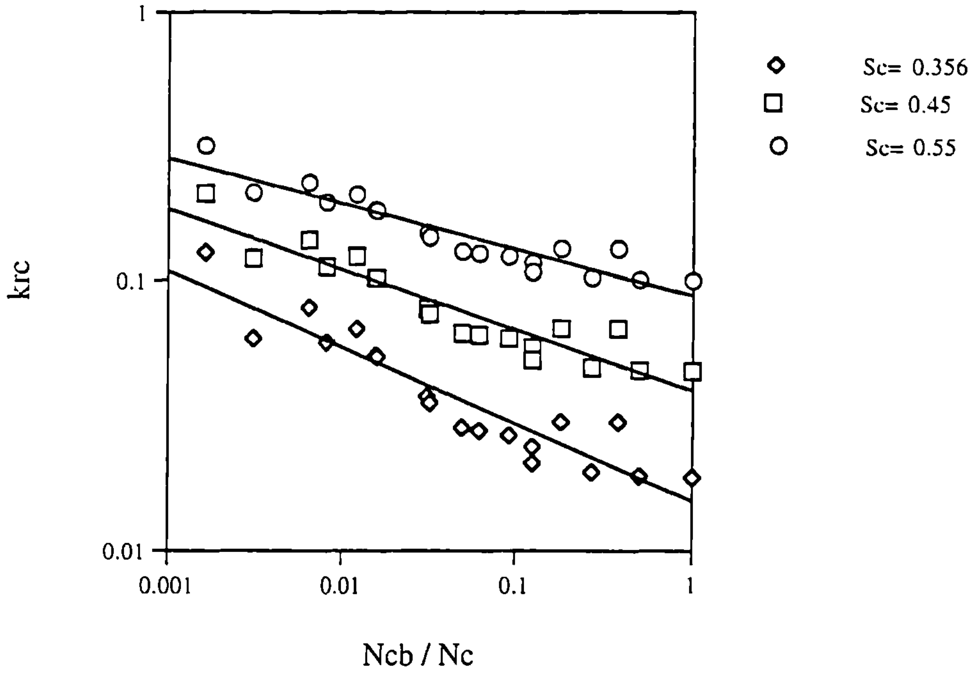

Figure 6.15: The variation of condensate relative permeability with capillary number ratio at selected constant phase saturations for all steady-state experiments measured on Berea Sandstone.

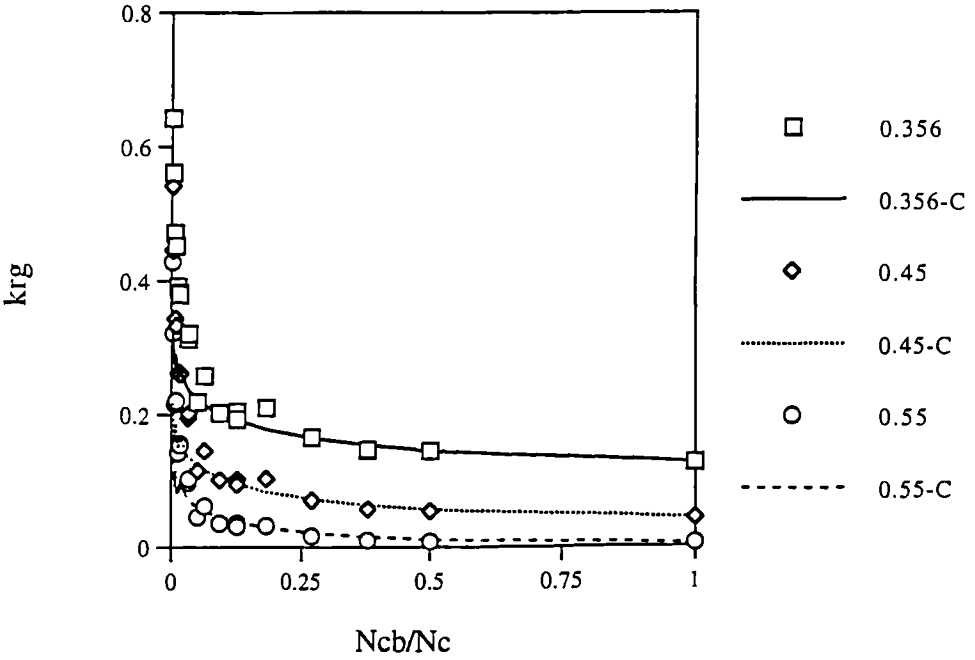

Figure 6.16: Predicted and measured gas relative permeability with capillary number ratio at selected constant phase saturations for all the steady-state experiments measured on Berea core.

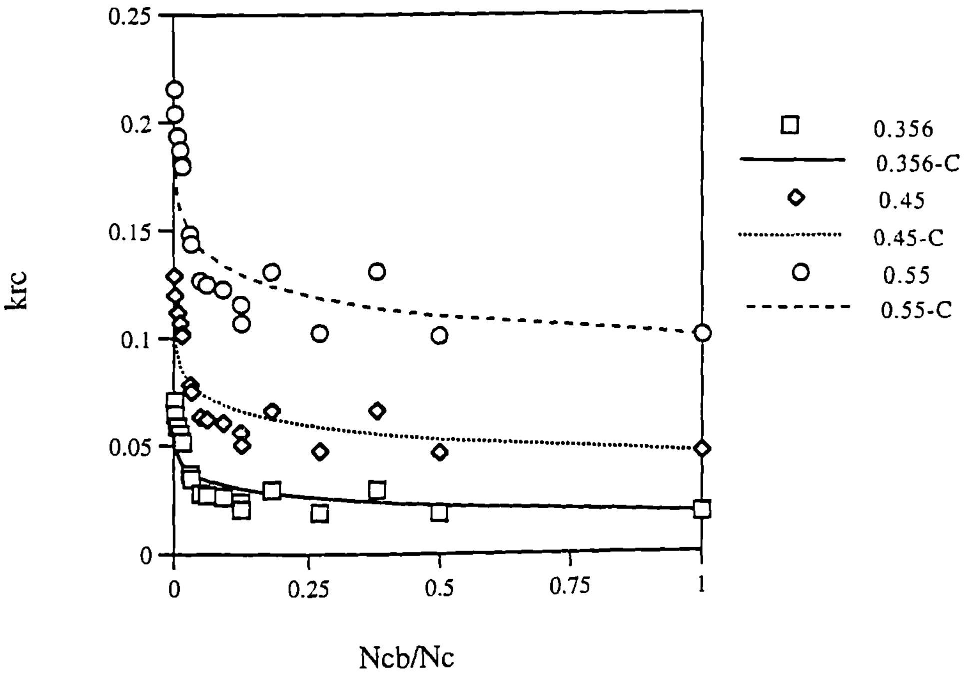

Figure 6.17: Predicted and measured condensate relative permeability with capillary number ratio at selected constant phase saturations for all the steady-state experiments measured on Berea core.

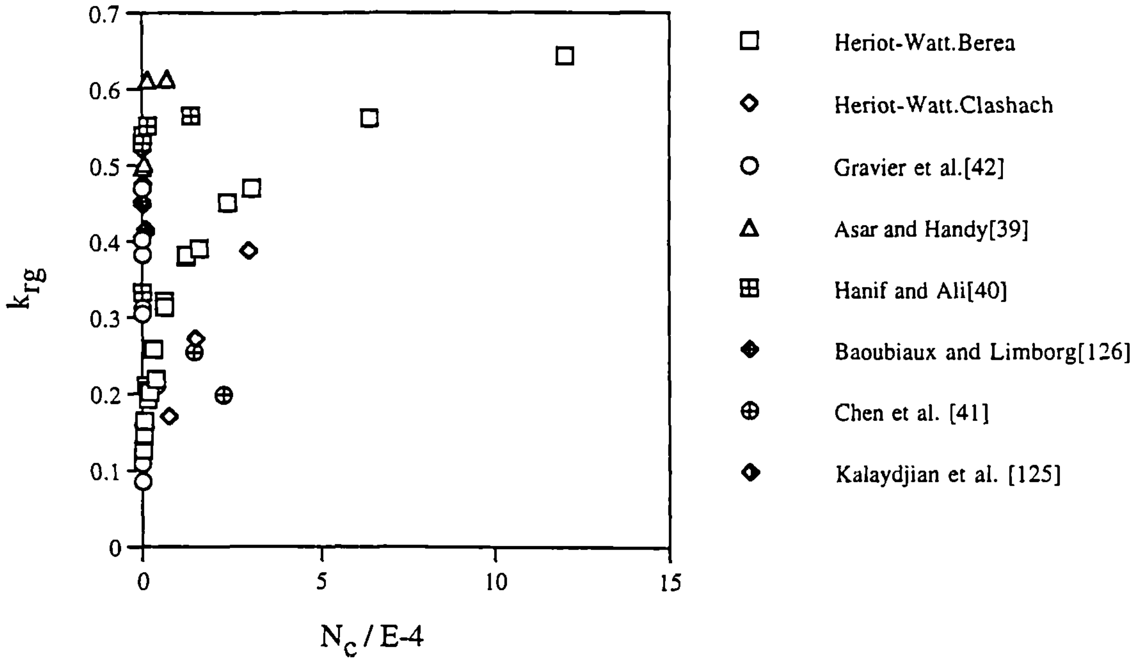

Figure 6.18: Steady-state gas relative permeability at S_c=0.356 for various cores types, IFT values, and flow rates as a function of capillary number ($N_c = \mu_g v_g / \sigma$).

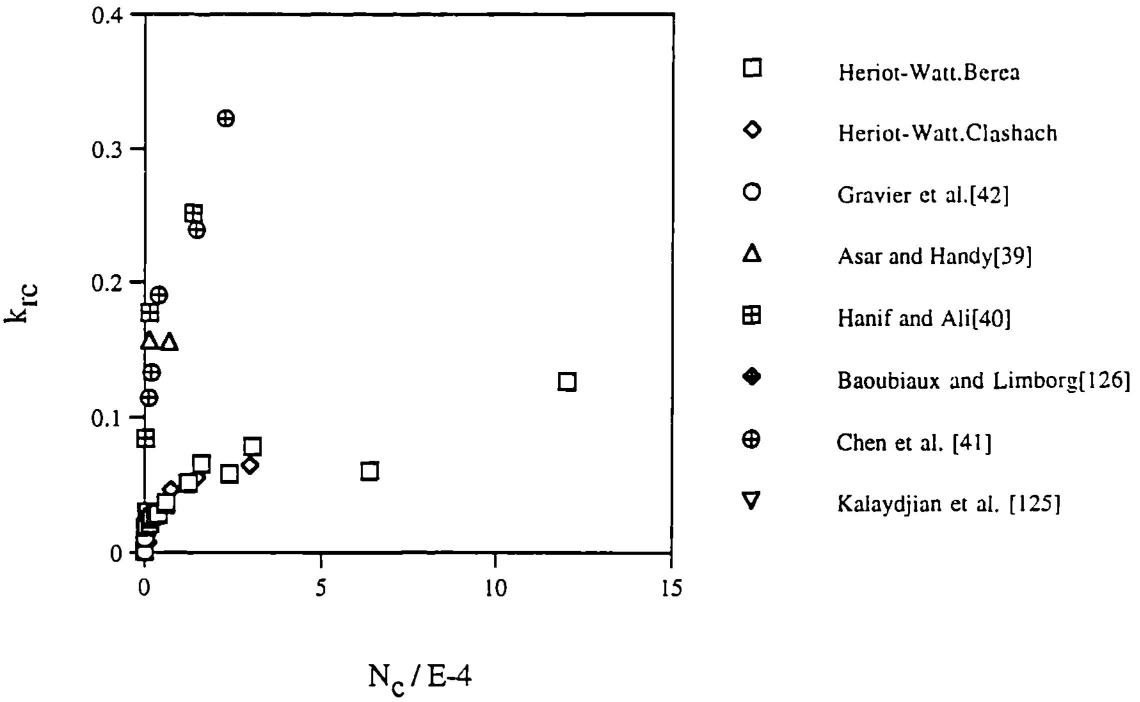

Figure 6.19: Steady-state condensate relative permeability at S_c=0.356 for various cores types, IFT values, and flow rates as a function of capillary number ($N_c = \mu_g v_g / \sigma$).

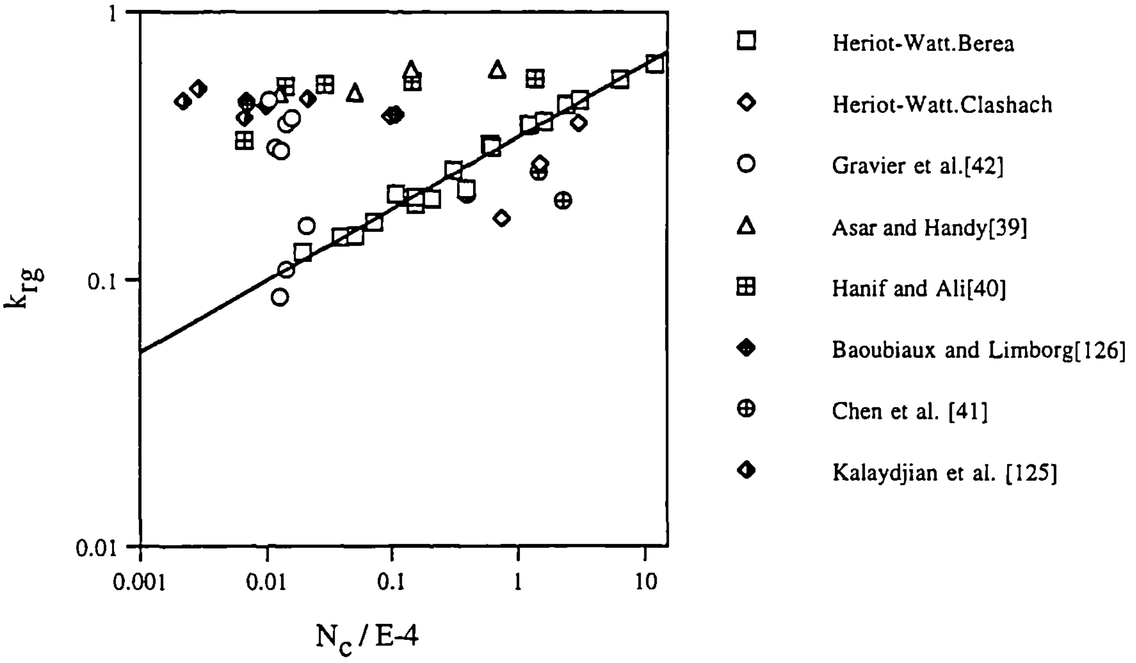

Figure 6.20: Steady-state gas relative permeability at S_c=0.356 for various cores types, IFT values, and flow rates as a function of capillary number ($N_c = \mu_g v_g / \sigma$).

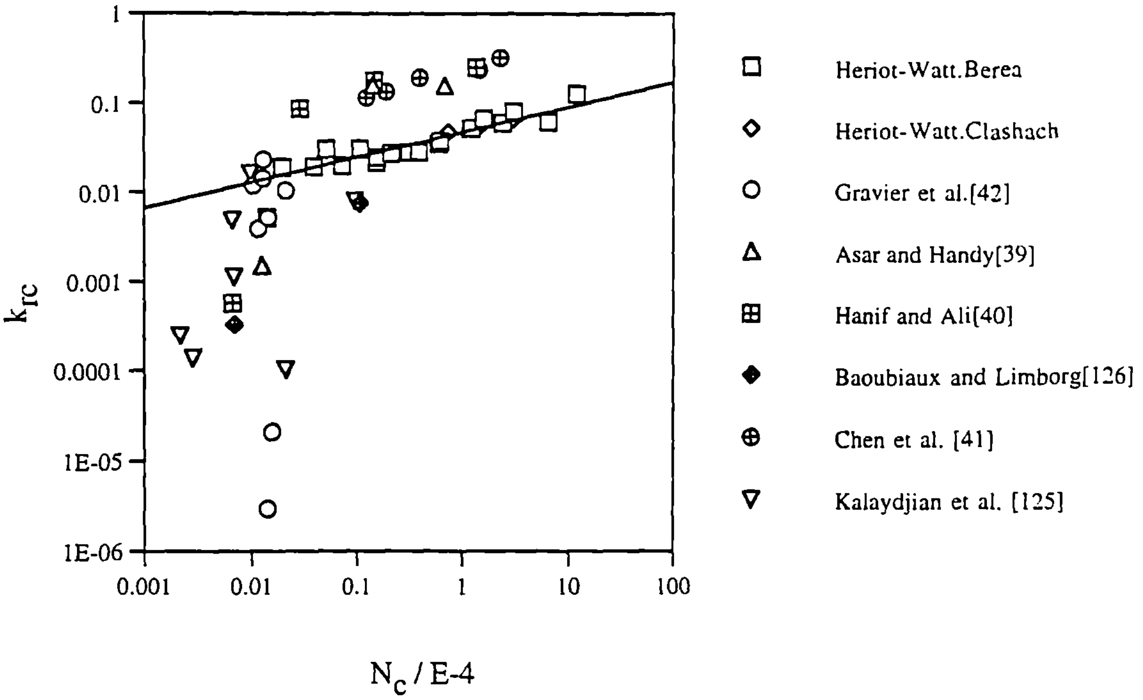

Figure 6.21: Steady-state condensate relative permeability at S_c=0.356 for various cores types, IFT values, and flow rates as a function of capillary number ($N_c = \mu_g v_g / \sigma$).

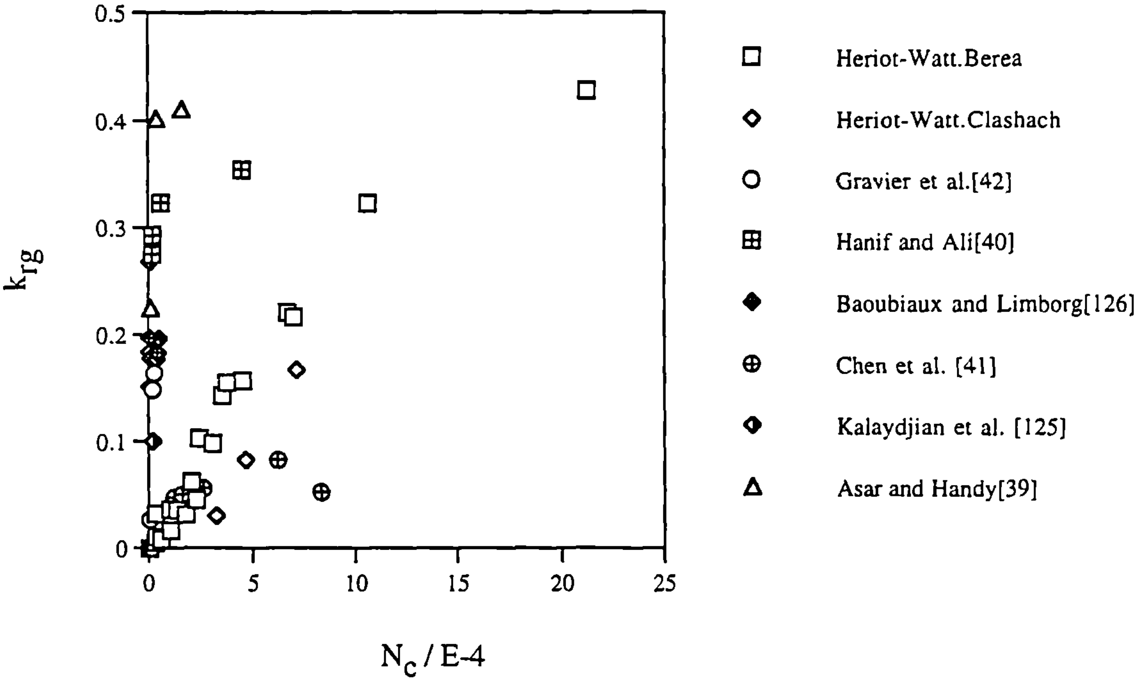

Figure 6.22: Steady-state gas relative permeability at Sc=0.55 for various cores types, IFT values, and flow rates as a function of capillary number ($N_c = k\Delta P / (\phi\sigma L)$).

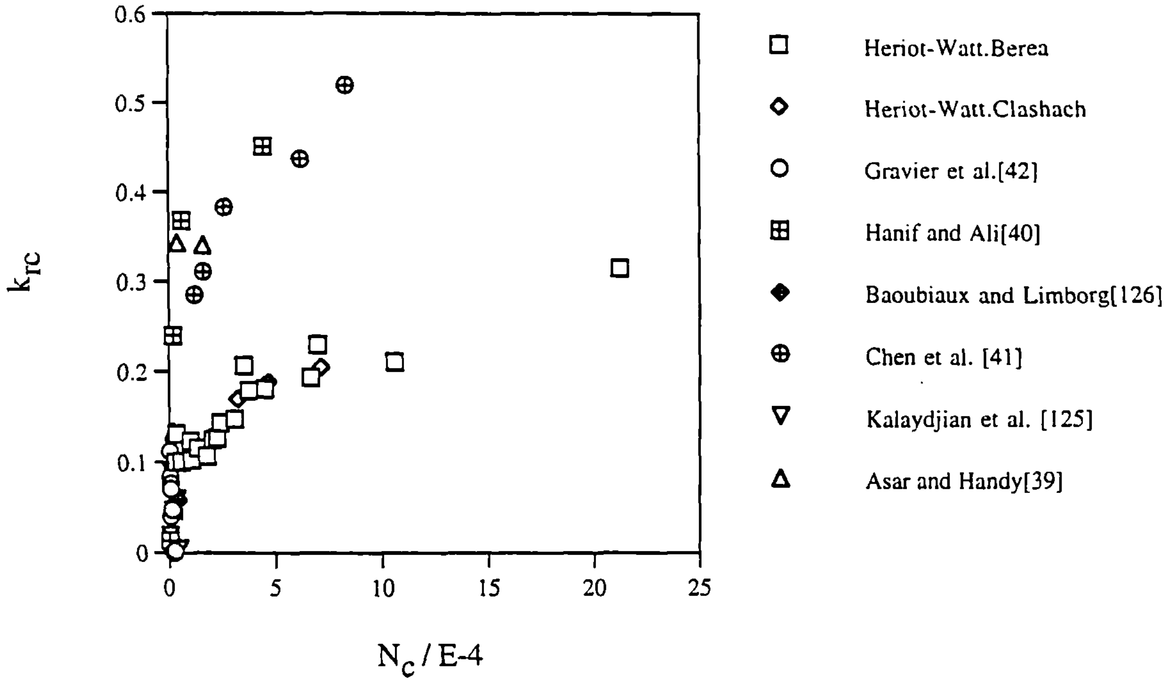

Figure 6.23: Steady-state condensate relative permeability at Sc=0.55 for various cores types, IFT values, and flow rates as a function of capillary number ($N_c = k\Delta P / (\phi\sigma L)$).

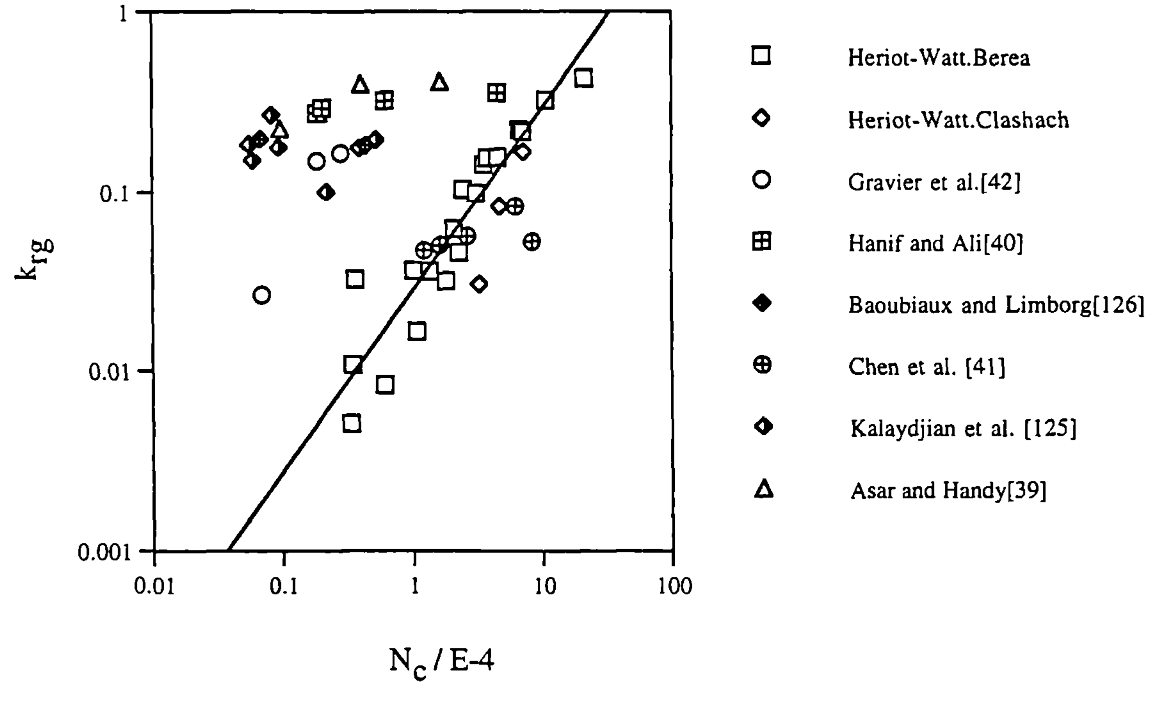

Figure 6.24: Steady-state gas relative permeability at Sc=0.55 for various cores types, IFT values, and flow rates as a function of capillary number ($N_c = k\Delta P / (\phi\sigma L)$).

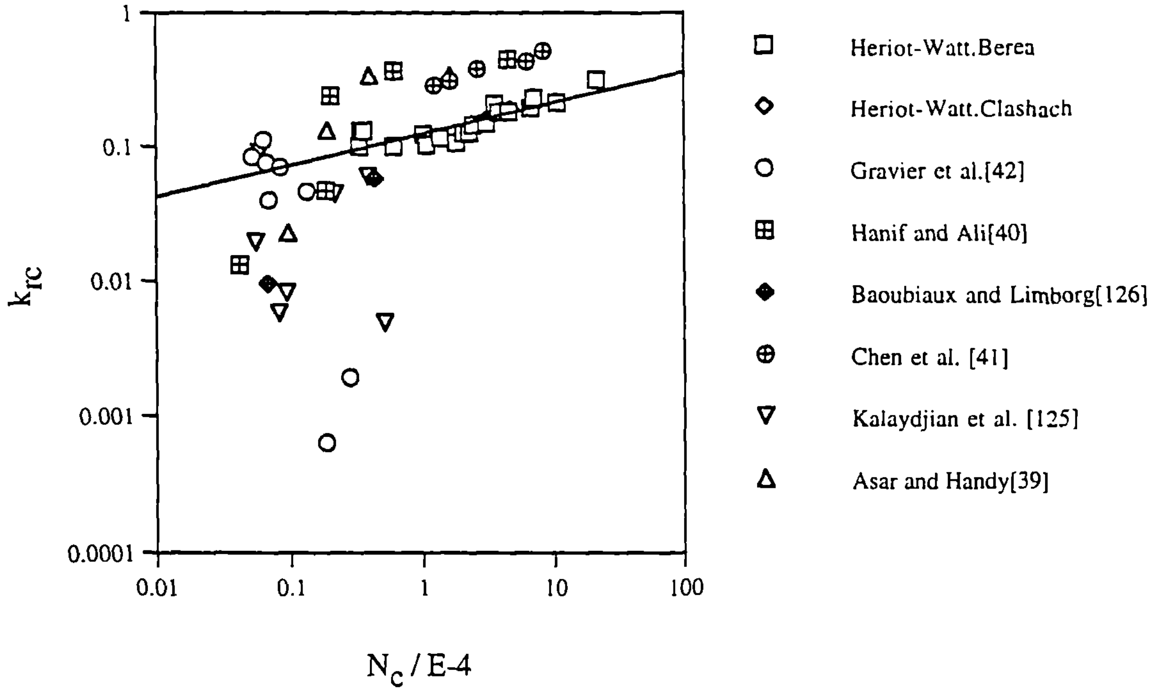

Figure 6.25: Steady-state condensate relative permeability at Sc=0.55 for various cores types, IFT values, and flow rates as a function of capillary number ($N_c = k\Delta P / (\phi\sigma L)$).

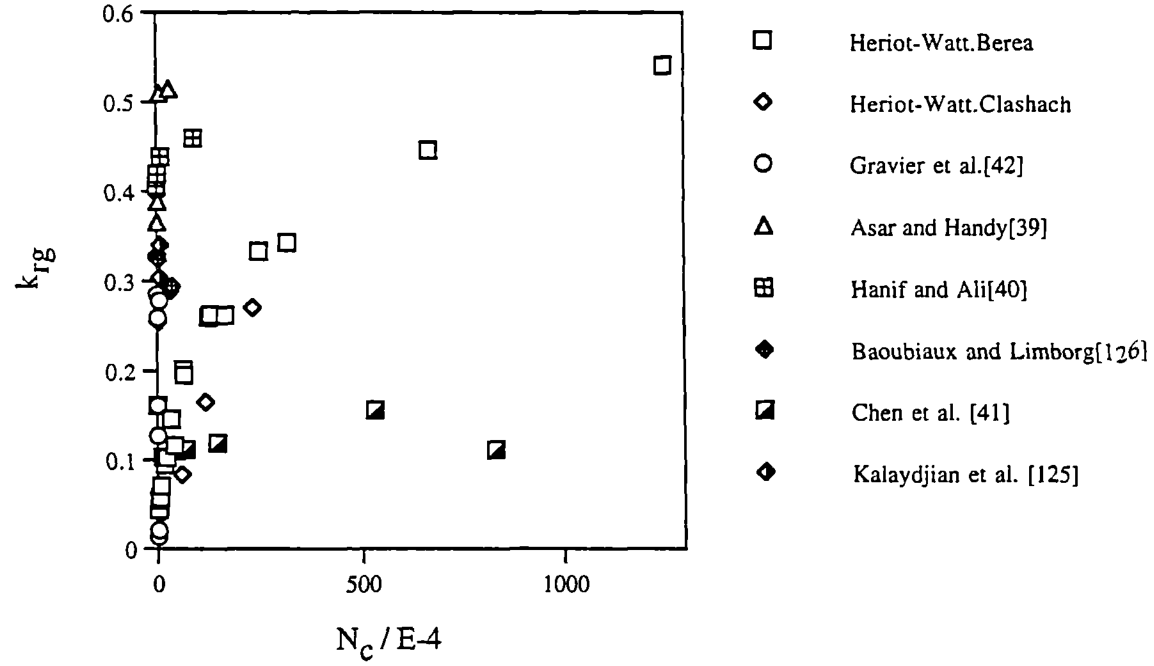

Figure 6.26: Steady-state gas relative permeability at S_c=0.45 for various cores types, IFT values, and flow rates as a function of capillary number $N_c = (4.\mu_g . v_g) / (\sigma. (8 k / \phi)$^0.5)

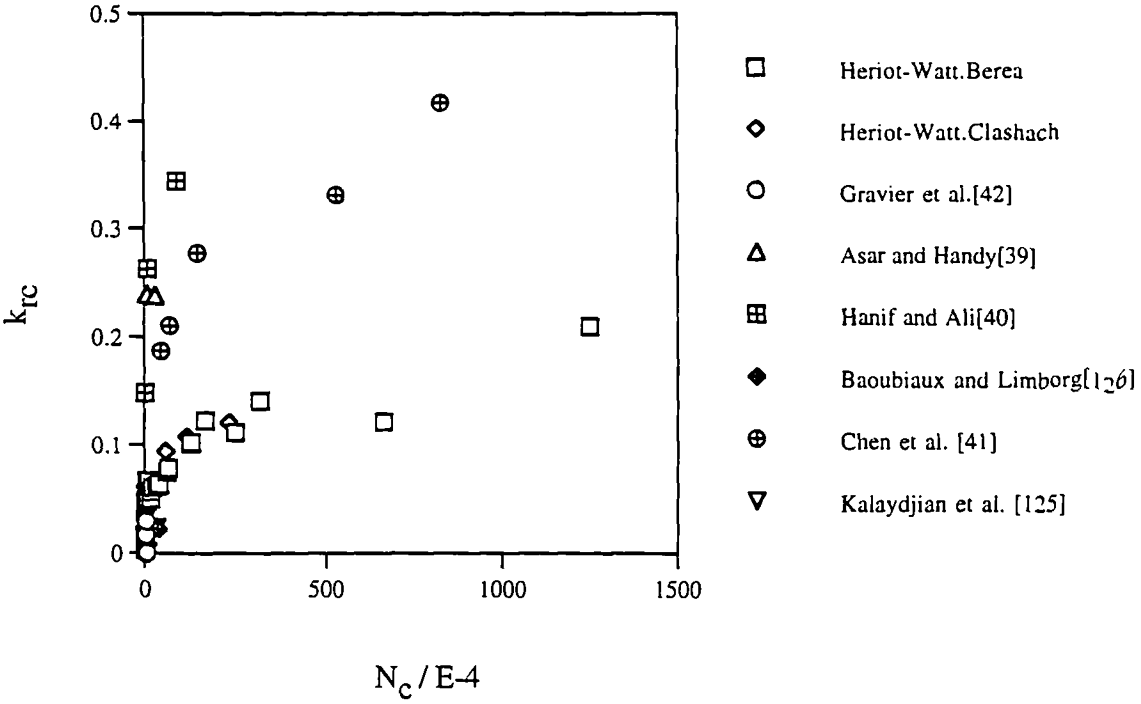

Figure 6.27: Steady-state condensate relative permeability at S_c=0.45 for various cores types, IFT values, and flow rates as a function of capillary numberN_c =$(4.\mu_g .v_g) / (\sigma. (8 k / \phi)$^0.5)

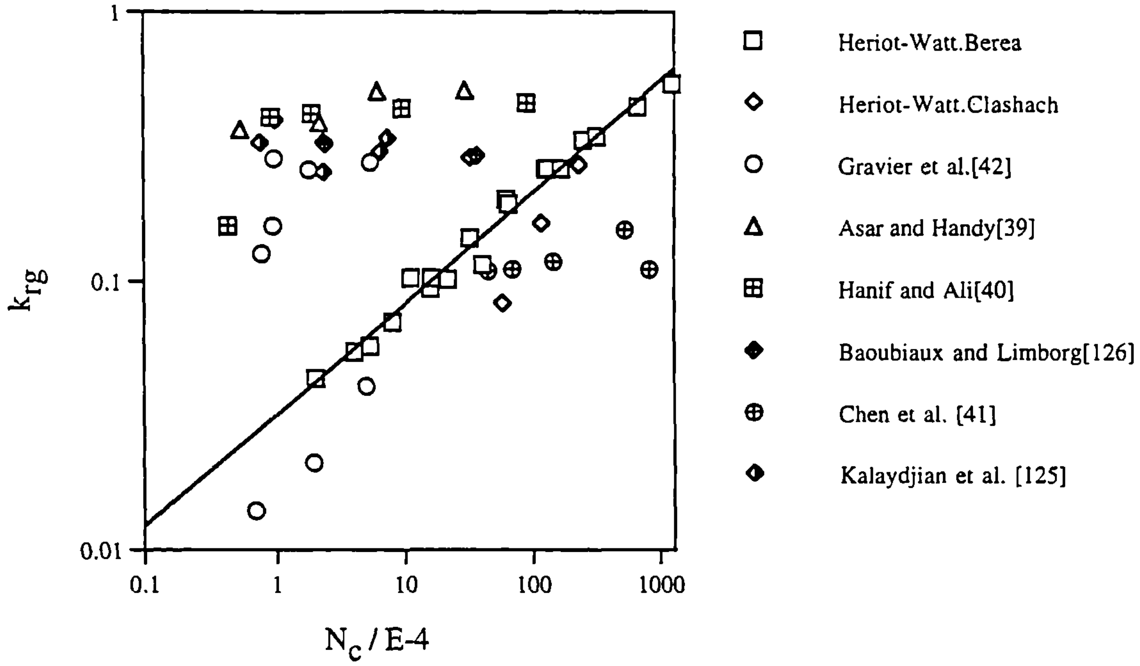

Figure 6.28: Steady-state gas relative permeability at S_c=0.45 for various cores types, IFT values, and flow rates as a function of capillary number N_c =$(4.\mu_g .v_g) / (\sigma. (8 k / \phi)$^0.5)

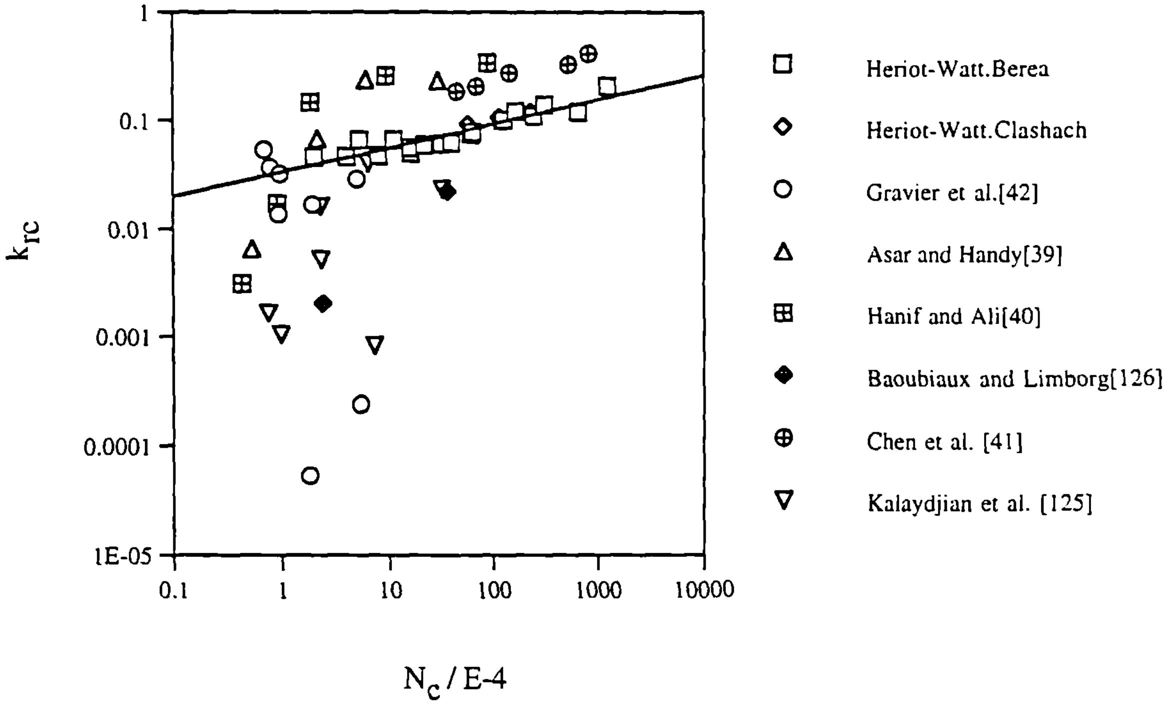

Figure 6.29: Steady-state condensate relative permeability at S_c=0.45 for various cores types, IFT values, and flow rates as a function of capillary numberN_c =(4.μ_g .v_g) / (σ. (8 k / ϕ)^0.5)

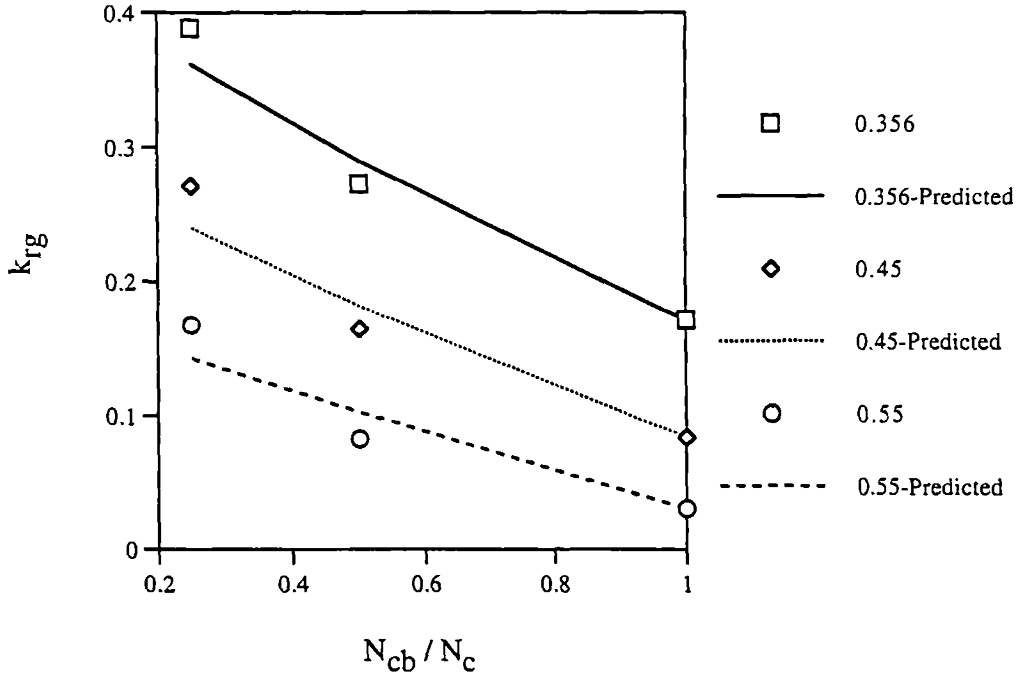

Figure 6.30: Experimental and predicted gas relative permeability values for the steady-state data measured in-house on the Clashach core.

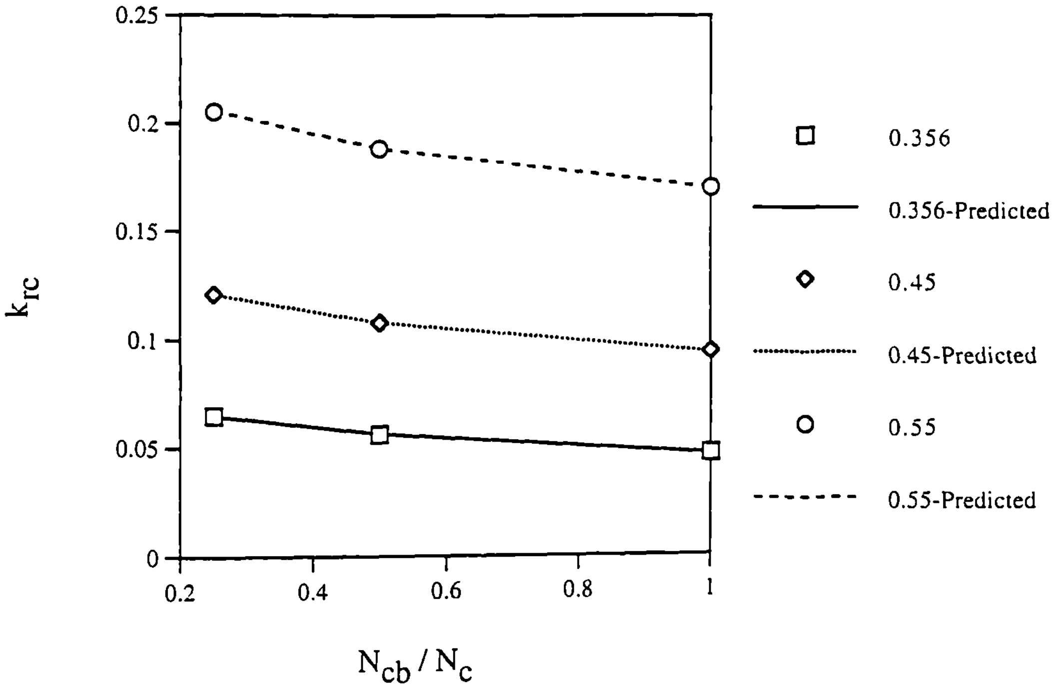

Figure 6.31: Experimental and predicted condensate relative permeability values for the steady-state data measured in-house on the Clashach core.

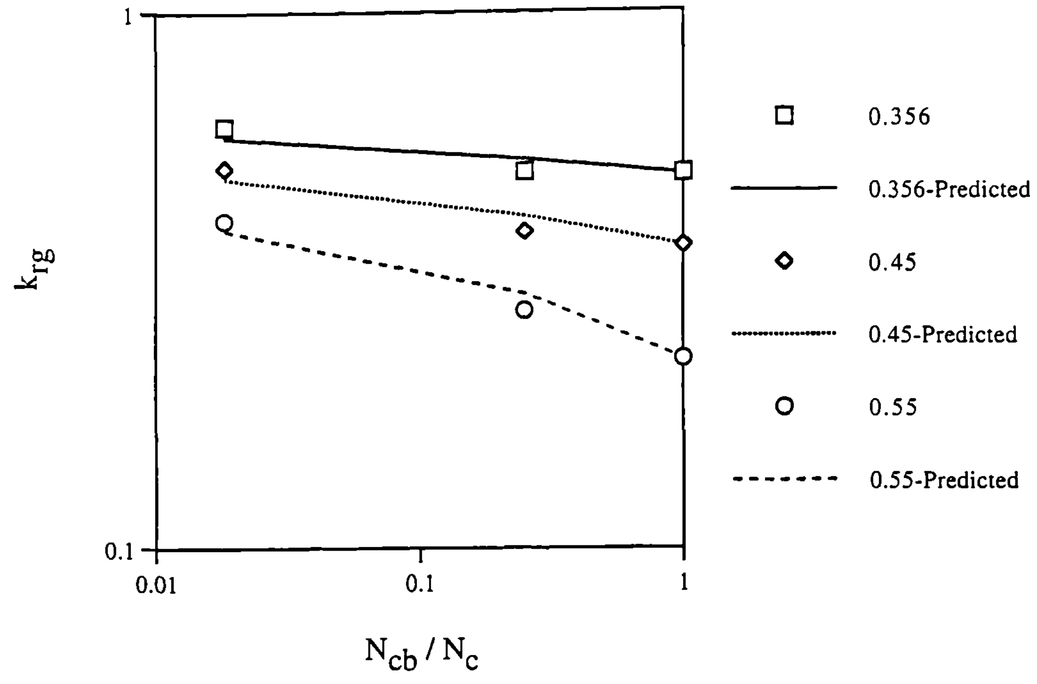

Figure 6.32: Experimental and predicted gas relative permeability values for the steady-state data measured on the fired Berea core by Asar and Handy[39]

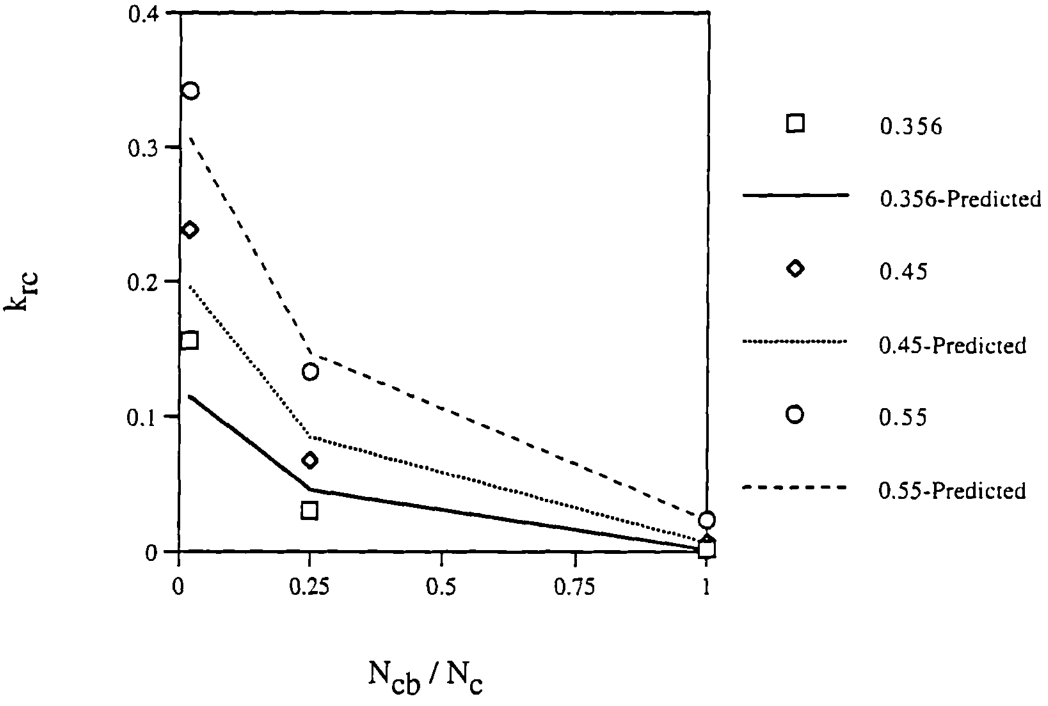

Figure 6.33: Experimental and predicted condensate relative permeability values for the steady-state data measured on the fired Berea core by Asar and Handy[39]

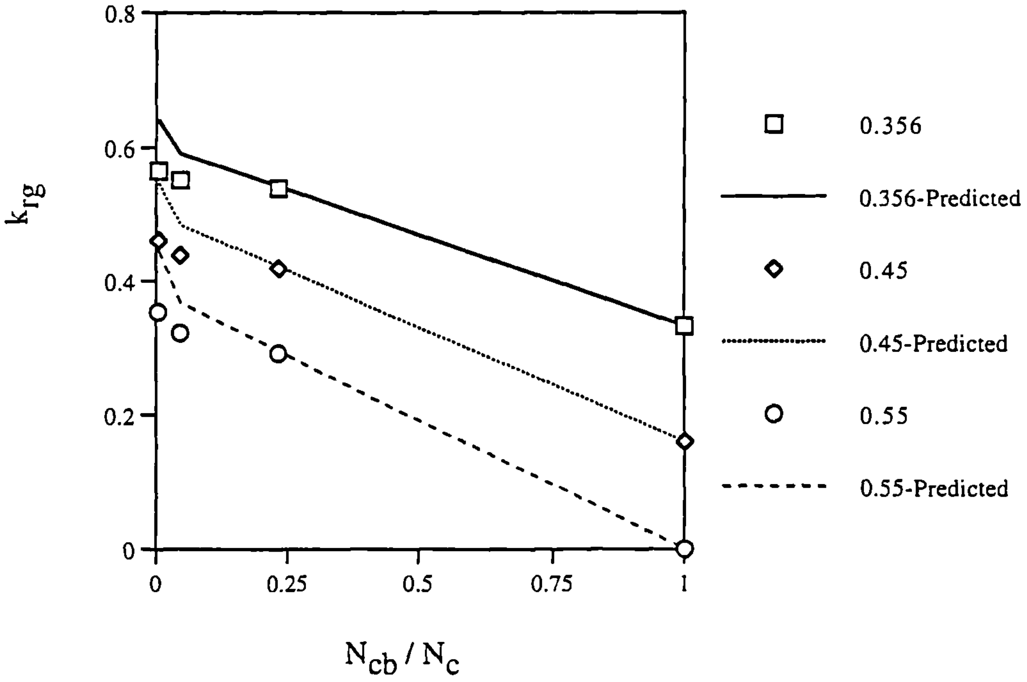

Figure 6.34: Experimental and predicted gas relative permeability values for the steady-state data measured on the Spynie core by Hanif and Ali[40]

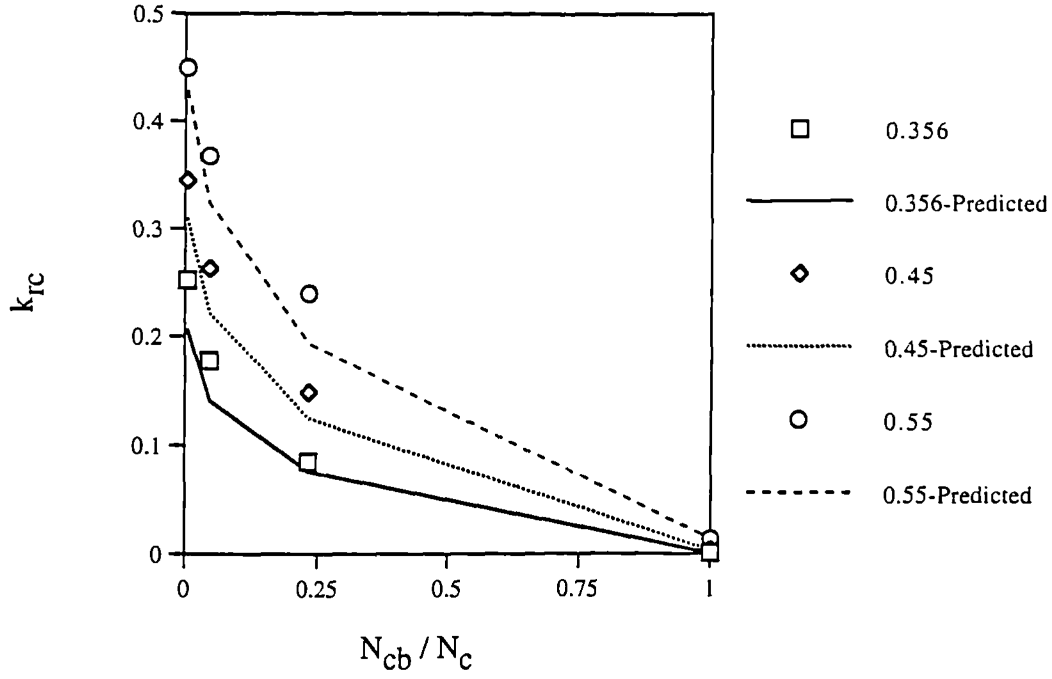

Figure 6.35: Experimental and predicted condensate relative permeability values for the steady-state data measured on the Spynie core by Hanif and Ali[40]

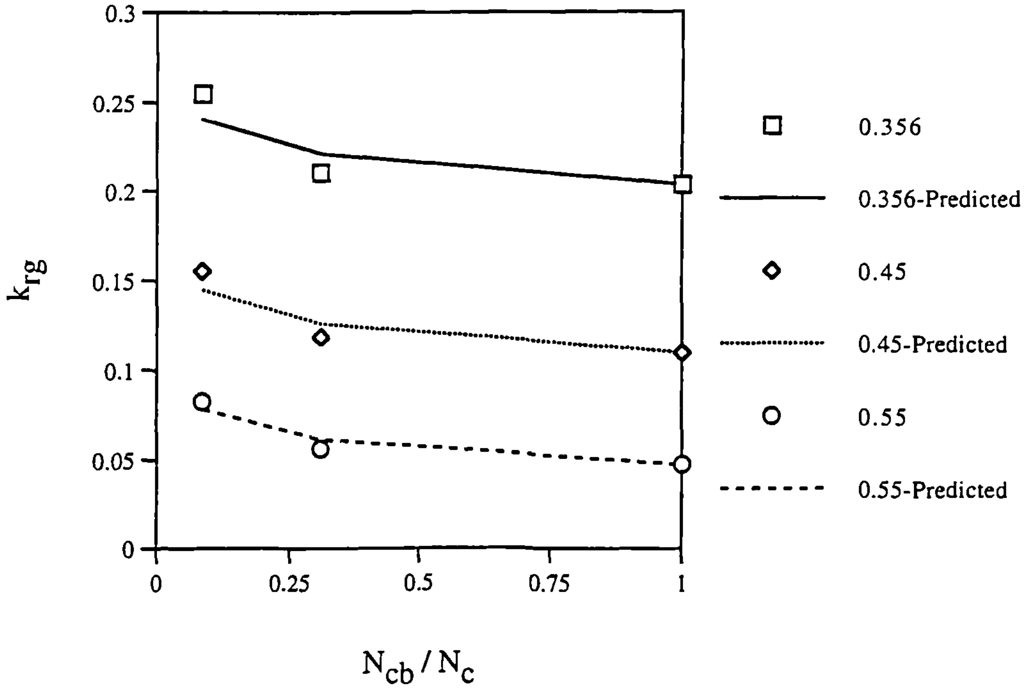

Figure 6.36: Experimental and predicted gas relative permeability values for the steady-state data (mobile condensate) measured on composite core B by Chen et al.[41]

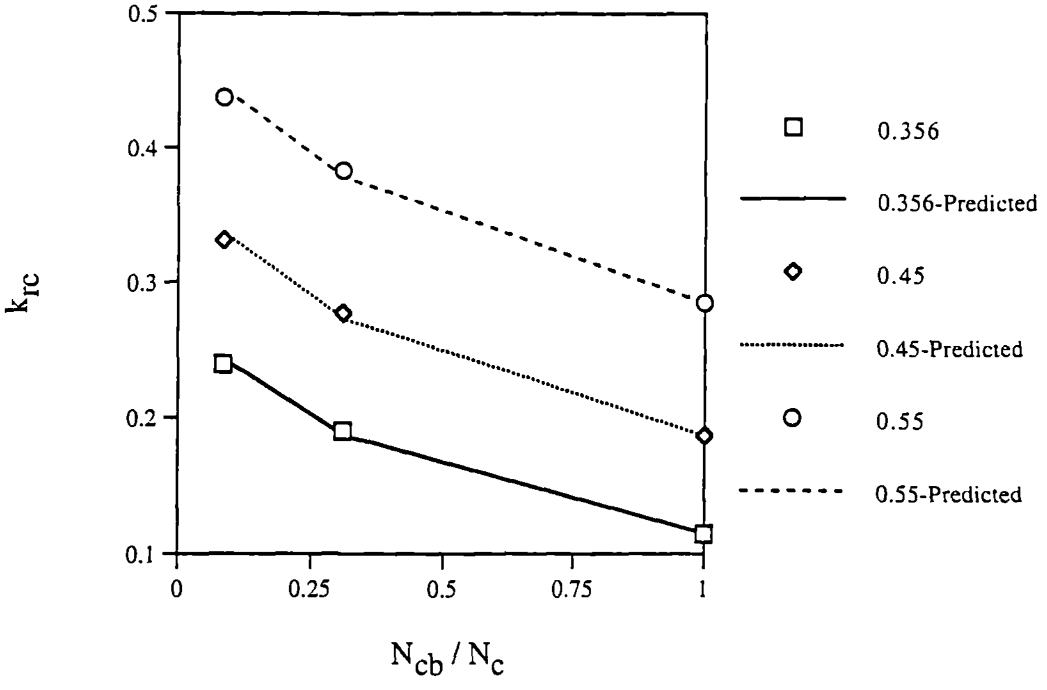

Figure 6.37: Experimental and predicted condensate relative permeability values for the steady-state data (mobile condensate) measured on composite core B by Chen et al.[41]

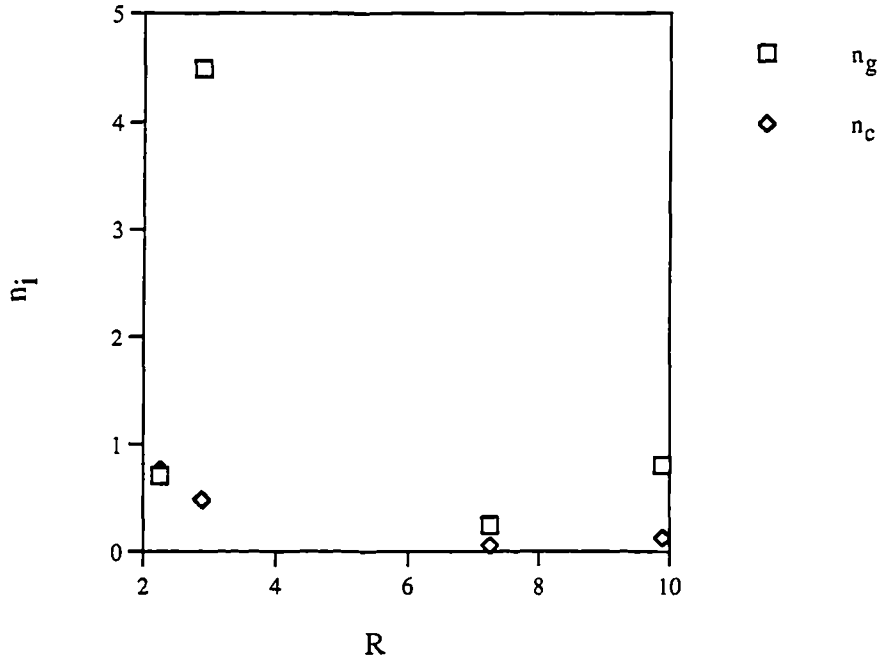

Figure 6.38: The variation of gas and condensate exponents with pore-size distribution index, R.

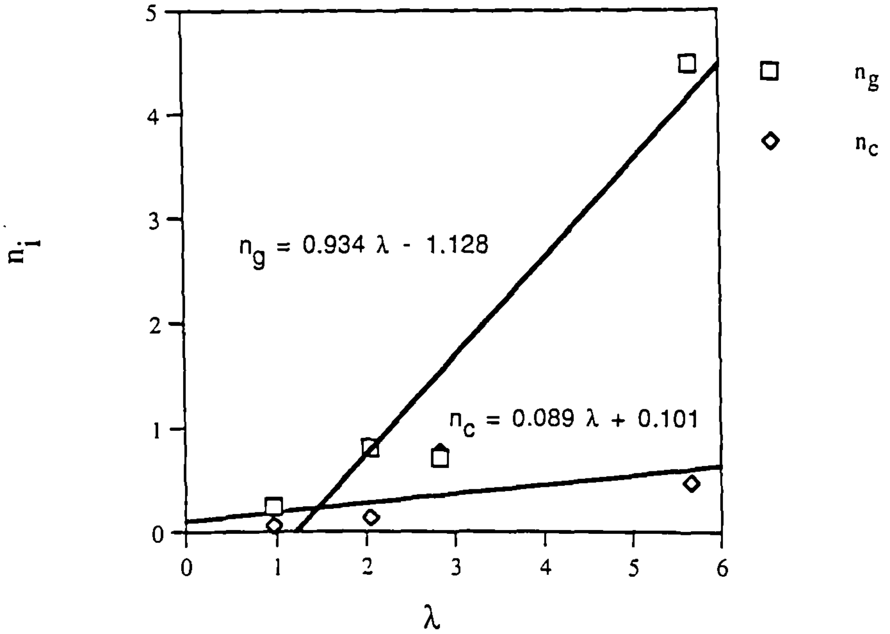

Figure 6.39: The variation of gas and condensate exponents with pore-size distribution index, λ.

CHAPTER 7
WELL DELIVERABILITY STUDY

7.1 INTRODUCTION

The influence of both interfacial tension (IFT) and Forchheimer (Inertia) effects on well-productivity have long been incorporated into simulators. However, no detailed attempts have been reported on incorporating the recently proven rate-effects of gas-condensate flow in porous media[44-45,61-62]. Furthermore, most of the correlations incorporated into simulators have been developed for either water-oil or gas-oil systems which not may be applicable to gas-condensate systems. Also only limited work has been reported on studying the total impact of these three effects on well deliverability[3, 24, 25, 150, 151]. Therefore, the modified relative permeability correlation, as detailed in chapter 6, has been supplied to GeoQuest Reservoir Technologies Inc. to be incorporated into their commercial compositional simulator Eclipse (E300). This modified E300 (1997A version) is used in a more comprehensive gas condensate wellbore deliverability study.

In this well deliverability study, a real North Sea gas condensate fluid is used together with a simple 200 feet thick radial reservoir of 3000 feet radius. Hence, the impact of rate, IFT and Forchheimer effects on gas condensate well deliverability are investigated in several idealised reservoir conditions. These conditions include the influence of production rate, reservoir absolute permeability, and gas-condensate liquid drop-out. This study offers an increased understanding of a typical gas condensate well deliverability through the modified relative permeability correlation as detailed in chapter

6. It also offers the ability to compare its conclusions with those obtained from other gas condensate well deliverability studies

7.2 THEORY

7.2.1 Introduction

The mathematical expressions for IFT and N_c effects which are either originally in the Eclipse compositional simulator or recently incorporated have been detailed in the previous chapters. The functions of IFT effect are those of Coats' correlation for which either chapter 6 or Eclipse 300 technical appendix A17.1-2 can be consulted. A detailed review of the Forchheimer functions are presented in chapter 4. The following section describes the combination of the Forchheimer effect and the N_c-effect functions which are incorporated in Eclipse compositional simulator (E300).

7.2.2 Capillary Number and Forchheimer Effects

The Forchheimer effect is incorporated into the model by modifying the gas-phase relative permeability values. To accomplish this, the Forchheimer effect-influenced gas-phase relative permeability is calculated by equating the Forchheimer expression (Eq. 4.3) to Darcy's law for multi-phase flow in porous media, so that,

$$\frac{\mu v}{k\,k_{rt}} = \frac{\mu v}{k\,k_{rb}} + \beta \rho v^2$$

Therefore, the Forchheimer effect-influenced gas-phase relative permeability, k_{rt}, can be calculated as:

$$\frac{1}{k_{rt}} = \frac{1}{k_{rb}} + \beta . k \frac{\rho v}{\mu} \qquad \text{...(7.1)}$$

Hence, capillary number effect is combined, optionally, with Forchheimer effects by applying Eq. 7.1 to capillary number affected relative permeabilities (k_{rvi}). and, Eq. 7.1 takes the following general form:

$$k_{ri} = \frac{1}{\left[F_i.\left(C.k.\beta_i.R_{ei}\right) + \dfrac{1}{k_{rvi}} \right]} \qquad \text{...(7.2)}$$

where,

k_{ri}: relative permeability of phase ‘i’, accounting for both the capillary number and Forchheimer effects.

C: conversion factor from the self consistent SI units to the field units, $C = 1.83 \times 10^{-16}$

F_i : a control parameter to specify whether the Forchheimer effect should be considered (F=1) or not (F=0), for each phase ‘i’.

k: reservoir absolute permeability, mD.

$$R_{ei} = \frac{\rho_i . v_i}{\mu_i} \qquad \text{...(7.3)}$$

where,

ρ_i: density of fluid ‘i’, lbs/cf.

v_i: Darcy velocity of phase 'i', ft/d.

μ_i: viscosity of phase 'i', cp.

β_i: Forchheimer factor, ft^{-1}, where it can be calculated through the following two different options,

$$\beta_i = B1_i\left(\frac{a_i}{\phi^{bi}.S_i^{ci}\left(k.k_{rvi}\right)^{di}}\right) + B2_i.\beta_{di}.S_i^{ci}.\left(k_{rvi}\right)^{di} \qquad \text{...(7.4)}$$

where,

$B1_i$, $B2_i$: option for Forchheimer factor equation (only one option must be active), 0 or 1.

S_i: saturation of phase 'i', fraction

ϕ: reservoir porosity, fraction

β_{di}: single phase Forchheimer factor, ft^{-1}

a_i, b_i, c_i, d_i: constants specific to each phase.

k_{rvi}: relative permeability of phase 'i', modified for the capillary number effect only. So that,

$$k_{rvi} = N_{cni}^{n_i}.k_{rbi} + \left(1 - N_{cni}^{n_i}\right).k_{rmi} \qquad ...(7.5)$$

where,

k_{rbi}: base relative permeability of phase 'i', fraction

k_{rmi}: miscible relative permeability of phase 'i', where,

$$k_{rmi} = \frac{S_i - X_i S_{rbi}}{1 - X_i S_{rbi}} \qquad ...(7.6)$$

where,

S_{rbi}: base residual saturation of phase 'i', fraction

X_i: residual saturation scale function of phase 'i', where,

$$X_i = 1 - e^{(-nr_i.N_{cni})} \qquad ...(7.7)$$

nr_i: constant, residual saturation exponent of phase 'i'.

N_{cni}: Normalised capillary number, where

$$N_{cni} = \frac{N_{cbi}}{N_{ci}} \qquad ...(7.8)$$

where,

N_{cbi}: base capillary number of phase 'i'. It can be supplied as a single value or defaulted as,

$$N_{cbi} = \frac{\mu_{gb} v_{gb}}{\sigma_b} \qquad \text{...(7.9)}$$

μ_{gb}: lowest gas phase viscosity.

v_{gb}: lowest gas superficial phase velocity.

σ_b: highest interfacial tension (IFT).

N_{ci}: capillary number of phase 'i', where it can be calculated by three different options,

$$N_{ci} = N1_i.\left(\frac{v_g.\mu_g}{\sigma}\right) + \mathrm{N}2_i.\left(\frac{k.k_{rvi}.\Delta P_i}{\sigma.L}\right) + N3_i.\left[\frac{\left(2\phi.S_i.k.k_{rvi}\right)^{0.5}\Delta P_i}{\sigma}\right] \qquad \text{...(7.10)}$$

$N1_i$, $N2_i$, $N3_i$: Options for capillary number calculations. (only one option must be active), 0 or 1.

μ_g: gas phase viscosity.

v_g: gas phase superficial velocity.

σ: interfacial tension (IFT).

ΔP_i: pressure drop across each grid-block.

L: Length of grid-block in the direction of flow.

Consistent units must be used for μ_g, v_g, and σ to calculate N_{ci} and N_{cbi}.

n_i: capillary number exponent function, where,

$$n_i = n_{i1} S_i^{n_{i2}} \qquad \text{...(7.11)}$$

where,

n_{i1}, n_{i2}: two constants (capillary number parameter) of phase 'i'.

Base relative permeability curves (k_{rbi}) and the corresponding base residual saturation values (S_{rbi}) must be supplied at the base capillary number values (N_{cbi}). The constants F_i, $B1_i$, $B2_i$, $N1_i$, $N2_i$ and $N3_i$ define the different options that are available for Forchheimer equations and the capillary number formulations respectively. Since the purpose of this study is not to compare the efficiency of the different options of such formulations, only one option is used to conduct this wellbore deliverability study. The other options are there to offer flexibility for further expansion to the on-going work in this study.

Further experimental investigation on the appropriate definition for the β-factor associated with high velocity flow of gas condensate at near the wellbore is required. Wong and Geertsma's Equation ($B1=1$, $B2=0$ in Eq. 7.4), is adopted for this study for its simplicity and consistency as it gives the correct unit for β, i. e. L^{-1}. Therefore, Forchheimer exponents a_i, b_i, c_i and d_i are those used by Geertsma[116] for multi-phase effect β-factor. The values for these exponents are listed in Table 7.1.

The residual saturation base values (S_{rbi}) and the exponent (nr_i) are those obtained for the Berea core measured data. All of these exponents are kept constant during the study and they are listed in Table 7.1 together with Coats IFT exponents (n, σ_b) which are used in Eq. 6.7 to represent the IFT effect. Ideally two different exponents for gas and condensate phases must be used in Eq. 6.7. However, the use of a single exponent for both phases is the existing conventional treatment for the IFT effect available in the Eclipse simulator. The capillary number exponents n_{i1} and n_{i2} vary with pore-size distribution index as defined by Eqs. 6.34 and 6.35 in the previous chapter, therefore, a separate treatment is given for these exponents in section 7.3.1.

7.3 WELL DELIVERABILITY STUDY

First, the N_c effect is established, in the presence of Forchheimer effect, by choosing the reservoir rock and fluid properties such that the N_c-effect is believed to be present (i.e. a rich gas condensate fluid in tight reservoir rock produced at a relatively high production rate). The impact of the N_c effect on well deliverability is then thoroughly investigated. This is performed by carefully analysing the impact of this phenomenon on total production of gas and oil, production rates, and well productivity indices. Also, careful inspection of the impact on pressure, and condensate saturation histories are performed. This is conducted on both single and double layer reservoir models.

Second, using the single-layer reservoir model, the important factors that control the N_c effect are varied to establish the boundaries of the importance of such effect. This process entails the variation of production rate, reservoir absolute permeability, and liquid drop-out independently. In each case, the possibility of establishing a range of the values of each parameter where the N_c effect is important will be examined.

This study is performed on a one-dimensional, fine-grid, single-well radial flow model.

7.3.1 Base Values

Capillary Number Base Value

As mentioned earlier, the base relative permeability curves must be supplied so that they correspond to base capillary number values (N_{cbi}). Therefore, the N_{cbi} value must be experimentally determined for each phase and base relative permeability curves must be measured at that N_{cbi} value. We can make use of the steady-state relative permeability data measured on the core to estimate the N_{cbi} value. For example, all the measured steady-state relative permeability data for the Berea Sandstone are given in Figs. 7.1 and 7.2 for the gas and condensate phases respectively. Each constant condensate saturation curve shown in these figures is analysed. k_{rc} and k_{rg} values, of each curve, are plotted as a function of $\log(N_c)$. The averaged minima for all curves are taken as the base capillary number (N_{cbi}) for each phase. The analysis resulted in N_{cbi} values of 2.0×10^{-6} and 4.5×10^{-6} for the gas and condensate phases respectively.

Base Relative Permeability Curves And N_c Exponents

The sensitivity of the base relative permeability curves to absolute permeability, and pore-size distribution index is recognised. The in-house measured relative permeability curves on the Berea Sandstone core shown in Figs. 7.1 and 7.2 are read at the N_{cbi} value of 2.0×10^{-6} for the gas base relative permeability curve and at N_{cbi} value of 4.5 x 10^{-6} for the condensate relative permeability curve. These base relative permeability curves are established and used for reservoir absolute permeability of 100 mD.

Furthermore, the pore-size distribution index (λ) is assumed to be constant but the reservoir absolute permeability can vary. Hence, the capillary number exponents n_{i1} and n_{i2} (determined in chapter 6) are kept constant throughout the study and they are included in Table 7.1. This assumption implies that only reservoir rocks with same depositional environment as those of the Berea Sandstone will be considered in this study. According to the Buckly-Levert definition for capillary pressure, as given in Eq. 6.14 of chapter 6, same depositional environment translates to different porosity and permeability of a reservoir with one J-function (Eq. 6.15) (i.e. J-function stays approximately the same as the Berea Sandstone J-function). This is a reasonable assumption for our practical purposes. Therefore, the effects of absolute permeability and the corresponding porosity on relative permeability curves must be investigated. Honarpour et al.(1986)[142] presented a comprehensive review of the effects of these two rock properties on relative permeability curves. In the review, the works of Wyckoff and Botset[143], Leverett and Lewis[144], Dunlap[145], Stewart et al.[146] and Morgan and Gordon[147], were summarised where the effect of absolute permeability and porosity on relative permeability curves were found to be insignificant. On the other hand, the dependence of irreducible water saturation as well as end-points relative permeability was established in the work of Keelan[148] and Leas et al.[149], however, this relationship is limited to particular cases where it is believed not to be true in general. Furthermore, the use of a single relative permeability curve to simulate reservoir performance despite the existence of different absolute permeability layers, is a conventional approach. This can be seen in the simulation work of Afidick et al.[150] in their multi-layer modelling of the Arun Field where a single relative permeability curve was used for all the six layers of the reservoir model with permeability variations from 1.5 to 49.0 mD.

Hence, the effect of absolute permeability and the corresponding porosity on the base relative permeability curve is assumed to be insignificant. Therefore, the measured base relative permeability curves of the Berea Sandstone core are used throughout this study. Also the permeability-porosity semi-log plot of Timur (1968)[141] is used to obtain an estimate of reservoir porosity for a given permeability because it predicts the porosity of the 100 mD Berea Sandstone core adequately (within 12% error margin). The base relative permeability curves used in this study are given in Fig. 7.3.

7.3.2 Fluid and Reservoir Properties

The fluid used in this analysis is a real North Sea gas-condensate fluid characterised by Whitson and Torp (1983)[104]. The heavy hydrocarbon components are grouped into five pseudo components. The composition is given in Table 7.2 and the properties of the pseudo components together with the binary interaction coefficient (BIC) between these components and methane are shown in Table 7.3. This fluid is chosen for this study because it was used by Fevang and Whitson (1995)[25] in their modelling of gas-condensate well deliverability. While the main objective of this study is different from theirs, both studies centre on the concept of well deliverability. Hence, by using the same model we can compare some aspects of the two studies. The key reservoir fluid properties at two different temperatures are given in Table 7.4 and the reservoir properties are given in Table 7.5.

7.3.3 Nc-Effect Investigation

Base Cases

In the base case runs none of the effects of IFT, N_C or Forchheimer are considered, referred to in all the figures as "None". First a single layer model with a uniform reservoir absolute permeability of 10 mD is considered. Second a double-layer reservoir model where an absolute permeability contrast of one order of magnitude is provided between the top and bottom layer (i.e. top layer k = 10 mD and bottom layer k = 100 mD). The layouts of the two reservoir models are detailed in Table 7.6.

Affected Cases

The IFT effect, Nc effect, and the combined N_C and Forchheimer effect are considered in three separate runs for the single-layer reservoir model. The impacts of the above three effects on total production of gas and oil, production rates, gas-oil ratio, and well productivity indeces are demonstrated in Figs. 7.4 to 7.9; and their impacts on pressure and condensate saturation histories at one-foot, 5, 40 feet radial distance from the wellbore, and at the external reservoir boundary are demonstrated in Figs. 7.10 to 7.17.

Only the combined N_C and Forchheimer effect (besides the base case) are considered for the double-layer reservoir model. Furthermore, since production potential of the double-layer reservoir is more than the single-layer one the gas-phase maximum production plateau rate is increased from 40 MMScf/d to 100 MMScf/d to maintain a reasonable annual hydrocarbon depletion rate from the reservoir (around 10% HCPV per annum). The impact of this effect on the recoveries, rates, and well productivity indices for both gas and oil phases are demonstrated in Figs. 7.18 to 7.23. The impacts on condensate saturation history at one-foot, 5, 40 feet radial distance from the wellbore, in both layers of the model, are demonstrated in Figs. 7.24 to 7.26.

7.3.4 Sensitivity Analysis

The purpose of this exercise is to try to define the boundaries that define the significance of N_C-effect on the recoveries from gas condensate reservoirs. Maximum liquid drop-out, maximum plateau production rate and reservoir absolute permeability are considered in this exercise. As mentioned earlier, the sensitivity analysis is conducted on the single-layer reservoir model.

Liquid Drop-out

First, the effect of reservoir fluid richness is investigated to determine whether this property can be used as a variable that can reflect the importance of the N_C-effect on the recoveries. For example, the significance of the N_C-effect that is established for recoveries from the rich gas condensate reservoir can be as important for the recoveries from a lean gas condensate one. The maximum liquid drop-out of the reservoir fluid is reduced from 23 to 3% by increasing reservoir temperature from 266 to 315 ^{O}F (the properties of this fluid at this temperature are listed in Table 7.4). Since the reservoir dew point pressure at this temperature is decreased from 5900 to 5400 psia initial reservoir pressure is also reduced to 5500 psia. For this lean gas condensate reservoir only the IFT and combined N_C and Forchheimer effects are considered. The impacts of IFT and combined N_C and Forchheimer effects on the recoveries, rates, and well productivity indices for both gas and oil phases are demonstrated in Figs. 7.27 to 7.32. Also condensate saturation histories at one foot, five feet, 40 feet and at external reservoir boundary are given in Figs. 7.33 to 7.36 respectively. The figures are discussed in detail in section 7.4 below.

Reservoir Absolute Permeability

Second, the impact of the reservoir absolute permeability on the significance of the N_C effect is determined. For both the rich and lean gas condensate reservoirs, the absolute permeability is varied between 10 mD and 400 mD. Also, the maximum gas production plateau rate is varied accordingly so that the annual hydrocarbon depletion rate from the reservoir for all the different permeability cases is kept constant. For each absolute permeability value, total gas and condensate recoveries of the base case (no effect) are compared with the recoveries of the N_C effectted in the presence of Forchheimer case.

For the rich gas condensate reservoir gas and condensate total production with and without the N_C and Forchheimer effect are shown in Figs. 7.37 and 7.38 for the various reservoir absolute permeabilities. The same is shown for the lean gas condensate reservoir in Figs. 7.39 and 7.40 (refer to section 7.4 for detailed analysis).

Maximum Plateau Production Rate

Third the impact of the maximum plateau gas production rate on the significance of the N_C effect is investigated. For both the rich and lean gas condensate single-layer reservoir models, the maximum plateau gas production rate is varied between 40 MMscf/d and 10 MMScf/d. For each production rate case, the total gas and condensate recoveries of the base case are compared with those of the N_C affectted in the presence of Forchheimer case.

For the rich gas condensate reservoir, the gas and condensate total productions are shown in Figs. 7.41 and 7.42 for the various maximum plateau gas production rates. The same is shown in Figs. 7.43 and 7.44 for the lean gas condensate reservoir.

7.4 ANALYSIS OF RESULTS

7.4.1 The Overall Impact

Single-Layer Reservoir Model

While N_C affected case and N_C affected in the presence of Forchheimer case are conducted, the latter case is believed to better represent the actual two-phase flow at near wellbore conditions than the former one. Hence, the comparison hereafter, is carried-out between the N_C affected in the presence of Forchheimer case and base case. The IFT-affected case is also performed. However, it is only reported for the sake of pointing-out the deficiency when compared with the alternative N_C dependent case.

For a rich gas condensate single layer model the effect of N_C dependent relative permeability is significant. Even when considering the effect of N_C in presence of the opposite Forchheimer effect, the net result is still quite a significant improvement. The accelerated production from the reservoir due to the improvement in the relative permeability is evident in terms of both the gas and the condensate total productions. After a six year production period the gas and condensate total production is increased by 27.5% and 19.2% from the base case respectively (refer to Figs. 7.4 to 7.7). This productivity enhancement is a reflection of significant improvement in both gas and condensate phase wellbore productivity indices, refer to Figs. 7.8 and 7.9. Over the same production period, the average gas-phase productivity index is higher by 26.9% than the base case value; and the average condensate-phase productivity index is higher by 14.3% than the base case value.

To understand the mechanics of the N_C effect in the two-phase flow in this single-layer reservoir, careful investigation of pressure and condensate saturation histories at various sections of the reservoir must be performed. With reference to Figs. 7.10 to 7.13 for the pressure histories, the N_C effect manifests itself differently at different locations of the reservoir. At near wellbore conditions (at both 1.0 and 5.0 feet from wellbore) the N_C effect retards pressure decline that characterises the early production period of the base case. On the other hand, pressure is depleted at much faster rate at conditions far from wellbore (at both 40 and 3000 feet from wellbore) than its slow depletion during the base case production.

With reference to condensate saturation histories, in Figs. 7.14 to 7.17, the condensate bank build-up is evident at near wellbore conditions as well as a gradual increase in condensate saturation throughout the reservoir as production continues. A much greater bank build-up (up to 56%) at near wellbore conditions due to the N_C-effect (Figs. 7.14 and 7.15) than in the base case. Also, a much greater efficiency in producing such a bank in the N_C-affected case than in the base case.

For comparison with the N_C-affected case, the IFT-affected case is shown in all the aforementioned figures. With reference to Figs. 7.4 to 7.9, the IFT effect does not capture the full potential for recovery improvement from such a rich gas condensate reservoir. It underestimates the recoveries of both gas and condensate phases where the above stated significant improvement in the recoveries due to the N_C effect is reduced to an indeed abysmal change due to the IFT compared to the base case.

Double-Layer Reservoir Model

With reference to Figs. 7.18 to 7.21 the improvement in the recovery in the gas-phase in the two-layer reservoir model due to the N_C effect in the presence of Forchheimer effect is not as significant as that in the single-layer reservoir model. On the other hand, this is compensated by a remarkable improvement in the condensate-phase total recovery. At the end of ten year production period, the double-layer reservoir model increased its total condensate production by 20.8% from the base case. The significance of the improvement is also evident in both the gas and condensate productivity indices as demonstrated in Figs. 7.22 and 7.23 especially during early production time.

There is a decrease in the significance of the N_C effect on total gas recovery and an increase in the significance on condensate phase recovery of the double-layer reservoir model than the single-layer one. The reason behind this reduction, is demonstrated in Figs. 7.24 to 7.26 where condensate saturation histories around the wellbore are shown. In these figures clearly the higher permeability bottom layer accumulates more condensate than the lower permeability top layer without the influence of N_C effect. Furthermore, the N_C effect reduces the condensate transport efficiency in this layer helping it accumulating an even more condensate. Therefore, the improvement in the gas-phase recovery due to the N_C effect in the lower permeability top layer is significantly diminished by the unfavourable flow conditions (i.e. high condensate accumulation) in the higher permeability bottom layer. On the other hand, the high condensate accumulation in the higher permeability, bottom layer, encourages more condensate production simply because there is more condensate available for production.

7.4.2 Boundaries of The Impact

Liquid Drop-out

It is clear from Figs. 7.27 to 7.32 that the N_c effect in the presence of Forchheimer is as significant for the recoveries from this lean gas condensate reservoir as those of rich one detailed in the previous sections. Total gas production is increased by 12.3% due to the N_c effect in the presence of Forchheimer effect after six years of production. The corresponding increase in the total condensate production is 12.5%. All other productivity indicators such as well productivity indices and condensate liquid build-up followed a similar trend as those of the rich gas condensate reservoir.

An important observation from the saturation histories (shown in Figs. 7.33 to 7.36 for the lean gas condensate reservoir case and in Figs. 7.14 to 7.17 for the rich gas condensate case) is that maximum condensate build-up near the wellbore for the lean case is not significantly different from that of the rich case (i. e. 46% for the lean case and 56% for rich case). This marginal difference persists throughout production and the different locations of the reservoir. This means that reservoir fluid richness is not the principal controller of the amount of liquid built-up at near the wellbore region. Therefore, the most likely criterion for controlling the condensate build-up is condensate transport efficiency between grid-blocks within the reservoir on one hand and between the reservoir and the wellbore on the other.

Reservoir Absolute Permeability

Table 7.7 shows the calculated increases, from the base case, in gas and condensate total recoveries after a six year production period. They are calculated for absolute permeability of 10, 100, 200, and 400 mD cases for the rich as well as the lean gas condensate reservoirs. It is evident from this table that the impact of the N_c effect in the presence of Forchheimer on gas total recovery is significant when reservoir absolute permeability is about 10 mD or less. On the other hand, its effect on the condensate-phase total recovery is significant at all reservoir absolute permeability levels for both the rich and the lean reservoirs.

Therefore, it can be stated that for both the rich and the lean gas condensate single-layer reservoir models, the impact of the N_c effect in the presence of Forchheimer can not be ignored regardless of reservoir absolute permeability.

Maximum Plateau Production Rate

Figures 7.41 and 7.42, show the impact of the N_c effect in the presence of Forchheimer on gas and condensate total recoveries respectively for the rich gas condensate reservoir, and Figs. 7.43 and 7.44, show the impact on the total recoveries for the lean gas condensate reservoir. As can be seen from these figures, low maximum production plateau rates reduce the impact on total recoveries. Table 7.8 gives the evaluated improvement in the total recoveries after six years of production. For the rich gas condensate reservoir, the improvement in the total recovery of the gas phase due to the effect is significant when the maximum plateau production rate is about 20 MMScf/d or greater. In the case of the lean gas condensate system, the improvement in the total recovery of the gas phase due to the effect is significant when the maximum plateau production rate is about 30 MMScf/d or greater. On the other hand, the improvement in the condensate total recovery due to this effect is found to be significant regardless of the maximum plateau production rate for both rich and lean gas condensate reservoirs. Indeed the significance of the effect on the condensate total recovery increases with decreasing such a maximum plateau production rate.

Hence, it can be stated that for both the rich and the lean gas condensate single-layer tight reservoir models the significance of the N_c effect can not be ignored regardless of the maximum plateau gas production rate.

7.5 DISCUSSIONS

Gas condensate well deliverability was modelled by Fevang[3] and reported by Fevang Whitson[25]. They used, in their simulation work, a one dimensional fine-grid single well and real gas condensate fluid similar to the one used in this study. They concluded that the impact of IFT on well deliverability was not significant. This finding is identical to finding in this study. Another important finding of their modelling work was that there is a minimal effect of critical or residual condensate saturation on gas condensate well deliverability. This finding enhances the findings in this study in the sense that the use of a critical or residual condensate saturation other than zero would not have a significance over the various conclusions reached in this study. On the other hand, in their study the importance of the improvement introduced by N_c dependent relative permeability was not considered. Therefore, the inefficiency of their reservoir model to reduce the condensate blockage at near wellbore from its maximum build-up is similar to our base case where few saturation percents reduction in condensate saturation was evident over the course of ten year production. As demonstrated in the saturation histories (analysed in section 7.4.1) the maximum condensate build-up at near the wellbore is reduced by more than 20 saturation percent over the same production period. This undoubtedly has a significant influence over the gas condensate well deliverability as shown by the various figures presented in this study.

Afidick et al.[150] modelled the production from Arun field, a tight and lean (< 1.2% liquid drop-out) gas condensate reservoir located in Northern Indonesia, using a multi-layer as well as single-layer one dimensional fine-grid single well and real gas condensate fluid similar to the one used in this study. They reported that a six-layer reservoir model was more realistic for the 765 feet thick formation than the single-layer model. The effects of neither IFT nor N_c were considered in their simulation work; however, a straight line gas relative permeability relation was used instead of the experimental "curved" relative permeability curves to history-match the actual production from the single well reservoir simulation. They also found that the higher permeability reservoir layers accumulate more condensate than lower permeability ones. This finding is identical to our finding in the double-layer rich gas condensate reservoir model for both N_c affected as well as the base cases.

van de Leemput et al.(Oct. 1995)[24] performed full field reservoir modelling of gas/condensate fields of Central Oman. They stated that they have used capillary number dependent gas condensate relative permeability curves to simulate deliverability enhancement due to velocity at near wellbore regions. They also incorporated Forchheimer effects via rate dependent skin. Because of the limited details provided in their paper a full comparison between the conclusions from their study and those of this study can not be performed. However, it was stated that the relative permeability linkage to capillary number was based on measurements obtained from centrifuge experiments and correlated with the bond number and not with the capillary number. Moreover, they emphasised the applicability of the use of capillary number dependent relative permeability to represent what they have termed viscous stripping at near the wellbore, yet they reported neither the specific relative permeability - capillary number correlation nor the mechanics of such linkage.

Diamond et al.[151] performed a probabilistic prediction of well performance of the Britannia gas condensate field located in the central North Sea. In their work radial simulation models were tuned to appraisal DST data to provide tuning parameters for the non-Darcy (Forchheimer) skin and capillary number effects. Gas condensate relative permeability curves were modified so that they change linearly from the base relative permeability curve to a miscible curve within transitional capillary number limits (i. e. 1.0×10^{-5} to 4.0×10^{-4}). When the capillary number exceeds the upper limit (4.0×10^{-4}) relative permeability curves will be those of miscible flow. Another constant determined from the tuning was Forchheimer β factor. While the importance of the impact of N_c effect on well deliverability has been acknowledged in this work, the relationship between the capillary number and gas condensate relative permeability has been oversimplified to provide a better control over history matching of DST data. This oversimplification compromises the physics governing the relationship between IFT and velocity (i.e. N_c) at one end and gas condensate relative permeability at the other. Furthermore, the upper limit for N_c of 4.0×10^{-4} is not physically meaningful because most relative permeability measurements, performed in house and elsewhere, have reached this N_c limit where flow is not yet miscible.

7.6 SUMMARY OF RESULTS AND CONCLUSIONS

A comprehensive gas condensate well deliverability study has been performed. Total recoveries and pressure and condensate saturation histories due to the impact of IFT, N_c, and Forchheimer effects have been carefully investigated in single and double-layer reservoir models. Also, the significance of the N_c effect combined with Forchheimer effect has been determined under various reservoirs and fluid conditions. Maximum liquid drop-out, reservoir absolute permeability and maximum gas plateau production rate have been varied to define the boundaries of the significance of such effects.

It is demonstrated that the IFT effect alone cannot be a true representative of the potential enhancement introduced by interaction of capillary and viscous forces at near wellbore conditions where viscous stripping is highly active. IFT effect is found to underestimate the improvement in gas condensate well deliverability that is due to N_c dependent two-phase flow at near wellbore region. Also, from the comparison between the rich and the lean gas condensate reservoir saturation histories, condensate transport efficiency between grid-blocks within the reservoir on one hand and between the reservoir and the wellbore on the other instead of reservoir fluid richness is more likely to be the principal controller of the amount of liquid built-up at near the wellbore region. The findings of this study are summarised in Tables 7.9 to 7.11. Table 7.9 shows the significance of the overall impact due to the N_c effect in the presence of Forchheimer in terms of the percent increase in the gas total production after six years of production. At the end of this production period, the improvement in the gas total recovery is significantly higher for the single-layer reservoir model than for the double-layer one. On the other hand, the improvement in the condensate total recovery is higher for the double-layer model than for the single-layer reservoir one.

Table 7.10 summarises the results from the sensitivity analysis conducted on the single-layer reservoir model where the boundaries of the importance of the significance are drawn for both the gas and condensate phases. The N_C effect in the presence of Forchheimer is significantly important for both gas and condensate phases whether the reservoir fluid is rich or lean. Also, the effect is significant for the gas-phase total recovery only when reservoir absolute permeability is 10 mD or less. Yet, the effect on the condensate-phase total recovery is significant regardless of the reservoir permeability. Furthermore, the significance of the effect on the condendsate-phase total recovery from this tight reservoir can not be ignored at any plateau production rate. Its impact on the gas-phase total recovery is only important when the gas plateau production rate is greater than 20 and 30 MMScf/d for the rich and lean reservoirs respectively.

Table 7.11 summarises the results from the sensitivity analysis conducted on the single-layer reservoir model where the tendencies of the significance are stated for both the gas and condensate phases. The significance of the N_C effect in the presence of Forchheimer effect on condensate-phase recovery is found to be directly proportional to gas plateau production rate, maximum liquid drop-out and reservoir absolute permeability. On the other hand, its significance on gas-phase recovery is found to be directly proportional to maximum liquid drop-out and gas plateau production rate, and inversely proportional to reservoir absolute permeability.

Therefore, for optimum gas-condensate reservoir management, phase production priorities must be established first. For example, a decision on what is the preferred phase of production must be achieved. To maximise the production of the preferred phase, therefore, a set of production parameters must be chosen. Provided that such a decision has been taken and other borehole and facility related factors are controlled, by recognising reservoir fluid richness and reservoir absolute permeability an optimum maximum production plateau rate can be identified. The finding from this study can therefore be used as a guideline for the tailoring of such an optimising process for a specific field.

This study has shown that for accurate field performance prediction a simulator should be used that has the facility to account for N_c and Forchheimer effects. Operators, therefore, should perform tests to determine the required parameters for their particular reservoir fluids and rock properties.

Table 7.1: Scale function exponents, base values, and constants

Exponent / Constant	Equation	IFT Effects		Nc + Forchheimer Effects	
		Gas	Cond.	Gas	Cond.
F_i	7.1	-	-	1	0
$B1_i$, $B2_i$	7.3	-	-	1, 0	-
a_i		-	-	48193.11	-
b_i		-	-	2.00	-
c_i		-	-	2.00	-
d_i		-	-	0.50	-
S_{rbi}	7.5	-	-	0.48	0.00
nr_i	7.6	-	-	51	0.00
N_{cbi}	7.7	-	-	2.0×10^{-6}	4.5×10^{-6}
$N1_i$, $N2_i$, $N3_i$	7.9	-	-	1, 0, 0	1, 0, 0
ni_1	7.10	-	-	1.00	1.00
ni_2		-	-	0.25	0.08
n	6.1	20.0	20.0	-	-
σ_b,(mN/M)		0.78	0.78	-	-

Table 7.2: Gas-condensate fluid composition

Abbreviation	Description	Value %
CO_2	Carbon dioxide	2.37
N_2	Nitrogen	0.31
C_1	Methane	73.19
C_2	Ethane	7.80
C_3	Propane	3.55
iC_4	isobutane	0.71
nC_4	n-butane	1.45
iC_5	isopentane	0.64
nC_5	n-pentane	0.68
C_6	Hexanes	1.09
PST1	C_7-C_9	3.2466
PST2	C_{10}-C_{13}	2.1410
PST3	C_{14}-C_{17}	1.1421
PST4	C_{18}-C_{24}	0.9749
PST5	C_{25+}	0.7054

Table 7.3: Pseudo component fluid properties

Name	Pc (psia)	Tc (°R)	MW kg/kmol	Accentric factor	Bp (°R)	Methane BIC
PST1	425.50	1016.5	106.1	0.3044	382.39	0.03659
PST2	313.10	1163.6	152.7	0.4348	463.89	0.04292
PST3	237.40	1304.5	209.2	0.5856	546.89	0.04807
PST4	182.70	1446.0	281.5	0.7832	637.17	0.05254
PST5	168.80	1584.2	462.3	0.8819	708.94	0.16500

Table 7.4: Key Fluid Properties

Reservoir Fluid Classification	Rich gas	Lean Gas
Temperature, °F	266	315
Initial Reservoir Pressure, psia	6500	5500
Dewpoint Pressure, psia	5900	5400
Maximum Liquid Drop-out, %	23	3
Initial CGR, STB/MMscf	175	45
API Gravity, °API	55	45

Table 7.5: Key Reservoir Properties, common to both models

Property	Value
Rock compressibility, psia^{-1}	5.0×10^{-6}
Reservoir thickness, ft.	200
Porosity ϕ, %	18.75
Irreducible water saturation S_{wi}, %	25
Reservoir Area, acres	650

Table 7.6: Single and double layered simulation models

Property / Dimension	Single Layer	Double Layer
No. of Gridblocks	20	40
Δ theta, Degree	20@360	40@360
Permeability, mD	20@10.0	20@10.0, 20@100.0
Gas maximum plateau production rate, MMScf/d	40	100
Δz, ft	20@200	40@100
Δr, ft (r_e =3000 ft) (r_w =0.35 ft)	0.36, 0.50, 0.76, 1.20, 1.85, 2.87, 4.46, 6.93, 10.77, 16.71, 25.96, 40.30, 61.81, 98.00, 150.96, 234.44, 364.08, 565.39, 878.02, 534.10	2*(0.36, 0.50, 0.76, 1.20, 1.85, 2.87, 4.46, 6.93, 10.77, 16.71, 25.96, 40.30, 61.81, 98.00, 150.96, 234.44, 364.08, 565.39, 878.02, 534.10)
k_v / k_h	1.0	1.0

Table 7.7: Sensitivity Analysis of the impact of the N_c effect: Improvement in total production at end of plateau period for different reservoir permeabilities

Permeability	Rich		Lean	
mD	Gas %	Cond. %	Gas %	Cond. %
10	27.5	19.2	12.3	12.5
100	0	23.2	0	18.3
200	0	31.9	0	22.7
400	0	36.2	0	27.0

Table 7.8: Sensitivity analysis of the impact of the N_C effect: Improvement in total production for different maximum gas production plateau rates after 6.0 years of production

Plateau Rate	Rich		Lean	
MMScf/d	Gas %	Cond. %	Gas %	Cond. %
40	27.5	19.2	12.3	12.5
20	10.1	12.3	0	6.2
15	0	5.9	0	5.7

Table 7.9: Overall impact of the N_C effect: Improvement from base case after six years for the rich gas condensate fluid

Reservoir Model	Gas	Cond.
	%	%
Single-Layer	27.5	19.2
Double-Layer	0	20.8

Table 7.10: Sensitivity Analysis of the impact of the N_C effect: Boundaries of the significance for both rich and lean gas condensate reservoirs

Category	Rich		Lean	
	Gas	Cond	Gas	Cond
Reservoir Permeability, mD	< 10	N	< 10	N
Maximum Production Plateau rate, MMScf/d	> 20	N	> 30	N

Table 7.11: Sensitivity Analysis of the impact of the N_C effect: Tendency of the significance

Phase	↑ Liquid Drop-out	↑ Production Rate	↑ Reservoir Permeability
Gas Phase	↑	↑	↓
Condensate Phase	↑	↑	↑

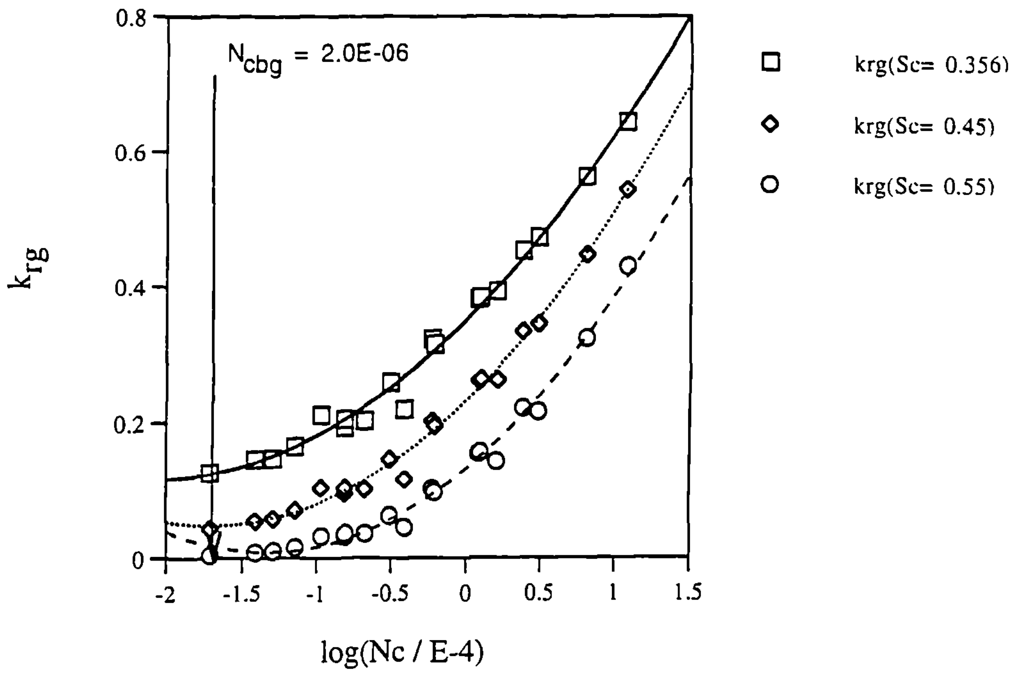

Figure 7.1: An estimate of gas-phase base capillary number (N_{cbg}) using the steady-state experiments measured on Berea Sandstone core, Nc = $\mu_g v_g / \sigma$.

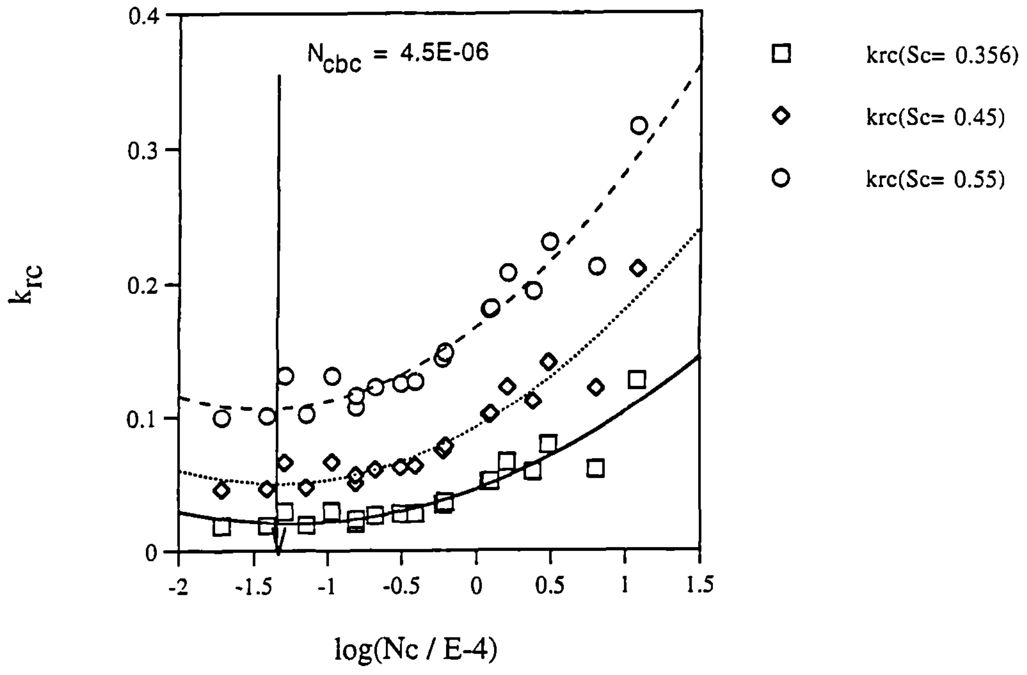

Figure 7.2: An estimate of condensate-phase base capillary number (N_{cbg}) using the steady-state experiments measured on Berea Sandstone core, Nc = $\mu_g v_g / \sigma$..

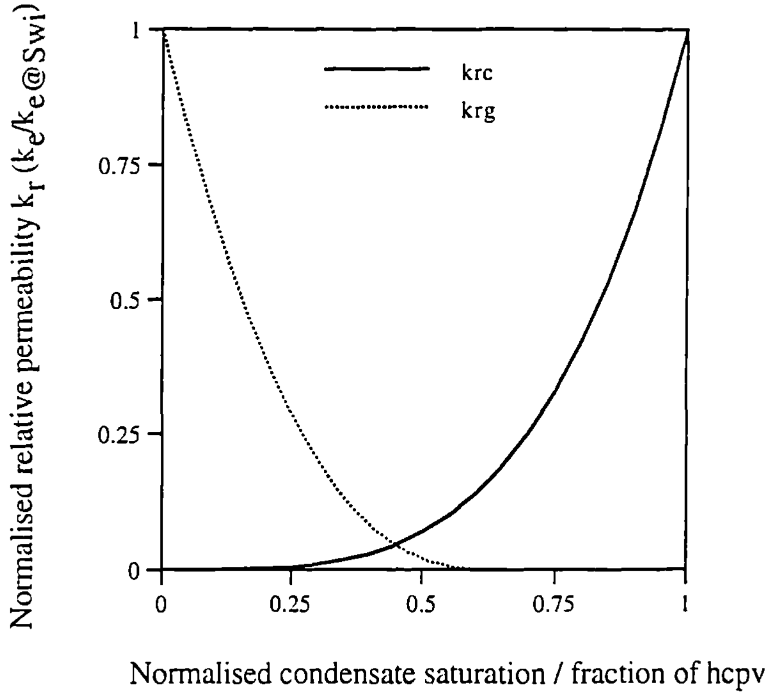

Figure 7.3: Base relative permeability curves used in the study at Ncb= 2.0 x 10^{-6}

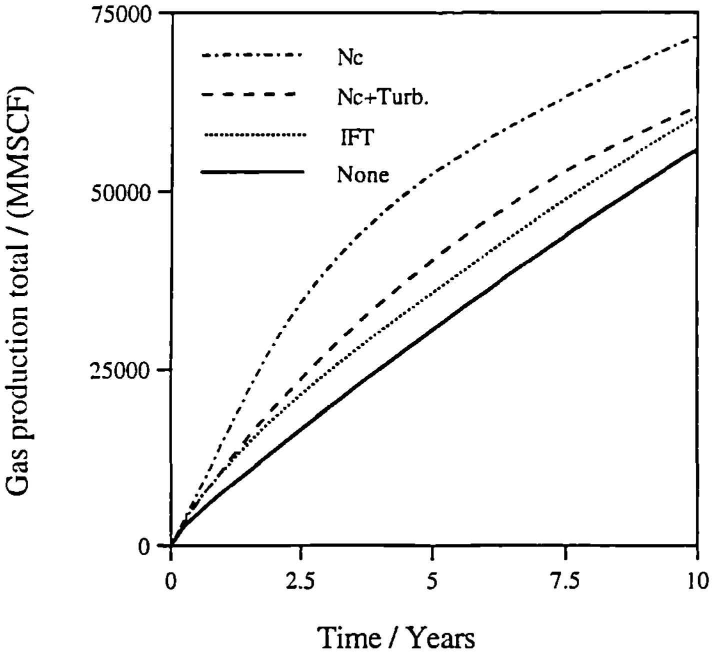

Figure 7.4: The impact of various effects on gas total production from a tight rich gas condensate reservoir (single layer model)

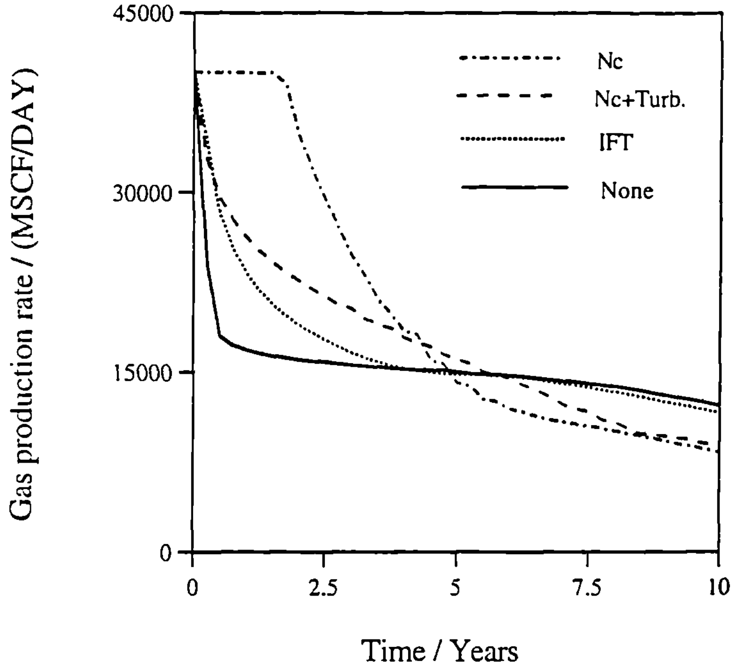

Figure 7.5: The impact of various effects on gas production rate from a tight rich gas condensate reservoir (single layer model)

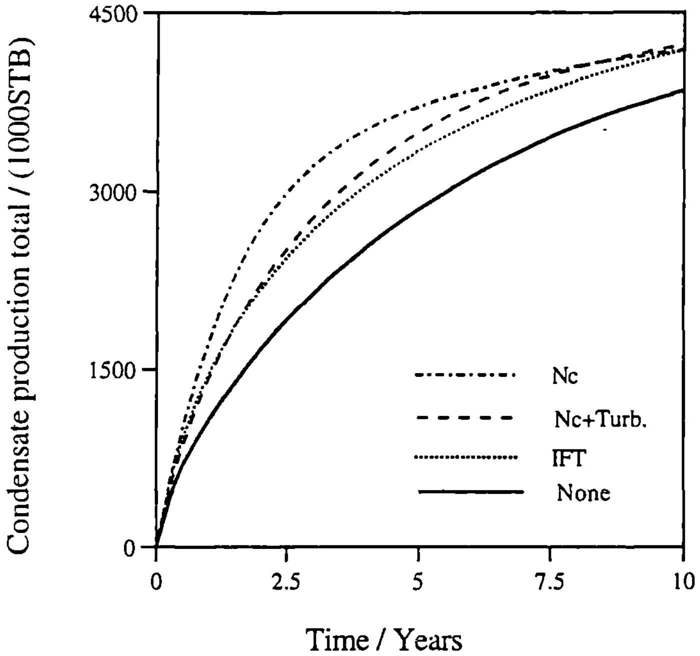

Figure 7.6: The impact of various effects on condensate total production from a tight rich gas condensate reservoir (single layer model)

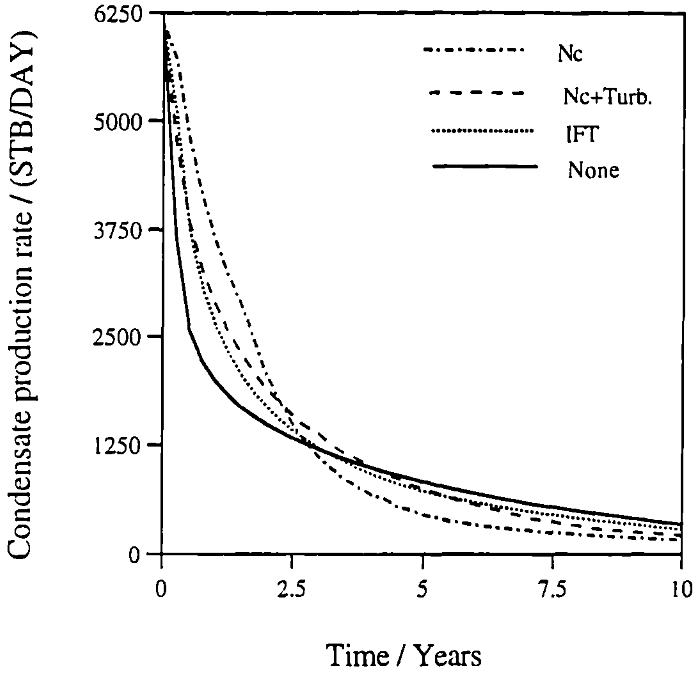

Figure 7.7: The impact of various effects on condensate production rate from a tight rich gas condensate reservoir (single layer model)

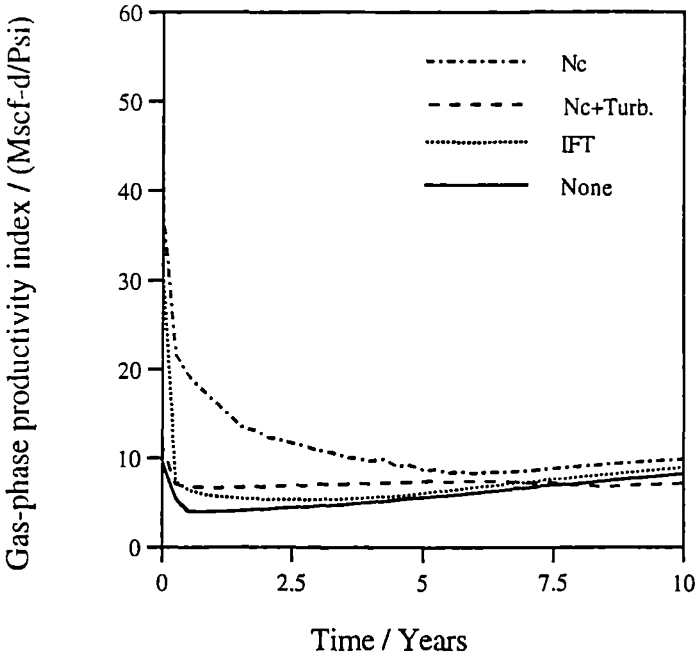

Figure 7.8: The impact of various effects on well gas-phase productivity index from a tight rich gas condensate reservoir (single layer model)

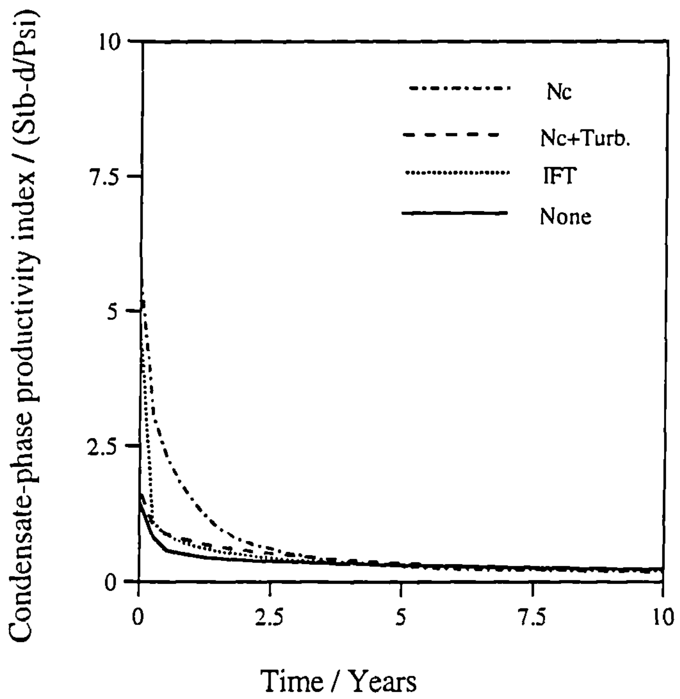

Figure 7.9: The impact of various effects on well condensate-phase productivity index from a tight rich gas condensate reservoir (single layer model)

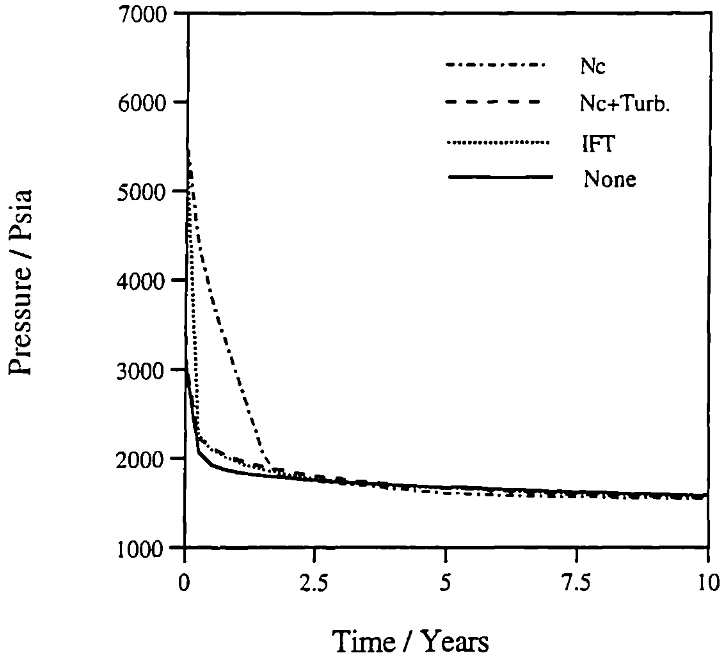

Figure 7.10: The impact of various effects on pressure history at 1.0 foot from wellbore for a tight rich gas condensate reservoir (single layer model)

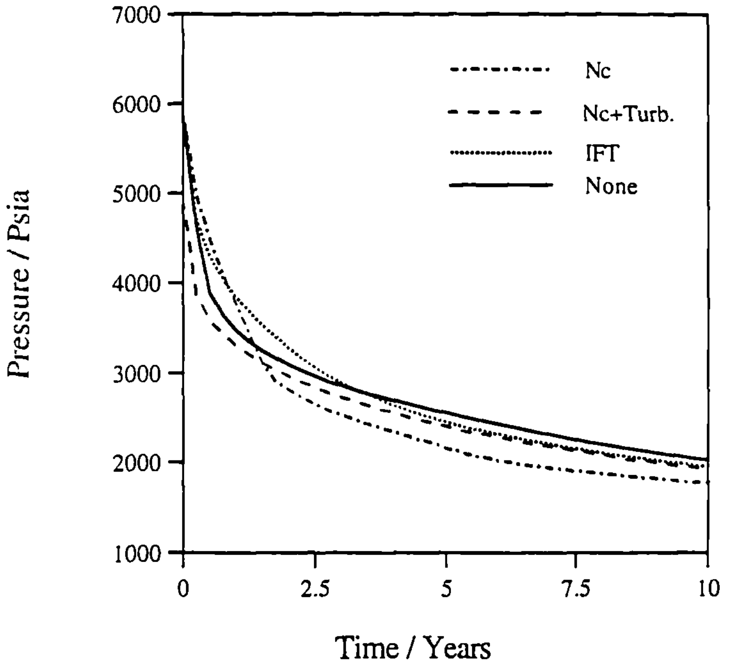

Figure 7.11: The impact of various effects on pressure history at 5.0 feet from wellbore for a tight rich gas condensate reservoir (single layer model)

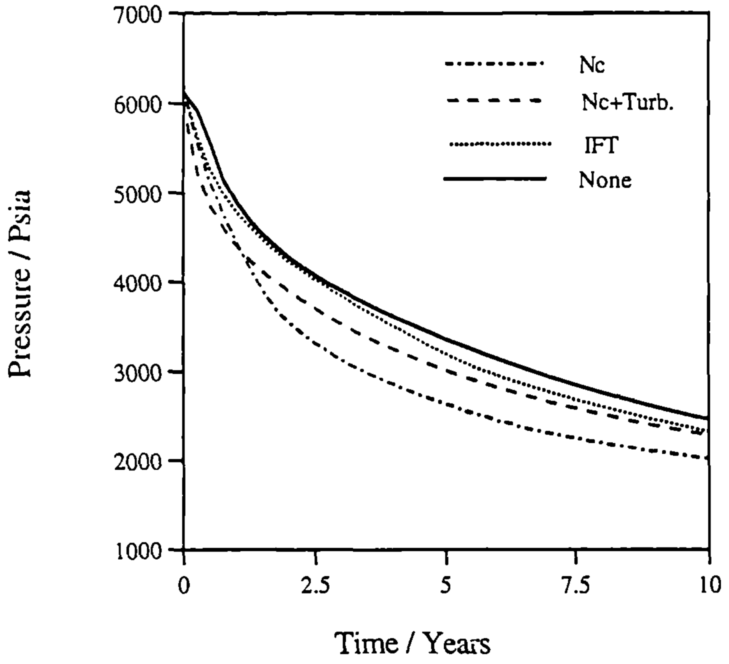

Figure 7.12: The impact of various effects on pressure history at 40.0 feet from wellbore for a tight rich gas condensate reservoir (single layer model)

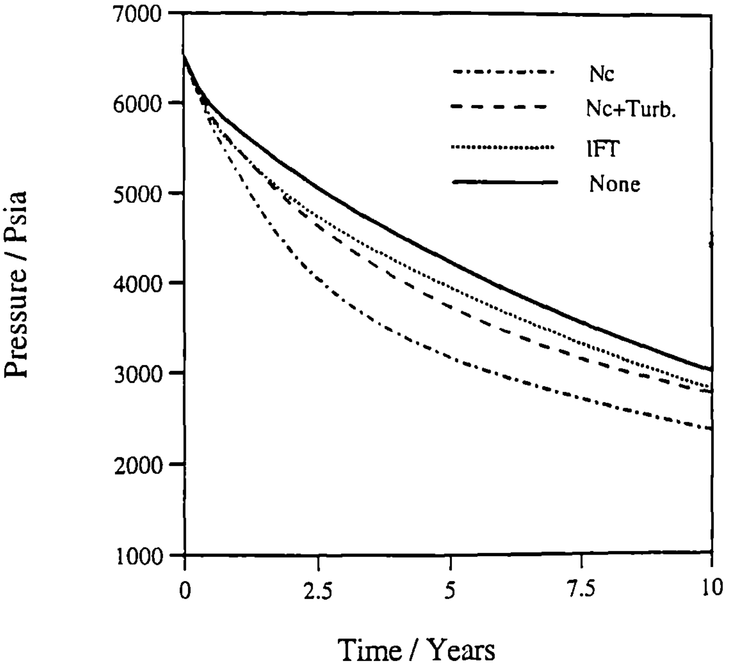

Figure 7.13: The impact of various effects on pressure history at external boundary of a tight rich gas condensate reservoir (single layer model)

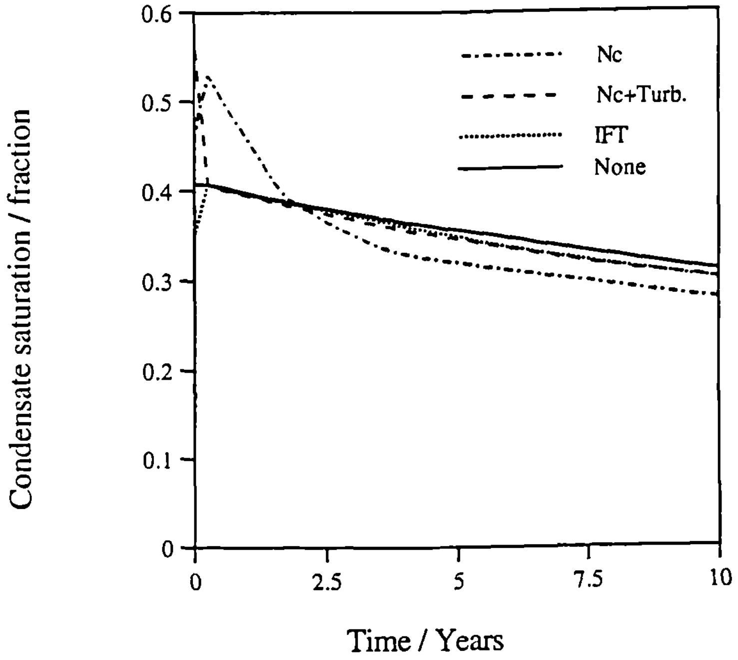

Figure 7.14: The impact of various effects on condensate saturation history at 1.0 foot from wellbore for a tight rich gas condensate reservoir (single layer model)

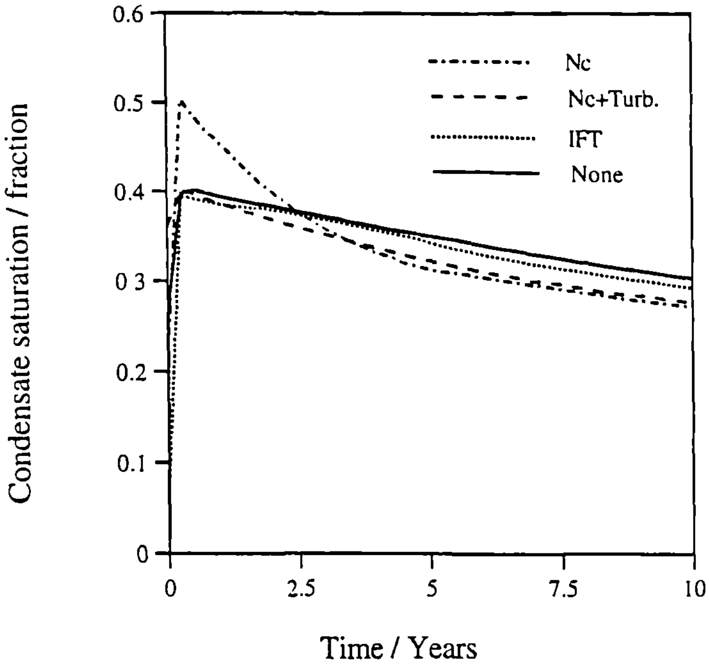

Figure 7.15: The impact of various effects on condensate saturation history at 5.0 feet from wellbore for a tight rich gas condensate reservoir (single layer model)

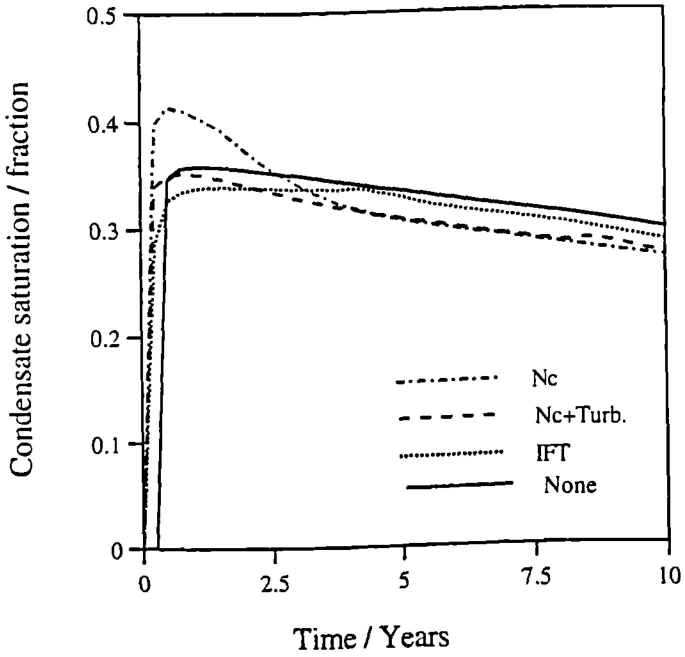

Figure 7.16: The impact of various effects on condensate saturation history at 40.0 feet from wellbore for a tight rich gas condensate reservoir (single layer model)

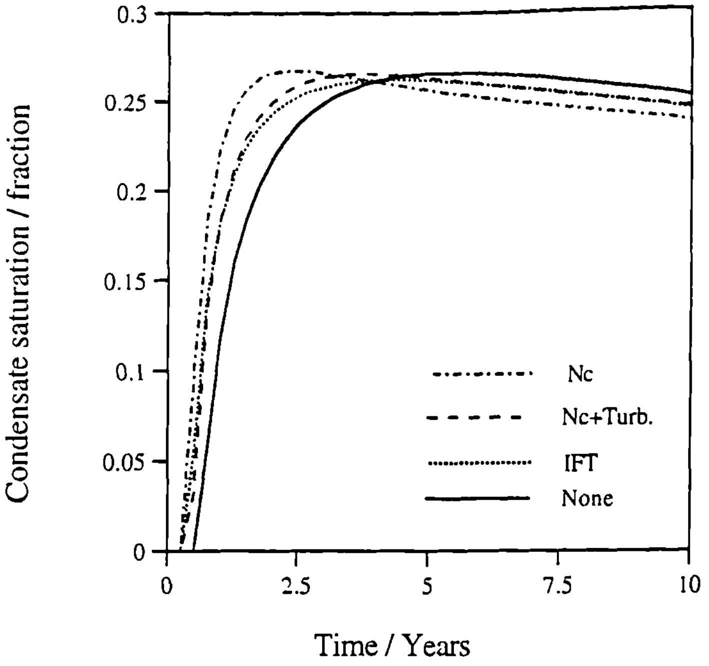

Figure 7.17: The impact of various effects on condensate saturation history at external boundary of a tight rich gas condensate reservoir (single layer model)

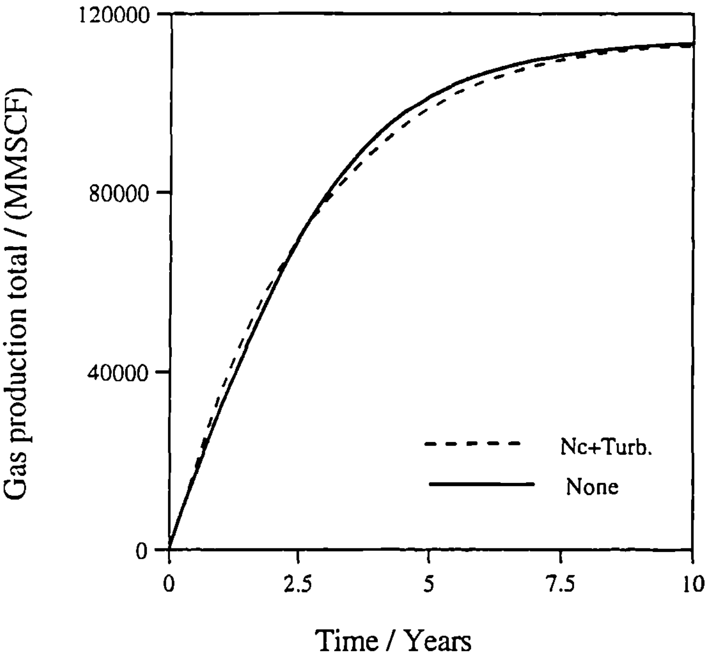

Figure 7.18: The impact of capillary number and turbulence on gas total production from a tight rich gas condensate reservoir (Two-layer model)

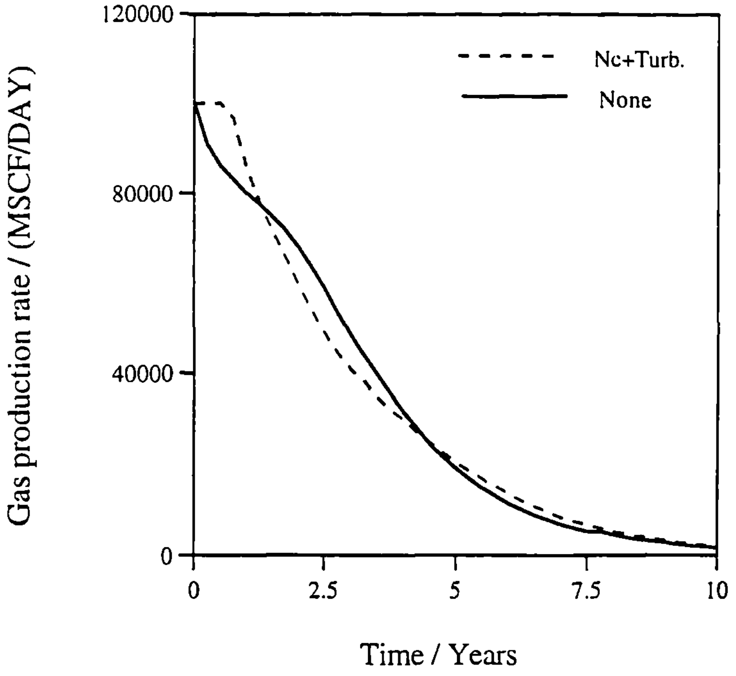

Figure 7.19: The impact of capillary number and turbulence on gas production rate from a tight rich gas condensate reservoir (Two-layer model)

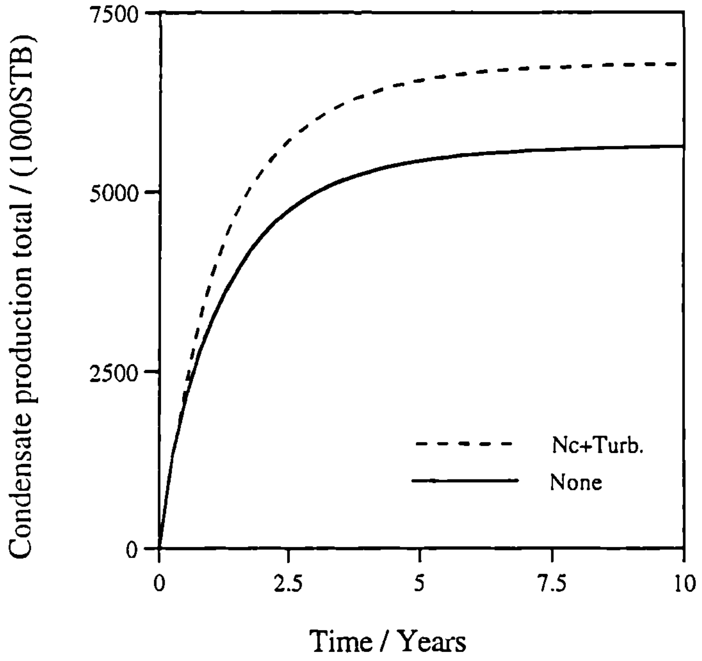

Figure 7.20: The impact of capillary number and turbulence on condensate total production from a tight rich gas condensate reservoir (Two-layer model)

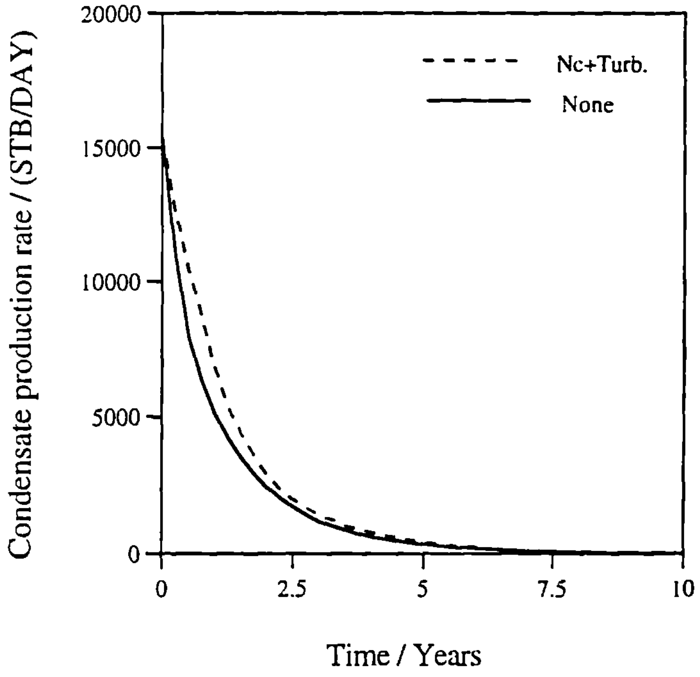

Figure 7.21: The impact of capillary number and turbulence on condensate production rate from a tight rich gas condensate reservoir (Two-layer model)

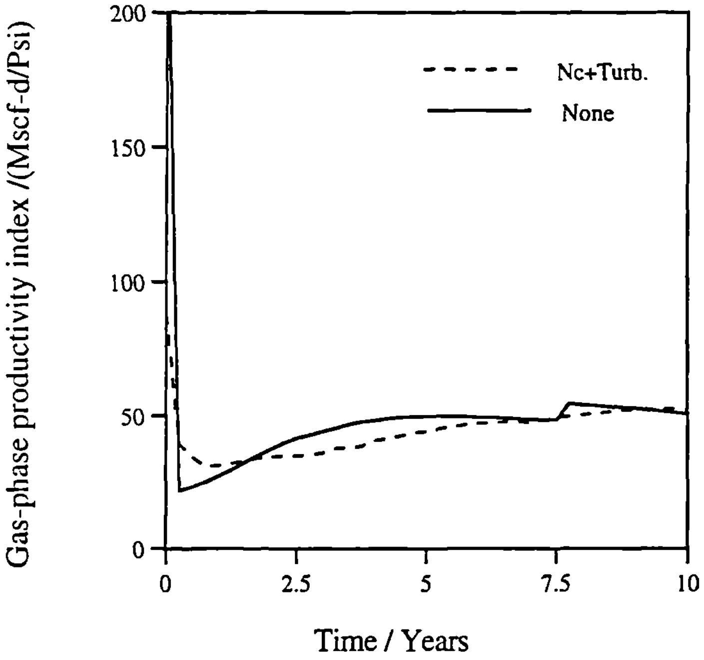

Figure 7.22: The impact of capillary number and turbulence on well gas-phase productivity index from a tight rich gas condensate reservoir (Two-layer model)

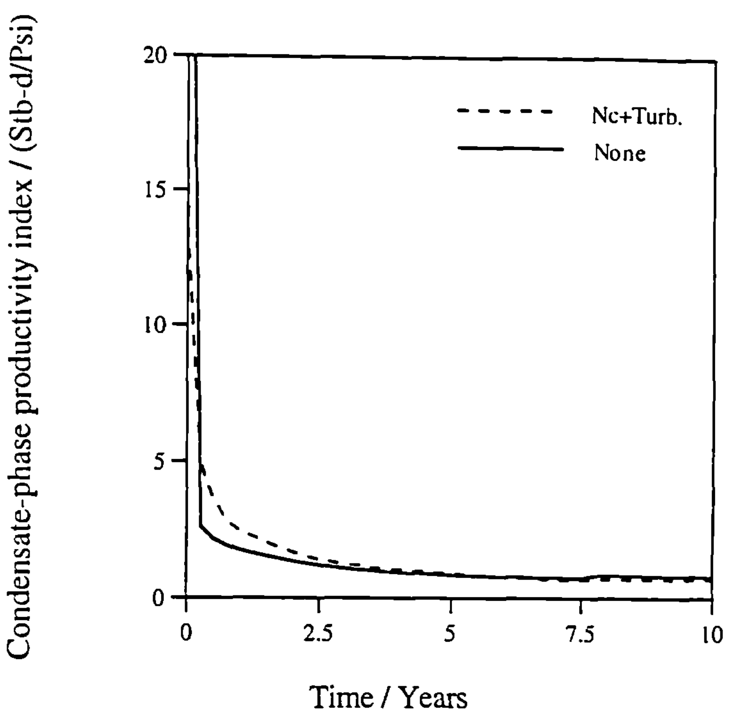

Figure 7.23: The impact of capillary number and turbulence on well condensate-phase productivity index from a tight rich gas condensate reservoir (Two-layer model)

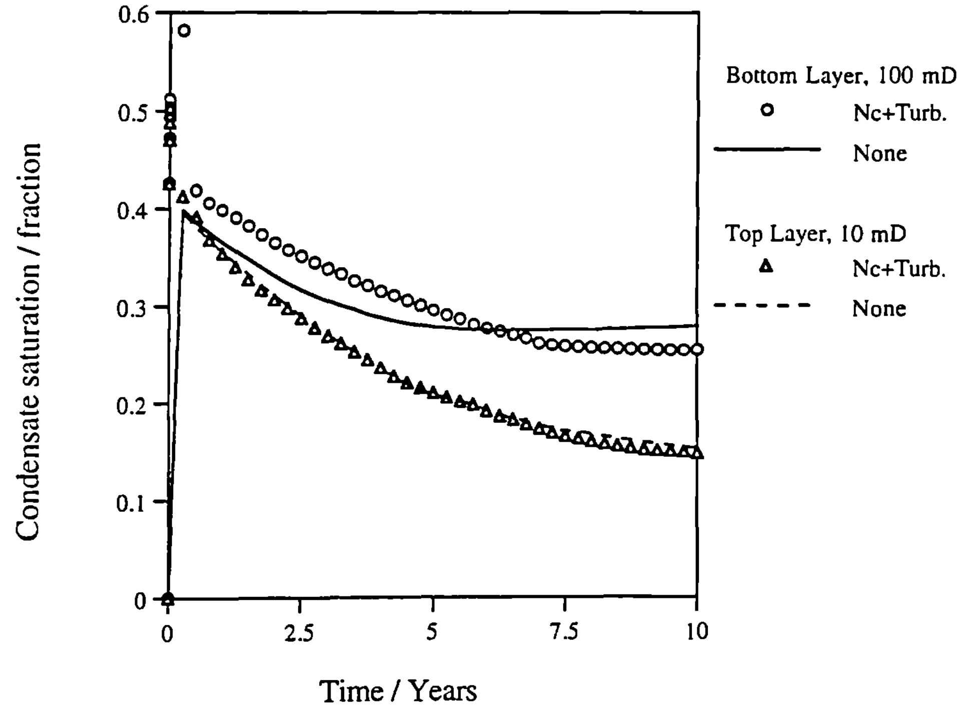

Figure 7.24: The impact of capillary number and turbulence on condensate saturation history at 1.0 foot from wellbore for a tight rich gas condensate reservoir (Two-layer model)

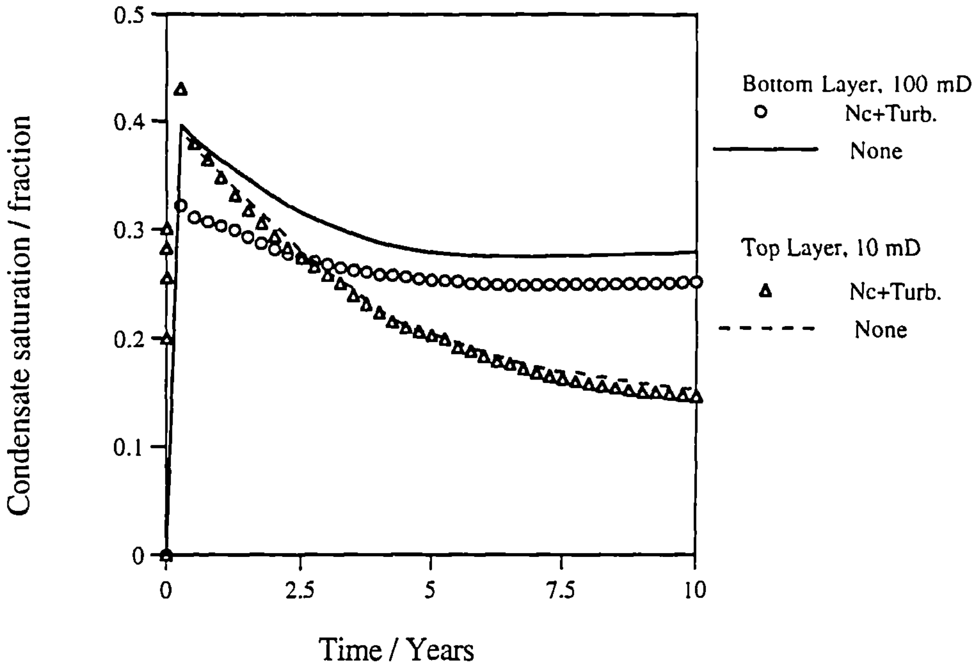

Figure7.25: The impact of capillary number and turbulence on condensate saturation history at 5.0 feet from wellbore for a tight rich gas condensate reservoir (Two-layer model)

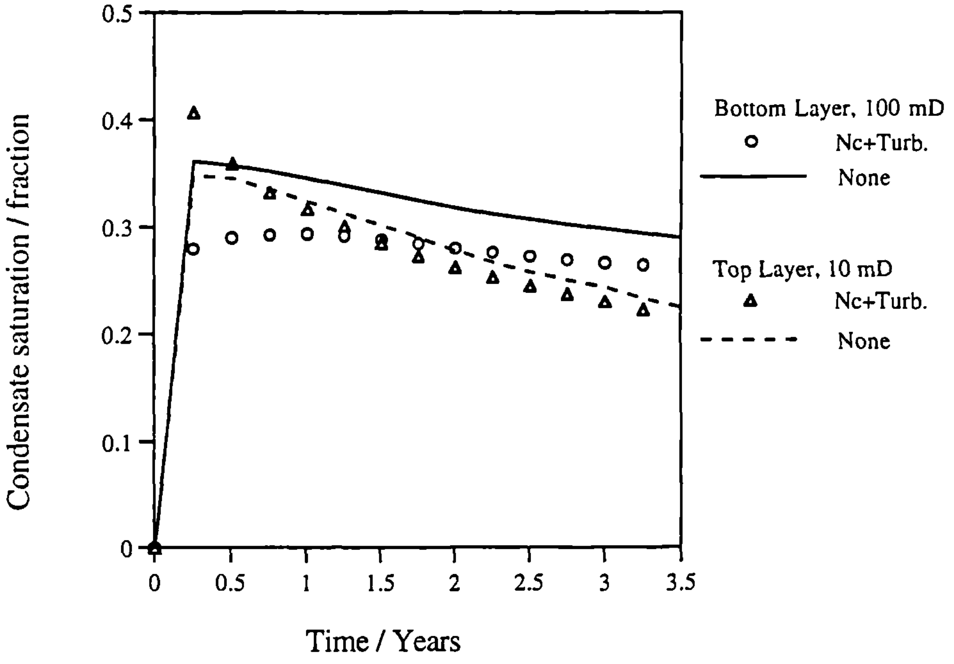

Figure 7.26: The impact of capillary number and turbulence on condensate saturation history at 40.0 feet from wellbore for a tight rich gas condensate reservoir (Two-layer model)

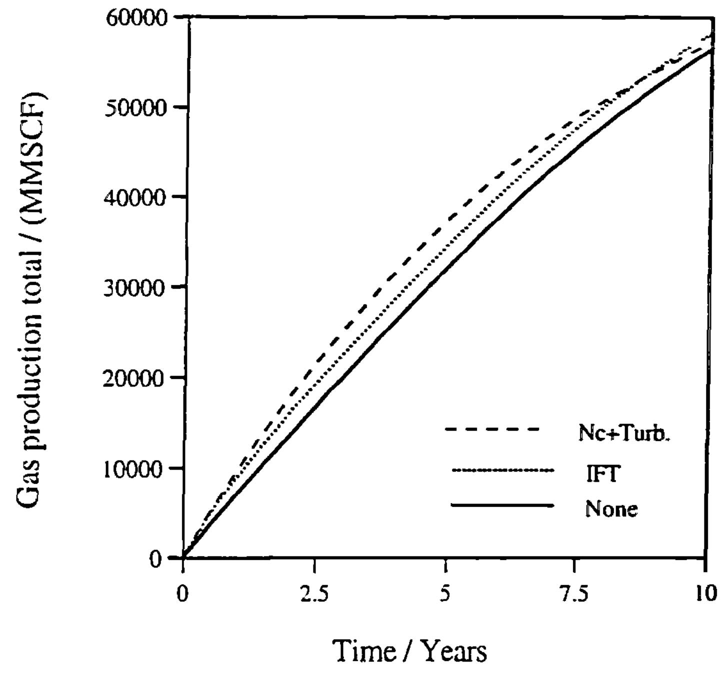

Figure 7.27: The impact of various effects on gas total production from a tight lean gas condensate reservoir (single layer model)

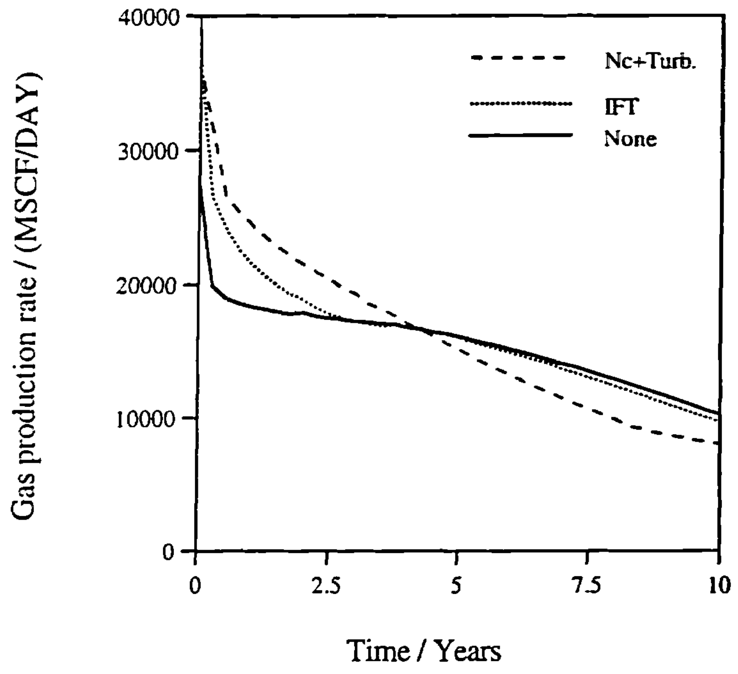

Figure 7.28: The impact of various effects on gas production rate from a tight lean gas condensate reservoir (single layer model)

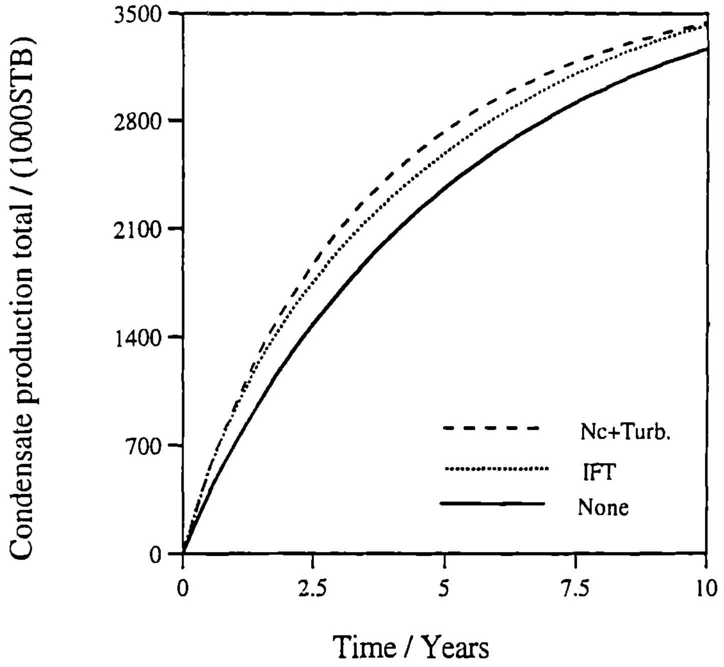

Figure 7.29: The impact of various effects on condensate total production from a tight lean gas condensate reservoir (single layer model)

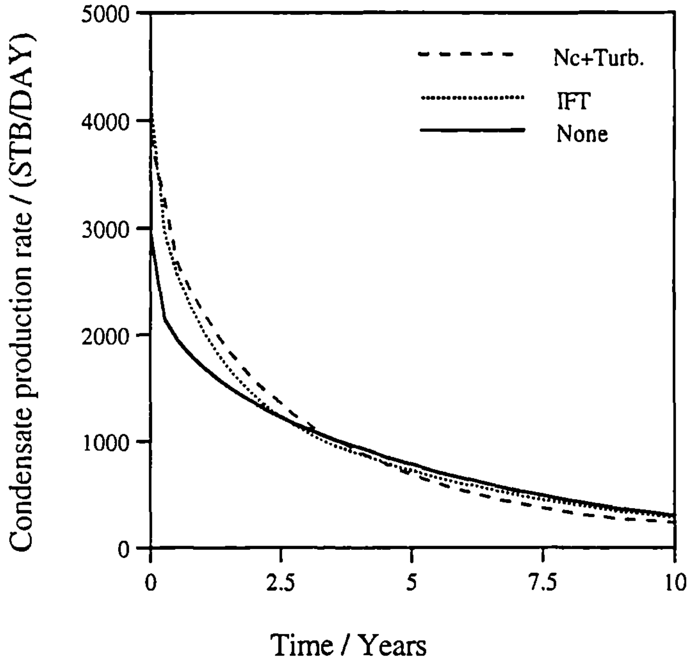

Figure 7.30: The impact of various effects on condensate production rate from a tight lean gas condensate reservoir (single layer model)

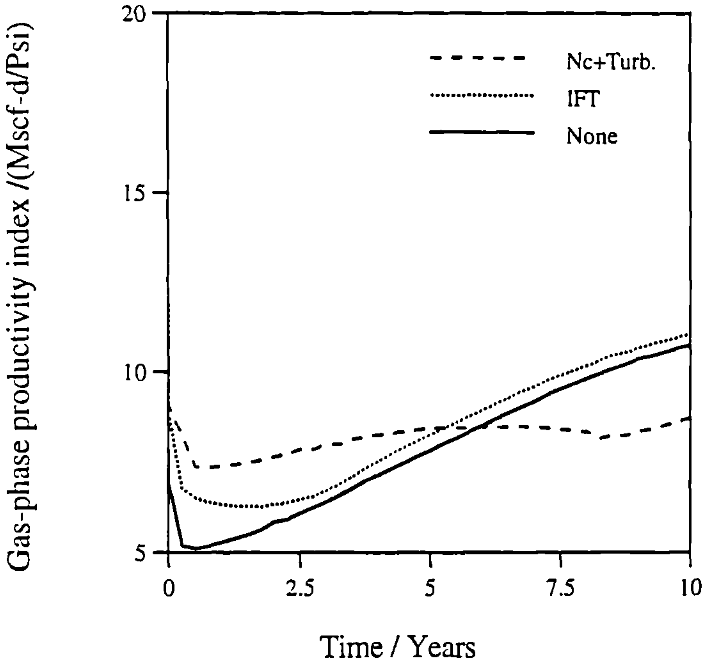

Figure 7.31: The impact of various effects on well gas-phase productivity index from a tight lean gas condensate reservoir (single layer model)

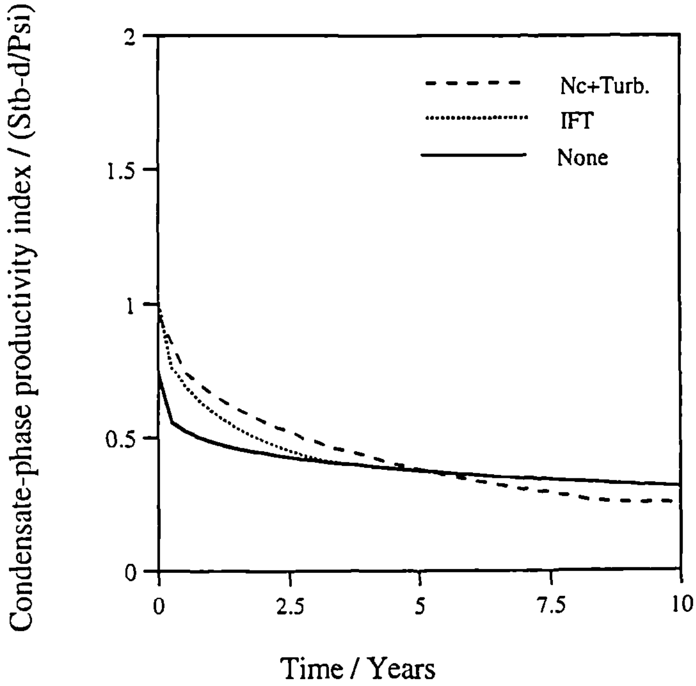

Figure 7.32: The impact of various effects on well condensate-phase productivity index from a tight lean gas condensate reservoir (single layer model)

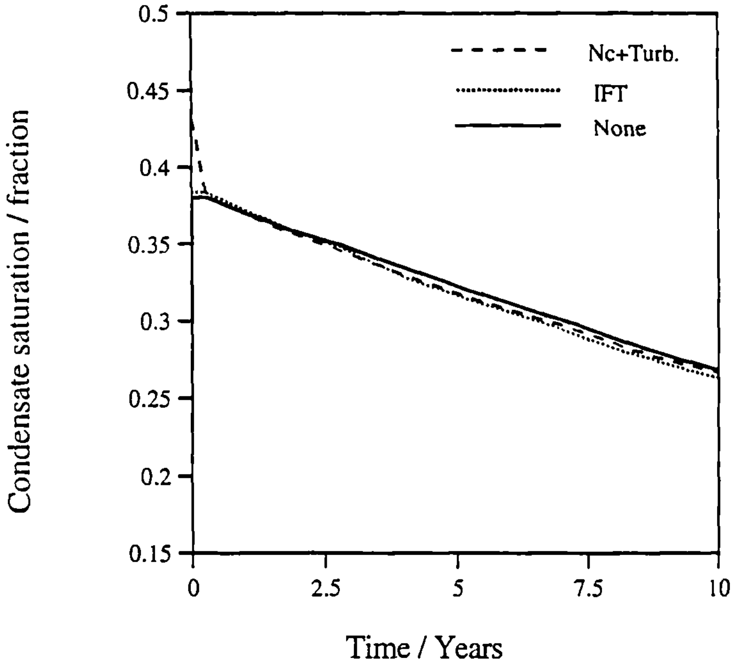

Figure 7.33: The impact of various effects on condensate saturation history at 1.0 foot from wellbore for a tight lean gas condensate reservoir (single layer model)

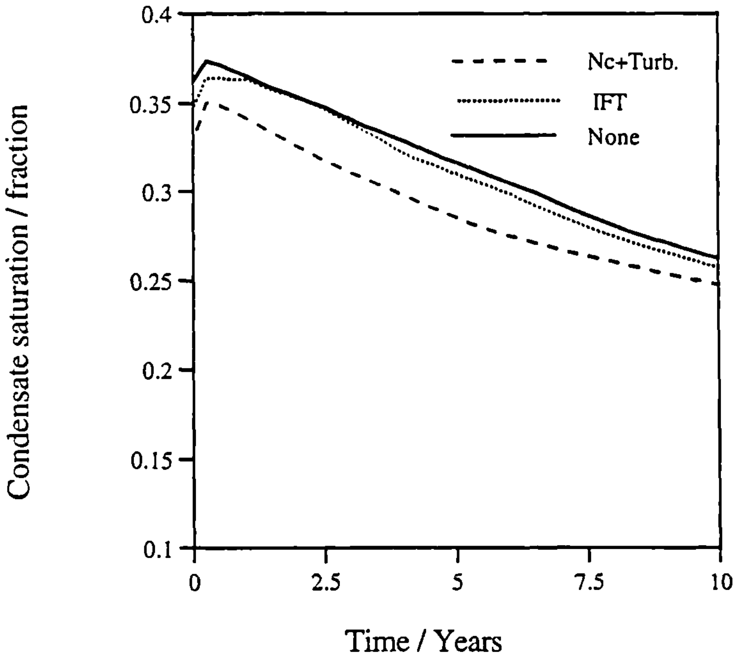

Figure 7.34: The impact of various effects on condensate saturation history at 5.0 feet from wellbore for a tight lean gas condensate reservoir (single layer model)

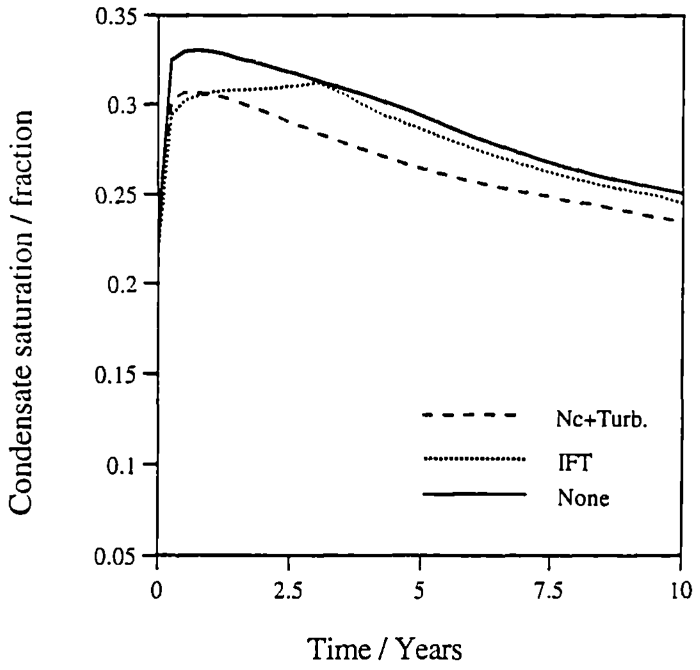

Figure 7.35: The impact of various effects on condensate saturation history at 40.0 feet from wellbore for a tight lean gas condensate reservoir (single layer model)

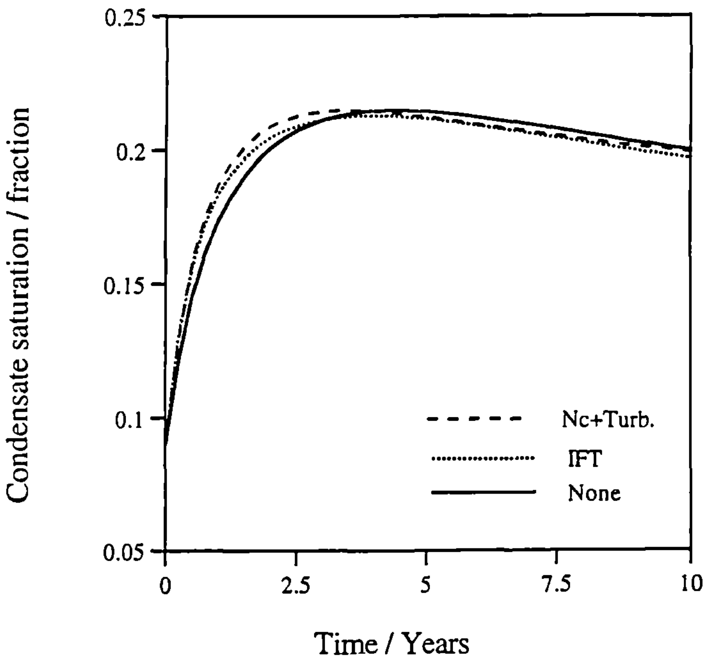

Figure 7.36: The impact of various effects on condensate saturation history at external boundary of a tight lean gas condensate reservoir (single layer model)

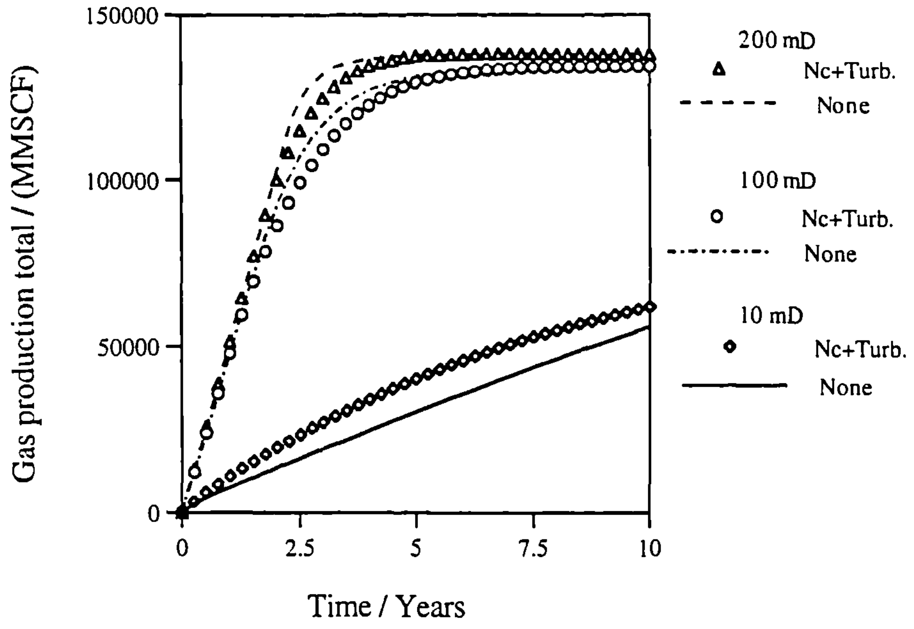

Figure 7.37: The significance of the Nc effect in terms of gas total production at different reservoir absolute permeabilities from a rich gas condensate single layer reservoir model

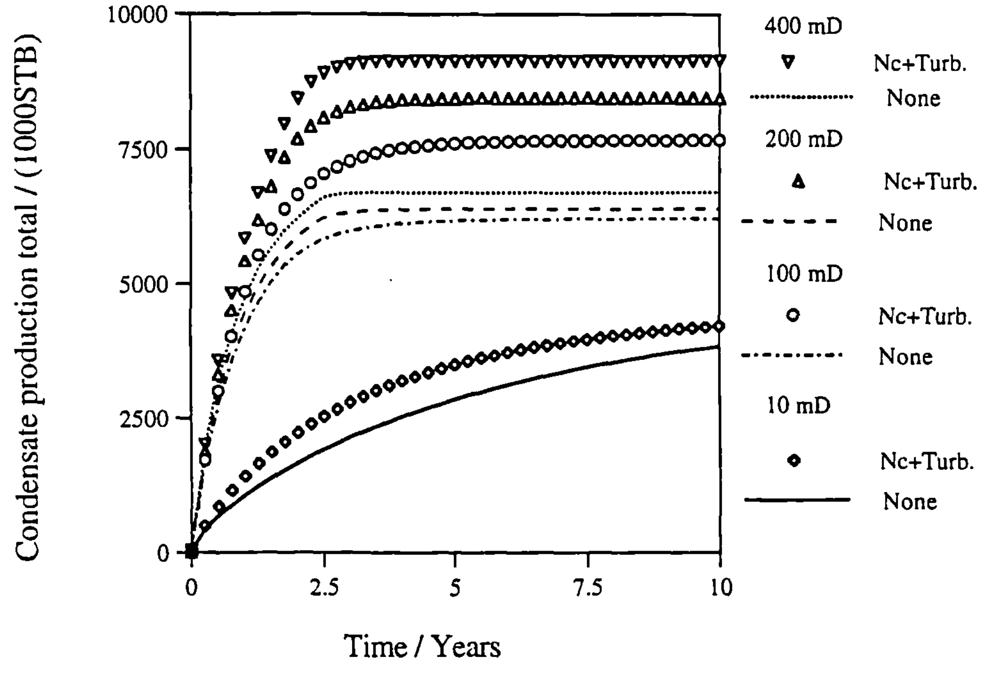

Figure 7.38: The significance of the Nc effect in terms of condensate total production at different reservoir absolute permeabilities from a rich gas condensate single layer reservoir model

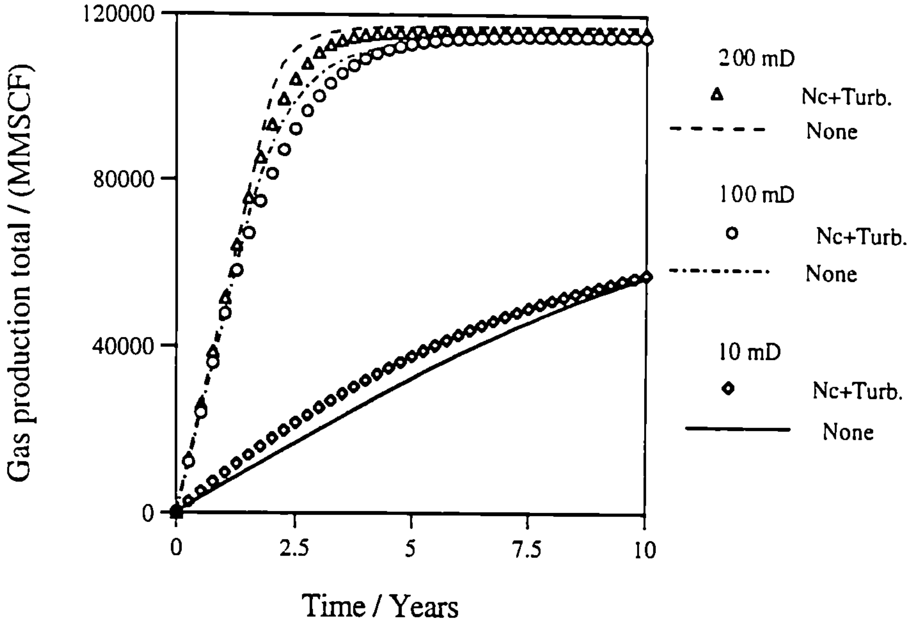

Figure 7.39: The significance of the Nc effect in terms of gas total production at different reservoir absolute permeabilities from a lean gas condensate single layer reservoir model

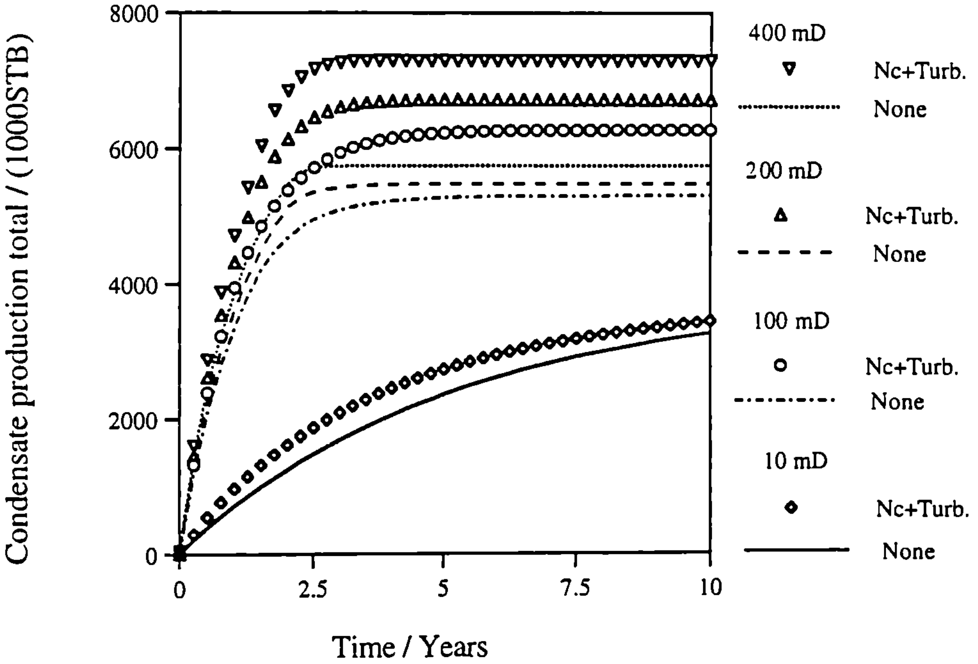

Figure 7.40: The significance of the Nc effect in terms of condensate total production at different reservoir absolute Permeabilities from a lean gas condensate single layer reservoir model

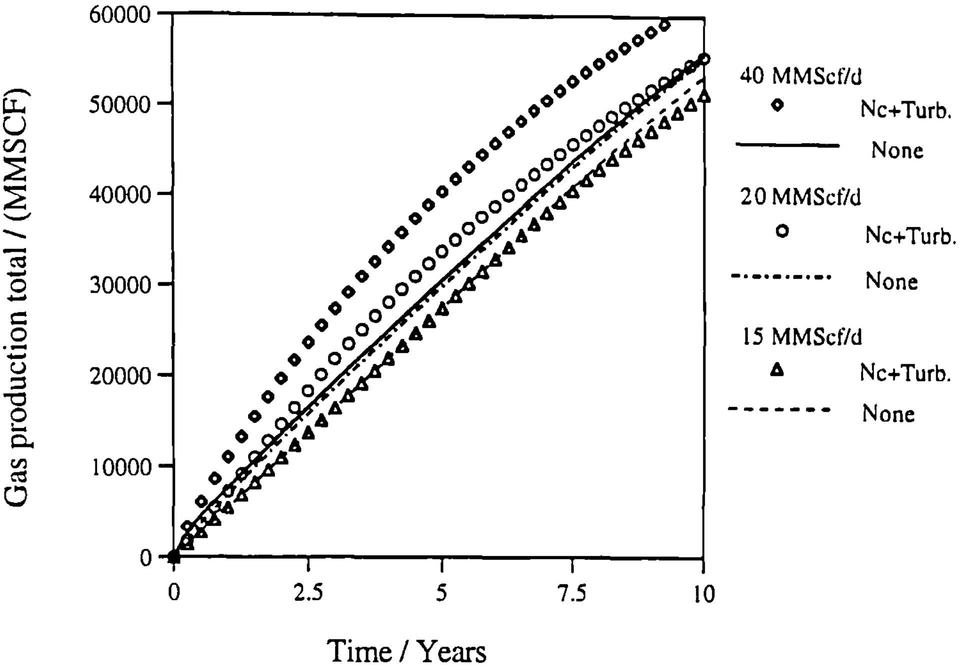

Figure 7.41: The significance of the Nc effect in terms of gas total production for different maximum gas plateau production rate from a rich gas condensate single layer reservoir model

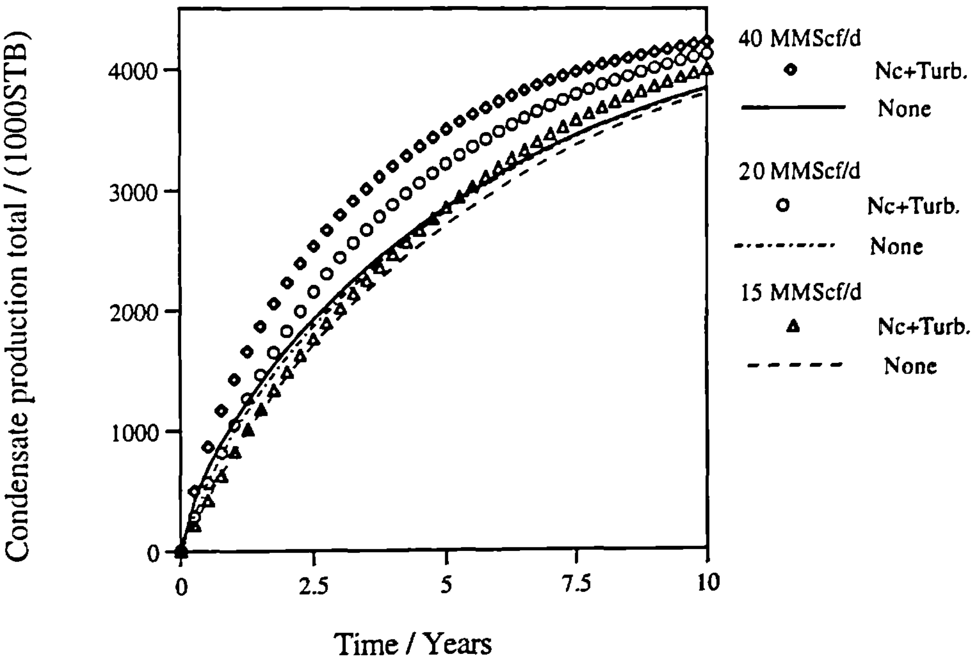

Figure 7.42: The significance of the Nc effect in terms of condensate total production at different maximum gas plateau production rate from a rich gas condensate single layer reservoir model

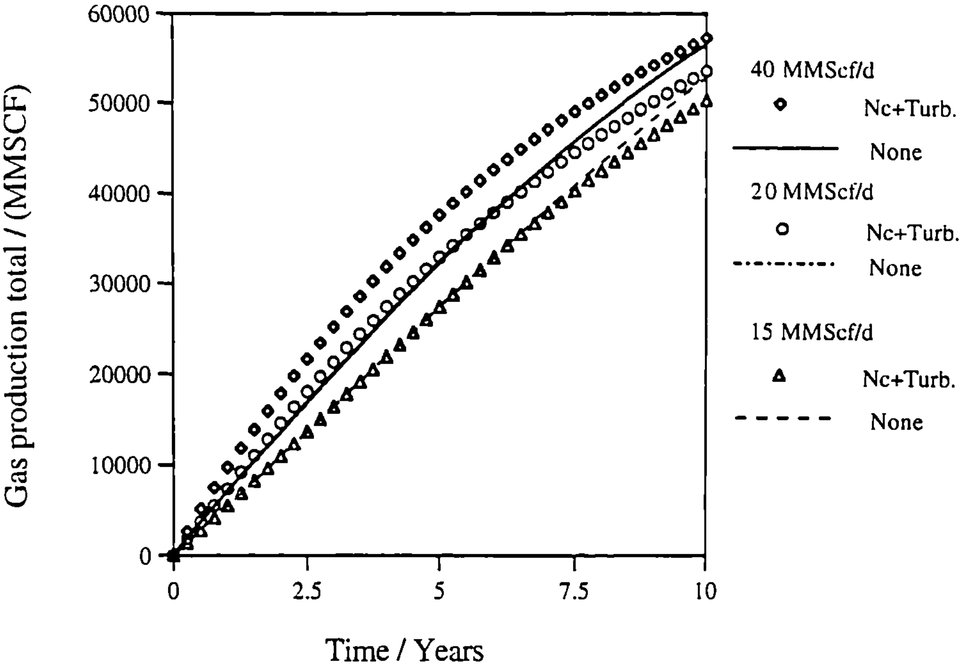

Figure 7.43: The significance of the Nc effect in terms of gas total production for different maximum gas plateau production rate from a lean gas condensate single layer reservoir model

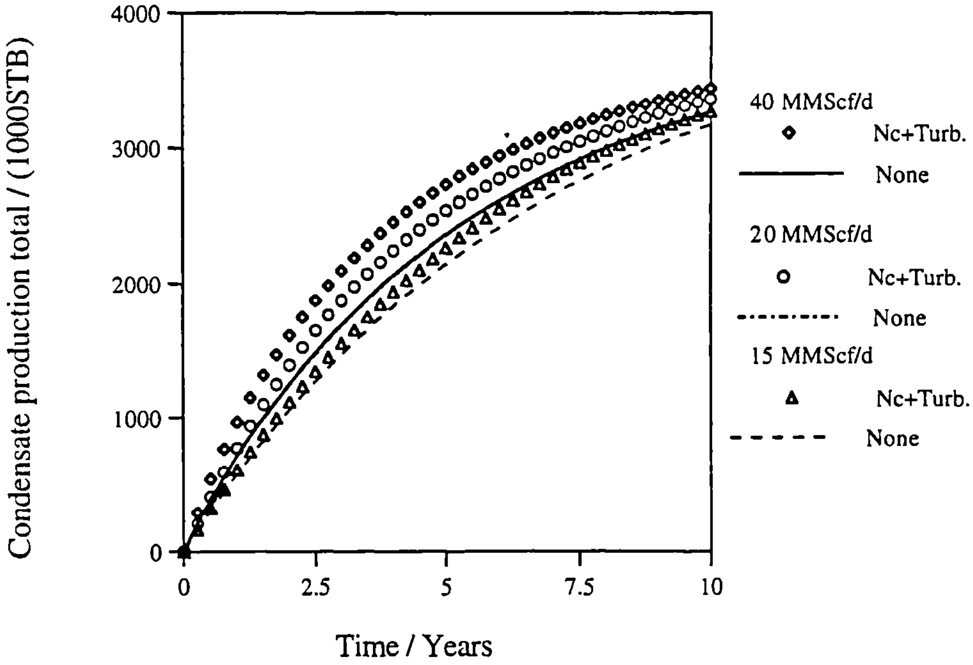

Figure 7.44: The significance of the Nc effect in terms of condensate total production at different maximum gas plateau production rate from a lean gas condensate single layer reservoir model

CHAPTER 8

CONCLUSIONS AND RECOMMENDATIONS

The different conclusions and recommendations stated at the end of each chapter reflect the gained understanding at that stage of the research. However, in the next few sections the overall conclusions and recommendations are listed according to their order in the thesis.

8.1 CONCLUSIONS

1. The use of in situ saturation monitoring by X-ray devices is a viable technique for gas condensate systems when model fluids such as methane/bromeopropane are employed. The optimum operational conditions have been identified in this work.

2. The relative permeability functions resulting from a mechanistic model developed for the flow in perforated regions have shown rate-dependent relative permeabilities. A favourable rate effect, similar to laboratory observations during the core tests, results for the condensate phase. However, unlike experimental observations, an unfavourable rate effect results for the gas phase. Fluid distribution which is believed to be responsible for the phase coupling during the core tests is not adequately represented by the assumed annular mist-flow in perforations.

3. It is evident that the experimentally proven positive rate effect on the gas condensate relative permeability tested in this laboratory is occurring in the upper region of the laminar flow regime but still away from the conventional turbulent zone.

4. A pragmatic approach has resulted in the development of a general and simple yet efficient relative permeability correlation for gas condensate systems at near wellbore conditions. The final form for the relative permeability correlation using the capillary number, N_C, predicts both in-house data as well as literature data efficiently.

5. A study of the impact of the positive rate effect (N_C effect), Forchheimer (inertia) effect and the conventional IFT effect on well deliverability has been successfully completed. Both single-layer and a double-layer reservoir models were considered. Also, the influences of reservoir fluid richness, reservoir absolute permeability, and production rate on the significance of the N_C-effect are quantified. The main conclusions of this study are as follows:

(a) The N_C-effect in the presence of the Forchheimer effect is found to accelerate gas and condensate production from the reservoir. This acceleration is reflected in a significant improvement in the total recoveries at a given point in the early production time and in a remarkable extension in the gas production rate plateau period.

(b) The N_C-effect in the presence of the Forchheimer effect is also found to show both higher condensate accumulation and higher condensate clearance from near the wellbore region, over the course of production, than the base conventional case.

(c) The level of condensate blockage "accumulation" near the wellbore region may be more dependent on condensate transport efficiency near the wellbore (i.e. two-phase flow) than on reservoir fluid richness. For example, condensate blockage is as important in lean gas condensate reservoirs as it is in rich ones.

(d) The significance of the N_C effect in the presence of the Forchheimer effect on condensate-phase recovery is found to be directly proportional to the gas plateau production rate, liquid drop-out and reservoir absolute permeability. On the other hand, its significance on gas-phase recovery is found to be directly proportional to maximum liquid drop-out and gas plateau production rate, and inversely proportional to reservoir absolute permeability.

(e) At practical gas plateau production rates, the N_c-effect should not be ignored regardless of reservoir fluid richness or absolute permeability.

8.2 RECOMMENDATIONS

1. On the basis of on this analysis, the installation of an X-ray device is recommended for the use of saturation monitoring during gas condensate relative permeability measurements particularly in unsteady-state displacement tests.

2. To capture the actual fluid distribution responsible for the coupling of the gas and condensate phases to produce the rate effect, mechanistic modelling must be conducted alongside visual micro-model experiments showing the observed rate-effect. This should give the experimentalist a first hand account enabling better reconstruction of both fluid distribution and unit cell optimisation.

3. The upper and lower boundaries of the dependence of relative permeability on velocity or capillary number must be experimentally established. The base velocity or base capillary number where the viscous forces are balanced by capillary forces must be measured. Also the upper limit for the velocity or capillary number where such a positive rate effect is balanced by inertial effect must be determined.

4. The core characteristic parameter in the general relative permeability correlation must be updated to include any future measurement of relative permeability especially the possible measurement of base relative permeability curves.

5. The developed relative permeability correlation for gas condensate system at near wellbore conditions is for steady-state data. The possible improvement of the approach

by including the unsteady-state gas condensate relative permeability data must be investigated.

6. The Forchheimer factor, β, used in the well deliverability study is based on functions and exponents found in the literature domain. Most of these functions are derived from experimental as well as theoretical investigations performed on gas-oil systems. Such functions may be improved or the exponents are validated by experimentally measuring the two-phase β-factor for gas-condensate systems.

7. Simulators that offer improved gas and condensate relative permeabilities due to the N_c-effect in the presence of Forchheimer effect should be used to history-match actual gas condensate reservoir production data. A procedure similar to one followed in this wellbore deliverability study can be used to obtain an optimum production rate to achieve optimum phase-production from gas-condensate reservoirs.

APPENDIX A

MECHANISTIC MODEL EQUATIONS DERIVATION

A.1 DERIVING VELOCITY PROFILES

The steady-state flow in the UC was modelled as flow in two concentric cylinders: a mixture of gas and condensate flows in the inner cylinder (referred hereafter by phase m) and the condensate phase flows in the annular space between the cylinders. The UC is L long and the pressure drop associated with it is ΔP; so that,

Peforming a momentum balance on a shell cylinder that has thickness of ∂r yields:

$$\frac{\partial}{\partial r}\left(r\,\tau_{rx}^{i}\right) = \left(\frac{\Delta P}{L}\right) r \qquad \text{...(A.1)}$$

where,

τ_{rx}^{i} : is the shear stress in phase i.

Integrating the above equation for the two regions yields:

$$\tau_{rx}^{m} = \left(\frac{\Delta P}{2L}\right) r + \frac{C_1^{m}}{r}; \quad 0 \le r \le \kappa R \qquad \text{...(A.2)}$$

$$\tau_{rx}^{f} = \left(\frac{\Delta P}{2L}\right) r + \frac{C_1^{f}}{r}; \quad \kappa R \le r \le R \qquad \text{...(A.3)}$$

where,

f, m : refer to the film and the mixture respectively.

C_1 : is the integration constant.

κ : $(0 \prec \kappa \prec 1)$ the ratio between the radius at fluid-fluid interface and the outer radius of the flow.

Since the shear stress at r=0 must be finite ($\tau_{rx}^{m} \neq \infty$), therefore, C_1^m=0; and

$$\tau_{rx}^{m} = \left(\frac{\Delta P}{2L}\right)r; \quad 0 \leq r \leq \kappa R \qquad \text{...(A.2a)}$$

Asuumption 3: No-slip at the fluid-fluid interface (r=κR); therefore, the two fluids have the same value of shear ($\tau_{rx}^{m} = \tau_{rx}^{f}$). Therefore, C_1^f=0, and

$$\tau_{rx}^{f} = \left(\frac{\Delta P}{2L}\right)r; \quad \kappa R \leq r \leq R \qquad \text{...(A.3a)}$$

Assumption 4: The two fluids behave like Newtonian fluids. Hence,

$$\tau_{rx}^{i} = -\mu^{i}\left(\frac{dv_x^i}{dr}\right) \qquad \text{...(A.4)}$$

and it follows,

$$\left(\frac{dv_x^i}{dr}\right) = \left(\frac{-\Delta P}{2L\,\mu^i}\right)r \qquad \text{...(A.5)}$$

Therefore, by itegrating equation A.5 for the two regions,

$$v_x^m = \left(\frac{-\Delta P}{4L\,\mu^m}\right)r^2 + C_2^m; \quad 0 \leq r \leq \kappa R \qquad \text{...(A.6)}$$

$$v_x^f = \left(\frac{-\Delta P}{4L\,\mu^c}\right)r^2 + C_2^f; \quad \kappa R \leq r \leq R \qquad \text{...(A.7)}$$

where,

C_2 : integration constant

c: refer to condensate.

At the outer radius (r=R) fluid velocity is zero ($v_x^f = 0$), therefore,

$$C_2^f = \left(\frac{-\Delta P}{4L\mu^c}\right)R^2 \qquad ...(A.8)$$

substituting this into Eq. A.7,

$$v_x^f = \left[\left(\frac{\Delta P R^2}{4L\mu^c}\right)\right]\left[1-\left(\frac{r}{R}\right)^2\right]; \quad \kappa R \le r \le R \qquad ...(A.7a)$$

According to assumption 3: at fluid-fluid interface ($r=\kappa R$) the fluids must flow at the same velocities ($V_x^f = V_x^m$), therefore a value for the constant C_2^m is found and substituted back into Eq. A.6 to give:

$$v_x^m = \frac{\Delta P R^2}{4L\mu^m}\left[\frac{\mu^m\left(1-\kappa^2\right)+\mu^c\kappa^2}{\mu^c} - \left(\frac{r}{R}\right)^2\right]; \quad 0 \le r \le \kappa R \qquad ...(A.6a)$$

A.2 DERIVING AVERAGE FLUXES

The flow rates associated with each region now can be calculated by integrating the above velocity profiles over the appropriate limits. To determine the total flow rate associated with each phase for the entire unit-cell the total mass flow rate of each phase must be determined. The average velocities (Fluxes) of each phase for the whole unit cell can then be calculated by dividing the total mass flow rate associated with each phase by cross sectional area of the unit cell.

For the centeral portion the limits are r=0 and r=κR, so that

$$q^i = \int_0^{2\pi}\int_0^{\kappa R}\left(v_x^i . r\right) dr\, d\theta \qquad ...(A.9)$$

and for the annular portion the limits are r= κR and r=R, so that

$$q^{i} = \int_{0}^{2\pi} \int_{\kappa R}^{R} \left(v_{x}^{i} . r \right) dr \, d\theta \qquad \text{...(A.10)}$$

Applying equations A.9 and A.10 to the velocity profiles resulted in the flollowing flow rates:

$$q^{m} = \frac{\pi \, \Delta P \, R^{4}}{8 \, L \, \mu^{c}} \left[2\kappa^{2} \left(1 - \kappa^{2} \right) + \left(\frac{\mu^{c} \kappa^{4}}{\mu^{m}} \right) \right] \qquad \text{...(A.11)}$$

$$q^{f} = \frac{\pi \, \Delta P \, R^{4}}{8 \, L \, \mu^{c}} \left(1 - \kappa^{2} \right)^{2} \qquad \text{...(A.12)}$$

Therefore, the total flow rate for the both the two phases:

$$q_{T} = q^{f} + q^{m}$$

$$q_{T} = \frac{\pi \, \Delta P \, R^{4}}{8 \, L \, \mu^{c}} \left\{ \left[2\kappa^{2} + \left(\frac{1}{\vartheta} - 2 \right) \kappa^{4} \right] + \left(1 - \kappa^{2} \right)^{2} \right\} \qquad \text{...(A.13)}$$

where

m, f: refer to the flow in the “core” region A and to the film in the “annular” region B of the UC respectively.

$$\vartheta = \frac{\mu^{m}}{\mu^{g}}.$$

Let, the total mass flow rate of the entrained condensate droplets in the “core” region A be equal:

$$M^{ce} = \rho^{c} A^{ce} u^{ce} \qquad \text{...(A.14)}$$

Collier and Hewitt (1961)[69] and Gill, Hewitt, and Lacy (1965)[71] and reported by Govier and Aziz (1972)[72] have approximated the mass flow rate of the entrained droplets in the "core" region A by setting u^{ce} equal to the gas superficial velocity flowing in the core u_g; so that,

$$q^{ce} = \omega\, \kappa^2\, A\, u_g = \omega\, \kappa^2\, q_g$$

where ω is the volume fraction of entrained droplets of condensates in the "core" region A (refer to section A.4 for exact definition of ω); therefore,

$$q^m - q_g = \omega\, \kappa^2\, q_g$$

from which,

$$q^m = (\omega\, \kappa^2 + 1)\, q_g$$

hence, substituting equation A.11 for q^m yields the following expression for the total flow rate of the gas phase:

$$q_g = \frac{\pi\, \Delta P\, R^4}{8\, L\, \mu^c \left(1 + \omega\, \kappa^2\right)} \left[2\kappa^2 \left(1 - \kappa^2\right) + \left(\frac{\mu^c \kappa^4}{\mu^m} \right) \right] \qquad \text{...(A.15a)}$$

Also, the flow rate of the condensate phase can be calculated by subtracting the flow rate of the gas phase from the total flow rate for the UC; i. e.,

$$q_c = q_T - q_g$$

Hence, substituting in Eqs. A.13 and A.15 yields:

$$q_c = \frac{\pi \Delta P R^4}{8 L \mu^c}\left\{\left(\frac{\omega \kappa^2}{1+\omega \kappa^2}\right)\left[2\kappa^2\left(1-\kappa^2\right)+\left(\frac{\mu^c \kappa^4}{\mu^m}\right)\right]+\left(1-\kappa^2\right)^2\right\} \quad \text{...(A.15b)}$$

Therefor the average velocities of both the condensate and gas phases can now be calculated by dividing the above total flow rates by total cross sectional area of the UC; so that,

$$v_g = \frac{q_g}{\pi R^2}; \text{ and } v_c = \frac{q_c}{\pi R^2}$$

Substituting equation A.14 and A.15 the following average velocities are obtained:

for the gas phase

$$v_g = \frac{\Delta P R^2}{8 L \mu^c\left(1+\omega \kappa^2\right)}\left[2\kappa^2\left(1-\kappa^2\right)+\left(\frac{\mu^c \kappa^4}{\mu^m}\right)\right] \quad \text{...(A.16)}$$

and for the condensate phase

$$v_c = \frac{\Delta P R^2}{8 L \mu^c}\left\{\left(\frac{\omega \kappa^2}{1+\omega \kappa^2}\right)\left[2\kappa^2\left(1-\kappa^2\right)+\left(\frac{\mu^c \kappa^4}{\mu^m}\right)\right]+\left(1-\kappa^2\right)^2\right\} \quad \text{...(A.17)}$$

A.3 DERIVATION OF RELATIVE PERMEABILITIES

In order to calculate the relative permeabilities for the two phases, Equations A.16 and A.17 are equated to the conventional Darcy's / Poiseuille's law; for two-phase flow in a pipe the average velocity of phase i can be expressed as follow:

$$v_i = \left[\frac{k_{ri} R^2 \Delta P}{8\mu^i L}\right] \quad \text{...(A.18)}$$

where,

k_{ri} : the relative permeability of phase i.

therefore, rearranging Eq.A.21, we obtain:

$$k_{ri} = \left[\frac{v_i 8\mu^i L}{R^2 \Delta P}\right] \tag{A.18a}$$

Substituting this in Eqs. A.16 and A.17 together with the other appropriate terms for the two phases in Eq. A.18a yields:

for the gas phase

$$k_{rg} = \frac{1}{\vartheta_1\left(1+\omega\kappa^2\right)}\left[2\kappa^2\left(1-\kappa^2\right)+\left(\frac{\vartheta_1\kappa^4}{\vartheta}\right)\right] \qquad ...(A.19)$$

and for the condensate phase

$$k_{rc} = \left\{\left(\frac{\omega\kappa^2}{1+\omega\kappa^2}\right)\left[2\kappa^2\left(1-\kappa^2\right)+\left(\frac{\vartheta_1\kappa^4}{\vartheta}\right)\right]+\left(1-\kappa^2\right)^2\right\} \qquad ...(A.20)$$

where,

$$\vartheta_1 = \frac{\mu^c}{\mu^g}$$

Checking the above relative permeability expressions for the case of one phase flow at κ=1.0 or at κ=0.0 the above expressions reduce to 1.0 or 0.0 as expected for one phase flow in pipe.

A.4 DERIVATION OF PHASE SATURATIONS

The saturations associated with each phase can be calculated by taking the ratio of the area occupied by each phase at any cross section along the UC. Hence the task is to determine the area associated with each phase.

Let,

$$\omega = \frac{\text{area of all the entrained condensate droplets}}{\text{total area of the mix flow in te center of the pipe}} = \frac{A^{ce}}{\pi \kappa^2 R^2}$$

therefore, the area of the condensate phase entrained in the gas region equals

$$A^{ce} = \omega \pi \kappa^2 R^2 \qquad \text{...(A.21)}$$

hence, the area associated with the gas phase equals:

$$A^{g} = (1-\omega)\, \pi \kappa^2 R^2 \qquad \text{...(A.22)}$$

and consequently the gas phase saturation equatls

$$S_g = \frac{\textit{the gas phase area}}{\textit{total cross sectional area of the UC}}$$

$$= \frac{(1-\omega)\, \pi \kappa^2 R^2}{\pi R^2} = (1-\omega)\, \kappa^2$$

$$S_g = \left(\kappa^2 - \omega \kappa^2\right) \qquad \text{...(A.23)}$$

Hence, the condensate phase saturation is

$$S_c = 1 - \kappa^2 + \omega \kappa^2 \qquad \text{...(A.24)}$$

A.5 DERIVATION OF THE VISCOSITY RATIO EQUATION

Eaton et al. (1967)[70] investigated "Annular-Mist flow" in the flow of natural gas-water, natural gas-crude oil, and natural gas-distilate systems in 2-, 4-, and 17-inch pipelines. They defined the two-phase mixture viscosity in terms of in situ average volume fraction of liquid and the viscosity of each of the phases. For our gas and entrained droplets flowing as a mixture in the "core" region of the UC the viscosity of the mixture can be expressed as follow:

$$\mu^{m} = \omega\mu^{c} + (1-\omega)\mu^{g} \qquad \text{...(A.25)}$$

dividing both sides by the viscosity of the gas phase to get,

$$\frac{\mu^{m}}{\mu^{g}} = \omega\vartheta_{1} + 1 - \omega$$

rearranging the above equation yields, $\vartheta = 1 + \left(\vartheta_{1} - 1\right)\omega$

But the the value for ω can be expressed in terms of κ and the saturation of the condensate phase as indicated by equation A.24; so that,

$$\omega = \frac{\kappa^{2} + S_{c} - 1}{\kappa^{2}}$$

substituting this into the above equation and rearranging we get,

$$\vartheta = \frac{\kappa^{2} + \left(\vartheta_{1} - 1\right)\left(\kappa^{2} + S_{c} - 1\right)}{\kappa^{2}} \qquad \text{...(A.26)}$$

A.6 SIMPLIFICATION OF LEVY'S CORRELATION

Levy's correlation[73] estimates the film dimensionless thickness δ, in terms of the total pressure gradient across the tube (ΔP), the gas flow rate (q_g), fluid properties, and UC dimensions; such that,

$$C_1\,\delta^{C_2} = \left(\frac{\Delta P R}{2L\,\rho^c}\right)^{1/2}\left(\frac{\rho^c}{\rho^g}\right)^{1/3}\left(\frac{1}{q_g}\right) \qquad \text{...(A.27)}$$

where,

δ: is the dimensionless thickness of the film.

equals to the thickness of the film over the total redius of the UC.

in the terms of our mechanistic flow model:

$$\delta = 1 - \kappa \qquad \text{...(A.28)}$$

C_1, and C_2: are constants and can be evaluated from the graphical representation of the Levy's Function correlation reported by Govier and Aziz (1972); their values were found to be 10^{19} and 20 for C_1 and C_2, respectively. C2 takes a dimensinless form but C_1 has units of m^{-2}.

$\frac{\Delta P}{L}$: the total pressure gradient along the UC.

For a two-phase laminar flow in a tube the total pressure gradient across the UC can be expressed in terms of the total flow rate and equivalent viscosity of the two-phase system. Also, for the equivalent viscosity the Eaton et al. (1967)[70] correlation can be used; this correlation, as stated above, gives the two-phase mixture viscosity in terms of phase saturations. Therefore,

$$\frac{\Delta P}{L} = \frac{8\left(q_g + q_c\right)\mu^e}{A\,R^2} \qquad \text{...(A.29)}$$

and

$$\mu^{e} = S_{c}\,\mu^{c} + \left(1 - S_{c}\right)\mu^{g} \qquad \text{...(A.30)}$$

incorporating equations A.28, A.29 and A.30 into Levy's Correlation yield the following simplified definition of the dimensionless flow radius ratio κ:

$$\kappa = 1 - \left(\frac{a}{C_1}\right)^{1/C_2} \qquad \text{...(A.31)}$$

where,

$C_1 = 10^{19}$

$C_2 = 20$

substituting the values of C_1 and C_2 yields:

$$\kappa = 1 - b.a^{0.05} \qquad \text{...(A.31)}$$

where,

$$a = \left[\frac{4\left(q_g + q_c\right)\mu^{e}}{A\,R\,\rho^{c}}\right]^{1/2} \left(\frac{\rho^{c}}{\rho^{g}}\right)^{1/3} \left(\frac{1}{q_g}\right) \qquad \text{...(A.32)}$$

$b = 0.1122,\ m^{0.1}$.

Equation A.32 is not dimensionless and the following units must be used:

A: the cross sectional area of the pipe, m^2.

ρ^c : the condensate phase density, kg/m^3.

ρ^g : the gas phase density, kg/m^3.

μ^c : the condensate phase viscosity, pa.s.

μ^g : the gas phase viscosity, pa.s.

D (=2R): the diameter of the pipe, m.

APPENDIX B

DETAILED LITERATURE REVIEW

The sources are listed chronologically according to their year of publication,

1. Bardon and Longeron (1980)[42]:

"Influence Of Very Low Interfacial Tension On Relative Permeability"

Study Details and Description:

Process: 100% liquid phase saturation vertically displaced by a vapour phase. USS method with injection introduced from the top of the core.

Injection rate: 0.01 cc/s or velocity of $5.6X10^{-3}$ cm/s

Fontainebleau sandstone core was used which has the following properties:

k (mD)	ϕ (%)	L (cm)	D (cm)
0.082w Swi	9.9	38.2	5.0

system is classified as gas-oil where,

7 experiments performed on binary C1-nC7 @Temperature: 71.1 °C (only 6 experiments are given).

2 experiments performed on binary C1-nC5 @Temperature: 37.7 °C (only 1 experiment is given).

1 experiment performed on binary C1-nC10 @Temperature: 37.7 °C (not given)

Author's Conclusions:

Strong dependence of kr on IFT at very low IFT values $\leq$ 0.04 mN/m.

Comments:

Experimental data may be incorporated into our USS data-base especially. However, our USS data are conducted on a horizontal core and not vertical like these tests.

2. Chatizis And Morrow (1984)[91]:

"Correlation Of Capillary Number Relationships For Sandstone"

Study Details and Description:

38 Unsteady-state short core displacement experiments performed on 16 different core types; these cores are all water wet sandstones. The experiments conducted on water-oil system at high IFT value (34.8 mN/m) with relatively low Nc values (4 x 10^{-5}). Three definitions for Nc were provided

$$N_{c1} = \frac{\mu_w \, v_w}{\sigma} \qquad \text{...(B.1)}$$

$$N_{c2} = \frac{k_w \, \Delta P}{L \, \sigma} \qquad \text{...(B.2)}$$

$$N_{c3} = \frac{k_{air} \, \Delta P}{L \, \sigma} \qquad \text{...(B.3)}$$

Correlations of residual saturations with N_{c1}, N_{c2}, and N_{c3} were created. Also air absolute permeability (k_{air}) were correlated with critical displacement ratio ($\frac{\Delta P}{L \sigma}$).

All the correlations were presented as plots rather than functional format.

Author's Conclusions:

1. The residual saturation and the relative permeability to air are correlateable with N_{c2} or N_{c3}.
2. Care must be administered when applying these correlation to fluid system with phases that have equal viscosities.

Comments:

1. Experimental data can not be used for our work because of both the high IFT value of the system and the low Nc values .
2. The use of definition of N_{c2} and its functionality is in line with our work.

3. Chierici (1984)[122]:

"Novel Relations for Drainage and Imbibition Relative Permeabilities"

Study Details and Description:

A set of a drainage (unsteady-state) gas-oil kr-curves.

No other information supplied

The following new formulations for kr as function of Saturation were provided:

$$k_{ro} = e^{\left(-A\left(\frac{S_g - S_{gc}}{1 - S_{wi} - S_g}\right)^{L}\right)} \quad ...(B.2)$$

$$k_{rg} = e^{\left(-B\left(\frac{S_g - S_{gc}}{1 - S_{wi} - S_g}\right)^{-M}\right)} \quad ...(B.5)$$

with,

$S_g - S_{gc} = 0$ for $S_g \leq S_{gc}$

A, L,B, and M are empirical constants.

Author's Conclusions:

These formulations given above are better representation of gas-oil kr as a function of saturation than the classical Corey's type particularly at end points kr prediction.

Comments:

1. We can not use the experimental data because no information on IFT, rate, k, ϕ, and μ were provided.
2. We may try to use the formulation to better fit our base-kr curve.

4. Morrow And Chatzis (1985)[134]:

"Entrapment And Mobilization Of Residual Oil In Bead Packs"

Study Details and Description:

10 Unsteady-state vertical displacement experiments on consolidated and un-consolidated glass bead packs. The experiments conducted on water-oil system with a range of IFT values (2.5 to 22.37 mN/m) at relatively low Nc values (1 x 10^{-5}) and bond number rang from 1-40 x 10^{-5}.

The definitions for Nc is

$$N_{c1} = \frac{\mu_w v_w}{\sigma} \qquad \text{...(B.6)}$$

Correlations of trapped and residual saturations with N_c were created.

All the correlations were presented as plots rather than functional format.

Author's Conclusions:

1. The residual saturation and the relative permeability to air are correlateable with N_c.
2. Base capillary number value estimated for the residual oil saturation for this fluid system flowing in un-consolidated bead pack is 2 x 10^{-4}, and for consolidated (sintered) bead packs it is around 2 x 10^{-4}, and for sandstone it is valued around @1x10^{-6}. For gas oil systems these values are expected to by 25 times lower.

Comments:

1. Experimental data can not be used for our work because of both the high IFT value of the system and the low Nc values. Also because of the fact, also highlighted by this study, that the base capillary number is dependent on the flowing fluid system (i.e. the base capillary number for gas condensate system is much lower than for water oil systems).
2. As long as we are incorporating data of similar systems (i.e. gas condensate systems and gas-oil systems at low IFT) base capillary number should not be an issue and one value can be used as a representative base capillary number.

5. Gravier, Lemouzy, Barroux, Abed (1986)[123]:

"Determination of gas-condensate Relative Permeability on Whole Cores Under reservoir Conditions"

Study Details and Description:

Fluid: gas-condensate system , ternary 78.8% Methane, 21.0% n-Pentane, and 3.2% n-Nonane

A total of 61 different experiments have been conducted on eight (8) different cores also critical condensate saturations were measured for these cores.

steady-sate, imbibition

Sample	k (mD)	ϕ (%)	L (cm)	D (cm)
1	17.2	25.8	20.2	6.6
2	0.37	16.5	13.1	6.6
3	31.8	22.7	17.3	6.6
4	6.0	18.6	19.5	6.6
5	39.2	19.6	21.5	6.6
6	7.4	19.6	19.9	6.6
7	14.5	23.4	16.6	6.6
8	0.9	14.5	15.6	6.6

Core: Packstone Carbonate with intergranular in some samples and vugular porosities in other.

Darcy velocity: 10^{-6} to 10^{-4} m/s

IFT: 0.5 to 1.5 mN/m.

Temperature: 158 - 266 ^{o}F (70 - 130 ^{o}C).

pressure: 1740 - 2320 psia.

Author's Conclusions:

1. No IFT effects can be considered because the range of IFT >> 0.07 mN/m which they believed to be the critical value for the dependence of kr on IFT.

2. The different cores have different initial water saturation (S_{wi}).
3. Temperature effect may exist but with negligible correction to kr values.

Comments:

The experimental data provided in this paper can be incorporated into our data to further enhance our data-base.

---

6. Kerig and Watson (1986)[124]:

"Relative permeability Estimation From Displacement Experiments: An Error Analysis"

Study Details and Description:

No experimental data provided. The paper discusses the fact that Corey's type representation of kr values is not adequate because of the rigidity of the function; i.e. only one parameters is determined from regression and other techniques, This one parameters is supposed to explain all the different phenomena which differentiate one kr-curve from another. Therefore, the choice of a particular functional formulation to represent kr as function of saturation on its own introduces a bias error because the chosen formulation might not be adequate to represent al other curves; this deficiency can be alleviated or eliminated by increasing the number of parameters in the representative formulation.

Author's Conclusions:

A cubic spline with three segments type of formulation can introduce substantial improvements in the accuracy of relative permeability prediction. i.e.

$$k_{ri} = a_{ij}S_i^3 + b_{ij}S_i^2 + c_{ij}S_i + d_{ij} \qquad \text{...(B.7)}$$

Comments:

This formulation might be worth looking into for our base kr curves.

7. Asar And Handy (1988)[39]:

"Influence Of Interfacial Tension On Gas/Oil Relative Permeability In A Gas-Condensate System"

Study Details and Description:

A total of 22 SS experiments using methane/propane mixture as a volatile oil on fired Berea core They have the following properties

k (mD)	k (mD)	ϕ (%)	L (cm)	D (cm)
100	193fired	20	30	5.0

IFT = 0.03 - 0.82 mN/m; viscosity ratio = 0.55 - 0.85

deferential pressure = 0.2 - 1.5 psia (for a single curve); Temperature = 21 °C

Author's Conclusions:

1. kr curves seem to straighten themselves to approach the 45° line as IFT decreases.
2. Higher residual condensate saturations at higher IFT values..
3. Impact of saturation history is limited for such experiments.
4. kr values at the highest IFT (0.82 mN/m) value are almost the same as those for nitrogen/kerosene system (IFT = 30 mN/m).
5. Gas condensate relative permeability curves are similar to those of gas-oil system except at low IFT values(less than some value).
6. For low IFT (near critical) fluids, liquid can flow at low liquid saturation.
7. Low IFT conditions appear to drive the system to be less oil-wet and more vapour-wet.

Comments:

1. The SS Experimental data can be used.

8. Munkerud (1989)[135]:

"Measurement Of Relative Permeability And Flow Properties Of Gas Condensate System During Pressure Depletion And Pressure Maintenance"

Study Details and Description:

Combination of three depletion followed by dynamic displacement tests were conducted. The fluid is a six-component gas condensate system (methane / ethane / propane / hexane / decane) with due point of 2784.72 psia. The core is Berea with the following properties:

k	ϕ	L	D	PV
(mD)	(%)	(cm)	(cm)	(cm^3)
150.0	15.3	50	5.08	155.0

Flow rates : 13.38 to 216.78 cc/hr.

IFT values: $\leq$ 0.09 mN/m.

Dynamic displacement tests were conducted at constant IFT values of 0.04, 0.07, and 0.09 mN/m.

Author's Conclusions:

1. The unsteady-state relative permeability values measured in these tests are dependent on IFT.
2. The relative permeability tests measured at different stages of the depletion are independent of injection rate.
3. These conclusions are more valid for the gas phase than for the condensate phase because of the difficulties encountered in measuring the recovered liquid.

Comments:

1. The dependence of relative permeability on IFT is evident.
2. The possible improvement in the relative permeability values induced by the rate effect during the depletion tests is completely masked by the increase in IFT at every

stage of the depletion, hence, no rate effect can be observed. A better way of presenting the data is to plot the constant pressure (IFT) kr values on a single curve. Therefore, the kr data reported here are not in any conflict with our rate sensitive kr data.

3. The kr data reported here (from the depletion tests) is quite valuable as unsteady-state data.

---

9. Haniff And Ali (1990)[40]:

"Relative Permeability And Low Tension Fluid Flow In Gas Condensate Systems"

Study Details and Description:

The number of steady-state data points were not reported, however, five different sets of kr curves are reported at five different IFT values: 0.001, 0.01, 0.05, 0.1, 0.2 mN/m.

Fluid system: a binary gas condensate system 62% Methane / 38% propane.

Temperature: 31.7 °C. The Spynie Sandstone core has the following characteristics:

k (mD)	ϕ (%)	L (cm)	D (cm)	PV (cm^3)
23	22	15	5.0	64.8

The range of velocities or pressure drops across the core are not reported; only a plot of the Bond number versus pressure is given.

$$N_b = k_a\, g \left(\frac{\Delta\rho}{\sigma} \right) \quad ..(B.8)$$

<u>Author's Conclusions:</u>

1. The authors stipulate that liquid exist as thin film along the walls of the pores at low IFT values $\leq$ 0.05 mN/m.

2. Gravity has an important role to play, therefore, the Bond number as given by equation (1) is a better correlating parameter for kr values than the capillary number.

Comments:

1. Via Dr. Joe Ali he told me that they measured 6-8 points along each curve, these points can be used.

---

10. Morel, Lomer, Marineau, And Putz (1992)[136]:

"Mobility Of Hydrocarbon Liquids In Gas Condensate Reservoir: Interpretation Of Depletion Laboratory Experiments"

Study Details and Description:

Combination of depletions followed by gravity drainage tests were conducted. The fluid is actual reservoir gas condensate fluid with due point of 5569.45 psia. The composite core is oriented vertically; it consists of 10 vertically stacked homogeneous dolomite rocks with the following overall properties:

k (mD)	ϕ (%)	L (cm)	D (cm)	PV (rcm^3)
8air(5water)	26	182.8	7.3	1993.5

Initial water saturation: 20%

Flow rates : 0.08333 cc/hr.

The two gravity drainage tests were conducted at constant IFT values about 0.22 and 2.2 mN/m.

Temperature: 141 °C.

IFT values are both measured and calculated using Ping-Robinson EOS.

Author's Conclusions:

1. Condensate is mobile as soon as pressure drop below the dew point pressure; however low its mobility is.

2. The existence of a base (critical) IFT value, below which residual condensate saturation is decreasing with lower IFT values, is possible (expected to be around 0.15 mN/m).

Comments:

1. The kr data reported here (from the depletion tests) can be used as unsteady-state kr data.

---

11. Ronde-1 (1992)[130]:

" Effect Of Low Interfacial Tensions On Relative Permeabilities In Some Gas-Condensate Systems"

Study Details and Description:

No experiments were performed.

Conclusions were based on experimental data gathered from literature. Not all the details regarding these experiments were mentioned (i.e. velocity of SS experiments).

Author's Conclusions:

1. Viscous forces dominate over gravity and capillary forces at the critical domain conditions.
2. Heavier phase is the wetting one.
3. Annular mist flow is possible for critical flow domain.
4. Such a domain (where the relative permeability curves starts to straighten) correspond to the start of the so called Cahn wetting transition to an annular flow regime; starts at 0.3 mN/m for methane-propane system in Berea core.

Comments:

1. From conclusion 1 Nc is a better correlating parameter than IFT.
2. Base IFT value can be taken around the 0.3 mN/m value.
3. Based on the conclusions of this study, our earlier attempt to model the flow of low IFT gas condensate systems as annular-mist flow is actually not completely off-the-mark.

12. Ronde-2 (1992)[87]:

"Relative Permeability At Low Interfacial Tensions"

Study Details and Description:

Same as above in addition to the explanation of condensate trapping on a Non-Newtonain fluid behaviour (Bingham Plastic model).

Comments:

Gas-condensate fluid can be modelled as a non-Newtonian fluid.

---

13. Ali, Butler, Allen, and Wardle (1993)[42]:

"The Influence Of Interfacial Tension On Liquid Mobility In Gas Condensate Systems"

Study Details and Description:

No kr experimental values reported. only liquid and vapour recoveries are given. kr values were estimated from simulating the horizontal displacement experiments and history matching such recoveries.

Berea sandstone was used which has the following properties

$k_{@Swi}$ (mD)	ϕ (%)	L (cm)	D (cm)
100.0	19.0	100.0	5.0

Fluid: gas-condensate synthetic mixture: C1, C2, C3, C5, C8, and C16.

Author's Conclusions:

1. There are many uncertainties in the mechanism of condensate flow in porous media; these uncertainties are associated with the impact of IFT on liquid mobility.
2. Low-tension pressure maintenance is viable production strategy.
3. Gravity can have strong effect on low-tension depletion.

Comments:

While their conclusions are generally helpful, no experimental kr data can be used from this study.

---

14. Hartman And Cullick (1993)[88]:

"Oil Recovery By Gas Displacement At Low Interfacial Tension"

Study Details and Description:

5 Unsteady-state slim tube experiments were conducted. These slim tubes were designed to suppress any possible gravitational or viscous effects. Therefore, the product kr curves are purely a function of IFT. A correlation of kr with IFT, similar to Coats, was created.

Also a correlation of residual gas saturation with IFT was created.

Author's Conclusions:

1. The relationship between kr together with residual saturation and IFT plays a major role in the recovery process for a multi-contact or nearly miscible (low IFT values) fluids.
2. Correlation of kr with IFT can successfully represent the effect of IFT on kr observed in laboratories.

Comments:

1. Slim-tube experimental data can be used in our work because the effect of IFT, hence capillary number, on kr are represented.
2. The logarithmic form of the residual gas saturation can be looked into.

15. Wang, Pope, Sepehrnoori (1993)[121]:

"Compositional modelling of low interfacial tension effects on flow behavior of gas condensate"

Study Details and Description:

system: gas-condensate 7-components (N2 and C1), (CO2, C2, and C3), (C3 and C4), (C5, C6, and C7), (C8, C9, and C10), (C11), and (C12)

vertical depletion experiment 100 grid-blocks.

kr. curves are reported in the form of two models where the exponents are generated from experimental kr-curves; therefore we can generate some curves at any Nc value we wish.

No information on whether the experimental data used to generate the two models are steady or unsteady-sate data. However, because they are used into a depletion study (long regarded as a unsteady-state process) the data may be classified as steady-sate data.

The work is a gas-condensate relative permeability study. Simulation of experimental vertical depletion experiments in long cores (1.8m long). Studied range of IFT is 0.02-0.12 mN/m.

ϕ = 0.226-0.289

k = 4.2-46.8 mD.

Two models were used to represent the effect of kr on IFT:

Model I: Corey type representation of kr curves where both the Corey exponents are a function of residual saturation and residual saturations are a function of capillary number.

Model II: Modified Coats correlation where the exponents for miscible relative permeability (krm), residual saturation, as well as relative permeability are all a function of IFT.

$$k_{ri} = \left[1 - e^{-a\left(\frac{\sigma}{b\sigma_b}\right)} \right] . k_{rbi} + \left[e^{-a\left(\frac{\sigma}{b\sigma_b}\right)} \right] . k_{rmi} \qquad \text{...(B.9)}$$

where,

$$k_{rmo} = k_{ro}^{o}\left(\frac{s_o - \left(\frac{\sigma}{b\sigma_b}\right)s_{orb}}{1 - s_{rw} - s_g - \left(\frac{\sigma}{b\sigma_b}\right)s_{orb}}\right)^{\left[1+(n_o-1)\left(\frac{\sigma}{b\sigma_b}\right)\right]} \qquad \text{...(B.10)}$$

$$k_{rmg} = k_{rg}^{o}\left(\frac{s_g - \left(\frac{\sigma}{b\sigma_b}\right)s_{grb}}{1 - s_{rw} - s_o - \left(\frac{\sigma}{b\sigma_b}\right)s_{grb}}\right)^{\left[1+(n_g-1)\left(\frac{\sigma}{b\sigma_b}\right)\right]} \qquad \text{...(B.11)}$$

where,

a = 5 and b=0.18 were found to represent their experimental data.

n_o, and n_g : Corey's exponents which are functions of σ or Nc.

Author's Conclusions:

The models showed a reasonable variation of kr with IFT compared to their experimental data.

For the fluid used in this study the critical IFT value below which capillary forces can be neglected is 0.048 mN/m.

Comments:

The ideas given in this work are helpful in correlating kr with Nc or IFT.

The following are important points raised in this paper:

1. I do not agree with conclusion taken in this study that the curvature of the predicted kr curve (in the coats original model) is solely influenced by the curvature of the base curve. Actually, in our approach which is similar to Coats, both the curvature of miscible term (straight line) and the curvature of the base term do play a role in determining the exponents of the predicted relative permeability curve (as demonstrated in our correlation). The only assumption regarding this issue, in our approach, is the fact that such a contribution is considered to be equal for both terms. This is a valid

assumption in the absence of experimental relative permeability data to support the contrary.

2. Base Nc (or IFT) for the kr curves can be different than the base Nc (or IFT) for the residual saturations. This is equivalent to using different functions representing kr or residual saturation as function of Nc (IFT) (as demonstrated in this correlation).

3. Exact measured experimental data were not reported; if we try to use relative permeability values calculated from one of the models they can not be considered as measured vales.

16. Bourbiaux and Limborg (1994)[126]:

"An Integrated Experimental Methodology For A Better Prediction Of Gas-Condensate Flow Behaviour"

Study Details and Description:

2 Steady-state and 7 unsteady-state experiments conducted.

Procedure: One phase depleted to desired IFT followed by equilibrium gas-injection for USS krg values then two-phase gas-condensate injection for SS krc and krg values.

Core: Palatinate sandstone with the following properties

k (mD)	ϕ (%)	L (cm)	A&Shape (cm^2)	PV (cm^3)	Swi (%)
4.1w/o Swi	19.3	38.4	10.20 squarre	75.4	16.6

Fluid types: binary C1C3 gas-condensate system.

Temperature: 37.8 oC

Pressures: 8.7 & 7.3 MPa.

Total flow rate: 2.8-3.1 x 10^{-9} m3/s (10-11 cc/hr)

Local saturation were measured using γ-ray attenuation scanning to make sure that a uniform saturation profile is established during the steady-state tests. The errors reported in measuring such a profile using the γ-ray attenuation coefficient is between 4-7 %PV on top the error in measuring S_{wi}.

Author's Conclusions:

1. Steady-state method overestimate the value of critical condensate saturation because of condensate accumulation within the core before breakthrough.
2. Both kr and critical condensate saturation are affected by IFT with krc having greater dependence on IFT than krg.

Comments:

Experimental data may not be incorporated into our data base especially the SS data points. Condensate accumulation gave erroneous steady-state measurements. Rotation of the core through 360 degrees (similar to our in-house measurement) may help elevate the problem.

---

17. Boom, Schulte, Oedai, Zeelenberg, and Maas (1995)[128]:

"Experimental Evidence For Improved Condensate Mobility At Near Wellbore Flow Conditions"

Study Details and Description:

Centrifuge experiments on water- heptane mixtures at 4 different IFTs. Different IFT conditions and viscosity contrast were obtained by adding specific amounts of Isopropyl alcohol and glycerol. These experiments can be classified as USS experiments.

Core plugs of different absolute permeability sorted into 6 groups of similar permeabilities. They cover 30- ft long reservoir rock section: With the following properties

Core	$k_{@Swi}$ (mD)	ϕ (%)	Swi (%)
(1)	101±1	30.1±0.3	0
(2)	117±3	28.8±0.4	0
(3)	169±2	29.4±0.6	0

(4)	173±1	29.1±0.4	0
(5)	189±1	27.9±0.4	0
(6)	184±4	26.6±0.3	0

IFT = 0.05 - 35.1 mN/m.

viscosity ratio = 11 - 47

process: core sample is fully saturated with the heavy phase, placed in the centrifuge core holder which is full of the light phase then centrifuged at a constant speed and recovery are measured. A new definition for capillary number is given:

$$N_c = \frac{k\,\Delta P}{\sigma} \qquad \ldots(\text{B.12})$$

In this study (centrifuge experiments) the capillary number is assumed to be represented by the bond number

$$N_b = \frac{\Delta\rho g\, k}{\sigma} \qquad \ldots(\text{B.13})$$

Author's Conclusions:

1. There are some evidence, in simulation, that indicate improvements of gas-condensate relative permeability at near wellbore conditions.
2. Increase in condensate mobility of up to 3 order of magnitude at near wellbore flow conditions.
3. The bond number which is assumed to represent the capillary number, in practical terms, is the controlling parameter for condensate mobility rather than IFT.
4. At high bond number the shape of wetting phase relative permeability to be similar regardless of the origin or absolute permeability of the sample .
5. The centrifuge-base model is firmly believed to give less ambiguous results and its less limiting and less time consuming.

Comments:

1. Experimental data can not be considered in our analysis because it does not take proper account of velocity effects.

2. The definition N_c is not dimensionless, therefore, it can not be,as is, of much use to our work.

---

18. Chen, Wilson, and Monger-McClure (1995)[127]:

"Determination Of Relative Permeability And Recovery For North Sea Gas-Condensate Reservoirs"

Study Details and Description:

86 Steady-state experiments conducted.

Procedure: One phase depleted to desired IFT followed equilibration time of between 18-40 hours then equilibrium gas is injected until steady-state conditions are reached for krg values; this is followed by two-phase gas-condensate injection for SS krc and krg values.

Two composite cores are used; each composite core is made from 13 different core plugs of similar absolute permeability:

They have the following properties

Core	k@Swi (mD)	ϕ (%)	L (cm)	D (cm)	PV (cm^3)	k (Klinkenberg) (%)	Swi (%)
(A)	73.39	17.4	73.28	3.81	143.35	255.8	20.9
(B)	11.76	18.5	73.67	3.81	155.63	39.10	21.5

Two North Sea gas-condensate reservoirs fluids were recombined using separator oil and synthetic gas then used: Fluid A and Fluid B:

	Fluid A	Fluid B
Dew Point, psiag	7070	6074
Smax, %	31.7	42.5
Temperature, ^{o}F	250	259

Pressures, psia	4892-7255	5826-6034
Gas flow rates, cc/hr	20-160	20-160.

Error due to non-uniform saturation profile across the core during the SS experiments : 1.4%PV.

Author's Conclusions:

1. Increasing gas injection rate increased krg.
2. Rate effect is more pronounced at higher condensate saturation (at least for case A).
3. A concave down curve for krc as a function of condensate saturation at a constant flow rate.
4. Condensate saturation accumulation reduced krg by 6 to 10 folds.
5. A critical condensate saturation was observed for the richer gas-condensate but not for the leaner one; this was attributed to the near critical behaviour of the richer gas-condensate system (i.e. lower IFT values).

Comments:

1. Experimental data can be incorporated into our data base especially the SS data points.
2. The trend of the rate effect on krg agrees with our finding (higher at higher condensate saturation).
3. The downward concavity of krc versus condensate saturation curve is not unusual because of the increasing IFT value along the curve. This behaviour can be peculiar if it maintain its down-ward concavity when IFT is constant throughout the curve.
4. The effect of rate, or IFT can not be clearly quantified from these experiments because during all of these experiments neither one is kept constant in order to study the other. However, these experiments should be useful to identify the relationship between krg and capillary number.

19. Boom, Wit, Zeelenberg, Weeda, and Maas (1996)[132]:

"On The Use Of Model Experiments For Assessing Improved Gas-Condensate Mobility Under Near-wellbore Flow Conditions"

Study Details and Description:

This paper provides more justification of the assumption made when applying experimental conclusions (concluded from the experimental work detailed in Boom et al.[128]) to field conditions. The authors sought to justify the following assumptions about their previous experimental work:

1. Are viscous forces in the filed can be represented by centrifugal forces in the lab?
2. The impact of connate water (as the case in the field conditions) on the overall conclusions obtained in experiments without considering the presence of connate water.
3. The role of elevated field conditions on the such experimental conclusions.

Author's Conclusions:

1. The conclusions obtained in the previous work[128] of the authors are valid.
2. The conclusions are validated by steady-state relative permeability experiments carried out earlier at Heriot-Watt University.

Comments:

1. No new material presented for us here.

20. Fang, Firoozabadi, Abbasazadeh, and Radke (1996)[131]:

"A phenomenological Modeling of Critical Condensate Saturation"

Study Details and Description:

No experiments were performed.

Conclusions were based on theoretical investigation of the understanding of critical condensate and residual saturations and contact angle. The conclusions reached here are primarily by investigating the balance between capillary and gravity forces; therefore, they are applicable for vertical systems.

Author's Conclusions:

1. Critical condensate saturation, S_{cr}, is a result of retrograde condensation (in-situ liquid formation) in porous media and it is in the range of 10 to 50%.
2. Critical condensate saturation is different than residual condensate saturation, S_r, which is established by displacement.
3. S_{cr} is similar for both network of capillary tubes and for a single tube.
4. At low contact angles ($< 10^o$) Scr increases with increasing contact angle in the network model; however no such dependence observed at high contact angles ($10 < \theta < 30^o$).
5. This dependence of S_{cr} on contact angle suggest that model fluids such as C1/nC4 may not be representative of real fluids at such low contact angle conditions.
6. At IFT below critical value (0.25 mN/m) S_{cr} is also a function of surface tensions both in the network and in the single tube models; No such dependence observed for S_r.

Comments:

1. Distinction must be made between Scr and Sr in our analysis.
2. Contact angle may have a role in the viscous dominated regimes as in our tests. In our analysis we are balancing viscous forces and capillary forces, therefore, contact angle or Capillary pressure can have a role, no matter how insignificant.

21. Jerauld (1996)[129]:

"Gas-Oil Relative Permeability Of Prudhoe Bay"

Study Details and Description:

No experiments were performed. Conclusions were based on Prudhoe Bay lithological Data in conjunction with other data gathered from literature. Correlations between trapped gas saturation as function of lithology (k & ϕ) and sorting were presented. Also correlations of kr as function of Saturation and residual Saturation is presented.

Author's Conclusions:

1. Lithologies (porosity, permeability, sorting, and microporosity) dictate governs drainage efficiency (relative permeability) and trapped gas.
2. Carman-Kozeny equation can be inverted to provide an estimate of an effective grain size.

Comments:

1. Carman-Kozeny equation can be used to define the typical size of pore radius (R) in the Nc definition proposed by Kalaydjian at al. (1996). Actually this is the equation we used in our analysis of the flow regimes during the steady-state experiments. As given in chapter 4 of this thesis.

---

22. Kalaydjian, Bourbiaux, and Lombard (1996)[125]:

"Predicting gas-condensate reservoir performance: how flow parameters are altered when approaching production wells"

Study Details and Description:

12 Steady-state and 17 unsteady-state experiments conducted.

Procedure: One phase depleted to desired IFT followed by equilibrium gas-injection for USS krg values then two-phase gas-condensate injection for SS krc and krg values.

Two different cores:

(1)Palatinate sandstone; and (2) Belgium Chalk with the following properties

Core	k (mD)	ϕ (%)	L (cm)	A&Shape (cm^2)	PV (cm^3)	Swi (%)
(1)	4.1w/o Swi	19.25	38.4	10.20 squarre	75.4	11.4
(2)	2.0	39.9	34.0	9.61 square	130.4	6.0

Three different fluid types: binary C1C3, ternary C1C3C7, and real gas-condensate systems.

Author's Conclusions:

1. No dependence of kr on IFT even at very low IFT values 0.03 - 1.41 mN/m.
2. This uncustomary result is explained by the authors due to the very low viscous forces at the pore level. The authors believes that the dependence of kr on IFT at low IFT values is due to the interaction between the viscous and capillary forces rather than on IFT alone; hence low IFT values alone can not be responsible for such a dependence and in order to produce such a dependence the low IFT condition must be accompanied by relatively high pore velocities. Therefore, not only low IFT values are needed but also high capillary number values in order to observe the dependence of kr on IFT at low IFT values.
3. Different formulation for capillary number is used to explain the authors findings:

Conventional capillary value definition: $$N_c = \frac{\mu_g v_g}{\sigma} \qquad \text{...(B.14)}$$

Proposed definition: $$N_{cA} = \frac{4.N_c L}{R} \qquad \text{...(B.15)}$$

where,

L: the length of the core.

R: typical size of pore radius

$$R = \frac{2\sigma\cos(\theta)}{P^*} \qquad \text{...(B.16)}$$

P^*: the pressure at which mercury starts invading the porous medium in a mercury intrusion curve.

alternatively, R can be approximated as follow:

$$R = \sqrt{\frac{8k}{\phi}} \qquad \text{...(B.17)}$$

All in self consistent SI units.

The authors claim that the new capillary number values has to greater or at least equal to 1.0 in order to find any dependence of kr on IFT even at low IFT values.

Comments:

1. Experimental data can be incorporated into our data base especially the SS data points.
2. The new form of the capillary number can be put to the test using our data and the newly literature data when possible.

---

23. Nikravesh and Soroush (1996)[133]:

"Theoretical Methodology for Prediction of Gas-Condensate Flow Behavior"

Study Details and Description:

No experimental measurements performed. Theoretical conclusions are based on theoretical modeling of an assumed behaviour of three phase-flow in porous media: water, vapour, and condensate are typically exist in a gas-condensate systems and they interact with the rocks of porous media.

A correlation of kr with IFT is given: it takes the same form as Coats formulation; and another correlation of critical condensate saturation as a function of pore geometry, gravitational force, and IFT is also given.

The analysis is based on the following main assumptions:

1. The existence of a critical IFT value below which both the shape of kr values as well as the critical condensate saturations will be affected.
2. Condensation occurs via two mechanisms: dropwise condensation, and filmwise condensation. The former mechanism occurs at poorly wetted surfaces or when the fully- wetting phase is contaminated with other impurities; while the latter mechanism is only possible when the liquid phase is fully wetting the rock surface.
3. Gas-condensate relative permeability depends on IFT, gravity, and velocity. The effect of IFT on relative permeability and the effect of gravity on the vertical condensate saturation were studied; however, the effect of velocity which referred to as "depletion rate effect" was acknowledged only.

Author's Conclusions:

1. Critical IFT value is a characteristic of the surface chemistry of the solid alone and it does not depends on the fluid which comes into contact with the surface.
2. Below such a critical IFT value the condensation occurs via film flow mechanism where the critical condensate saturation can be considered zero.
3. The shape of relative permeability curves are greatly influenced by IFT below the critical value.
4. The effect of gravity on critical condensate saturation can not be neglected; its neglection can lead to an overestimation of the critical condensate saturation.
5. Interstitial water helps the early formation of film condensation on the water surfaces.

Comments:

1. While the chemistry of the surface rock may have a complementary role in determining the value of the critical condensate saturation, the primary factor on determining the exact value of a such critical IFT value ought to be the fluid itself.
2. The correlation and some of the conclusions are valid for the case of gravity dominated flow where viscous forces are not considered i.e. in the bulk of the reservoir.

REFERENCES

1. Chopra, A. K. and Carter, R. D.: "Proof of the two-phase Steady-State Theory for Flow Through Porous Media," SPEFE (1986) 603-608.

2. Raghavan, R. and Jones, J. R.: "Depletion Performance Of Gas-Condensate Reservoirs," JPT August (1996) 725-731.

3. Fevang, ϕ.: Modeling Gas Condensate Well Deliverability, PhD. Thesis, University of Trondheim, NTH, (1995).

4. Khazam, M.: Application of Phase Behaviour and Flow Models to Gas Injection and Gas-Condensate Recovery Processes, PhD. Thesis, Heriot-Watt University, (November, 1994).

5. Ali, J. K. and Butler, S., Allen, L., and Wardle, P.: "The Influince of Interfacial Tension on Liquid Mobility in Gas Condensate Systems' SPE 26783 presented at the 1993 Offshore Eutopean Conference, Aberdeen, Sep. 7-10.

6. O'Dell, H. G. and Miller, R. N.: "Successfully cycling a Low Permeability, High-Yield Gas Condensate Reservoir," JPT January (1967) 41-47; Trans., AIME, 240.

7. Petroleum Development Oman, Mina Al-Fahal, Muscat, Oman. Marmul Field Team, Private Communication.

8. Peng, D. Y. and Robinson, D. B.: "A New Two-Constant Equation of State," Ind. Eng. Chem. Fund. (1976) 59-64.

9. Soave, G.: "Equilibrium Constants from a Modified Redlich-Kwong Equation of State," Chem. Eng. Sci., 27, 2297-1203, (1972).

10. Zudkevitch, D. and Joffe, J: "Correlation and Prediction of Vapour-Liquid Equilibria with the Redlich-Kwong Equation of State," AIChe J., 16 (1), 112 (1970).

11. Patel, N. C. and Teja, A. S.: "A New Cubic Equation of State for Fluids and Fluid Mixtures," Chem. Eng. Sci., 77 (3), 463-473, (1982).

12. Archer, J. S. and Wall, C. G.: Petroleum Engineering, Principle and Prectice, Graham & Trotman, London (1986).

13. Petroleum Engineering Handbook, Bradly, H. B., Ed., SPE, Dallas, 1987, chapter 39.

14. Koedertiz, L. F., Harvey, A. H., and Honapour, M.: Introduction to Petroleum Reservoir Engineering, Gulf Publishing Co., Houston, Texas, 1989, chapter 10.

15. Muscat, M.: Physical Principles of Oil Production, McGraw-Hill Book Company, Inc. (1949).

16. Fetkovich, M. J.: "The Isothermal Testing of Oil Wells," SPE paper 4529 presented at the 1973 SPE ATCE, las Vegas, USA, Sept. 30- Oct. 3.

17. Kniazef, V. J. and Naville, S. A.: "Two-phase Flow of Volatile Hydrocarbons," SPEJ (1965) 37-44; Trans., AIME, 234.

18. Eilerts, C. K., Sumner, E. F., and Potts, N. L.: "Integration of Partial Differential Equation for Transient Radial Flow of Gas-Condensate Fluids in Porous Structures," SPEJ (1965) 141-152.

19. Eilerts, C. K. and Sumner, E. F.: "Integration of Partial Differential Equation for Multicomponent, Two-phase Transient Radial Flow," SPEJ (1967) 125-135.

20. Gondouin, M, Iffly, R., and Husson, J.: "An Attempt to Predict the Time Dependence of Well Deliverability in Gas Condensate Fields," SPEJ (1967) 112-124; Trans., AIME, 240.

21. Fussel, D. D.: "Single-Well Performance Predictions for Gas Condensate Reservoirs," JPT (1973) 258-268, 860-870; Trans., AIME, 255.

22. Coats, K. H.: "Simulation of Gas Condensate Reservoir Performance," JPT Oct. (1985) 1870-1886.

23. Hinchman, S. B. and Barree, R. D.: "Productivity Loss in Gas Condensate reservoirs," SPE paper 14203 presented at the 1985 SPE 60th ATCE, las Vegas, USA, Sept. 22-25.

24. van de Leemput, L. E. C., Bertram, D. A., Bentley, M. R., and Gelling R.: "Full Field Reservoir Modelling of Central Oman Gas/Condensate Fields" SPE paper 30757 presented at the 1995 SPE ATCE, Dallas, USA, Oct. 22-25.

25. Fevang, ϕ. and Whitson, C. H.: "Modeling Gas Condensate Well Deliverability," SPE paper 30714 presented at the 1995 SPE ATCE, Dallas, USA, Oct. 22-25.

26. Jones, J. R. and Raghavan, R.: "Interpretation of Flowing Well response in Gas Condensate Wells," SPE paper 14204 presented at the 1985 SPE ATCE, Las Vegas, USA, Oct. 22-25.

27. Alonso, M. E. and Nectoux, A. C.: "Experimental and Numerical Investigations of Primary Depletion of a Critical Fluid", Paper SPE 13266 presented at the 1984 SPE Annual Technical Conference and Exhibition, Houston, Sept. 16-19.

28. Danesh, A. Krinis, D., Henderson, G. D., and Peden, J. M.: "Visual Investigation of Retrograde Phenomena and Gas Condensate Flow in Porous Media" Proceedings of the Fifth European Symposium on Improved Oil Recovery, Budapest (April 1989).

29. Danesh, A. Krinis, D., Henderson, G. D., and Peden, J. M.: "Pore Level Visual Investigation of Miscible and Immiscible Displacements", Journal of Petroleum Science and Engineering, Vol. 2 (April 1989).

30. Danesh, A., Henderson, G. D., Krinis, D., and Peden, J. M.: "Experimental Investigation of Retrograde Condensation in Porous Media at Reservoir Conditions", Proceedings of the 63rd Annual Conference of the Society of Petroleum Engineers, Houston, (October 1988).

31. Danesh, A., Henderson, G. D., and Peden, J. M.: "Experimental Investigation of Critical Condensate Saturation and its Dependence on Connate Water Saturation", SPE Reservoir Engineering Journal, 336-342, (August 1991), also in Transactions of SPE 1991.

32. 'Gas Condensate Recovery Project' Final Report, August 1996, Heriot-Watt University, Department of Petroleum Engineering.

33. Hanarpour, M. and Mahmood, S. M.: "Relative Permeability Measurement: An Overview", JPT. (August 1988), 963-966.

34. Buckley, S. E. and Leverett, M. C.: "Mechanism of Fluid Displacement in Sands", Trans., AIME (1942) 146, 107-116.

35. Johnson, E. F. Bossler, D. P., and Naumann, V. O.: "Calculation of Relative Permeability from Displacement Experiments", Trans., AIME(1959) 216, 370-372.

36. Welge, H. J.: "A Simplified Method for Computing Oil Recoveries by Gas or Water Drive", Trans., AIME(1952) 195, 91-98.

37. Jones, S. C. and Roszelle, W. O.: "Graphical Techniques for Determining Rekative Permeability From Displacement Experiments", JPT. (May 1978) 807-817; Trans., AIME, 265.

38. Saiedi, A. and Handy, L. L.: "Flow and Phase Behavior of Gas Codensate and Volatile Oils in Porous Media," paper SPE 4891 presented at the 1974 44th Annual California Regional Meeting of the SPE, San Francisco, April 4-5.

39. Asar, H. and Handy, L. L.: "Influence of Interfacial Tension on Gas/Oil Relative Permeability in Gas-Condensate Systems," SPERE (Feb. 1988), 258-264.

40. Haniff, M. S. and Ali, J. K.: "Relative Permeability and Low Tension Fluid Flow in Gas-Condensate Systems' SPE 20917.

41. Gravier, J. F., Lemouzy, P., Barroux, C. and Abed, A. F.: "Determination of Gas-Condensate Relative Permeability in Whole Cores under Reservoir Conditions, " Paper SPE 11493 presented at the 1983 Middle East Oil Technical Conference of the SPE, Manama, March 14-17.

42. Bardon, C. and Longeron, D. G.: "Influence of Very Low Interfacial Tensions on relative Permeability," SPEJ, (Oct. 1980).

43. Munkerud, P. K.: "Measurements of relative permeability and flow properties of a gas-condensate system during pressure depletion and pressure maintenance", Paper SPE 11493, 1983.

44. 'Gas Condensate Recovery Project' Progress Report No. 1, Jan. 1994, Heriot-Watt University, Department of Petroleum Engineering.

45. 'Gas Condensate Recovery Project' Progress Report No. 2, July 1994, Heriot-Watt University, Department of Petroleum Engineering.

46. Dullien, F. A.: Porous Media Fluid Transport and Pore Structure. (1992). 2nd Ed. 333-484. Academic Press, Inc. San Diego, California 92101, USA.

47. Rose, W. (1972). The Iran Pet. Inst. Bull. 46, 23.

48. Rose, W. (1974). The Iran Pet. Inst. Bull. 48, 25.

49. Rose, W. (1988). Transport in Porous Media 3, 163-171

50. de Gennes, P. G. (1983). Phys. Chem. Hydr. 4, 175.

51. de la Cruz, V. and Spanos, T. J. T. (1983). AIChE J. 29, 854.

52. Auriault, J. L. and Sanchez-Palencia, E. (1986). J. Theor. Appl. Mech. Special Issue, 141.

53. Whitaker, S. (1986). Transport in Porous Media 1, 105-125.

54. Auriault, J. L. (1987). Transport in Porous Media 2, 45.

55. Spanos T. J. T., de la Cruz, V., Hube, J., and Sharma, R. C. (1986). Can. J. Petr. Technol. 25, 71.

56. Kalaydijian, F. (1987). Transport in Porous Media 2, No. 6, 537-552.

57. Kalaydijian, F. and Legait, B. (1987). C. R. Acad. Sc. Paris Ser. II 304, 869.

58. Spanos T. J. T., de la Cruz, V. and Hube, J. (1988). AOSTRA Journal of Research 4, 181.

59. Kalaydijian, F. (1990). Transport in Porous Media 5, No. 3, 215-229.

60. Payatakes, A. C., Tien Chi, and Turian, R. (1973). AIChE J. 19, 58, 67.

61. 'Gas Condensate Recovery Project' Progress Report No. 3, January 1995, Heriot-Watt University, Department of Petroleum Engineering.

62. 'Gas Condensate Recovery Project' Progress Report No. 4, July 1995, Heriot-Watt University, Department of Petroleum Engineering.

63. 'Gas Condensate Recovery Project' Progress Report No. 5, January 1996, Heriot-Watt University, Department of Petroleum Engineering.

64. Dybbs, A. and Edwards, R. V. A New Look at Porous Media Fluid Mechanics - Darcy to Turbulent. Fundamentals of Transport Phenomena in Porous Media, 1984. 201-256. Martinus Nijhoff Publishers. Dordrecht, The Netherlands.

65. Bird, R. B., Stewart, W. E., and Lightfoot, E. N. *Transport Phenomena.* 1960. 180-207. John Wiley & Suns Inc. New York. USA.

66. Cornell, D. and Katz, D. L.: Ind. Eng. Chem. (1953), 45, 2145.

67. Stutzman, L. F. and Thodos, G.: Pet. Trans., AIME (1956), 376, 352.

68. Aziz, K., and G. W. Govier, *Can. J. Chem. Eng.*, 40, 51, (1962).

69. Collier, J. G., and G. F. Hewitt, *Trans. Inst. Chem. Engrs.*, 39, 127 (1961).

70. Eaton, B. A., D. E. Andrews, C. R. Knowles, I. H. Silberberg, and K. E. Brown, *J. Petrol. Technol.*, 19, 815 (1967).

71. Gill L. E., G. F. Hewitt, and P. M. Lacy, *Chem. Eng. Sci.*, 20, 71 (1965).

72. Govier, G. W., and Aziz, K. *The Flow of Complex Mixtures in Pipes.* New York, NY.: Van Nostrand Rheinhold, 1972.

73. Levy, S., *Int. J. Heat and Mass Transfer*, 9, 171 (1966).

74. Wicks, M., and A. E. Duckler, *A. I. Ch. E. Journal*, 6, 463 (1960).

75. M. M. Khazam, Ali Danesh, D. H. Tehrani, A. C. Tod, and R. Burgass. “Dynamic Validation of Phase Behaviour Models for Reservoir Studies of Gas Injection Schemes" SPE 28627 (1994).

76. Moore, T. F. and Slobod, R. L., 1956. The effect of viscosity and capillarity on the displacement of oil by water. Prod. Month., 20 (Aug.): 20-30.

77. Pirson, S. J. (Editor), 1958. Oil Reservoir Engineering. McGraw Hill, New York, N.Y.

78. Mungan, N., 1966. Interfacial effects in immiscible liquid-liquid displacement in porous media. Soc. Pet. Eng. J., 6 (Sep.): 247-253.

79. Wagner, O. R. and Leach, R. O., 1966. Effect of interfacial tension on displacement efficiency. Soc. Pet. Eng. J., 6 (Sep.): 335-344.

80. Lafebvre du Prey, 1968. Influence des parametres interfacing sur les permeabilities relatives. Comm. 13, C. R. 3eme Colloque Assoc. Recherche sur les Technique de Forage et de Produits, Pau, France.

81. Coats, K. H., 1980. An equation of state compositional model. Soc. Pet. Eng. J., 20 (Oct.): 363-367.

82. Amaefule, J. O. and Handy, L. L.: "The Effect of Interfacial Tension on Relative Oil/Water Permeabilities on Consolidated Porous Media," Soc. Pet. Eng. J. (June 1982): 371-381.

83. Bette, S., Hartman, K. J., and Heinemann, R. F., 1991. Compositional modelling of interfacial tension effects in miscible displacement processes. J. Pet. Sci. Eng., 6: 1-14.

84. Fultcher, R.A., Ertekin, T., and Stahl, C. D., 1985. Effect of capillary number and its constituents on two-phase relative permeability curves. J. Pet. Technol., 37 (Feb.): 249-260.

85. Jankovic, M. S., 1985. Analytical miscible relative permeability curves and their usage with compositional and Pseudo-miscible simulators. Pap. 85-36-48, presented at 36th annu. Tech. Conf. Pet. Soc. CIM, Edmonton, Alta.

86. Pusch, G. and Muller, T., 1989. Modelling of multiphase flow with respect to low interfacial tension by pseudo-two-phase relative permeability fractions. 5th Eur. Symp. Improved Oil Recovery, Budapest, Hungary. Rev. Inst. Fr. Petrole, 45 (1): 63-70.

87. Ronde, H., 1992. Relative permeability at low interfacial tensions. SPE 24877, presented at the 67th Annu. Tech. Conf. Soc. Pet. Eng. Washington, D. C.

88. Hartman, K. J., and Cullick A. S. 1994. Oil recovery by gas displacement at low interfacial tension. J. Pet. Sci. Eng., 10: 197-210.

89. Taber, J. J. "Dynamic and Statis Forces Required to remove a Discontinuous oil Phase from Porous Media Containing Both Oil and Water," Soc. Pet. J. (March 1969) 3-12.

90. Melrose, J. C. and Brandner, C. F.:"Role of Capillary Forces in Determining Microscopic Displacement Efficiency for Oil Recovery by Waterflooding," J. Cdn. Pet. Tech. (Oct.-Dec. 1974) 54-62.

91. Chatizis, I. and Morrow, N. R.: "Correlation of Capillary Number Relationships for Sandstones," S. P. E. J. (Oct. 1984) 555-562.

92. Stegemeier, W.: Oil Recovery by Surfactant and Polymer Flooding, Academic Press Inc., Washington, D. C. (1977).

93. Marquaedt, D. M. "An Algorithm for Least-Squares Estimation of Nonlinear Parameters," J. Soc. Indust. Appl. Math., 11, 431-441, 1963.

94. Kuester, J. L. and Mize, J. H.: Optimisation Techniques With Fortran, McGraw-Hill Inc., New York, NY, U.S.A. (1973) 240-250.

95. Taylor, John R.: An Introduction to Error Analysis, The Study of Uncertainities in Physical Measurements, University Science Books, Oxford University Press, Mill Vally, CA, U.S.A. (1982) 40-98.

96. Fussell, L. T. and Fussell, D. D.: "An Iterative Technique For Compositional Reservoir Models," SPEJ, (August 1979) 211-220.

97. Nghiem, L. X., Fong, D. K., and Aziz, K.: "Compositional Modeling with an Equation of State," SPEJ, (Dec. 1981) 688-698.

98. Kazemi, H. Vestal, C. R., and Shank, G. D.: "An efficient Multicomponent Numerical Simulator," SPEJ, (Oct. 1978) 355-368.

99. Young, L. C. and Stephenson, R. E.: "A generalised Compositional Approach for Reservoir Simulation," SPEJ, (Oct. 1983) 727-742.

100. Sarker, R.: "Application of Quaternary Diagrams to the Compositional Modeling of Gas Miscible Processes". PhD. Thesis, Heriot-Watt University, (Nov. 1987).

101. Peaceman, D. W.: Fundamentals of Numerical Simulation, Elsevier Scientific Publishing Co., Amsterdam (1977).

102. Lantz, R. B.: "Quantitative Evaluation of Numerical Diffusion (Truncation Error)," EPEJ (Sept. 1971) 315-320; Trans., AIME, 251.

103. Wilson, G.: "A Modified Redlich-Kwong Equation of State, Application to General Physical Data Calculations," paper 15C presented at the 1968 AIChe Natl. Meeting, Cleveland, May 4-7.

104. Whitson, C. H. and Trop, S. B.: "Evaluating Constant Depletion Data," JPT (March 1983) 610-620.

105. Standing, M. B.: Volumetric and Phase Behaviour of Field Hydrocarbon Systems, SPE, Richardson, TX (1977).

106. Varotsis, N.: "A Robust Prediction Method for Rapid Phase- Behaviour Calculations," SPERE, (May 1989), 237-243.

107. Jhaveri, B. S., and Youngren, G. K.: "Three-Parameter Modified Peng-Robinson Equation of State to Improve Volumetric Predictions," SPE paper 13118' presented at the 1984 SPE Annual Technical Conference, Houston, September 16-19.

108. Peneloux, A., Rauzy, E., and Freze, R.: "A Consistent Correlation for Redlich-Kwong-Soave Volumes," Fluid Phase Equilibria, 1982, Vol. 8, 7-23.

109. Lohrenz, J., Bary, B.G., and Clark, C. R.: "Calculating Viscosities of Reservoir Fluids from Their Compositions," JPT, pp. 1171-1176, (Oct. 1964).

110. Weinaug, C. F. and Katz, D. L.: "Surface Tensions of Methane-Propane Mixtures," Ind. Eng. Chem. (1943) [35], 239.

111. Danesh, A., Dandekar, A., Todd, A. C., and Sarker, R.: "A Modified Scalling Law and Parachor Method Approach for Improved Prediction of IFT of Gas-Condensate Systems," SPE 22710, (1990).

112. Hough, E. W. and Stegemeier, G. L.: "Correlation of Surface and interfacial Tension of Light Hydrocarbons in the Critical Region," SPEJ. (Dec. 1961) 259-263; Trans., AIME, 222.

113. Firoozabadi, A., Katz, D. L., Soroosh, H. and sajjadian, V. A.: "Surface tension of Grude-Oil/Gas Systems Recognising the Asphalt in Heavy Fractions," SPERE (Feb. 1988) 265-272.

114. Penny, G. S. and Liang, J. "The Development of Laboratory Correlations Showing The Impact of Multiphase Flow, Fluid, and Proppant Selection Upon Gas Well Productivity". SPE Annual Technical Conference & Exhibition, Dallas, TX, USA, 22-25 October, 1995. SPE Paper No. 30494.

115. Wong, S. W.: "Effect of Liquid Saturation on Turbulence Factors for Gas-Liquid System." J. Canadian Pet. Tech. (Oct. -Dec. 1970) 274.

116. Greetsma, J.: "Estimating the Coefficient of Inertial Resistance in Fluid Flow Through Porous Media," SPEJ (Oct. 1974), 445-450.

117. Tek, M. R., Coats, K. H., and Katz, D. L.: "The Effect of Turbulence on The Flow of Natural Gas through Porous reservoirs," JPT (July 1962) 299.

118. Fredrick, D. C. and Graves, R. M.: "New Correlations to Predict Non-Darcy Flow Coefficients at Immobile and Mobile Water Saturations," Annual Technical Conference, New Orleans, LA, USA, 25-28 Sept., 1994. SPE Paper No. 28451.

119. Noman, R. and Archer, J. S. :"High Velocity Gas Flow in Liquid-Saturated Porous Media and its Visualization," J. Cand. Pet. Tech., 27, no 3, May-June, 1988, 64-69.

120. Hagoort, J.: "Oil Recovery By Gravity Drainage," SPEJ (June 1980) 139-50.

121. Wang, P., Pope, G. A., and Sepehrnoori, K.: "Compositional Modeling Of Low Interfacial Tension Effects On Flow Behaviour Of Gas Condensate," Proceedings of the Seventh European Symposium on Improved Oil Recovery, Moscow, Russia (October 27-29, 1993).

122. Gian Luigi Chierici: "Novel Relations For Drainage and Imbibition Relative Permeabilities," SPEJ (June 1984) 275-276.

123. Gravier, J. F., Lemouzy, P., Barroux, C. and Abed, A. F.: "Determination of Gas-Condensate Relative Permeability in Whole Cores under Reservoir Conditions, " SPEFE (February 1986), 9-15.

124. Kerig, P. D. and Watson, A. T.: "Relative-Permeability Estimation From Displacement Experiments: An Error Analysis, " SPERE (March 1986), 175-182.

125. Kalaydjian, F. J-M., Bourbiaux, B. J., and Lombard, J-M.: "Predicting gas-condensate Reservoir Performance: How Flow Parameters are Altered When Approaching Producing Wells," SPE paper 36715 presented at the 1996 SPE ATCE, Denver, Colorado, USA, October. 6-9.

126. Bourbiaux, B. J. and Limborg, S. G. An Integrated Experimental Methodology for a Better Prediction of Gas-Condensate Flow Behaviour. SPE 28931 presented at the SPE Annual Technical Conference and Exhibition held in New Orleans, LA, U.S.A., 25-28 September 1994.

127. Chen, H. L., Wilson, S. D., and Monger-McClure, T. G.: "Determination Of Relative Permeability And Recovery For North Sea Gas Condensate Reservoirs," SPE paper 30769 presented at the 1995 SPE ATCE, Dallas, Texas, USA, October, 22-25.

128. Boom, W., Wit, K., Schulte, A. M., Oedai, S., Zeelenberg, J. P. W., and Mass, J. G.: "Experimental Evidence For Improved Condensate Mobility At Near-Wellbore Flow Conditions," SPE paper 30766 presented at the 1995 SPE ATCE, Dallas, Texas, USA, October, 22-25.

129. Jerauld, G. R.: "Gas-Oil relative Permeability Of Prudhoe Bay," SPE paper 35718 presented at the 1996 SPE Western Regional Meeting, Anchorage, Alaska, USA, May. 22-24.

130. Ronde, H.: “Effect of Low Interfacial Tension On Relative Permeabilities In Some Gas Condensate Systems,” SPE Paper 25072 presented at The European Petroleum Conference, Cannes, France (November 16-18, 1992).

131. Fang, F., Firoozabadi, A., Abbaszadeh, M., Radke, C.: "A Phenomenological Modeling Of Critical Condensate Saturation," SPE paper 36716 presented at the 1996 SPE ATCE, Denver, Colorado, USA, October. 6-9.

132. Boom, W., Wit, K., Zeelenberg, J. P. W., Weeda, H. C., and Mass, J. G.: "On The Use Of Model Experiments For Assessing Improved Gas-condensate Mobility Under Near-Wellbore Flow Conditions," SPE paper 36714 presented at the 1996 SPE ATCE, Denver, Colorado, USA, October. 6-9.

133. Nekravesh, M. and Soroush, M.: "Theoretical Methodology For Prediction of Gas-Condensate Flow Behaviour," SPE paper 36704 presented at the 1996 SPE ATCE, Denver, Colorado, USA, October. 6-9.

134. Morrow, N. R. and Chatizis, I.: "Entrapment And Mobilization Of Residual Oil In Bead Packs," SPE paper 14423 presented at the 1985 SPE 60th ATCE, Las Vegas, NV, USA, Sept. 22-25.

135. Munkerud, P. K.: "Measurement Of Relative Permeability And Flow Properties Of A Gas Condensate System During Pressure Depletion And Pressure Maintenance," SPE paper 19071 presented at the 1989 SPE Gas Technology Symposium, Dallas, Texas, USA, June, 7-9.

136. Morel, D. C., Lomer, J-F., Morineau, Y. M., and Putz, A. G.: "Mobility Of Hydrocarbon Liquids In Gas Condensate Reservoirs: Interpretation Of Depletion Laboratory Experiments," SPE paper 24939 presented at the 1992 SPE ATCE, Washington, D. C., USA, October, 4-7.

137. Oak, M. J. and Ehrlichl, R. ‘‘A New X-Ray Absorption Method for Measurement of Three-Phase Relative Permeability’’ SPE Res. Eng. February 1988.

138. Nicholls, C. I. and Heaviside, J. "Gamma Ray Absorption Techniques Improve Analysis of Core Displacement Tests", SPE14421, Presented at 60th Annual Technical Conference of SPE, Las Vegas, NV, Sept. 1985.

139. Hartman, K. "Bromated Hydrocarbon PVT data" Private communication, Mobil Exploration and Producing Technical Center Fluid Flow Characterization. August 1994.

140. Henderson, GD, Danesh, A, Tehrani, DH, and Al-Shaidi, S, JM:"Measurement and Correlation of Gas Condensate Relative Permeability by the Steady-State Method", SPE Journal, 191-201 (June 1996).

141. Jordan, J. R. and Campbell: Well Logging I - Rock Properties, Borehole Environment, Mud and Temperature Logging., Monograph Series, SPE, Dallas (1984) 9, Chapter 2, 11-39.

142. Honarpour, M., Koedertiz, L. F., and Harvey, A. H.: IRelative Permeability of Petroleum Reservoirs, CRC Press Inc., Boca Raton, FL (1989) 27-29; 79-82.

143. Wyckoff, R. D. and Botset, H. G.: Flow Of Gas Liquid Mixtures Through Sands, Physics, 7, 325, 1936.

144. Leverett, M. C. and Lewis, W. B.: Steady Flow Of Gas-Oil-Water Mixtures Through Unconsolidated sands, *Trans. AIME*, 142, 207, 1941.

145. Dunlap, E. N.: Influence Of Connate Water On Permeability Of Sands To Oil, *Trans. AIME*, 127, 215, 1938.

146. Stewart, C. R., Craig, F. F., Jr., and Morse, R. A.: Determination of Limstone Performance Characteristics by Model Flow Tests, *Trans. AIME*, 198, 1953.

147. Morgan, T. J. and Gordon, D. T.: Influence Of Pore Geometry On Wate-Oil Realtive Permeability, *JPT*, 1199, 407, 1970.

148. Keelan, D. K.: A practical Approach To Determination Of Imbibition Gas-Water Relative Permeability, *JPT*, 4, 199, 1976.

149. Leas, W. J., Jenks, L. H., and Russell, C. D.: Relative Permeability To Gas, *Trans. AIME*, 189, 65, 1950.

150. Afidick, D., Kaczorowski, N. J., and Bette S.: Production Performance Of A Retrograde Gas Reservoir: A case Study Of The Arun Field. SPE paper 28749

presented at the SPE Asia Pacific Oil & Gas Conference, Melburne, Austratlia, 7-10 November 1994.

151. Diamond, P., Pressney, R. A. and Snyder, D. E.: "Probabilistic Prediction of Well Proformance in Gas Condensate Reservoir," SPE paper 36894 presented at the 1996 SPE European Petroleum Conference, Milan, Italy, 22-24 October.

Vita

Salman Ibin Mohammed Al-Shidi was born in the state of Saham located on the Gulf of the Sultanate of Oman. He is the sixth child of Mohammed Ibin Salman Al-Shidi and his wife Salimah Bint Salem Al-Bureiki.

Salman graduated from Drexel University in Philadelphia, Pennsylvania, USA with a Bachelor of Science in Civil Engineering in June 1991 and had a Master of Science in Engineering (Petroleum Engineering) from the University of Texas at Austin in Austin, Texas, USA in December 1993. He has been a scholar for Petroleum Development of Oman LLC., a Royal Dutch Shell subsidiary, since 1991; now, he is on a PhD. scholarship at the Department of Petroleum Engineering of Heriot-Watt University in Edinburgh, Scotland, UK.

Permanent Address: P. O. Box 630
Sohar, 311
Oman.

This Thesis was typed by the author.